University of Louisville
ThinkIR: The University of Louisville's Institutional Repository

Electronic Theses and Dissertations

12-2022

# Voltage-gated potassium channel dependent mechanisms of cardiovascular adaptation to chronic exercise.

Sean Raph
*University of Louisville, School of Medicine*

Follow this and additional works at: https://ir.library.louisville.edu/etd

Part of the Exercise Physiology Commons

## Recommended Citation

Raph, Sean, "Voltage-gated potassium channel dependent mechanisms of cardiovascular adaptation to chronic exercise." (2022). *Electronic Theses and Dissertations.* Paper 3992.
Retrieved from https://ir.library.louisville.edu/etd/3992

This Doctoral Dissertation is brought to you for free and open access by ThinkIR: The University of Louisville's Institutional Repository. It has been accepted for inclusion in Electronic Theses and Dissertations by an authorized administrator of ThinkIR: The University of Louisville's Institutional Repository. This title appears here courtesy of the author, who has retained all other copyrights. For more information, please contact thinkir@louisville.edu.

# VOLTAGE-GATED POTASSIUM CHANNEL DEPENDENT MECHANISMS OF CARDIOVASCULAR ADAPTATION TO CHRONIC EXERCISE

By

Sean Raph

B.A., University of Maine at Farmington, 2012

M.Sc. Bio, University of Southern Maine, 2015

M.S., University of Louisville, 2021

A Dissertation

Submitted to the Faculty of the

School of Medicine of the University of Louisville

In Partial Fulfillment of the Requirements

For the Degree of

Doctor of Philosophy

In Pharmacology and Toxicology

Department of Pharmacology and Toxicology

University of Louisville

Louisville, Kentucky

December 2022

VOLTAGE-GATED POTASSIUM CHANNEL DEPENDENT MECHANISMS OF CARDIOVASCULAR ADAPTATION TO CHRONIC EXERCISE

By

Sean Raph

B.A., University of Maine at Farmington, 2012

M.Sc. Bio, University of Southern Maine, 2015

M.S., University of Louisville, 2021

A Dissertation Approved on

December 6th, 2022

By the Following Dissertation Committee:

_____

Dissertation Director

Matthew A. Nystoriak, Ph.D.

_____

Aruni Bhatnagar, Ph.D.

_____

Steven P. Jones, Ph.D.

_____

Bradford Hill, Ph.D.

_____

Amanda J. LeBlanc, Ph.D.

_____

Zhoa-Hui Song, Ph.D.

# DEDICATION

This dissertation is dedicated to my friends and family, my children Ronan, Kieran and Eamon, and my wife Sara Jane.

# ACKNOWLEDGEMENTS

I acknowledge the Herculean support of everyone in the lab since I joined Dr. Nystoriak and the Diabetes and Obesity Center (now the Center for Cardiometabolic Science) in 2018. Importantly, I am grateful for the guidance of my committee members. Most emphatically my mentor Dr. Matthew Nystoriak, who has always kept his expectations high and encouraged me to succeed. I would also like to think Xuemei Hu and Li Luo for their support and guidance with various molecular techniques and for assisting in maintaining our animal colonies. I am also thankful for the help and support of Dr. Marc Dwenger, for teaching and advising me various electrophysiological patch clamp techniques and in the writing of manuscripts. I would also like to thank our collaborators Drs. William Chilian and Vahagn Ohanyan and Northeast Ohio Medical University.

# ABSTRACT

VOLTAGE-GATED POTASSIUM CHANNEL DEPENDENT MECHANISMS OF CARDIOVASCULAR ADAPTATION TO CHRONIC EXERCISE

Sean M. Raph

December 6, 2022

Exercise increases cardiac workload, escalating the demand for oxygen. The myocardial vasculature responds to the greater demand for oxygen by increasing blood flow to match the needs of the heart during augmented work. Increasing blood flow requires the coronary arteries dilate (a.k.a. vasodilation); this is mediated predominantly by vascular smooth muscle cell relaxation. Vasodilation is driven through inhibition of calcium influx into vascular smooth muscle cells. The prevention of calcium influx is largely mediated by efflux of potassium via potassium channels causing membrane hyperpolarization, which in turn closes voltage-dependent (or gated) calcium channels (VDCC). Changes in vascular smooth muscle cell membrane potential are influenced by the movement of potassium ions through $K^+$ channels such as the voltage gated potassium (Kv) channels. Kv channels form heteromeric octomeric complexes consisting of four membrane bound α-subunits that comprise the voltage-sensitive pore complex, and associate with four intracellular auxiliary β-subunits (Kvβ). The auxiliary β-

subunits are members of the aldo-keto reductase (AKR) super family, enzymes that catalytically react with carbonyl substrates. These β-subunits sense changes in oxygen availability, metabolic signal transducer ratios (e.g., NADH:$NAD^+$) and metabolites (e.g., $H_2O_2$). In this study I investigated the role of Kv channels and their auxiliary Kvβ2 subunits in vasodilation response to conditions of altered metabolism, physiological cardiac adaptation, and myocardial blood flow in response to 4 weeks of exercise. I found that Kvβ2 is necessary to induce Kv driven vasodilation under hypoxic conditions. Loss of Kvβ2 significantly impaired exercise capacity in both naïve and 4-week exercised (exe) mice, relative to sedentary and wildtype controls. Chronic exercise also enhanced myocardial perfusion in WT mice but not $Kv\beta2^{-/-}$ male mice. Additionally, 4-weeks of exercise significantly increased Kv1 associated Kvβ2, in proximity ligation assay experiments. In isolated arteries from SM22α-rtTA single transgenic mice, the perfusion of external 10 mM L-lactate in the presence of $10^{-5}$ M $H_2O_2$ induced significantly greater vasodilation. Interestingly, this effect was not seen in arteries from SM22α-rtTA:TRE β1 double transgenic mice. Administration of NADH and $H_2O_2$ induced significant increases in Kv channel open probability (nPo). Additionally, in vascular smooth muscle cells, isolated from SM22α-rtTA mice, externally perfused with 1 mM NADH plus of $10^{-5}$ M $H_2O_2$ we observed a significant increase in Kv nPo. Hence, we conclude that loss of Kvβ2 impairs vasodilatory capacity in response to conditions that reflect increased work. Also, exercise capacity and myocardial perfusion are impaired in the absence of Kvβ2. Additionally, the increased presence of Kvβ1 relative to Kvβ2 in the Kv channel complex opposes the

vasodilatory response to metabolites and signal transducers of increased work (e.g., NADH and $H_2O_2$). In conclusion, the presence of the Kvβ2 protein in arterial myocytes is crucial for adaptation following chronic exercise training.

# TABLE OF CONTENTS

*DEDICATION* ..... *iii*

*ACKNOWLEDGEMENTS* ..... *iv*

*ABSTRACT* ..... *v*

VOLTAGE-GATED POTASSIUM CHANNEL DEPENDENT MECHANISMS OF CARDIOVASCULAR ADAPTATION TO CHRONIC EXERCISE ..... v

*LIST OF FIGURES* ..... *x*

*CHAPTER 1: LITERATURE REVIEW* ..... *1*

Introduction ..... 1

Cardiac form and function ..... 2

Cardiac metabolism ..... 5

Exercise ..... 6

Circulatory system ..... 9

Arteries ..... 10

Vasodilation and vasoconstriction ..... 12

Ion channel ..... 18

Membrane polarization of excitable cells ..... 21

Comparative physiology: Regulation of myocardial blood flow, cardiac health, and disease ..... 22

Cardiovascular health and regulation of myocardial blood flow ..... 23

Cardiovascular disease ..... 24

*HYPOTHESIS AND SPECIFIC AIMS* ..... *26*

Aim 1: Determine how coronary Kvβ molecular composition influences the relationship between myocardial blood flow and $O_2$ demand. ..... 28

Aim 2: Elucidate the contribution of Kvβ molecular remodeling to enhanced myocardial blood flow in the exercise-conditioned heart. ..... 28

*CHAPTER 2: MATERIALS AND METHODS* ..... *29*

*CHAPTER 3: MYOCARDIAL BLOOD FLOW CONTROL BY OXYGEN SENSING VASCULAR $K_V\beta$ PROTEINS*[2] ..... *46*

Introduction ..... 46

Results ..... 49

Discussion ..... 58
Figures ..... 65
*CHAPTER 4: INTEGRATED REDOX SENSITIVITY OF VASCULAR $K_V1$ CHANNELS ..... 76*
Introduction ..... 76
Results ..... 80
Discussion ..... 83
Figures ..... 86
*CHAPTER 5: EXERCISE-ENDHANCED CARDIAC FUNCTION AND MYOCARDIAL PERFUSION REQUIRE THE VOLTAGE-GATED POTASSIUM CHANNEL AUXILIARY SUBUNIT $K_V\beta2$. ..... 93*
Introduction ..... 93
Results ..... 96
Discussion ..... 103
Figures ..... 106
*CHAPTER 6: DISCUSSION, CONCLUSIONS AND FUTURE DIRECTIONS ..... 123*
Discussion ..... 123
Conclusions ..... 124
Future directions ..... 129
Study limitations ..... 130
*REFERENCES ..... 132*
*APPENDIX A ..... 150*
Pyridine nucleotide redox potential in coronary smooth muscle couples myocardial blood flow to cardiac metabolism. ..... 150
*APPENDIX B ..... 191*
Diversification of potassium currents in excitable cells via Kvβ proteins ..... 191
*APPENDIX C ..... 217*
Biochemical and physiological properties of $K^+$ channel associated AKR6A (Kvβ) proteins ..... 217
*CURRICULUM VITAE ..... 236*

# LIST OF FIGURES


FIGURE 1-1. LOSS OF KVB2 IMPAIRS CARDIAC PUMP FUNCTION DURING STRESS. ..... 65
FIGURE 1-2. RELATIONSHIP BETWEEN MYOCARDIAL BLOOD FLOW AND CARDIAC WORKLOAD IN KVB-NULL MICE. ..... 66
FIGURE 1-3: ABLATION OF KVB2 ATTENUATES HYPOXIA-INDUCED CORONARY VASODILATION. ..... 67
FIGURE 1-4. L-LACTATE ENHANCES IKV IN CORONARY ARTERIAL MYOCYTES AND PROMOTES CORONARY VASODILATION VIA KVB2. ..... 69
FIGURE 1-5. KVB2 CONTROLS REDOX-DEPENDENT VASOREACTIVITY IN RESISTANCE MESENTERIC ARTERIES. ..... 71
FIGURE 1-6. INCREASING THE RATIO OF KVB1.5:KVB2 SUBUNITS IN SMOOTH MUSCLE INHIBITS L-LACTATE-INDUCED VASODILATION AND SUPPRESSES MYOCARDIAL BLOOD FLOW. ..... 74
FIGURE 2-1. ELEVATION OF L-LACTATE PROMOTES VASODILATION VIA LDH ACTIVITY. (A) ..... 86
FIGURE 2-2. NADH INDUCES SIGNIFICANT INCREASE IN NPO OF ISOLATED ARTERIAL MYOCYTES. ..... 87
FIGURE 2-3. 10 MM $H_2O_2$-INDUCED INCREASED VASODILATION AND KV OPEN CHANNEL PROBABILITY... 88
FIGURE 2-4. DIRECT EFFECTS OF $H_2O_2$ ON NATIVE VASCULAR KV1 CHANNELS IN THE PRESENCE OF NADH. (A) ..... 89
FIGURE 2-5. $H_2O_2$-INDUCED DILATION IS NOT AFFECTED BY OVER-EXPRESSION OF KVB1 IN SMOOTH MUSCLE. ..... 90
FIGURE 2-6. SMOOTH MUSCLE OVEREXPRESSION OF KVB1 PREVENTS REDOX MODULATION OF $H_2O_2$-INDUCED VASODILATION. ..... 91
FIGURE 3-1. EXERCISE CAPACITY IS IMPAIRED IN NAÏVE KVB2-KNOCKOUT MICE. ..... 106
FIGURE 3-2. POST 4-WEEK FORCED TREADMILL RUNNING (FTR) EXERCISE INDUCED GREATER ADAPTATION IN WT MALE MICE. ..... 108
FIGURE 3-3. 4-WEEKS EXE. ENHANCED CARDIAC FUNCTION IN WT MALE MICE. ..... 110
FIGURE 3-4. 4-WEEK EXE. INCREASES KV1.5:B2 PROXIMITY IN ISOLATED CORONARY VASCULAR SMOOTH MUSCLE CELLS. ..... 112
FIGURE 3-5. 4-WEEKS OF EXERCISE ENHANCED CARDIAC FUNCTION, AND MYOCARDIAL BLOOD FLOW IN WT MALE MICE. ..... 113
FIGURE 3-6. 4-WEEKS EXE. HAD MINIMAL IMPACT ON IMPROVING CARDIAC FUNCTION IN KVB2-/- MALE MICE. ..... 114
FIGURE 3-7 4 WEEKS OF EXERCISE DID NOT ENHANCE MYOCARDIAL BLOOD FLOW IN $KVB2^{-/-}$ MALE MICE. ..... 116
FIGURE 3-9. ADAPTATIONS IN EXERCISE CAPACITY FOLLOWING FOUR WEEKS OF TREADMILL RUNNING ARE ATTENUATED IN KVB2-NULL ANIMALS. ..... 118
FIGURE 3-10. ADAPTIVE INCREASES IN HEART SIZE IN WILD TYPE, BUT NOT KVB2-NULL ANIMALS FOLLOWING TREADMILL EXERCISE CONDITIONING. ..... 119
TABLE 1: BODY MASS OF SEDENTARY AND EXERCISED WILD TYPE AND KVB2-/- MICE. ..... 120
TABLE 2: COMPARISON OF ECHOCARDIOGRAPHIC PARAMETERS IN WILD TYPE AND KVB2-/- EXERCISED AND SEDENTARY MICE AND AT BASELINE AND DURING DOBUTAMINE CHALLENGE. ..... 121

# CHAPTER 1: LITERATURE REVIEW

## Introduction

Cardiovascular disease persists as the leading cause of death around the globe.[1,2] Despite numerous pharmacological interventions meant to mitigate these pernicious conditions, the greatest means to alleviate and or prevent premature death due to cardiovascular disease continues to be exercise.[3,4] Exercise has played a major role in human physiological and cultural evolution from the prehistoric era to modern day.[5,6] For example, the modern-day Olympics is a direct imitation of the ancient Greek Olympiads, in which athletes of superior fitness would display their physical prowess. The cultural and physiological importance of exercise to our society is made most apparent when watching the modern-day Olympic marathon that precedes the lighting of the great torch: a replication of the ancient story of the Greek messenger Pheidippedes (a.k.a. Philippides) and his race to deliver the message of victory at the Battle of Marathon.[7-9] Despite numerous studies investigating the importance of exercise there still remain numerous unanswered questions. How does exercise improve our cardiovascular health? How does exercise change our cardiovascular system response to stress? By what mechanism(s) does exercise improve heart and vascular function? Are cardiac adaptations preceded or followed by adaptations to the coronary vasculature? In this thesis, I endeavor to address these questions and further our

understanding of the cardiovascular benefits of exercise. However, before communicating my scientific results addressing these questions, I will present a comprehensive review of what is known about exercise induced physiological changes to the heart and coronary perfusion to improve understanding of the outcomes of this project and provoke discussion of this thesis's implications.

## Cardiac form and function

The heart is comprised of four chambers, that work in paired unison to pump oxygen poor blood through the vasculature of the pulmonary circuit, and oxygen rich blood out to through the systemic circuit. For reference, when facing an individual, the heart resides, tilted slightly, just left of the center of the sternum. The top of the heart, a.k.a. the base, is pointed up and to the left toward the subject's right shoulder. The bottom of the heart, a.k.a. the apex, points down and away to the right. The base of the heart is comprised of the left and right atria, these are separated from the two other chambers by a septal wall. Inferior to the atria, reside the left and right ventricles, these are separated by a thick septal wall.

The cardiac cycle is divided into two major phases: systole, the contraction phase of the heart, and diastole, the relaxation and ventricular filling phase of the heart. During mid to late diastole, the ventricles are relaxed and the pressure in these chambers is lower than in the atrial chambers. Due to this lower ventricular pressure as compared to atrial pressure, the tricuspid and bicuspid valves are open between the atrial and ventricular chambers. Because these valves remain open during this phase of the cardiac cycle, deoxygenated blood from the systemic circulation passively flows via the superior and inferior vena cava through the right

atrium into the right ventricle. Simultaneously, oxygenated blood from the pulmonary circulation passively flows via the pulmonary veins through the left atrium and into the left ventricle. Approximately 80% of blood passively fills into the ventricles during mid to late diastole. At the beginning of cardiac contraction (systole), the sinoatrial (SA) node cells spontaneously inducing action potentials throughout both atrial chambers. This contraction allows for the remaining 20% of blood in the atria to pass into the ventricles. The action potentials continue to spread towards the ventricles at the apex of the heart. Eventually, the action potentials from the SA node cells converge on another type of nodal cells, the atrioventricular (AV) bundle, an electrical conduit to the ventricles that lies near the interface between the interatrial septum and the atrioventricular septum. A conduction delay occurs at the atrioventricular node allowing for completion of atrial contraction and ventricular filling. Following this delay, action potentials propagate into the ventricular myocardium by following myocardial fibers that lie near the interventricular septum, named bundle of His and the left and right bundle branches. From the bundle branches, the action potentials spread to the rest of the ventricular myocardium via the Purkinje fiber system. As the action potentials spread to the ventricular myocardium, the ventricles begin to contract, initiating ventricular systole. As ventricular systole progresses, the ventricular myocardium squeezes the blood in the ventricles. Eventually, ventricular pressure exceeds atrial pressure and the atrioventricular valves, tricuspid and bicuspid respectively, snap shut. During initial period of ventricular contraction, the volume in the ventricles remains the same as ventricular pressure remains lower than the

pressure in the pulmonary and systemic circulation; thus, the semilunar valves remain closed, inhibiting blood flow from the ventricles. Eventually the isovolumetric contraction phase in the ventricles ends as ventricular pressure exceeds the pressure in the pulmonary trunk and aorta. When ventricular pressure reaches this peak, the semilunar valves open and blood flows from the right ventricle into the pulmonary circulation and from the left ventricle into the systemic circulation via the aorta. Eventually, systole ends, initiating diastolic relaxation again. The semilunar valves close and the atrioventricular valves opens as ventricular pressure decreases below pulmonary, systemic, and atrial pressure and ventricular filling begins again. The cardiac cycle lasts approximately 0.6 to 1 second in humans.

Due to this constant workload on the heart, the myocardial tissue must be continuously perfused by oxygenated blood. This constant perfusion is partially assisted by the anatomy of the vasculature. Immediately after oxygenated blood is ejected from the left ventricle during systole, a portion of blood is diverted into the left and right coronary arteries that branch off the aorta. The coronary arteries supply oxygenated blood to the left and right sides of the heart, respectively. The left and right coronary arteries split into several branches to efficiently perfuse the myocardium. For example, the right coronary artery branches into the marginal artery and posterior interventricular artery, which perfuse the right and a majority of the posterior ventricular myocardium. The left coronary artery divides into circumflex and left anterior descending (LAD) artery. Furthermore, these branches supply oxygen rich blood to the myocardial tissue to prevent ischemia.[10-12] Blood

flow in the coronary circulation must be tightly regulated as the heart has limited anaerobic capacity. Thus, a discussion on how the coronary circulation regulates blood flow to the myocardium is warranted, especially in the context of exercise in which workload is increased; however, this discussion of the regulation of blood flow during several physiological states requires a basic understanding of cardiac metabolism, exercise, and arterial function.

## Cardiac metabolism

In the human body, there remains the constant struggle of resource allocation for energy production, with the brain and the heart being the largest consumers of ATP.[13,14] The three predominant resources that the heart relies on for ATP production are glucose, free fatty acids (FFA), and lactate.[15-17] Resource utilization depends on several factors: increased work (e.g., exercise), growth (e.g., hypertrophy), injury. At rest, the heart predominantly utilizes FFA and glucose which produce 40–70% and 20–30% of the ATP consumed, respectively.[15] Both FFA and glucose are eventually converted to molecules of acetyl-CoA and enter the TCA cycle.[18] During exercise the reliance on glucose significantly declines, and the utilization of FFA, lactate, and ketone bodies significantly increase.[15] FFA utilization results in increased lipolysis of adipose tissues, while lactate levels increase as a byproduct of cellular mitochondrial respiration, increased skeletal muscle lactate production, and other local changes in metabolism.[19-21] Increased FFA and lactate utilization can drive increased concentrations of metabolic signaling transducers (e.g., NADH) and reactive oxygen species (e.g., $H_2O_2$), which have also been proposed as signaling

molecules for vasodilation.[22-24] Exercise induced changes in cardiac metabolism are linked to greater coronary flow reserve and enhanced vasodilatory capacity. However, the signaling mechanisms behind enhanced coronary perfusion during increased cardiac work and altered are not well established.

## Exercise

Exercise can be defined as participation in regularly repeated activity where physical effort is greater than normal, for the purpose of sustained or improved health and fitness.[25] This can include regular participation in activities such as running, walking, biking, and playing numerous sports. The regular repetition of these activities improves not only skeletal muscle strength, but arguably and most importantly, cardiovascular health.[26] Regular exercise is a crucial tool in preventing and ameliorating cardiovascular disease and its associated risks.[27]

Cardiovascular disease (CVD) and associated co-morbidities (e.g., obesity) are a leading cause of global mortality and morbidity.[1] Sedentary lifestyle behavior is one of the most detrimental risk factors contributing to CVD deaths.[28] Introducing regular exercise to previously sedentary individuals, those with diabetes, obesity, or other diseases, improves endothelial function,[29,30] anti-inflammatory response,[31] blood flow,[32] cardiac function,[33] and cognition.[34]

Crucial considerations when researching exercise and changes to cardiac function are work and functional measures of cardiac performance. Work can simply be assessed using forced running on a treadmill and an exercise capacity test.[35] The weight of the animal is multiplied by the vertical distance travelled at each stage of the capacity test. Additionally, by comparing exercise capacity prior

training, researchers can assess subject improvement.[36] Functional measures of cardiac performance can include or are derived from heart rate (beats per minute), ejection fraction, end diastolic (relaxed) and end systolic (contracted) volumes, blood pressure, and stroke volume. From these data we can calculate more complex determinants of cardiac work such as cardiac output (CO, stroke volume x heart rate). Additionally, contrast echocardiography can be used to determine perfusion (i.e., blood flow) in myocardium and determine relative blood flow to the heart.[37] Regular increases in cardiac work (i.e., exercise) have been associated with improved heart rate recovery and cardiac function, and improved myocardial perfusion in humans.[38-41] Additionally, Yang et al., 2007 have shown that with exercise training the whole cell potassium currents significantly increase.[42] This is represented as a sensitization of the potassium channel currents at more hyperpolarized states after exercise. From these findings it can be inferred that exercise sensitizes arterial myocytes membrane potential at a hyperpolarized state[42], confers a greater propensity of arteries to dilate.[43] In turn, the enhanced potassium channel activity contributes to vasodilation that leads to greater coronary perfusion,[44] increased oxygen and nutrients supplied to the myocardial tissue, and sustained cardiac function during increased work.[41,44,45]

With the introduction of regular exercise, the heart adapts by growing.[46] There are two ways in which the heart can grow in response to increased work, physiological and pathological hypertrophy. Pathological cardiac hypertrophy is often characterized by a growth of the myocardium in such a manner that volume of the ventricular chambers decreases,[47] this can drive decreased function and

develop into heart failure. Physiological hypertrophy, often observed in athletes, increases ventricular wall thickness without loss in ventricular chamber volumes. Researchers have observed enhanced left ventricular function in athletes with physiological cardiac hypertrophy.[48,49] As discussed in previous sections, exercise results in a greater contribution of potassium channels to enhance coronary blood flow. However, several questions remain; how do $K^+$-channels sense rapid changes in $O_2$ or nutrients and confer greater coronary perfusion? Is the Kv channel or its intracellular subunit component the sensor of altered metabolic conditions? Does impaired coronary flow confer a decrease in cardiac work capacity?

Increased work (e.g., exercise) requires the matching of oxygen and nutrients supplied to the heart to prevent tissue ischemia and damage.[50] This is achieved in part through the vasodilatory responsiveness of the coronary arteries to changes in metabolic redox ratios and oxygen saturation. As cardiac workload increases, the ratios and concentrations of metabolic byproducts (e.g., lactate) and endogenous stimuli (e.g., $H_2O_2$) increase.[41,51] In resting conditions, these factors are well established as vasodilators.[37,52] Additionally, increases in NADH (via lactate conversion to pyruvate by lactate dehydrogenase)[53] and ROS influence vasodilation via interactions with $K_V$ channels.[54,55] In addition to enhanced sensitivity to altered metabolites, exercise enhances the myocardial flow reserve in part by enhancing the vasodilatory capacity of the coronary artery.[56] The vascular benefits of exercise have been attributed to increased levels of endothelial derived nitric oxide (NO), or sensitivity of calcium sensitive potassium

channels ($BK_{Ca}$), and or ATP-sensitive potassium channels ($K_{ATP}$).[56-59] However, these have been displaced as major contributors of increased coronary perfusion in response to increased cardiac workload during exercise. Tune et al., 2004 and others have shown that individual and paired blockade of NO, $K_{ATP}$, adenosine, and $BK_{Ca}$, causes a downward shift in coronary blood flow but does not impair increased coronary flow during exercise or increased cardiac work.[60] If the contributing mechanism of coronary flow were blocked, or impaired it would most likely translate to no observable increase in coronary perfusion during increased cardiac work. Therefore, the question remains, what regulates the change in myocardial perfusion in response to increased cardiac work (i.e., exercise)?

## Circulatory system

A common deleterious event to the organs in the body is a rapid, significant starvation of oxygen and/or nutrients.[61] Our circulatory systems pervade our bodies organs and innervate our tissues. Comprised of a high-pressure delivery circuit (arteries) and a low-pressure return circuit (veins), described generally as the vasculature, these systems supply essential resources throughout the body. These circuits are further grouped into the pulmonary and systemic circulatory systems, each comprised of a tree of arteries and veins. The pulmonary circuit cycles blood to the lungs where oxygen and carbon dioxide are exchanged in the alveolar sacs. Similarly, the systemic arterial circuit dispenses recently oxygenated blood throughout the body. The structural components of arteries and veins differ from one another to better serve their physiological function. These anatomical functions will be described in more detail in their individual sections.

Some of the earliest observations of vascular physiology were made by Hippocrates and Galen. These monumental forebearers of modern medicine and science interpreted the world around them as best they could. In 340 BC Praxagorus first differentiated arteries which originate from the heart from veins which originated from the liver.[62] Erasistratus proposed the heart as the origin of both arteries and veins. That arteries were a transport for air, that only become filled with blood from the veins via invisible anastomoses when the arteries empty of air. It was Galen, the physician to the Emperor of Rome, and others who proposed an open system model of circulation in which blood ebbed and flowed slowly.[62] This also included blood having originated in the liver and air (termed pneuma) exchanged in the lungs and delivered to tissues via the veins and arteries. Once the blood and air had reached the end of a vein or artery it would dissipate into the tissues. This flawed knowledge of the body and its mechanisms permeated the understanding and interpretations of generations of historical figures.[62]

For centuries humors and pneuma and an open circulatory system were accepted as fact until in 1628 William Harvey published his works, *On the Motion of the Heart and Blood in Animals*.[63,64] Harvey used a matured scientific deduction, reasoning and importantly experimentation to investigate and demonstrate that blood circulated in a closed system. Harvey demonstrated the importance of the cardiac mechanical strength as the force behind the movement of blood throughout the circulatory system.

## Arteries

Arteries deliver oxygen and nutrients throughout the body, ensuring that tissues are not deprived of oxygen (i.e., hypoxia).[65] The most distinct feature of arteries is the maintained rigid tube structure, comprised of multiple layer(s) of vascular smooth muscle cells (VSMC), arrayed in such a way that they confer significant changes in arterial diameter.[66] Arteries are comprised of three distinct layers or tunica (derived cognate from the Latin for “tunic” or layer). The first being the inner or tunica intima, which is comprised predominantly of endothelial cells. The tunica media or middle, which is comprised of the vascular smooth muscle cells, tightly controls the diameter of the vessel. Finally, the tunica adventitia or outer layer, which is composed of connective tissues that provide the structural and connective support.[66,67]

The vascular smooth muscle cells that encompass the tunica media are arranged in longitudinal, radial, and circumferential fashion to allow for control of vascular diameter.[68,69] The tight regulation and great range of changes to arterial diameter play important roles as arteries become progressively smaller. The typical human aorta, is ~25 millimeters in diameter, they have the greatest diameter but the least dynamic range instead retaining a greater elasticity to cushion the forceful output from the heart.[70] Progressing down the arterial tree the diameter of individual arteries decreases, however the density and dynamic range (~100-300 μm) of arteries increases significantly.[71,72] Following the same principle observed in electrical circuits with resistors, in which resistors in parallel have a multiplied effect compared to resistors in series which have only an added effect.[45] In humans arterioles are typically 50-200 micrometers in diameter,[73] this has a

significant impact on restricting or enhancing blood flow. Early work done in small resistance arteries show that these artery beds have the greatest impact on vascular resistance, and thus blood flow.[73]

## Vasodilation and vasoconstriction[1]

As mentioned above, changes in small resistance arterial diameter greatly impact blood pressure through modifying vascular resistance.[37] This important function can either increase (vasoconstriction) or decrease (vasodilation) vessel diameter and influence blood flow. The flow of blood through the vasculature follows Poiseuille's law, loosely stated, "the velocity of a liquid flowing through a tube is directly proportional to the change in pressure at two points of the tube and the fourth power of the radius of the tube and inversely proportional to the viscosity of the liquid and tube length."[74] Simply put, assuming that pressure, viscosity, and tube length are constant, the most significant contributing factor to changing flow is the diameter of the tube. In the case of the human body, our vascular network (e.g., arteries) is continuously looping and therefore the length is not an influential factor. However, the capacity of resistance arterials to change their diameter (50-300 μm) creates a significant range in potential resistance. For instance, a change in arterial diameter of 100 μm to 80 μm (Δ20μm) decreases flow in that artery by approximately 50%. Therefore, when many resistance arteries decrease their diameter, total resistance increases, and this decreases blood flow.

[1] Portions of these topics were also discussed previously in the Masters thesis Raph, Sean M, "Role of KVβ2 subunits in regulation of resistance arterial tone." (2021). *Electronic Theses and Dissertations.* Paper 3589.

Changes in arterial diameter are driven predominantly through increased calcium influx and sarcoplasmic release in vascular smooth muscle cells. As with dilation, numerous endogenous and exogenous factors can induce vasodilation. Here, I will focus on the basic principle of calcium influx and constriction, describing several pertinent examples of vasomotor function (i.e., vasoconstriction and dilation).

*Regulation of calcium ([$Ca^{2+}$]) in vascular smooth muscle cells (VSMC)*: Calcium is the driving force for nearly every signaling pathway in the human body, such as insulin and neurotransmitter release, and smooth muscle contraction.[75-77] There are two major contributing sources of calcium for VSMC, the extracellular calcium and sarcoplasmic pools. The intracellular and sarcoplasmic concentrations of [$Ca^{2+}$] typically reside around 100-140 nM.[78] Meanwhile, extracellular $Ca^{2+}$ can exceed concentrations of 2mM.[78] As such, the influx of extracellular $Ca^{2+}$ or sarcoplasmic release can significantly increase $[Ca^{2+}]_i$ by 10-1000x times greater. Therefore, the regulation of $[Ca^{2+}]_i$ is crucial to maintain proper cellular function. In vascular smooth muscle cells, the predominant means of calcium influx into the VSMC is via the L-type voltage-dependent $Ca^{2+}$ channels (VDCC).[79] The opening of VDCC is dependent on the VSMC membrane depolarizing to a more positive potential.[80] Sarcoplasmic $Ca^{2+}$ release can be induced via activation of ryanodine receptors after increases in $[Ca^{2+}]_i$ and membrane depolarization.[81,82] Additionally, the inositol triphosphate receptors (IP3R) are able to liberate $Ca^{2+}$ from local stores in the endoplasmic reticulum where $Ca^{2+}$ far exceeds $[Ca^{2+}]_i$.[83]

*Myogenic tone*: Self-regulation of vessel diameter by resistance arteries is crucial to maintain blood pressure and flow. To provide sufficient and consistent blood flow the arteries respond to changes in intravascular pressure and shear forces to induce a myogenic i.e., muscle derived, tonic response. This is a physiological vasoconstriction response that occurs in response to increased intraluminal pressures (roughly in the range of 60–100 mmHg). This response is mediated via the regulation of arterial smooth muscle cell (a.k.a. arterial myocyte) intracellular calcium ($[Ca^{2+}]_i$). Increased arterial myocyte $[Ca^{2+}]_i$ stimulates the vasoconstriction pathway of the calmodulin-myosin light chain kinase activity induced constriction.[84] This pathway involves $[Ca^{2+}]_i$ binding to calmodulin, the $Ca^{2+}$-calmodulin activates myosin light chain kinase (MLCK). MLCK phosphorylates light chain myosin allowing myosin to interact with actin. In the presence of ATP this leads to arterial myocyte contraction, that translates on the tissue level to arterial constriction, and in response to increased intraluminal pressure, myogenic tone.[85]

*Shear stress-induced regulation of arterial tone*[2]: Changes in intravascular pressure alone do not sufficiently explain every condition of arterial tone regulation. Additional factors, such as shear stress are capable of inducing endothelium dependent tone development.[86-88] As is the case with numerous effectors in the blood stream, the endothelium lining the arterial walls are the first layer exposed to native and foreign molecular stimuli, and mechanical forces i.e., shear stress.

[2] Portions of these topics were also discussed previously in the 'nitric oxide' section of the Masters thesis Raph, Sean M, "Role of KVβ2 subunits in regulation of resistance arterial tone." (2021). *Electronic Theses and Dissertations.* Paper 3589.

This can also be described as the shear force in laminar flow, in which the velocity of the fluid at the center of the artery is greater than at the point of contact with the tube wall. This difference in fluid velocity is due to the friction exerted on the fluid by the tubes 'stationary surface' (i.e., the vessel wall). It is the friction between the fluid (i.e., flowing blood) and the tube wall (i.e., artery) that exerts a shear stress. Increased blood flow drives greater shear stress on the microvascular endothelium this drives endothelium dependent vasodilation.[89-91] There are a number of endothelium derived vasodilators such as calcium-activated potassium channels (a.k.a., $SK_{Ca}/IK_{Ca}$) as well as nitric oxide (NO), that play a role in shear stress induced endothelial response. The $SK_{Ca}/IK_{Ca}$ channels have been shown as important contributors that induce increased endothelial NO in response to increased shear stress.[89,92] The induction of shear stress induces the conversion of L-arginine to L-citrulline by the nitric oxide synthase (NOS) pathway, this increases the byproduct NO. The readily diffusible NO moves from the endothelium to adjacent vascular smooth muscle cells and activates the soluble guanylate cyclase (sGC). In turn, this increases cGMP that activates PKG that then inhibits IP3R driven sarcoplasmic $Ca^{2+}$ release paired with decreased intracellular $Ca^{2+}$, results in vasodilation. [93-97]

*Hypoxia induced vasodilation*: Decreases in available oxygen to tissues, also known as hypoxia, can have severe effects on the body. Hypoxia can occur when too little oxygen is available to enter the blood via the lungs (such as at very high altitudes), during a vascular obstruction (such as during an ischemic stroke), or when the heart is weak and incapable of proper function (such as with ischemia).

In systemic circulation, hypoxia can induce vasodilation via inward rectifying potassium channels ($K_{IR}$) in the endothelium.[98] Park et al., 2005 revealed in isolated rabbit hearts, that hypoxia increased coronary blood flow was significantly diminished with the addition of barium ($Ba^{2+}$), a known inhibitor of $K_{IR}$ channels.[99] The increase in $K_{IR}$ mediated vasodilation was attributed to cyclic-adenosine monophosphate (cAMP) driven phosphokinase-a (PKA) signaling cascades. Although $K_{IR}$ induced membrane hyperpolarization has also been attributed to increased cellular release of potassium during hypoxia or ischemia. Additionally, others have shown that hypoxia induced vasodilation can be attributed to endothelial derived nitric oxide, prostaglandins, and adenosine via $K_{ATP}$ channels.[100-102]

*Nitric oxide induced vasodilation*: Another significant vasodilator is nitric oxide (NO), a byproduct of nitric oxide synthase (NOS) conversion of L-arginine to citrulline in vascular endothelial cells. Experiments conducted in the early 1900's by F.W. Mott et al., revealed that in anaesthetized animals the "organic substance" choline suppressed arterial blood pressure.[103] It was not until the 1980's that scientists identified acetylcholine induced endothelial dependent vasodilation via NO.[104,105] Endothelial cells comprise the interior face of arteries, and are capable of influencing vascular smooth muscle cells and vasomotion via signaling molecules NO.[106]

*Reactive oxygen species mediated vasodilation*: Increases in cellular metabolism and thus respiration is necessary to meet the needs of highly active tissues. However, the resulting change in respiration can drive increases in

reactive oxygen species (ROS).[107,108] This includes the superoxide anion and hydrogen peroxide ($H_2O_2$), these species can be derived from aerobic respiration, and NADPH oxidase (NOX) activity.[109,110] Classically ROS have been considered as only detrimental, due to the damaging effects on DNA and tissues.[111,112] However more recently studies have considered ROS, specifically $H_2O_2$ as crucial signaling molecules.[113] For instance increases in $H_2O_2$ have been shown to induce vasodilation via activation of potassium channels.[114] However, the exact mechanism of $H_2O_2$ mediated vasodilation and activation of these channels are not well established. It has been proposed that $H_2O_2$ induces oxidation of the thiols to affect channel opening and induce vasodilation.[115,116] Interestingly, sustained increases in ROS uncouple endothelial derived NO mediated vasodilation.[117,118] These observations demonstrate the importance of maintaining a balance of ROS so that signaling capacities are preserved and tissue damage is prevented.

*Endothelial derived relaxing factors:* The nomenclature, endothelial derived relaxing factors (EDRF), encompasses several identified and yet unidentified potential mediators. Those that have been identified include but are not limited to, ADP, thrombin, $H_2S$, and $H_2O_2$.[119,120] Typically, the accepted mechanism of these EDRF molecules is an activation of soluble guanylate cyclase. For instance, under conditions of sheer stress endothelial cells endogenous NOS converts L-arginine to citrulline, and as a byproduct NO is released. NO readily diffuses across the endothelial membrane into the surrounding tissues, for example smooth muscle cells. The diffused NO binds to and activates the guanylyl cyclase which induces increased cyclic-GMP (c-GMP).[121] cGMP in turn activates cGMP-dependent

protein kinases (PKG1) that feed into further cascades that lead to decreased $[Ca^{2+}]_i$ and vasorelaxation.[122,123] Another EDRF, endothelial derived hydrogen sulfide ($H_2S$) induces vasodilation via posttranslational cysteine *S*-sulfhydration that activates $K_{ATP}$ and $K_{IR}$ channels.[124] EDRF molecules can influence local or direct changes to vascular tone in response to shifts in metabolic demands.

**Ion channel**

Ion channels are purposed with selectively filtering the passage of ions across the membranes of cells to enhance or alleviate the driving force of the electro-chemical gradient. There are consistent mechanisms, such as voltage sensitivity, or thiolation, which activate or sensitize different channels to serve their purpose.

*Inwardly rectifying channels:* Inwardly rectifying potassium ($K_{IR}$) channels greatly differ from other $K^+$ channels (e.g., $K_V$) in that they are made up of two membrane spanning helices, they more readily allow for influx of $K^+$ rather than efflux when membrane potential is negative to $E_K$ and have voltage independent mechanisms of activation such as gating by pH and ATP.[125] $K_{IR}$ currents are lower in arterial myocytes due in large part to their positive membrane potential relative to $E_K$.[126] The $K_{IR}$-mediated efflux of $K^+$ occurs with increased external $K^+$ and drives hyperpolarization.[125] Park et al.,2007 showed that in the presence of the $K_{ATP}$ inhibitor glibenclamide, hypoxia enhanced coronary blood flow in isolated rabbit hearts via $K_{IR}$.[127] While $K_{IR}$ are well studied in the vascular smooth muscle cells, where they contribute to resting membrane potential and basal tone, in endothelial

cells $K_{IR}$ have been proposed to “cooperatively” regulate arterial vasomotor responses.[128-131]

*Voltage-gated potassium channels*: Comprising 40 genes that make up approximately 12 subfamilies depending on their location, structural composition, voltage sensitivity, and applied function, the voltage-gated potassium channel are the most prolific ion channels.[132] For instance, the voltage-gated potassium channels (KCNA1) include the sub family Kv1.x.[132] These channels are comprised of membrane bound alpha and intracellular beta-subunits. The alpha subunits contain six distinct regions, and further associate as membrane integrated heteromeric alpha subunit complexes, comprised of 4 α-subunits. Within the membrane bound region of each alpha subunit is a voltage sensitive structure. This specialized region is comprised of 4 arginine residues per α-subunit that make up the “gating charges”.[133-135] MacKinnon, 2003 and Jiang et al., 2003 have described the voltage sensors as “paddles” that confer the positive charges of the arginine residues across the membrane in response to voltage changes.[133-135] The movement of these charged residues through the electrical field of the membrane confer electrical work that is coupled to the channel opening. The pore region of the α-subunit channel makes up the selectivity filter of the channel. The selectivity of the Kv channel allows the passage of potassium and water in a multi-step transition through the alpha (α) complex.[136] There is an intracellular segment of the alpha subunits termed the T1 binding domain. This region is the interface point between the alpha and beta-subunit (β) components. The Kvβ-subunits (KCNAB) are members of the aldo-keto reductase (AKR) super family and retain their

catalytic function, reducing carbonyls with the help of cofactors.[137-140] While several cofactors, such as NADH, have been found to interact with the catalytic binding pocket the identification of endogenous carbonyl substrates has continued to elude the field.[138-140]

## Pharmacological intervention to control vascular tone and modify blood flow

Cardiovascular disease (CVD) is the leading cause of death around the globe, accounting for more than 17-million deaths annually.[141] The physical burden of CVD is paired with a large financial burden calculated to exceed $300 billion dollars per year and expected to continue increasing.[142] A large contribution of CVD related injury and death results from diminished vasodilatory capacity or physical obstructions that impair blood flow to the myocardial tissue a condition known as coronary ischemic heart disease (IHD).[143] A number of lifestyle factors such as diet, obesity, diabetes, and sedentary lifestyle, are known to significantly contribute to the development of IHD and CVD.[144-146] The most common forms of treatment for these diseases have predominantly been pharmacological interventions to enhance blood flow.[147] The cause of the ischemia, whether obstruction or impaired vasodilatory capacity, determine the intervention. For instance, individuals are often prescribed medications to reduce the risk of blood and cholesterol derived clots (aspirin and statins). Additionally, to increase blood flow drugs like nitrates (nitroglycerine) are often prescribed that activate vasodilatory pathways like the soluble guanylyl cyclase cascade.[148] Additionally, the use of calcium channel blockers is known to cause relaxation in vascular

smooth muscle cells.[149] For the purpose of this review I will focus on pharmacological interventions targeting Kv channels and the Kvβ-subunit.

Humans were not the first to develop compounds able to target Kv channels, several animals including snakes, scorpions and marine snails, independently adapted Kv targeting venoms.[150] Use of Kv channel targeting small molecules, and venom derived peptides could be used in neurological clinical settings in an attempt to decrease or increase the frequency of Kv-mediated action potential firing.[151] In the context of cardiovascular disease, Kv targeting therapies are used to correct or alleviate arrythmia in cardiomyocyte tissues.[152,153] However, the majority of Kv targeting compounds in use overlook the β-subunit its influence on Kv channel activity. There is a current lack in the knowledge base of drugs, or small molecules with the potential to target the catalytic capacity of Kvβ to enhance or impair Kv channel activity. Although, there are studies investigating compounds that can disrupt Kv-α/β and potentially impact Kv current, there are as of yet no drugs known to target Kvβ.[154] Despite this, what is known about enhanced Kv channel activity in response to Kvβ sensing or interacting with cofactors, $H_2O_2$-mediated thiolation, and carbonyls, support a possible target with wide ranging influence on cardiovascular health.[138-140,151,155-157]

## Membrane polarization of excitable cells

The driving factor of membrane potential and excitability is driven predominantly through differences in intracellular and extracellular ion concentrations and the subsequent electro-chemical gradient. Movement of potassium ($K^+$) ions across the membrane exhibit the greatest influence on

changes to membrane potential. At rest, vascular smooth muscle cells maintain a hyperpolarized membrane potential of -60 to -35 mV.[158,159] Using the Nernst equation $(RT/z)*\ln([\Sigma X]_{out}/[\Sigma X]_{in})$ I can calculate the effect on membrane potential for each ions concentration. R is the universal gas constant, T is temperature in Kelvin, z is the ionic charge, $[\Sigma X]_{out}$ is the sum of all external ions e.g., $K^+$, $Na^+$, $Cl^-$, $Ca^{+2}$; $[\Sigma X]_{in}$ is the sum of the intracellular ion concentrations. So, when calculating membrane potential, the greatest influencing factor is the concentration of $K^+$. Therefore, I can simply state that changes in extracellular $[K^+]$ relative to intracellular $[K^+]$ drive membrane potential more negative (hyperpolarize) or positive (depolarized). For example, in arterial functional assays (e.g., myography) it is common to induce calcium influx through inducing membrane depolarization by externally administering 60 mM $[K^+]$ (normal extracellular $[K^+]$ is roughly 4–6 mM). The difference in potassium concentration between the inside (140 mM) and outside (4–6 mM) of the cell creates an electro-chemical gradient. Using techniques such as electrophysiological patch clamp, researchers in the 1940's and 50's were able to determine the depolarization of neuronal cells using giant squid axons. By measuring the current across the axon membrane after the addition of different external stimuli (e.g., 60 mM potassium, or external voltage increase) Hodgkin and Huxley were among the first to elucidate membrane potential polarization was linked to the movement of ions.[107,160]

## Comparative physiology: Regulation of myocardial blood flow, cardiac health, and disease

The use of animals in place of humans to study anatomical, physiological, and biological phenomena has been common practice since ancient times.[161] These early anatomists noted significant differences in organ location and size, as well as other anatomical structural differences.[161] Despite numerous classical anatomical observations few reliable physiological comparisons were ever made. However during the Renaissance era physiological inquiries would begin emerging as regular practice for early physicians and scientists included animal experimentation.[161] Experiments conducted by William Harvey in the early 1600's applied the scientific method to investigate physiological systems of the human body.[162] Thanks to these early physiological investigations into the cardiovascular system we understand the conservation of function across mammals.[163] Despite the similarities in cardiovascular function there are significant differences that are important to realize, for instance murine resting heart rate is in the range of 500-600 beats per minute (bpm), in humans it is 60-100 bpm.[164] Even with centuries of investigation into cardiovascular function, humans are still faced with the daunting reality that cardiovascular disease is the leading global killer.[141] The importance of understanding human cardiovascular function in healthy and diseased states is therefore of great importance. This includes further study of coronary physiology to better understand how myocardial perfusion may be impacted by altered metabolic load and disease. Therefore, it is crucial to include further discussion on the topics of regulation of myocardial blood flow, cardiovascular health, and disease as it pertains to human physiology.

## Cardiovascular health and regulation of myocardial blood flow

As described in earlier sections, the coronary artery branches from the aorta as it leaves the left ventricle. Branching off from the left coronary artery (LCA) into the circumflex and left anterior descending artery (LAD). These branches supply blood to the left side of the heart and are frequently the proverbial culprits of ischemic heart disease a contributing factor in poor cardiovascular health outcomes. Further, the LCA and LAD provide the required supply of oxygen and nutrients to the myocardium at rest and during stress by modifying arterial diameter and thus myocardial perfusion. Investigating myocardial perfusion in humans requires greater awareness of potential harm of contrast agents to patients.[165,166] At rest, coronary diameter and myocardial perfusion are maintained in large part by myogenic constriction.[95] During increased work $O_2$ demand, shear force, or other factors mediate increased coronary diameter and myocardial perfusion.[45,95,166-169] However, coronary artery disease, whether obstructive or non-obstructive, contributes to approximately 7 million deaths and leaves another 129 million patients with impaired cardiovascular function.[170]

## Cardiovascular disease

There is no singular disease that can be used to define or describe cardiovascular disease (CVD), and numerous contributing factors can lead to impaired cardiac function.[171] One of the most frequent causes of cardiac dysfunction is a lack of sufficient oxygen supply as a result of impaired arterial function. Decreased arterial dilatory capacity, impaired arterial sensitivity, obstructive plaques that narrow arterial diameter, diminished endothelial function, disrupted cellular metabolism, comprise only a brief list of possible causes of

decreased coronary perfusion and thus cardiac function.[1,2,27,28,70,96,141,143-145,171-176] Therefore, I endeavor to further expand the field of coronary physiology by investigating adaption of coronary perfusion regulation. Further expanding our understanding of this critical physiological response and can then apply our knowledge in the context of disease to develop better targeted therapies.

# HYPOTHESIS AND SPECIFIC AIMS

Regular exercise prevents and mitigates cardiovascular disease (CVD). Among the many beneficial cardiovascular effects of exercise, physical conditioning increases maximal myocardial perfusion and increases coronary flow reserve. Enhanced myocardial blood flow (MBF) following prolonged exercise may support exercise-induced adaptations of the heart, including documented changes in cardiac metabolism, electrophysiology, contractility, and structure that directly antagonize pathological signatures. Nonetheless, the molecular mechanisms by which the regulation of MBF adapts to exercise to promote cardiorespiratory fitness and reduced CVD risk are poorly understood. In an acute bout of exercise, increased myocardial $O_2$ demand requires instantaneous increases in MBF (i.e., increased $O_2$ supply) via coronary vasodilation. Coronary arterial tone is largely dependent upon global cytosolic [$Ca^{2+}$], which is controlled by membrane potential and $Ca^{2+}$ influx via voltage-dependent $Ca^{2+}$ channels. Acute increases in $O_2$ demand, such as those that occur during exercise, lead to the increased activity of voltage-dependent $K^+$ (Kv) channels in arterial myocytes, resulting in membrane potential hyperpolarization and relaxation. Nonetheless, a *major gap in knowledge* exists related to the molecular determinants of Kv channel activation during periods of heightened myocardial $O_2$ demand. Our preliminary studies reveal a fundamental role for intracellular regulatory subunits of voltage-gated $K^+$ channels in establishing the relationship between MBF and myocardial $O_2$ consumption. Our

findings suggest that intracellular Kvβ subunits (i.e., $K_V\beta1$ and $K_V\beta2$), interacting as heterotetramers with pore-forming Kv1 proteins in coronary arterial myocytes, differentially confer vasoreactivity to $O_2$ tension and demand. Consistent with this, ablation of *Kcnab2*, the gene encoding Kvβ2, abolished coronary vasodilation in response to acute hypoxia and elevated external L-lactate, and diminished MBF. Studies in large animal models suggest that enhanced Kv channel activity in coronary arterial myocytes may contribute to improved MBF following chronic exercise.[42,44,50,60,169,177] Consistent with the role for vascular Kvβ proteins in coupling MBF with myocardial $O_2$ consumption, which is augmented in the exercise-conditioned heart, the ratio of vascular $K_V\beta2$:Kvβ1 was increased following four weeks of treadmill running in mice. Furthermore, characteristic adaptive responses to exercise (e.g., improved exercise capacity, physiological cardiac growth) were abolished in $K_V\beta2^{-/-}$ mice. These findings are consistent with our global hypothesis that metabolic regulation of Kv1 activity, coronary vasoreactivity, and MBF is modified by the molecular identity of Kvβ proteins in arterial myocytes. Moreover, adaptive enhancement of MBF following exercise conditioning requires Kv channel remodeling leading to enhanced Kvβ2 function (Fig. 1). To test this hypothesis, I have established two aims.

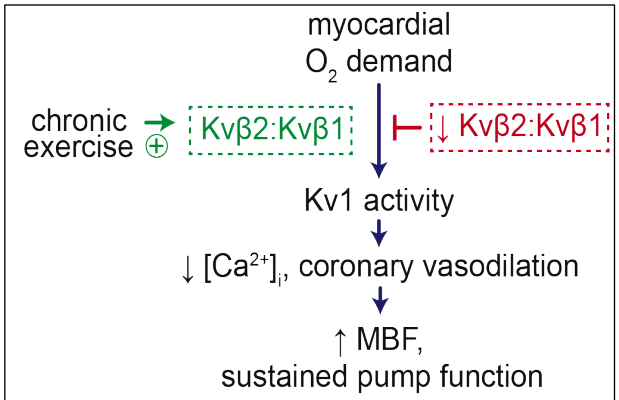


**Fig. 1: Proposed model of Kvβ regulation of MBF.**

**Aim 1: Determine how coronary Kvβ molecular composition influences the relationship between myocardial blood flow and $O_2$ demand.** Using a unique combination of genetically engineered mouse models, I will determine how modifying the heteromeric composition of the Kv1 auxiliary complex in coronary arterial myocytes impacts metabolic regulation of Kv currents ($I_{Kv}$), *ex vivo* coronary vasoreactivity, and *in vivo* MBF.

**Aim 2: Elucidate the contribution of Kvβ molecular remodeling to enhanced myocardial blood flow in the exercise-conditioned heart.** I will subject mice to an established treadmill running exercise regimen and determine how exercise alters the molecular composition of the Kvβ complex in coronary arterial myocytes. Using novel transgenic models that enable smooth muscle specific reconstitution of Kvβ proteins, I will determine the specific role for vascular Kvβ remodeling in exercise-induced adaptations in $I_{Kv}$, metabolic vasodilation, MBF, and cardiac performance.

# CHAPTER 2: MATERIALS AND METHODS[3]

*Animal genotypes, care, and use*: Male wild type (129SvEv, C57BL/6N, FVB) and Kvβ2$^{-/-}$, Kvβ$^{Y90F}$ (129SvEv background) and Kvβ1$^{-/-}$ (C57BL/6N background), sm22α-TRE and sm22α-TRE:KCNAB1 transgenic mice (FVB background), aged 12-20 weeks were used. For the transgenic mice sm22α-TRE and sm22α-TRE:KCNAB1, doxycycline was added to the animal's water at 2 mg/mL plus 5% sucrose and was provided *ad libitum*. This study was performed in compliance with the National Institutes of Health Guide for the Care and Use of Laboratory Animals and in strict accordance with protocols approved by the Animal Care and Use Committee of the University of Louisville.

*Exercise capacity test*: Age-matched wild type, Kvβ2$^{-/-}$, sm22α-TRE and sm22α-TRE:KCNAB1 transgenic mice were randomly assigned into sedentary and FTR exercise groups. All mice underwent a 2-day treadmill familiarization period (one familiarization session per day) before testing to assess baseline exercise capacity

[3] The majority of methods listed here have been previously published in the following manuscripts 37. Ohanyan V, Raph SM, Dwenger MM, Hu X, Pucci T, Mack G, Moore JBt, Chilian WM, Bhatnagar A, Nystoriak MA. Myocardial Blood Flow Control by Oxygen Sensing Vascular Kvbeta Proteins. *Circ Res*. 2021;128:738-751. doi: 10.1161/CIRCRESAHA.120.317715, 168. Dwenger MM, Raph SM, Reyzer ML, Lisa Manier M, Riggs DW, Wohl ZB, Ohanyan V, Mack G, Pucci T, Moore JBt, et al. Pyridine nucleotide redox potential in coronary smooth muscle couples myocardial blood flow to cardiac metabolism. *Nat Commun*. 2022;13:2051. doi: 10.1038/s41467-022-29745-z

on the third day. For familiarization sessions, mice were each placed in a lane of an Exer 3/6 motorized rodent treadmill (Columbus Instruments, Columbus, OH) that was set at a speed of 0 m/min for 10 min, at a 0$^{o}$ incline (with respect to the horizontal), and the shock grid set at an intensity of 0.3 - 0.7 mA (2 Hz). After the 10 min, treadmill speed was slowly increased from 0 to 10 m/min for 12 min. Prior to exercise capacity tests (ECT), the mice were weighed, and blood lactate levels were measured at rest with a hand-held Lactate Plus sensor (Nova Biomedical, Waltham, MA, U.S.A.) via a distal tail clip. Mice were then placed on the treadmill and allowed to familiarize with the environment for 3-5 minutes before the beginning of the ECT. The treadmill shock grid remained on throughout the duration of the ECT at the same intensity and frequency settings as described above for the familiarization procedure. ECTs consisted of an initial warmup period (9 min; 8.5 m/min; 0$^{o}$ incline), followed by speed increases at increments of 2.5 m/min every 3 min and incline increases at increments of 5$^{o}$ at minutes 9, 18, and 27 of the test (see Figure 1G). In this manner, the amount of work performed (vertical distance x body mass) over time incrementally increased as the test progressed. This type of high intensity, short duration ECT (e.g., Bruce protocol) is well established for assessment of exercise performance as a function of $VO_2$ max and anaerobic crossover points (assessed by initial and final blood lactate concentration from venous tail blood and respiratory quotient through indirect calorimetry).[178,179] The exhaustion criteria used to determine the fatigue point during the ECT and during the regular exercise sessions (discussed below) has been previously described[35] and was as follows: 1) Mouse is subjected to >10

seconds of consecutive shocks on electric grid, and/or 2) mouse spends >50% of the time spent receiving shocks, for any rolling time interval, and/or 3) mouse displays a lack of motivation to resume running upon manual prodding. After recording the fatigue point (distance, time and maximal speed achieved at fatigue) for each animal, the individual shock grid lane was turned off and the animals was immediately removed from the treadmill to measure post-fatigue blood lactate levels. Mice were then returned to their home cage with *ad libitum* access to food and water. All mice undergoing FTR training rested for 72 hours before beginning a 4-week training regimen.

*Echocardiography and microbubble perfusion*: Cardiac function was assessed by transthoracic echocardiography using either the Vevo 770 or Vevo 3100 (VisualSonics) as previously described.[180] Mice were anesthetized (isoflurane, 2.0% induction, 1.0-1.5% maintenance) and placed chest up on an examination board while body temperature was continuously monitored and maintained at 36.5-37.5ºC. Two dimensional images of the parasternal long axis were captured (100 fps) with a 707-B (30 MHz) scan head. The same anatomical position was used for M-mode imaging. Data collected for each animal were obtained from ≥5 independent cardiac cycles. The experimenter was blinded to experimental group for echocardiographic recordings and data analyses.

Microbubbles were made fresh weekly as needed. The lipid microbubbles contrast agent was comprised of distearoylphosphatidylcholine (2.mg/mL) and polyoxyetheylene-40-stearate (0.5 mg/mL) resuspended in calcium and

magnesium free phosphate buffered saline solution (PBS). The contrast agent was then sonicated for 10 minutes in a bath sonnicator at room temperature and briefly vortexed to ensure all components were dissolved. Approximately 800 µL of contrast agent stock solution was pipetted into 11 mm (or 13 mm) glass crimp-top vials. Secure gasket and metal lock lid were secured with hand-held crimping tool. In well ventilated chemical hood one 22-gauge needle was used as a vent. A second 22-gauge needle attached to a hose connected to perfluorobutane tank. The gas was slowly turned on to the point at which the surface of the contrast agent inflected, this was maintained for 30 seconds. After such time, both needles were removed, and the vial was carefully wrapped in parafilm and placed in the amalgamator for 45 seconds. At least one vial from each prepared batch of contrast agents was used to calculate the microbubbles attenuation.

Animals were anesthetized and the fur around the neck and chest were removed. ECG gel was applied to the he limbs of the animal which were then secured to the platform electrodes. An incision was made above the clavicle and fat and connective tissue around the carotid artery was removed. A catheter comprised of a 27 guage needle connected to PE tubing filled with heparinized saline at 10 units per mL, was secured in the carotid artery. The catheter connected to separate syringes containing either microbubbles and saline, or microbubbles and dobutamine. Microbubbles, saline, and dobutamine were delivered at a rate of 20 µL per minute. The individual concentration of dobutamine prepared was calculated based on the weight of each animal in order to administer 10 $\mu g \bullet kg^{-1} \bullet min^{-1}$.

*Pressure myography*: Resistance primary and secondary branches from the coronary and third and fourth order branches from mesenteric arterial trees were isolated in ice-cold buffer containing (mM): 134 NaCl, 6 KCl, 1 $MgCl_2$, 2 $CaCl_2$, 10 HEPES, 7 D-glucose, pH 7.4. Arteries were used within 8 hours of initial dissection and isolation, for assessment. Experiments were conducted as previously described in physiological saline solution, following equilibration.[37]

*Western Blot*: As previously described in Ohanyan, Raph et al., 2021 and Dwenger et al., 2022 tissue lysates from WT, Kvβ2$^{-/-}$, sm22α-rtTA:TRE β1, sm22α-rtTA, were collected from brain, and mesenteric arteries and were homogenized in lysis buffer containing (in mM): 150 NaCl, 50 Tris-HCl, and 1 EDTA with 0.25% deoxycholic acid, 1% NP-40, and Complete Mini protease inhibitor cocktail (Roche; per manufacturer's instructions), pH 7.4. Tissue homogenates were sonicated on ice and centrifuged (10,000 xg, 10 min, 4°C). Supernatants were transferred to another tube and boiled with Laemmli sample buffer (10 min) and run on a Stain-free Mini-PROTEAN 4-20% polyacrylamide gel (Bio-Rad). Total protein was assessed prior to transfer using a myECL imager (Thermo Fisher Scientific). Following transfer of proteins to polyvinylidene fluoride (PVDF), membranes were blocked for non-specific binding with 5% milk (wt/vol) in tris-buffered saline (TBS) and incubated (overnight, 4°C) in primary antibodies against Kvβ2 (Neuromab, 75-021, 1:400) or α-tubulin (Sigma Aldrich, T5168, 1:4000) in TBS containing 0.1% Tween-20 (TBSt). After washing with TBSt (5x, room temperature), membranes

were incubated with horseradish peroxidase (HRP)-conjugated secondary antibodies (anti-mouse IgG, Cell Signaling, 7076S, 1:3000). HRP was then detected with Pierce ECL Plus Western Blotting Substrate (Thermo Fisher Scientific) and a myECL imager (Thermo Fisher Scientific). Densitometry was performed for immunoreactive bands using FIJI software (NIH).[37,168]

*Aortic smooth muscle isolation for culture*: Preparation of solutions was described previously.[168] Enzyme digestion buffer consisted of 2.2 mg Collagenase type 2 and 1 µl of 20 mM calcium chloride solution, in 1 ml Tyrodes solution in sterile Eppendorf. Approximately 1 ml of enzyme digestion buffer is used per aorta isolated. Filter solution with 0.2 µm PES filter into clean sterile tube. Allow 5 ml Tyrodes solution to come to room temperature for use washing the aorta.

After anesthetizing the animal, made a horizontal incision in the lower abdominal/upper pubic region, cut horizontally from initial incision. Then cut up (toward the head) along the sides of the abdominal cavity. Carefully cut the ribs and remove the diaphragm to allow access into the thoracic cavity, making a flap that can be pinned to ease isolation. Remove all organs, except for the heart, from the thoracic and abdominal cavities. The aorta can be found running along the spine behind the esophagus. Remove the heart by grasping near the base and excising as close to the heart as possible. Carefully remove the connective tissue attaching the aorta to the spinal column, all the way to the abdominal cavity. Pin the aorta in a chilled dish containing DMEM/fungizone. Remove connective tissue and adventitia from aorta. Once the aorta is clean use a 1 ml syringe to inject

DMEM into the interior of the aorta to remove blood. Carefully, cut the aorta into 1 mm segments and transfer to sterile Eppendorf tube. Allow the segments to settle to the bottom. In a biosafety cabinet, wash the segments with filtered Tyrodes solution, then remove this solution and resuspend the segments in prepared enzyme digestion buffer. Loosen the cap of the tube and pace in cell culture incubator for four hours, gently agitating the tube every 30 to 60 minutes. At completion of this step the tissue should appear as a cloudy mass at the bottom of the tube. Spin down the Eppendorf tube at 300 g, 1500 rpm for 5 minutes. Resuspend the pellet in DMEM containing 10% FBS and 1% penicillin streptomycin. Resuspend the pellet in sufficient quantity for desired plating (i.e., 24-well, 6-well, or 35 mm Primeria dish). Cells are cultured for five to seven days to confluence and passaged into T-25 or utilized for experiments.

*Coronary artery vascular smooth muscle cell isolation*: Animals were anesthetized by intraperitoneal injection of sodium pentobarbital (150 mg/kg). An incision is then made inferior to the sternum and continued horizontally to the base of both left and right sides of the rib cage. Then separate the diaphragm from the rib cage being careful not to contact the heart. The rib cage is then cut as close to the thoracic lateral line to prevent cutting the ribs and potentially damaging the heart. Using curved forceps grasp the aorta above the base of the heart and cut superior to the forceps. Place the heart in ice cold calcium free magnesium phosphate buffered saline ($Ca^{+2}$ free MgPSS). Carefully transfer the heart to dissection dish containing ice cold $Ca^{+2}$ free MgPSS and pin the heart down so that the left atria is facing

away from the dish and is centered. It is recommended that the atria be pulled away from the heart and pinned in order to expose the face of the left ventricle (LV) and the aorta. The desired region of the coronary artery is the left anterior descending (LAD) artery. This will appear as a dark purple line within the wall of the LV starting at the aorta and directed toward the apex. Using sharpened D-tip forceps carefully grasp the heart tissue to the left of the LAD and using curved spring scissors with the curve facing away from the heart slowly cut away layers of the myocardium until the LAD is exposed. Be careful not to nick or cut the LAD as it will become extremely difficult to see if it loses all the blood. Continue using the curved spring scissors with the curve away from the heart down the length of the LAD until sufficient area is exposed. Carefully separate the LAD from the myocardium by using the scissors. Place the isolated artery in vial containing 1 mL $Ca^{+2}$ free MgPSS.

After allowing the LAD to settle to the bottom of the vial, remove as much of the $Ca^{+2}$ free MgPSS from the vial as possible without disturbing the tissue. Warm the vial and solutions 1 and 2 in 37oC water bath for 1 minute. Add solution 1 to the vial and gently agitate in 37$^{o}$C water bath for 5 minutes, then carefully remove solution 1 with minimal disturbance of the tissue. Add solution 2 to the vial and gently agitate in 37$^{o}$C water bath for 5 minutes. Carefully remove solution 2, add 1 mL $Ca^{+2}$ free MgPSS to the vial 3 times. Add 0.5-1 mL of $Ca^{+2}$ MgPSS depending on desired cell/volume ratio. Triturate the tissue to liberate vascular smooth muscle cells, first with large bore then medium and if desired small bore modified glass pipettes. Take a small sample of cell containing solution and check isolation quality

on light microscope. Isolated coronary vascular smooth muscle cells were isolated as described above and divided for use between proximity ligation assay and electrophysiological patch clamp.

*Proximity ligation assay*: We utilized the DuoLink proximity ligation assay kit (INFO). Slides were prepared with a designated location for the dispersement of the cells in solution. Using a hydrophobic Pap-pen, a small circle is made and allowed to dry for 5 minutes. Carefully outline the hydrophobic area with a permanent marker (Sharpie) and indirectly, gently rinse the prepared slides in distilled water. Isolated coronary vascular smooth muscle cells were dispensed onto the prepared glass slide and allowed to settle to the slide surface for 10 to 20 minutes. After this time the $Ca^{+2}$ MgPSS solution is carefully dabbed away using a Kimwipe by presenting the wipe at the edge of the hydrophobic circle. After removal of the $Ca^{+2}$ MgPSS solution, cover the same area with 4% paraformaldehyde (PFA) for 10 minutes. Wash the slides two times with fresh PBS. After the second wash slides can be stored in PBS for no more than two weeks. If continuing, cells are permeabilized by immersing the slides in 0.1% Triton X-100 in PBS for 10 minutes. Next, we followed the manufacturers recommendations for preparing our samples, briefly described here. Approximately 40 µl of Duolink blocking solution is added to each sample, enough to cover the designated area. Slides are then incubated in a heated humidity chamber for 60 minutes at 37$^{o}$C. During this step we prepared the primary antibody in the Duolink antibody diluent. We prepared slides and antibodies for the following target combinations: Kv1.5

(Ab), Kv1.5:Kvβ1 (Ab:Ab), Kv1.5:Kvβ2 (Ab:Ab). At the completion of blocking, the solution was gently tapped off from the slides and the primary antibody solutions were added. Slides are then incubated overnight at 4$^{o}$C. After this step, Duolink PLA probes “Plus” and “Minus” are prepared at a 1:5 ratio in Duolink antibody diluent. Primary antibody solution was gently removed from the slides which were then washed two times for 5 minutes each in 1x Wash Buffer A, at room temperature. After washing buffer was carefully removed, the PLA probe solution was added and incubated in a pre-heated humidity chamber for 1 hour at 37$^{o}$C. During this incubation period ligation solution was prepared by diluting 5x Duolink ligation buffer at 1:5 ratio in high purity water and mixing. PLA probe solution was gently removed from the slides which were then washed two times for 5 minutes in 1x Wash Buffer A at room temp. Retrieve the ligase solution and keep on freezer block, then add to ligation buffer at 1:40 dilution and mix. Tap off excess wash buffer and apply ligation solution. Incubate slides in pre-heated humidity chamber for 30 minutes at 37$^{o}$C. Next, prepare amplification buffer by diluting 5x amplification buffer 1:5 in high purity water. Gently tap off ligation solution from slides and wash two times for 5 minutes each in 1x Wash Buffer A at room temperature. Retrieve the polymerase from the freezer and keep on a freezer block. Add polymerase to 1x Amplification buffer at a 1:80 dilution and mix. Remove excess wash buffer and apply amplification buffer, incubate slides in pre-heated humidity chamber for 100 minutes at 37$^{o}$C. Finally, tap off amplification buffer and wash slides two times for 10 minutes in 1x Wash buffer B at room temperature followed by 0.01x Wash buffer B for 1 minute. Remove excess wash

buffer and mount coverslip using minimal volume of Duolink In Situ mounting medium with DAPI. The edges of the cover slips were sealed using clear nail polish. Slides were then protected from light and stored in a slide box at 4$^{o}$C for short storage or -20$^{o}$C for long term storage.

*Electrophysiological whole cell and single channel patch clamp techniques*: As previously described utilizing the inside-out configuration $K^+$ currents were recorded using the gap-free mode of an Axopatch 200B amplifier (Axon Instruments). Borosilicate glass pipettes are pulled using a P-87 micropipette puller (Sutter Instruments) to a resistance of 7-12 MΩ. Pipettes are filled with a pipette solution containing (in mM): 140 KCl, 1 HEDTA, 10 HEPES, 0.0001 iberiotoxin. Cells were allowed to adhere to a glass coverslip for at least 10 minutes in a 0.25 ml recording chamber (Warner Instruments) and bathed in a solution containing (in mM): 140 KCl, 1 HEDTA, 10 HEPES, 0.001 gliblenclamide.[168] Stochastic channel activity of excised patches held at constant potential were recorded in gap-free mode with a sampling frequency of 10 kHz. Data were analyzed using Clampfit (software version 10.6; Axon Instruments).

As described above, isolated arterial myocytes were allowed to adhere to the cover slip of the recording chamber. Using conventional whole-cell patch clamp configuration during voltage clamp mode of the Axopatch 200B amplified (Axon Instruments). Pipettes made of borosilicate glass were pulled using the P-87 micropipette puller (Sutter instruments). Acceptable pipette resistance of 5-7 MΩ and filled with pipette solution comprised of (in mM): 87 K,$^{+}$-aspartate 20 KCl, 1

$MgCl_2$,5 Mg-ATP, 10 EGTA, 10 HEPES and pH 7.2. After cells were allowed to adhere to the cover slip solution containing the following was added to the chamber (in mM): 134 NaCl, 5 KCl, 1 $MgCl_2$, 0.1 $CaCl_2$, 10 Glucose, 10 HEPES. Electronically compensated for series resistance ≥80%. Currents of ouward K+ were recorded during 500 msec stepwise depolarizations in increments of 10 mV from -70 to +50 mV from an initial holding potential of -70 mV. Voltage-dependence of activation was determined from tail currents elicited by repolarization to -40 mV. Voltage-dependence of inactivation was determined from standard two-pulse voltage protocol with cells underwent stepwise depolarizations from -100 to +50 mV for 8 seconds followed by a 200 ms pulse of 50 mV. Additionally, voltage-dependent outward $K^+$ currents were measured in the absence (-) and presence (+) of 10 mM lactate and psora-4 (500 nM) (-,+).

*Metabolic phenotyping:* WT and Kvβ2$^{-/-}$ mice were single-housed in cages (250 mm x 150 mm x 240 mm dimensions; 9 L) with *ad libitum* access to food and water, and metabolic and behavioral information was continuously recorded using a TSE PhenoMaster / LabMaster high-throughput phenotyping platform (TSE Systems, Bad Homburg, Germany). Indirect gas calorimetry was performed using an air flow rate of 0.35 L/min and sampling rate of 10 min with reference-air cage readings performed during each interval to account for changes in room air conditions. Recordings from each mouse were performed over a 24 hr period to monitor oxygen consumption ($VO_2$), carbon dioxide production ($VCO_2$) (both normalized to body weight), respiratory exchange ratio ($VCO_2$:$VO_2$), food and water

consumption, and movement. Energy expenditure (calories/min·kg) was calculated using the Weir equation (*heat, H = $CVO_2$ ($VO_2$) + $CVCO_2$($VCO_2$)/1000*), with coefficients for $CVO_2$ and $CVCO_2$ = 3.941 and 1.106, respectively.

*Forced treadmill running (FTR):* Age-matched wild type and Kvβ2$^{-/-}$ mice were randomly assigned into sedentary and FTR exercise groups. All mice assigned to FTR groups underwent a 2-day treadmill familiarization period (one familiarization session per day) before testing to assess baseline exercise capacity on the third, following day. For familiarization sessions, the mice were each placed in a lane of a Exer 3/6 motorized rodent treadmill (Columbus Instruments, Columbus, OH) that was set at a speed of 0 m/min for 10 min, at a 0$^o$ incline (with respect to the horizontal), and the shock grid set at an intensity of 0.3 - 0.7 mA (2 Hz). After the 10 min, treadmill speed was slowly increased from 0 to 10 m/min for 12 min.

Prior to exercise capacity tests (ECT), the mice were weighed, and blood lactate levels were measured at rest with a hand-held Lactate Plus sensor (Nova Biomedical, Waltham, MA, U.S.A.) via a distal tail clip. Mice were then placed on the treadmill and allowed to familiarize with the environment for a 3-5 minutes before the beginning of the ECT. The treadmill shock grid remained on throughout the duration of the ECT at the same intensity and frequency settings as described above for the familiarization procedure. ECTs consisted of an initial warmup period (9 min; 8.5 m/min; 0$^o$ incline), followed by speed increases at increments of 2.5 m/min every 3 min and incline increases at increments of 5$^o$ at minutes 9, 18, and 27 of the test (see Figure 1G). In this manner, the amount of work performed

(vertical distance x body mass) over time incrementally increased as the test progressed. This type of high intensity, short duration ECT (e.g., Bruce protocol) is well established for assessment of exercise performance as a function of $VO_2$ max and anaerobic crossover points (assessed by initial and final blood lactate concentration from venous tail blood and respiratory quotient through indirect calorimetry).[178,179] The exhaustion criteria used to determine the fatigue point during the ECT and during the regular exercise sessions (discussed below) has been previously described[35] and was as follows: 1) Mouse is subjected to >10 seconds of consecutive shocks on electric grid, and/or 2) mouse spends >50% of the time spent receiving shocks, for any rolling time interval, and/or 3) mouse displays a lack of motivation to resume running upon manual prodding. After recording the fatigue point (distance, time and maximal speed achieved at fatigue) for each animal, the individual shock grid lane was turned off and the animals was immediately removed from the treadmill to measure post-fatigue blood lactate levels. Mice were then returned to their home cage with *ad libitum* access to food and water. All mice undergoing FTR training rested for 72 hours before beginning a 4-week training regimen.

Regular forced treadmill running sessions were administered 5 days a week (Monday through Friday), for 4 weeks. Each session consisted of a 12 min warmup period (5 m/min, $10^o$ incline), immediately followed by either 40 (week 1), 50 (week 2) or 60 (weeks 3 and 4) min of running. Treadmill speed was assigned at ~50% of the average maximal speed attained during the initial ECT before fatigue (12.1 m/min at $10^o$ incline for both WT and $K\nu\beta2^{-/-}$ exercise groups). Animals meeting

criteria for fatigue as described above were removed from the treadmill for that day and returned to the training program on the next day. A cooldown period (5 m/min at 10$^{o}$ incline, 5 min) was allowed before returning mice to their home cage with *ad libitum* access to food and water. Following 4 weeks of exercise, mice underwent the same ECT protocol (described above) to assess changes in exercise capacity.

*Body mass composition analysis:* Following the completion of the four-week exercise training period, adipose content and lean mass were determined using a small animal Lunar PIXIMus X-ray densitomer (Dexascan). Mice were anesthetized with 2% isoflurane and subjected to Dexascan measurements of lean and fat mass percentages.

*Histology and immunohistochemistry:* Hearts were excised and flushed with 1M KCl in phosphate buffered saline via cannulation of the aorta. Transverse mid-ventricular sections with the right and left ventricles visible were fixed with 10% neutral buffered formalin for 24 hr. Following fixation, heart sections were embedded in paraffin, and sections (4 μm) were cut using a microtome. Following standard xylene/ethanol deparrafinization, antigen retrieval was performed with 0.1 M sodium citrate (pH 6.8) (Sigma), and slides were treated with Sudan Black to minimize autofluorescence. Sections were then stained with Alexa Fluor 555-conjugated wheat germ agglutinin (WGA) (Life Technologies) and Fluorescein-

conjugated anti-isolectin B4 (Vector Biolabs) and mounted using SlowFade Gold Anitfade mountant with dapi (Life Technologies).

All image acquisition and analyses were performed in a blinded manner. Images were acquired from the left ventricular free wall (anterior and posterior) for Alexa Fluor 555 (WGA) and Fluorescein (Isolectin B4) using a Nikon Eclipse-Ti epifluorescence microscopy system with a 20x objective lens. Myocytes in a cross sectional view within the subendocardial region were chosen for analysis using the following criteria: 1) oblong-to-circular cell outline, with centric and round nuclei with capillaries (Isolectin B4 positive staining) surrounding the cardiomyocyte in cross-sectional (rather than oblique) view. For analysis of cross sectional area, ≥100 cardiomyocytes were counted per animal.

*Quantitative real-time polymerase chain reaction:* Total RNA was isolated from hearts using a RNeasy Fibrous Tissue Isolation kit (Qiagen), and RNA purity was assured by treatments with proteinase K (Qiagen) and DNase (Qiagen). The quantity and quality of isolated RNA were determined using a NanoDrop 2000C spectrophotometer (Thermo Scientific). RNA was reverse-transcribed for the first strand cDNA synthesis with an RNA-directed DNA polymerase, the Avian Myeloblastosis Vi-rus (AMV) Reverse Transcriptase (Promega), and Oligo dT primers (IDT). Assays were performed in triplicate for each gene and condition, and real-time PCR amplification was performed using iTag Universal SYBR Green Supermix reagents (Bio Rad) on a 7900TH Fast Real-Time PCR System (Applied Biosystems). The threshold cycle (Ct) was obtained, and the relative transcript

level was calculated using the 2-ΔΔCt method. The relative expression levels of target genes were normalized to that of the endogenous reference gene hypoxanthine phosphoribosyltransferase 1 (HPRT1) in each sample, and differences in mRNA expression in exercise groups were expressed as fold relative to respective sedentary controls. The sequences of primers used are: C/EBPβ3, Forward: 5'-ACGACTTCCTCTCCGACCTCT-3', Reverse: 5'-AGGCTCACGTAACCGTAGTCG-3'; Cited4, Forward: 5'-CATGGACACCGAGCTCATC-3', Reverse: 5'-CTGACCCCAGGTCTGAGAAG-3'; NFAT, Forward: 5'-ACGGGAGTGACCCTCAAA-3', Reverse: 5'-CTGACCCCAGGTCTGAGAAG-3'; HPRT1, Forward: 5'-AGGACCACTCGAAGTGTTGG-3', Reverse: 5'-AGGGCATATCCAACAACAAAC-3'.

*Statistical analysis:* Data are expressed as mean ± SEM. Student's t-test was used to compare two groups. One-way and Two-way ANOVA followed by Tukey multiple comparisons test were used for comparison between >2 groups as is appropriate for the data sets being compared. A p-value of $<0.05$ was deemed significant.

# CHAPTER 3: MYOCARDIAL BLOOD FLOW CONTROL BY OXYGEN SENSING VASCULAR $K_V\beta$ PROTEINS[4,2]

## Introduction

An imbalance between myocardial oxygen supply and demand is a salient feature of heart disease, which remains the leading cause of death worldwide.[1] Impaired cardiac function associated with inadequate myocardial perfusion is commonly observed in patients with heart failure, hypertension, diabetes, and coronary artery disease.[2-5] Even in the absence of stenoses in large diameter conduit arteries, suppressed vasodilator capacity of small diameter coronary arteries and arterioles can lead to ischemia.[6,7] Despite the vital importance of oxygen delivery to the preservation of cardiac structure and function, the fundamental mechanisms by which the coronary vasculature responds to fluctuations in myocardial metabolic demand remain poorly understood.

[4] This is a final version of a peer reviewed article published as reference 37. Ohanyan V, Raph SM, Dwenger MM, Hu X, Pucci T, Mack G, Moore JBt, Chilian WM, Bhatnagar A, Nystoriak MA. Myocardial Blood Flow Control by Oxygen Sensing Vascular Kvbeta Proteins. *Circ Res*. 2021;128:738-751. doi: 10.1161/CIRCRESAHA.120.317715.

[2]This work was also used in part in my Masters thesis Raph, Sean M, "Role of KVβ2 subunits in regulation of resistance arterial tone." (2021). *Electronic Theses and Dissertations.* Paper 3589.

In the healthy heart, the coronary arteries and arterioles remain partially constricted, and they dilate or constrict further according to myocardial requirements for oxygen and nutrient delivery.[8,9] As myocardial oxygen consumption increases (e.g., due to an increase in heart rate, myocardial

contractility, or afterload), there is a corresponding demand for an increase in oxygen supply to sustain oxidative energy production. However, with little reserve for increased oxygen extraction, sustained cardiac function relies on the intimate link between local and regional metabolic activity and vasodilation of the coronary vascular bed to deliver adequate blood flow to the myocardium (i.e., metabolic hyperemia).[10] In searching for molecular entities that couple vascular function to myocardial oxygen demand, recent studies from our group[11, 12] and others[13] have found that increased cardiac work promotes coronary vasodilation and hyperemia via the activation of Kv1 channels in smooth muscle cells. Nonetheless, how vascular Kv1 channels sense changes in oxygen demand to regulate blood flow to the heart is unclear.

In this study, we tested the hypothesis that regulation of myocardial blood flow (MBF) by Kv1 channels depends upon their auxiliary Kvβ subunits. The Kvβ proteins are functional aldo-keto reductases that bind NAD(P)(H) and differentially regulate channel gating in response to changes in cellular redox status.[14, 15] Hence, these proteins represent a plausible molecular link between metabolic activity, oxygen availability, and Kv activity that could regulate

vasoreactivity.[16] The mammalian genome encodes three Kvβ proteins, which have been shown to control the voltage sensitivity, surface localization, and subcellular distribution of Kv1 channels in excitable cells of the cardiovascular and nervous systems.[17] Consistent with this, in our previous work, we reported that Kvβ proteins support the functional expression of Kv channels in cardiomyocytes and contribute to the metabolic regulation of cardiac repolarization.[18] The Kvβ proteins are expressed throughout the coronary vasculature of humans[19] and rodents,[20] and we have recently reported that native Kv1 channels of coronary arterial myocytes are heteromeric assemblies of Kvβ1.1 and Kvβ2 proteins.[20] Using a combination of genetically engineered mice with *ex vivo* and *in vivo* approaches, we now report that Kvβ1.1 and Kvβ2 have contrasting roles in regulating MBF and cardiac function under stress, and that they impart oxygen sensitivity to vascular tone.

## Results

*Kvβ2 is required for sustained cardiac pump function during stress.*

**Figure 1-1** shows exemplary effects of norepinephrine infusion on arterial blood pressure in WT and Kvβ2$^{-/-}$ mice. Norepinephrine infusion increased steady state blood pressure in both groups. Consistent with our previous report,[12] norepinephrine led to an increase in arterial blood pressure in WT animals that was sustained for the duration of drug administration. However, in Kvβ2$^{-/-}$ mice, norepinephrine-induced elevation of pressure was not sustained, but declined after ~40 s of infusion. This inability to maintain elevated blood pressure during stress is reminiscent of effects in Kv1.5-null mice.[12] Therefore, as is the case with Kv1.5, Kvβ2 appears to play an essential role in supporting cardiac contractile performance under conditions of catecholamine stress and enhanced cardiac workload.

*Relationship between myocardial blood flow and cardiac workload is disrupted in Kvβ2-null mice.*

The inability of Kvβ2$^{-/-}$ mice to sustain cardiac performance may reflect insufficient oxygen delivery during stress. Thus, we postulated that Kvβ proteins may be integral to the relationship between myocardial blood flow (MBF) and cardiac workload. To test this, we used myocardial contrast echocardiography (MCE)[11, 12] to compare MBF in WT and Kvβ-null mice. MCE uses high-power ultrasound to destruct lipid-shelled echogenic microbubbles in circulation.

Subsequent replenishment of signal intensity in a region of interest following disruption is used to calculate the tissue perfusion (**Fig. 1-2 A**). Because MBF responds to changes in ventricular workload and myocardial metabolic activity, we used MCE to evaluate MBF as a function of cardiac workload (i.e., double product of mean arterial blood pressure x heart rate),[12] monitored at baseline and during intermittent intravenous infusions of norepinephrine (0.5–5 μg/kg·min$^{-1}$). **Figure 1-2 B** shows representative contrast signal intensities plotted over a period of ~10 s after microbubble destruction and fit with a one-phase exponential function (see *inset*) in WT (129SvEv), Kvβ1.1$^{-/-}$, and Kvβ2$^{-/-}$ mice (5 μg/kg·min$^{-1}$ norepinephrine). The relationship between MBF and double product shows a modest elevation of MBF, albeit across a lower workload range in Kvβ1.1$^{-/-}$ mice compared with WT mice (**Fig. 1-2 C**). However, consistent with impaired cardiac function under stress conditions described above (see **Fig. 1-1**), levels of MBF recorded in Kvβ2$^{-/-}$ mice were markedly reduced. Specifically, linear regression analysis showed a significant reduction in the slope of the MBF-work relationship in Kvβ2$^{-/-}$ mice (**Fig. 1-2 D**). Note that cardiac workload in Kvβ1.1$^{-/-}$ mice was reduced due to lower MAP relative to corresponding wild type mice in the presence of 1-5 μg/kg·min$^{-1}$ norepinephrine (see **Fig. 1-2 C**). However, MAP, HR, and double product were not significantly different between WT and Kvβ2$^{-/-}$ mice over the tested range of norepinephrine. Taken together, these data reflect differential roles for Kvβ1.1 and Kvβ2 proteins in regulating MBF, whereby loss of Kvβ2 suppresses MBF and impairs cardiac function as the heart is subjected to increased workloads.

*Oxygen sensitivity of coronary arterial diameter is modified by Kvβ2.*

Impaired Kv1-mediated coronary vasodilation results in a markedly reduced myocardial oxygen tension during increased metabolic demand.[22] We therefore posited that coronary vasodilation in response to metabolic stress may be impaired by loss of Kvβ2. Arteries of the systemic circulation exhibit robust dilation in response to metabolic stressors such as hypoxia and intracellular acidosis via a number of purported mechanisms, including activation of Kv channels.[23, 24] Hence, we examined the *ex vivo* vasoreactivity of coronary arteries isolated from WT and Kvβ2$^{-/-}$ mice in response to an acute reduction in oxygen. When subjected to physiological intravascular pressures, isolated coronary arteries developed myogenic tone (i.e., 8 ± 2% and 11 ± 2% at 60 and 80 mmHg, respectively). To evaluate vasodilatory capacity, arteries were pressurized (60 mmHg), pre-constricted with 100 nM U46619, and subjected to hypoxic bath conditions (physiological saline solution aerated with 95% $N_2$/5% $CO_2$ and containing 1 mM hydrosulfite).[25-27] Direct measurement of bath $O_2$ levels confirmed a significant reduction in $O_2$ from control levels during application of hypoxic conditions (**Fig. 1-3 A**). As shown in **Figure 1-3 B (*top*)** coronary arteries isolated from WT mice responded to hypoxic perfusate with robust and reversible dilation. Vasodilation was not observed when 1 mM hydrosulfite was applied in the presence of 20% $O_2$. Consistent with the involvement of Kv1 channels, the selective Kv1 inhibitor psora-4 (500 nM) significantly attenuated (~58%) hypoxia-induced vasodilation. Likewise, hypoxia-induced dilation was

significantly reduced in arteries from Kvβ2$^{-/-}$ mice (19.6 ± 6.4%) compared with arteries from WT mice (56.9 ± 6.2%) (**Fig. 1-3 B–D**). Together, these data suggest that Kvβ2 proteins facilitate vasodilation to reduced $PO_2$ and support the notion that Kvβ proteins link tissue perfusion to local oxygen consumption.

*L-lactate augments $I_{Kv}$ in coronary arterial myocytes and induces coronary vasodilation via Kvβ2.*

We tested whether Kv1 activity in coronary arterial myocytes is sensitive to acute changes in oxygen due to alterations in cellular redox potential via elevation of L-lactate. Our reasoning for examining the effects of L-lactate was two-fold: first, myocardial underperfusion leads to a rapid decline in tissue $PO_2$, increased anaerobic metabolism, and net accumulation of L-lactate that can promote feedback coronary vasodilation to increase MBF.[21, 28-31] Second, it is plausible that Kv1 channels, via association with Kvβ proteins, may be acutely responsive to changes in lactate secondary to modification of cellular NADH:NAD$^+$ ratio after uptake and interconversion to pyruvate via the lactate dehydrogenase reaction.[15, 17, 32-35] Consistent with this expectation, using the perforated whole cell configuration of the patch clamp technique, we observed a significant increase in outward $K^+$ current density (pA/pF) in isolated coronary arterial myocytes immediately following (1-3 min) application of 10 mM L-lactate in the bath (**Fig. 1-4A, C**). However, this effect was abolished when L-lactate was applied in the presence of the Kv1 blocker psora-4 (500 nM, **Fig. 1-4B, D**). The change in $I_K$ induced by application of 10 mM L-lactate in coronary arterial

myocytes in the absence and presence of psora-4 is shown in Figure 4E. These data indicate that L- lactate acutely potentiates $I_{KV}$ in coronary arterial myocytes.

We next examined the vasodilatory response of preconstricted coronary arteries to increasing concentrations of extracellular L-lactate. As shown in **Fig. 1-4 F** and consistent with previous studies,[36, 37] isolated coronary arteries that were pre-constricted with 100 nM U46619 exhibited step-wise vasodilation in response to elevation of external L-lactate (5-20 mM). This effect was abolished when L-lactate was applied in the presence of 500 nM psora-4 (**Fig. 1-4 G, I**), consistent with involvement of $I_{KV}$ described above. Furthermore, L-lactate-induced vasodilation was also abolished in arteries isolated from Kvβ2$^{-/-}$ mice, indicating a key role for this subunit in L-lactate-induced vasodilation (**Fig. 1-4 H, I**). These data are consistent with the notion that the regulation of Kvβ2 via vascular intermediary metabolism controls coronary vasodilatory function upon acute changes in myocardial oxygen tension.

*Functional role for Kvβ2 in L-lactate-induced vasodilation of resistance mesenteric arteries.*

We next asked whether the role for Kvβ in redox-dependent vasoreactivity is confined to the coronary vasculature or is generally observed in peripheral resistance arterial beds where Kv1 prominently controls vascular tone. For this, we first compared Kvβ protein-protein interactions in arterial myocytes of coronary versus mesenteric (3$^{rd}$ and 4$^{th}$ order) arteries using *in situ* proximity ligation (PLA), as previously described.[18, 20, 38] The PLA method is

based on dual labelling of proteins that are located within close proximity (<40 nm), and thus, is an approach used to identify protein-protein interactions in complexes with molecular resolution. We observed robust PLA-associated fluorescent signals in coronary arterial myocytes that were co-labelled with Kv1.5 and Kv1.2, Kv1.5 and Kvβ1, Kv1.5 and Kvβ2, or Kvβ1 and Kvβ2 (**Fig. 1-5 A**), consistent with heteromeric oligomerization of Shaker channels.[20, 39] The number of fluorescent sites assigned to these - α/α, α/β, and β/β interactions were similar between coronary and mesenteric arterial myocytes (**Fig. 1-5 A, B**). PLA-associated fluorescence in cells labeled for Kv1.5 alone was negligible for arterial myocytes of both beds. These data suggest that Kv α/β subunit expression patterns and interactions are similar in arterial myocytes of these two distinct vascular beds.

Next, we tested whether knockout of Kvβ1.1 or Kvβ2 alters the regulation of mesenteric arterial diameter. Note that ablation of either of these Kvβ proteins had no statistically significant effect on the active (i.e., myogenic tone) or passive responses to increases in intravascular pressure, nor did it impact vasoconstriction responses to direct membrane potential depolarization with 60 mM $K^+$ or the stable thromboxane $A_2$ receptor agonist U46619 (100 nM). Similar to observations in isolated coronary arteries (see **Fig. 1-4 F**), application of L-lactate (5-20 mM) resulted in robust and reversible dilation of isolated mesenteric arteries (**Fig. 1-5 C)**. L-lactate-mediated vasodilation was insensitive to endothelial denudation but was abolished when arteries were constricted with elevated external $K^+$, rather than U46619. Consistent with observations in

isolated coronary arteries, vasodilation in response to L-lactate was eliminated by the Kv1-selective inhibitor psora-4 and loss of Kvβ2 (**Fig. 1-5 C–E**). The dilatory response to L-lactate was not significantly different between arteries from Kvβ1.1$^{-/-}$ mice when compared with arteries from corresponding WT animals. Moreover, in contrast to the disparate effects of L-lactate, vasodilation induced by adenosine (1 - 100 μM) was not significantly different between Kvβ1.1$^{-/-}$ or Kvβ2$^{-/-}$ arteries, when compared with corresponding WT arterial preparations. Together with results shown in **Fig. 1-2–1-4**, these data identify Kvβ2 as a functional regulatory constituent of Kv1 channels that imparts stimulus-dependent redox control of vascular tone.

*Increasing the Kvβ1.1: Kvβ2 ratio suppresses redox-dependent vasodilation and MBF.*

Native Kv1 channels are comprised of pore-forming subunits associated with more than one Kvβ subtype. This combinatorial variability may contribute to the diversity and cell-specific adaptability of channel function to a wide range of physiological and pathological stimuli. In coronary arterial myocytes, both Kvβ1.1 and Kvβ2 proteins are present in native Kv1 auxiliary subunit complexes;[20] however, our data suggest that these proteins may have divergent roles in the regulation of arterial diameter and myocardial perfusion. That is, in contrast to our observations made in Kvβ2$^{-/-}$ mice, deletion of Kvβ1.1 did not impede MBF. Structural comparison of the two subunits shows a clear difference in the N-termini of Kvβ1 and Kvβ2 subunits. The N-termini of Kvβ1 proteins form

a ball-and-chain-like inactivation domain, a feature that is lacking in Kvβ2.[17] Thus, we hypothesized that the association of Kvβ1.1 with Kv1 channels may serve to counter the regulatory function imparted by Kvβ2. A testable prediction based on this hypothesis is that increasing the ratio of Kvβ1.1:Kvβ2 subunits in arterial myocytes would recapitulate the effects of Kvβ2 deletion. To examine this possibility, we generated transgenic mice with conditional doxycycline-inducible overexpression of Kvβ1.1 in smooth muscle cells (**Fig. 1-6 A**). Briefly, this model consists of transgenic mice with a reverse tetracycline trans-activator driven by the SM22α promoter (SM22α-rtTA)[40] crossed to transgenic mice with Kcnab1 downstream of the tetracycline responsive element (TRE-Kvβ1) to yield double transgenic (SM22α-rtTA:TRE-Kvβ1) and single transgenic littermate control (SM22α-rtTA) mice. Western blot revealed elevated Kvβ1 protein abundance in arteries of SM22α- rtTA:TRE-Kvβ1 mice after doxycycline treatment, compared with arteries from doxycycline-treated SM22α-rtTA mice (**Fig. 1-6 B, C)**. Consistent with a lack of doxycycline effects on Kvβ1 protein in peripheral tissues, no statistically significant differences were observed in Kvβ1-associated band intensities in brain lysates of SM22α-rtTA:TRE-Kvβ1 versus SM22α-rtTA mice.

We next measured the relative levels of Kv1α:Kvβ protein interactions in coronary arterial myocytes via PLA. We observed PLA-associated fluorescent punctae in coronary arterial myocytes from SM22α-rtTA that were either co-labelled with Kv1.5 and Kvβ1, or with Kv1.5 and Kvβ2. Consistent with results of Western blot experiments described above, we observed a significant increase

in Kv1.5:Kvβ1- associated PLA signal in coronary arterial myocytes from SM22α-rtTA:TRE-Kvβ1 when compared with myocytes from SM22α-rtTA mice (**Fig. 1-6 D, E**). Notably, Kv1.5-Kvβ2-associated PLA signal was reduced in myocytes from SM22α-rtTA:TRE-Kvβ1 when compared with myocytes from SM22α-rtTA mice, suggesting that double transgenic mice express vascular Kv1 complexes with increased ratios of Kvβ1.1:Kvβ2 subunits. Functionally, enhanced Kvβ1.1:Kvβ2 subunit composition in arterial myocytes from SM22α-rtTA:TRE-Kvβ1 was associated with significantly blunted vasodilation of isolated mesenteric arteries in response to extracellular L-lactate when compared with arteries from single transgenic control mice (**Fig. 1-6 F, G**). Indeed, these observations in SM22α-rtTA:TRE-Kvβ1 arteries were similar to those made in coronary and mesenteric arteries from $Kv\beta2^{-/-}$ mice, as well as arteries from WT mice pre-treated with the Kv1-selective inhibitor psora-4 (see **Fig. 1-4 F–I and 1-5 C–E**). *In vivo* evaluation of the relationship between MBF and cardiac workload revealed significantly suppressed MBF in SM22α- rtTA:TRE-Kvβ1 mice when compared with SM22α-rtTA mice (**Fig. 1-6 H**). No differences in heart rate or MAP were observed between groups of mice. Together, these results indicate that Kvβ1.1 in arterial myocytes functions as an inhibitory regulator of vasodilation, and that the control of MBF is balanced on the juxtaposing functional influences of Kvβ1.1 and Kvβ2 proteins.

## Discussion

In this study we identify vascular Kvβ proteins as key regulators of myocardial blood flow. Our findings suggest that the auxiliary Kvβ subunits impart oxygen sensitivity to Kv1 channel function, enabling them to trigger vasodilation in response to an increase in oxygen demand. A functional role of Kvβ proteins in imparting oxygen-sensitivity to Kv1 channels and thereby regulating vasodilation is supported by the following key findings: 1) $Kv\beta2^{-/-}$ mice exhibit acute cardiac failure during administration of norepinephrine; 2) MBF is significantly suppressed across the physiological range of cardiac workload in $Kv\beta2^{-/-}$ mice, yet is moderately enhanced in $Kv\beta1.1^{-/-}$ mice; 3) vasodilation of isolated coronary arteries in response to hypoxia and elevation of extracellular L-lactate is strongly attenuated by loss of Kvβ2; 4) whereas ablation of Kvβ proteins does not impact vasoconstriction of resistance caliber mesenteric arteries, vasodilation of these vessels in response to L-lactate is abolished by ablation of Kvβ2, comparable to effects of Kvβ2 deletion in coronary arteries; and 5) increasing the Kvβ1.1:Kvβ2 ratio in smooth muscle impairs L-lactate-induced vasodilation and suppresses MBF, similar to observations made in $Kv\beta2^{-/-}$ arteries and mice. Collectively these results support the concept that Kvβ1.1 and Kvβ2 cooperatively control vascular function and regulate MBF upon changes in metabolic demand.

Kv1 channels belong to one of several Kv subfamilies that regulate membrane potential and $[Ca^{2+}]_i$ in arterial myocytes to control vessel diameter and blood flow.[41] Pharmacological blockade of Kv1 channels reduces whole-cell

outward $I_K$ by ≥50%,[42] whereas increased steady-state $I_{Kv}$ results in membrane hyperpolarization and reduced $Ca^{2+}$ influx via voltage-gated $Ca^{2+}$ channels.[43] The resultant reduction in cytosolic $[Ca^{2+}]_i$ leading to myocyte relaxation, and vasodilation increases local tissue perfusion. Considering the relatively high resting input resistance (1-10 GΩ) of arterial smooth muscle cells, the opening or closure of few $K^+$ channels can generate substantial changes in membrane potential and vascular tone.[44, 45] Consequently, the functional expression of native Kv channels of arterial myocytes is dynamically controlled by multiple molecular processes, which include post-transcriptional regulation (e.g., phosphorylation, glycosylation), subcellular trafficking and recycling, redox modifications, as well as association with accessory subunits and regulatory proteins.[21, 31, 46-48] Adding to this complexity, our observation that deletion of Kvβ2 disrupts Kv1-dependent vasodilation is consistent with a functional role of this subunit in regulating the vasodilatory response to metabolic stress.

Kv channels in excitable cells assemble as either homomeric or heteromeric structures with varied $\alpha_4\beta_4$ configurations of pore-forming and auxiliary subunits.[49-52] This 'mix-and-match' capability of Kv channels contributes to the wide heterogeneity of $K^+$ currents that enables diverse physiological roles across different cell types. In our previous work we found that Kv1 channels in murine coronary arterial myocytes interact with Kvβ1.1/Kvβ2 heteromers,[20] and our present findings suggest a divergent functional regulation of vascular tone and blood flow by these proteins. These divergent roles are revealed by the

observation that even though Kvβ2 ablation suppressed vasodilatory function and MBF, the loss of Kvβ1.1 had little impact on arterial diameter *ex vivo*, but elevated MBF *in vivo*. These findings suggest that Kvβ1 and β2 have somewhat divergent and potentially antagonist roles, which may relate to differences in their structures. The Kvβ1 has a ball-and-chain inactivation domain at the N-terminus, a feature that is lacking in Kvβ2. Potentially as a result of these differences, individual subunits have differential effects on the gating of non- and slowly-inactivating Kv1α channels.[53] Specifically, Kvβ1 induces N-type inactivation in non-inactivating Kv1α proteins whereas Kvβ2 increases current amplitude and shifts the voltage-dependence of activation towards more hyperpolarized potentials, with little impact on channel inactivation.[15, 32, 53] These effects are consistent with a greater steady-state activity of non-inactivating Kv1α channels (e.g., Kv1.5) when assembled with Kvβ2, as compared with those predominantly consisting of Kvβ1 proteins.

How the net competing influences of multiple Kvβ subtypes impact the function of native Kv1 channels remains to be resolved; however, it has been reported that within the same auxiliary complex, the N-terminal inactivation function of Kvβ1 is inhibited by Kvβ2 subunits,[54] an effect which may be due to competition between Kvβ subtypes for the intracellular domain of pore-forming Shaker subunits, or through modification of Kvβ1 function via β:β subunit interactions. We found that in arterial myocytes both Kvβ1.1 and Kvβ2 proteins are expressed in native Kv1 channels, and therefore, it is plausible that the

greater abundance of Kvβ2 relative to Kvβ1.1 in Kv1 channels of coronary arterial myocytes underlies its functional dominance under physiological conditions. Consistent with this are the apparent differences in inactivation kinetics between slowly inactivating outward $K^+$ currents measured in coronary arterial myocytes in comparison with rapidly inactivating (i.e., A-type) currents recorded in retinal arteriolar myocytes, which predominantly express Kv1.5 + Kvβ1 proteins.[55-57] Indeed, our current data obtained from novel double transgenic mice overexpressing Kvβ1.1 in smooth muscle suggest that increased abundance of Kvβ1 proteins effectively diminishes the vasodilatory function attributed to Kvβ2. Thus, based on these findings, we speculate that Kvβ1 and β2 play antagonistic roles and that Kv channel remodeling which results in functional upregulation of Kvβ1.1 or downregulation of Kvβ2 (i.e., elevated Kvβ1.1:Kvβ2 ratio) could impair vasodilation and limit tissue perfusion.

The Kvβ proteins were discovered as functional AKRs, a group of enzymes that catalyze the reduction of carbonyl compounds by NAD(P)H.[58, 59] In our previous work, we found that the binding of oxidized and reduced pyridine nucleotides to Kvβ proteins differentially modifies channel gating,[15, 18, 32, 60, 61] thus, raising the possibility that the Kvβ subunits provide a molecular link between the metabolic state of a cell and Kv channel activity. Given the high affinity of Kvβ proteins for pyridine nucleotides,[14, 62] it is plausible that rapid changes in intracellular redox potential of pyridine nucleotides in arterial myocytes may underlie Kv-mediated control of blood flow in the heart upon

changes in metabolic demand.

We recently reported that Kvβ2 subunits facilitate surface expression of Kv1 and Kv4 channels in cardiomyocytes and that they impart redox and metabolic sensitivity to cardiac Kv channels, thus coupling repolarization with intracellular pyridine nucleotide redox status;[18] however, to the best of our knowledge, the current study is the first to suggest a fundamental role for these subunits in controlling resistance vascular tone and blood flow.

Although our data show that Kvβ proteins regulate the diameter of resistance arteries subsequent to the modulation of NAD(H) redox via elevation of L-lactate, the precise identity of the factors responsible for coupling between myocardial oxygen consumption and coronary arterial tone remain unclear. Several myocardium-derived 'metabolites' (e.g., local $O_2$/$CO_2$ tensions, reactive oxygen species such as $H_2O_2$, lactate, endothelial-derived factors such as arachidonic acid metabolites)[9] could conceivably alter intracellular pyridine nucleotide redox potential and further work is required to identify specific metabolic processes that link intracellular redox changes to Kv activity. The function of coronary Kv1 channels could also be affected by other long-term biochemical processes. For example, the Kvβ proteins could plausibly alter patterns of basal post-transcriptional regulatory pathways (e.g., PKC-mediated channel phosphorylation)[63] or the surface density of functional channels.

However, such differences would likely manifest as differences in myogenic tone development or differential responses to vasoconstrictor stimuli,[64] which were not seen in our study, suggesting that the vasoregulatory effects of Kvβ may reflect more dynamic modifications of channel function.

Even though our study has many strengths, some limitations should be considered. Our studies were performed in mice, which exhibit greater heart rates and MBF relative to larger mammals, including humans.[65] Nonetheless, the positive correlation between myocardial oxygen consumption and MBF is highly conserved across species, and the parallel importance of Kv1 channels in the regulation of MBF is established in small rodents and larger mammals (i.e., swine).[11-13] Thus, it is likely that regulation of MBF by Kvβ proteins, observed in our current study, extends to larger species. Additionally, we cannot exclude the possibility that deletion of Kvβ proteins in non-vascular cell types (e.g., cardiomyocytes, neurons) may contribute to effects on MBF in vivo. However, this is unlikely for several reasons. First, prior work from our group indicates that suppression of blood flow in animals lacking Kv1.5, a predominant Kv1α binding partner of Kvβ, is restored via its conditional reconstitution in smooth muscle.[12] Second, data from novel transgenic mice generated for the current study (SM22α-rtTA:TRE-Kvβ1) indicate that smooth muscle- selective overexpression of Kvβ1.1, which increases the ratio of Kvβ1.1:Kvβ2 subunits in native Kv1 channels in arterial myocytes, leads to robust suppression of vasodilation and MBF, similar to observations in global Kvβ2 knockout mice. Additional evidence

from *ex vivo* arterial diameter measurements further supports the role for vascular Kvβ proteins in the regulation of vasoreactivity and is consistent with the notion that Kvβ subunits of native arterial Kv1 channels facilitate the metabolic hyperemia response.

In summary, we report a novel role for intracellular Kvβ subunits in the differential regulation of resistance artery diameter and control of myocardial blood flow. Our results indicate that proper coupling between coronary arterial diameter and myocardial oxygen consumption relies on the molecular composition of Kv1 accessory subunit complexes such that the functional expression of Kvβ2 is essential for Kv1-mediated vasodilation. Moreover, the current study suggests that perturbations in Kvβ function or expression profile (i.e., Kvβ1.1:Kvβ2) may underlie the dysregulation of blood flow in disease states characterized by impaired microvascular function and ischemia-related cardiac dysfunction.

## Figures

### Figure 1-1

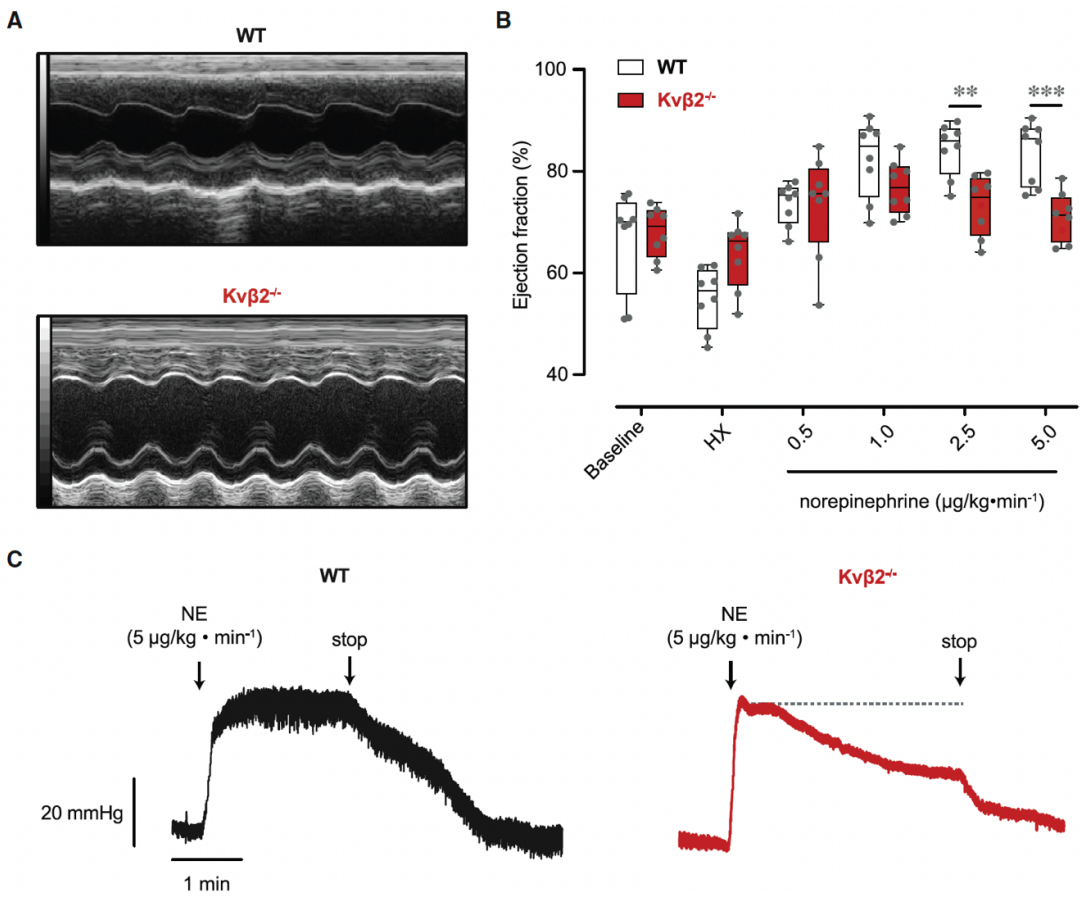


**Figure 1-1. Loss of Kvβ2 impairs cardiac pump function during stress.** (**A**) Representative M-mode echocardiographic images obtained from wild type (WT; 129SvEv), and Kvβ2$^{-/-}$ mice during infusion of 5 μg/kg·min$^{-1}$ norepinephrine. **(B)** Box-and-whisker plot of ejection fraction data for WT and Kvβ2$^{-/-}$ mice at baseline, after administration of hexamethonium (HX; 5 mg·kg$^{-1}$, i.v.), and during norepinephrine infusions (0.5 – 5 μg/kg·min$^{-1}$; 2-3 min duration). n = 8 each, **P<0.01, ***P<0.001 (two-way RM ANOVA). (**C**) Arterial blood pressure recordings obtained via femoral artery catheter in WT and Kvβ2$^{-/-}$ mice, before and after norepinephrine treatment (NE, 5 μg/kg·min$^{-1}$, indicated by arrows).

**Figure 1-2**

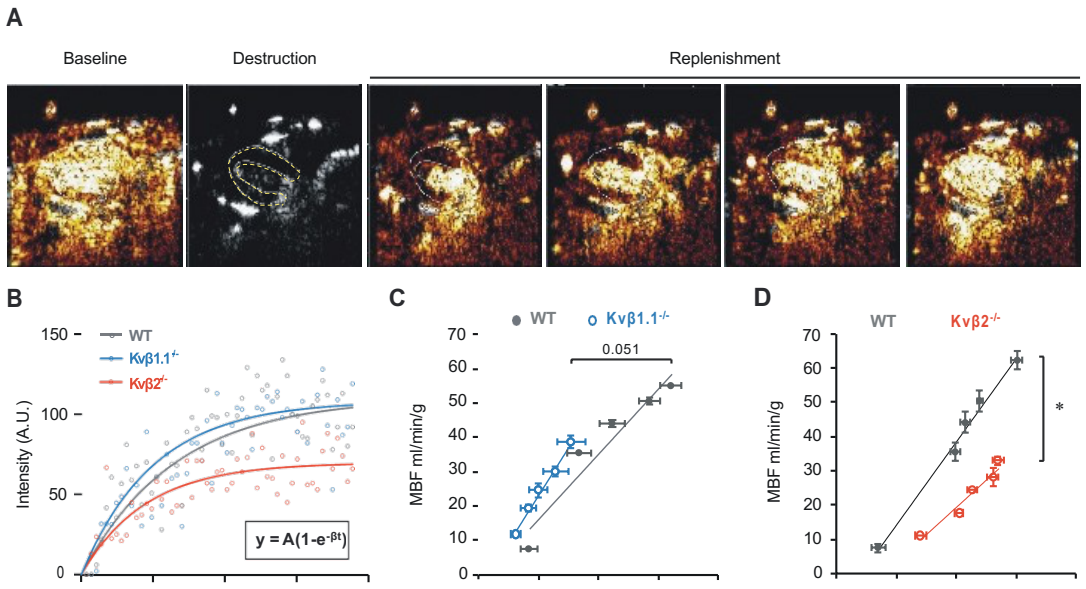


**Figure 1-2. Relationship between myocardial blood flow and cardiac workload in Kvβ-null mice.** (**A**) Long axis MCE images showing signal intensity from myocardial tissue and cavity before destruction frame and during replenishment phase (~10 sec). The left ventricular wall is outlined with a yellow dashed line in the destruction frame. (**B**) Signal intensity versus time (following destruction frame) in region of interest in the anterior left ventricular myocardial wall of WT (129SvEv), Kvβ1.1$^{-/-}$, and Kvβ2$^{-/-}$ mice. Data were fit with exponential function (*see inset*). (**C,D**) Summary of MBF as a function of cardiac workload (double product; heart rate x mean arterial pressure) in Kvβ1.1$^{-/-}$ (*C*) and Kvβ2$^{-/-}$ (*D*) versus strain-matched wild type (WT) control mice. Data were fit with a simple linear regression model with slopes: WT (0.00192 ± 0.00031), Kvβ1.1$^{-/-}$ (0.00279 ± 0.00016); n = 6-8 mice; WT (0.00241 ± 0.00014), Kvβ2$^{-/-}$ (0.00162 ±0.00022); n = 4-8 mice, *P<0.05, slope of Kvβ2$^{-/-}$ vs. WT.

**Figure 1-3**

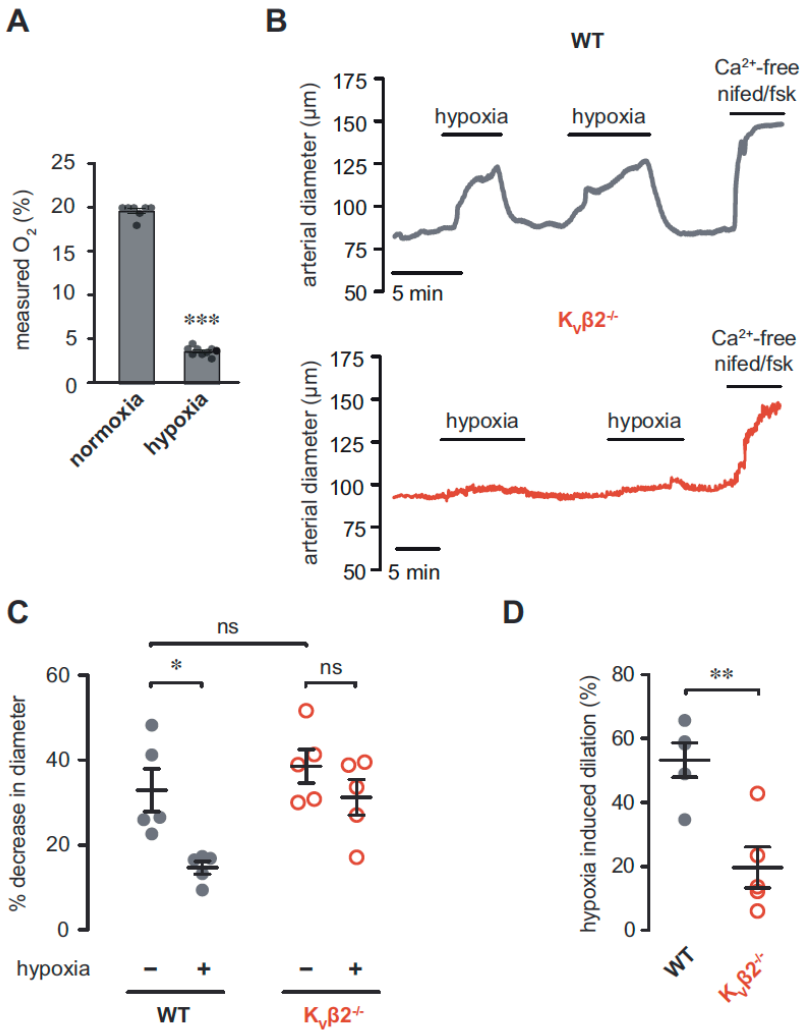


**Figure 1-3: Ablation of Kvβ2 attenuates hypoxia-induced coronary vasodilation.** (**A**) Summarized bath $O_2$ (%) measured in normoxic and hypoxic conditions (perfusate aerated with 5% $CO_2$, balance $N_2$, + 1 mM $Na_2S_2O_4$); data are pooled from measurements obtained with wild type (129SvEv) and Kvβ2$^{-/-}$ coronary arteries. n = 7-9, ***P<0.001 (Mann Whitney U). (**B**) Representative arterial diameter recordings in isolated preconstricted (100 nM U46619) coronary arteries from wild type (WT; 129SvEv) and Kvβ2$^{-/-}$ mice in normoxic and hypoxic

conditions. $Ca^{2+}$-free perfusate containing nifedipine (nifed; 1 μM) and forskolin (fsk; 0.5 μM) was introduced at the end of the experiment to induce maximum dilation. (**C**) Scatter-plot and mean ± SEM showing percent decrease in diameter recorded under normoxic (- hypoxia) and hypoxic (+ hypoxia) conditions for arteries from WT and $Kv\beta2^{-/-}$ mice. Normoxic and hypoxic conditions were both applied in continuous presence of U46619, see above (*B*). n = 5 arteries, 3-4 mice *P<0.05, ns: P≥0.05 (one-way ANOVA, Tukey). (**D**) Scatter-plot and mean ± SEM showing hypoxia-induced dilation (%) for arteries from WT and $Kv\beta2^{-/-}$ mice. **P<0.01 (Mann-Whitney U test).

**Figure 1-4**

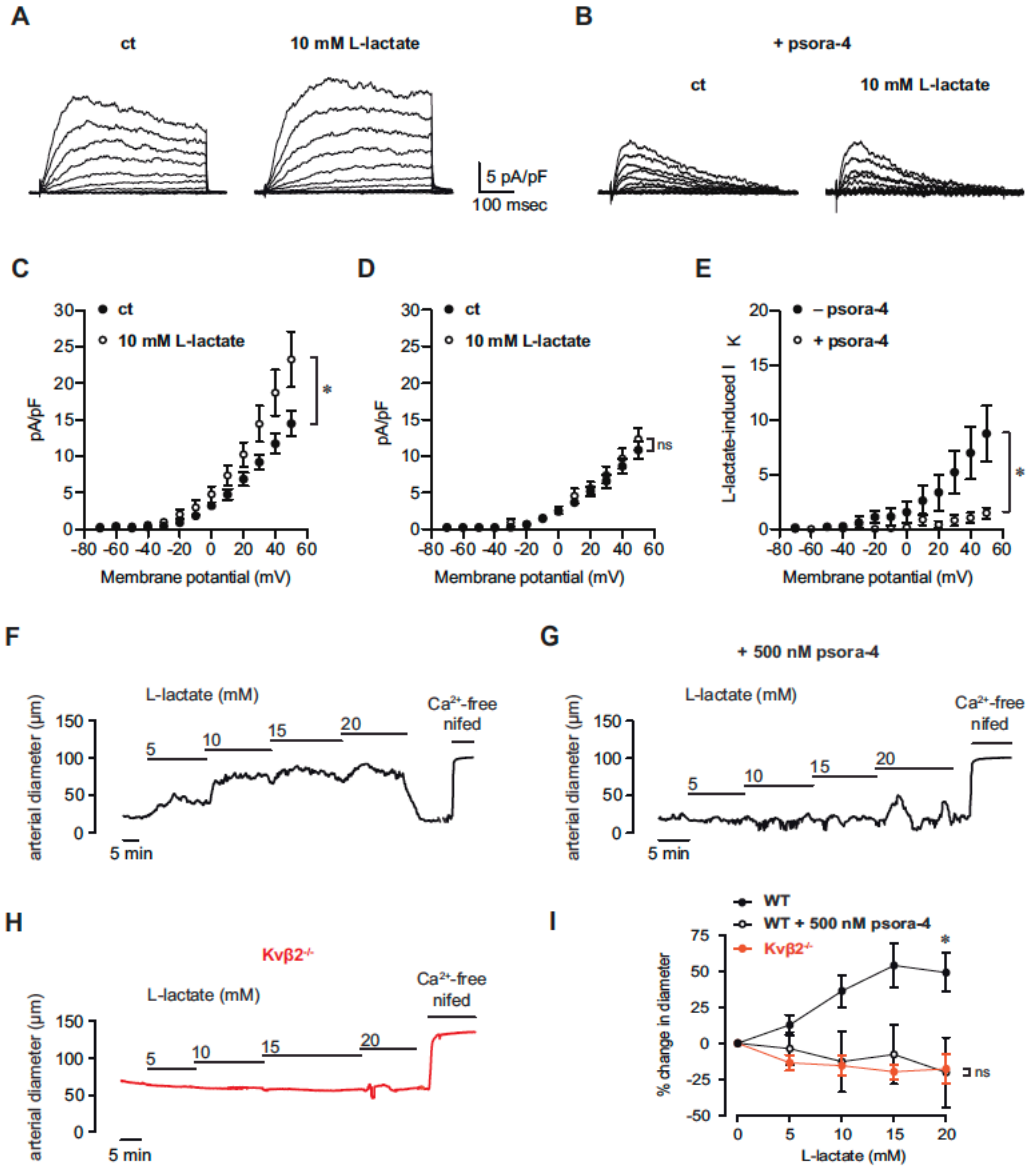


**Figure 1-4. L-lactate enhances IKv in coronary arterial myocytes and promotes coronary vasodilation via Kvβ2.** (**A, B**) Representative outward $K^+$ current recordings normalized to cell capacitance (pA/pF) in response to step-wise (10 mV) depolarization to +50 mV from a holding potential of –70 mV in isolated coronary arterial myocytes. Currents were recorded before and after

application of 10 mM L-lactate in bath solution lacking (*A*) or containing (*B*) 500 nM psora-4. (**C, D**) Summary current-voltage relationships obtained in coronary arterial myocytes before and after application of 10 mM L-lactate in bath solution lacking (*C*) or containing (*D*) 500 nM psora-4. n = 5-7 cells from 4-7 mice. *P <0.05, ns: P≥0.05 (two-way RM ANOVA). (**E**) Summary of L-lactate-induced currents recorded in the absence and presence of 500 nM psora-4. n = 5-7 cells from 4-7 mice. *P <0.05 (mixed-effects). (**F-H**) Arterial diameter traces obtained from pressurized (80 mmHg) coronary arteries isolated from wild type (WT; 129SvEv; *F,G*) and Kvβ2$^{-/-}$. (*H*) mice in the absence and presence of L-lactate (5-20 mM, as indicated). Arteries were preconstricted with 100 nM U46619; for WT arteries, L-lactate was applied in the absence (*top*) and presence (*bottom*) of psora-4 (500 nM). Maximum passive diameter was recorded at the end of each experiment in $Ca^{2+}$-free saline solution with nifedipine (nifed; 1 μM) and forskolin (fsk; 0.5 μM). (**I**) Summary plot showing L- lactate-induced dilation, expressed as a percent change from baseline diameter relative to maximum passive diameter, for arteries isolated from WT (129SvEv; ± 500 nM psora-4) and Kvβ2$^{-/-}$ mice. n = 4 arteries from 4 mice for each. *P<0.001; ns: P≥0.05, lactate vs. baseline (Friedman).

**Figure 1-5**

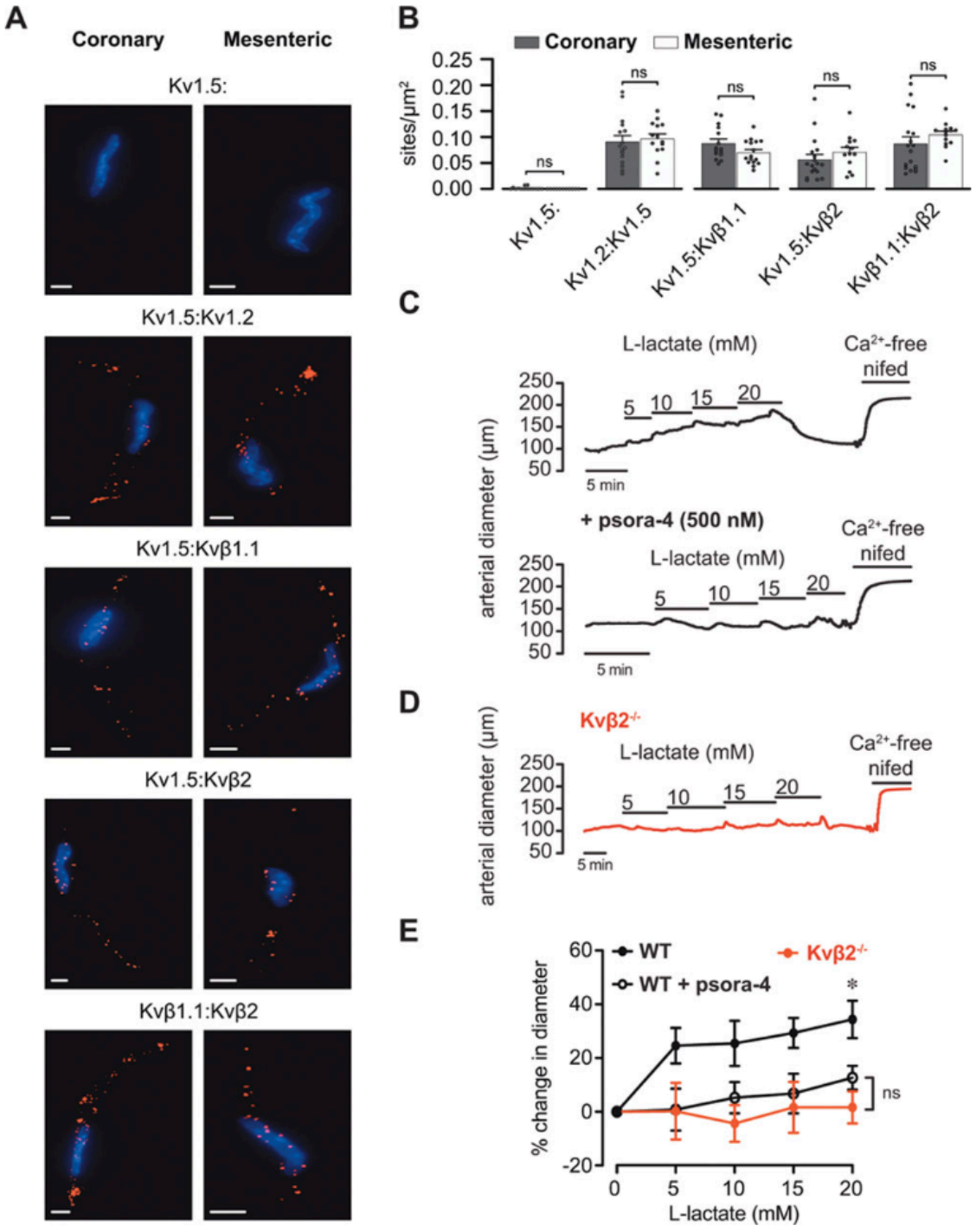


**Figure 1-5. Kvβ2 controls redox-dependent vasoreactivity in resistance mesenteric arteries.** (**A**) Representative fluorescence images showing PLA-

associated fluorescent punctae (red) in wild type coronary and mesenteric arterial myocytes. Cells were labelled for Kv1.5 alone, or co-labelled for Kv1.5 and Kv1.2, Kv1.5 and Kvβ1.1, Kv1.5 and Kvβ2, or Kvβ1.1 and Kvβ2 proteins. DAPI nuclear stain is shown for each condition (blue). Scale bars represent 5 μm. (**B**) Summary of PLA-associated punctate sites normalized to total cell footprint area for conditions and groups as in D. P values are shown for coronary versus mesenteric arteries (Mann Whitney U). (**C,D**) Arterial diameter traces obtained from pressurized (80 mmHg) mesenteric arteries isolated from wild type (*C*; 129SvEv) and $Kv\beta2^{-/-}$ (*D*) mice in the absence and presence of L-lactate (5-20 mM, as indicated). Arteries were preconstricted with 100 nM U46619 and L-lactate was applied in the absence (*top*) and presence (*bottom*) of the selective Kv1 channel inhibitor psora- 4 (500 nM). Maximum passive diameters were recorded at the end of each experiment in $Ca^{2+}$-free saline solution with nifedipine (nifed; 1 μM) and forskolin (fsk; 0.5 μM). (**E**) Summary plot of L-lactate-induced dilation, expressed as the percent change from baseline diameter relative to maximum passive diameter, for arteries isolated from WT (129SvEv; ± psora-4) and $Kv\beta2^{-/-}$ mice. n = 5 arteries from 4-5 mice for each.

*P<0.05; ns: P≥0.05, lactate vs. baseline (Friedman).

## Figure 1-6

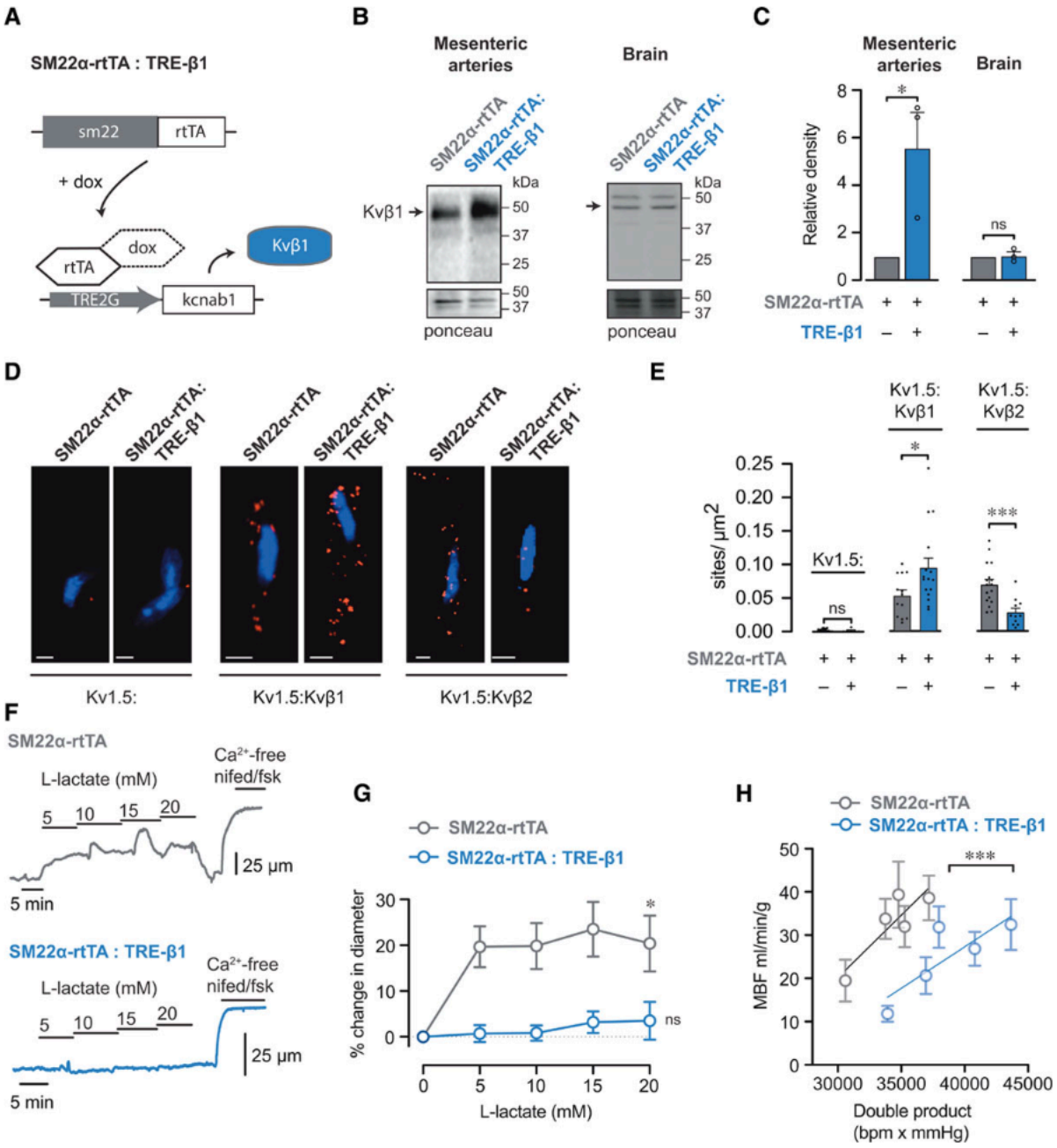
A
SM22α-rtTA : TRE-β1
sm22
rtTA
+ dox
rtTA
dox
Kvβ1
TRE2G
kcnab1
B
Mesenteric arteries
Brain
SM22α-rtTA
SM22α-rtTA: TRE-β1
kDa
Kvβ1
50
37
25
ponceau
C
Mesenteric arteries
Brain
Relative density
ns
SM22α-rtTA
TRE-β1
D
SM22α-rtTA
SM22α-rtTA: TRE-β1
Kv1.5:
Kv1.5:Kvβ1
Kv1.5:Kvβ2
E
Kv1.5: Kvβ1
Kv1.5: Kvβ2
sites/ μm2
Kv1.5:
ns
SM22α-rtTA
TRE-β1
F
SM22α-rtTA
L-lactate (mM)
5 10 15 20
Ca2+-free nifed/fsk
25 μm
5 min
SM22α-rtTA : TRE-β1
G
SM22α-rtTA
SM22α-rtTA : TRE-β1
% change in diameter
ns
L-lactate (mM)
H
SM22α-rtTA
SM22α-rtTA : TRE-β1
MBF ml/min/g
Double product (bpm x mmHg)

**Figure 1-6. Increasing the ratio of Kvβ1.5:Kvβ2 subunits in smooth muscle inhibits L-lactate-induced vasodilation and suppresses myocardial blood flow.** (**A**) Schematic diagram describing the SM22α- rtTA:TRE-β1 model. Double transgenic animals (+dox) results in activation of the reverse tetracycline trans-activator (rtTA) in smooth muscle cells, and drives expression of Kvβ1.1. (**B**) Western blots showing immunoreactive bands for Kvβ1 in whole mesenteric artery and brain lysates from SM22α-rtTA (single transgenic control) and SM22α-rtTA:TRE-β1 (double transgenic) mice after doxycycline treatment. Ponceau-stained membrane (mol. Wt.: ~30-55 kDa) is shown as an internal control for total loaded protein. (**C**) Summarized relative densities of Kvβ1.1-associated immunoreactive bands in mesenteric arteries and brains of SM22α-rtTA:TRE-β1 relative to SM22α-rtTA. n = 3 each. *P<0.05, ns: P≥0.05 (one sample t test). (**D**) Representative fluorescence images showing PLA-associated fluorescent punctae (red) in coronary arterial myocytes isolated from SM22α-rtTA and SM22α-rtTA:TRE-β1mice. Cells were labelled for Kv1.5 alone, or co-labelled for Kv1.5 and Kvβ1, or Kv1.5 and Kvβ2 proteins. DAPI nuclear stain is shown for each condition (blue). Scale bars represent 5 μm. (**E**) Summary of PLA-associated punctate sites normalized to total cell footprint area for conditions and groups as in D. n = 6-19 cells from 2-3 mice for each; *P<0.05, **P<0.001 (Mann Whitney U). (**F**) Representative arterial diameter recordings from 100 nM U46619-preconstricted mesenteric arteries isolated from SM22α-rtTA and SM22α-rtTA:TRE-β1 mice in the absence and presence of L-lactate (5-20 mM), as in Figure 5C,D. Passive dilation in the presence of $Ca^{2+}$-free solution

+ nifedipine (1 μM) and forskolin (fsk; 0.5 μM) is shown for each recording. (**G**) Summary plot of L-lactate-induced dilation for arteries isolated from SM22α-rtTA and SM22α-rtTA:TRE- β1 mice. n = 6-10 arteries from 5-6 mice; *P<0.05; ns: P≥0.05, lactate vs. baseline (Friedman). (**H**) Summary relationships between myocardial blood flow (MBF) and cardiac workload (double product; heart rate x mean arterial pressure) in SM22α-rtTA:TRE-β1 vs. SM22α-rtTA control mice. n = 5 each; ***P<0.001 (linear regression).

# CHAPTER 4: INTEGRATED REDOX SENSITIVITY OF VASCULAR $K_V1$ CHANNELS[5]

## Introduction

Resistance arterial blood flow is tightly regulated and crucial for preserving $O_2$ and nutrient supply to the surrounding tissues.[45,169] During increased work the resistance arteries dilate to match the $O_2$ and nutrient demands of the adjacent tissues.[50,60] The increased work alters the metabolic chemistry such that the ratio of crucial electron and hydride transport intermediates, the oxidized and reduced pyridine nucleotides ($NAD^+$ and NADH) shift in favor of NADH.[168] The increase in NADH as compared to $NAD^+$ is believed to be an important signaling molecule in the vasodilatory response of small resistance arteries. Additionally, it is well established that other known compounds, such as hydrogen peroxide ($H_2O_2$), increase from due to greater mitochondrial respiration, and affect vasodilation.[115,155] Importantly, voltage-gated potassium ($K_V$) channels have been identified as prominent regulators of resistance artery vasodilation.[55,181] These channels consist of membrane bound alpha ($K_{V\alpha}$) heteromeric complexes, and intracellular auxiliary beta-subunits ($K_V\beta$), which have been proposed as sensors of metabolic change.[55,114,167,182,183] The $K_V$-$K_V\beta$ complexes form octameric-heteromers comprised in an $\alpha_4/\beta_4$ formation.[43,128,184,185] In the vascular

[5]At the time of the writing of this dissertation the data presented in this chapter have been submitted to a scientific journal for peer review (December 2nd, 2022).

smooth muscle cell $K_V\beta$ isoforms $K_V\beta1$ and $K_V\beta2$ have been identified. These β-subunits differ structurally in that $K_V\beta1$ has a ball-and-chain component that rapidly inactivates the $K_V1$ channel. Meanwhile, the $K_V\beta2$ subunit does not contain this inactivating component, and has been shown to have an opposite effect on $K_V1$ channel activity and vasodilation in the presence of increased NADH. The $K_V$ subunit $K_V\beta$ is a member of the aldo-keto reductase superfamily (AKR) and retains the catalytic activity of its namesake. These catalytic subunits utilize a co-factor such as NADH, and $NAD^+$ to reduce carbonyl substrates.[138-140] Additionally, both $H_2O_2$ and NADH increase with greater cardiac work and have been shown to individually induce $K_V1$-mediated vasodilation.[155]

The complex signals that regulate vasomotor control of the vascular smooth muscle cells are individually well studied. Importantly, *in vivo* there is no singular signal but rather an entire milieu of vasoactive mediators at varying concentrations in response to different environmental factors. Therefore, it is crucial to understand how the presence of multiple different vasoactive compounds might affect vasomotor control.

The lipid membrane of the cell is sensitive to reactive oxygen species, including $H_2O_2$. Aldehydes are regular byproducts of cell membranes exposure to ROS ($H_2O_2$) and are potential substrates for $K_V\beta$ catalysis. The proximity of the $K_V1$-$K_V\beta$ complex to an increase in co-factor (NADH) and substrates (aldehydes) could result in increased catalytic activity of the $K_V\beta$ subunits. As both NADH and $H_2O_2$ increase with enhanced cardiac work it can be surmised that more NADH would bind to the $K_V\beta$ subunit, and that more lipid membrane peroxidation is

occurring. We tested the hypothesis that Kv1-mediated vasodilation in response to $H_2O_2$ is modified by smooth muscle metabolic state via intracellular pyridine nucleotide redox state. To address this hypothesis, we developed several questions which we then investigated using patch clamp electrophysiology in the single channel configuration and ex vivo pressure myography. 1) Does the presence or absence of either $K_V\beta1$ or $K_V\beta2$ impact $H_2O_2$ induced vasodilation; 2) does pretreating isolated vascular smooth muscle cells cells (or vessel) with 10 mM NADH (or lactate) affect $H_2O_2$ induced $K_V1$ channel activity and vasodilation; 3) does 10 mM $NAD^+$ (or pyruvate) differentially affect $K_V1$ channel activity and vasodilation; 4) does overexpression of $K_V\beta1$ impact $K_V1$ channel activity or vasodilation in the presence increased NADH or $NAD^+$ and $H_2O_2$.

**Schematic 1.**

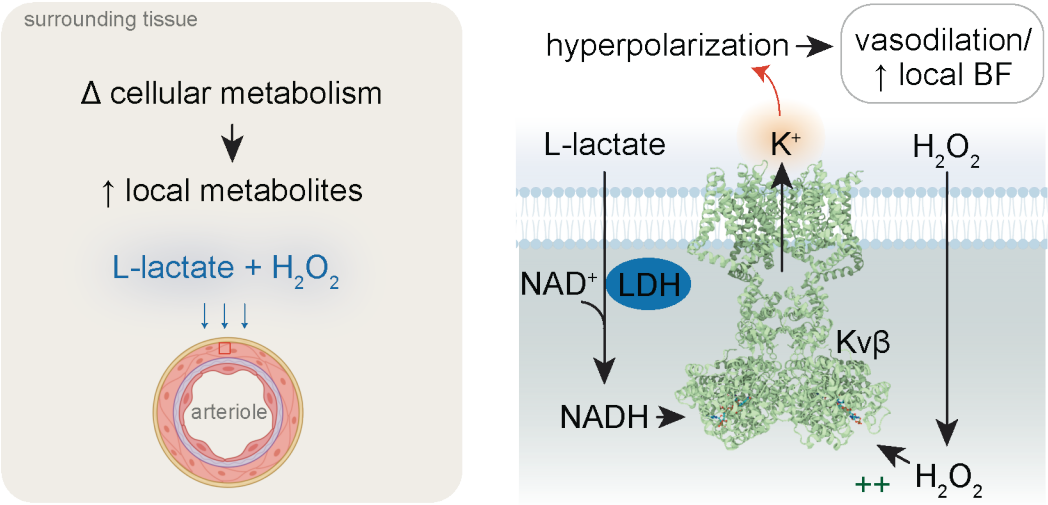


**Schematic 1. Proposed mechanism of the effects increased NADH and $H_2O_2$ during increased cellular metabolism.** This image represents the hypothesis

that local changes in cellular metabolism and thus metabolites significantly impacts vasodilation and in turn blood flow via enhanced Kv channel activation.

## Results

*Lactate induces vasodilation via LDH dependent activity.*

Lactate production increases during increased metabolic respiration. The balance of lactate:pyruvate is mediated via the lactate dehydrogenase enzyme (LDH). This balance is maintained by the modification of pyridine nucleotide reduced:oxidized ratio (i.e., NADH:$NAD^+$). Increases in NADH are known to enhance vasodilation and whole cell currents via Kv channels.[155] In isolated small resistance arteries, we have shown that external perfusion of increasing concentrations of lactate induces greater vasodilation (**Fig. 2-1A, top panel**). Additionally, that pharmacological inhibition of LDH enzymatic activity significantly impaired L-lactate and in turn NADH induced vasodilation (**Fig. 2-1A, bottom panel**).

*NADH in the absence and presence of $H_2O_2$ induces significantly greater Kv channel activity.*

As described above increases in cytosolic lactate induce an increase in NADH via LDH enzymatic activity in isolated mesenteric artery smooth muscle cells. In isolated arterial myocytes we compared single channel open probabilities under baseline conditions with those in the presence of 1 mM NADH (**Fig. 2-2 A**). Addition of 1 mM NADH significantly increased the nPo and nPO relative to control (F**ig. 2-2 B, C**). However, the channel dwell time was not significantly increased (**Fig. 2-2 D**). Increased endogenous $H_2O_2$ has previously been shown to induced

greater vasodilation. Here we reaffirmed the vasodilatory capacity of 10 μM $H_2O_2$ (**Fig. 2-3 A i.**) in resistance arteries from wild type mice (FVB). Additionally, we utilized single channel patch clamp and determined that 10 μM $H_2O_2$ significantly increased the nPo (**Fig. 2-3 B, C**) in isolated arterial smooth muscle cells. Representative traces of single channel patch clamp experiments of 1 mM NADH in the absence and presence of 10μM $H_2O_2$ show the events (**Fig. 2-4 A**). The nPo of 1 mM NADH was significantly greater in the presence of 10μM $H_2O_2$, as compared to 1 mM NADH alone (**Fig. 2-4 B**). Additionally, $H_2O_2$-induced ΔnPo was significantly greater in the presence of 1 mM NADH as compared to 10μM $H_2O_2$ alone (**Fig. 2-4 C**).

*$H_2O_2$ induced vasodilation is not impacted by overexpression of Kvβ1.*

Endogenous increases in reactive oxygen species (i.e., hydrogen peroxide) occur with enhanced cellular respiration. Previous studies have shown $H_2O_2$ induces Kv1 dependent vasodilation.[155] However, the mechanism of $H_2O_2$ induced modification of Kv1 via the Kv auxiliary beta subunits has not been elucidated. There have been no studies to our knowledge that have linked either Kvβ1 or Kvβ2 to different responses to $H_2O_2$-mediated vasodilation. In our SM22α-rtTA:Kcnab1 animals given doxycycline via drinking water we saw an increase in Kvβ1 protein isolated from mesenteric arteries (**Fig. 2-5 A**). From these observed increases in Kvβ1 protein and our previous publication utilizing the same animals, we infer that an increase in Kvβ1 expression displaces Kvβ2 in the Kvβ complex (**Fig. 2-5 B**). Our

data show that overexpression of Kvβ1 does not significantly impair or enhance $H_2O_2$-mediated vasodilation (**Fig. 2-5 C**).

*$H_2O_2$ induced vasodilation in NADH primed resistance arteries is impaired with overexpression of Kvβ1.*

During increased work, greater metabolic respiration produces increases in lactate and $H_2O_2$. As mentioned previously, increases in lactate drive greater NADH via LDH enzyme activity. In isolated resistance arteries perfusion of 10 mM L-lactate with 10 μM $H_2O_2$ induced significantly enhanced vasodilation (**Fig. 2-6 A i.**). However, in the presence of pyruvate the effect on vasodilation was not observed (**Fig. 2-6 A ii.**). The $H_2O_2$-induced increase in diameter was significantly greater in the presence of lactate as compared to control, and 10 mM pyruvate (**Fig. 2-6 B**). In isolated resistance arteries from SM22α-rtTA:TRE-β1 mice that exhibit increased Kvβ1 in the Kv-complex, perfusion of 10 mM L-lactate or 10 mM pyruvate in the presence of 10 μM $H_2O_2$ had no significantly vasodilatory response (**Fig. 2-6 C i. and ii.**).

## Discussion

The activity of native vascular Kv1 channels is in part regulated by the redox state of cytosolic pyridine nucleotides in smooth muscle as well as tissue-derived reactive species such as $H_2O_2$.[140,167,183,186-189] In a physiological perspective, by-products, and endogenous vasoactive signaling molecules are present on their own. Rather, the milieu of potential vasoactive agents, whether dilatory or constrictive in nature, are competing against their respective thresholds of activation. Respectively, in instances of increased work (i.e., exercise) both NADH and $H_2O_2$ have been shown to increase in vascular smooth muscle cells.[50,55,114,168] NADH has been shown to interact with the Kvβ-subunit acting as a hydrogen donor for the β-subunits catalytic function of modifying carbonyls.[138,140] Park et al., 2015, showed that $H_2O_2$ induced vasorelaxation and increased whole cell currents were impaired in the presence of Kv channel inhibitor 4-AP.[155] Further, in intact cells dialyzed with NADPH in the presence of 10 mM $H_2O_2$ an increased current density was observed, that was ablated with the addition of glutathione (GSH) reductase.[155] These support an interaction of Kv channel enzymatic co-factors, and *S*-glutathionylators that may sensitize the Kv channel. This could cause enhanced channel opening, extended dwell time, and rapid catalytic turn-over of endogenous substrates. Therefore, we endeavored to investigate whether L-lactate (i.e., NADH) sensitizes the Kv channel Kvβ-subunit to $H_2O_2$. We found that the elevation of reduced pyridine nucleotides (i.e., NADH) enhances the vasodilatory response to $H_2O_2$. Our results suggest that multiple vasoactive

metabolites may influence redox-dependent dilatory function via additive effects on Kv1 channels via the Kvβ auxiliary subunit complex.

During increased work, the concentration of metabolites lactate and $H_2O_2$ increase in local tissues.[168,190] Increases in local lactate concentration results in conversion by the lactate dehydrogenase (LDH) enzyme to pyruvate this increases the pool of NADH while decreasing $NAD^+$.[191] Lactate and NADH haven been shown to increase Kv currents in arterial smooth muscle cells.[168] By inhibiting LDH enzyme activity we have shown that the Kvβ-subunit is modifying Kv-mediated vasodilation in response to lactate conversion to NADH (**Fig. 2-1**). Additionally, both $H_2O_2$, a known endogenous vasodilatory, and NADH, induce significant increases in Kv channel opening (**Fig. 2-2 and 2-3**). From this increase in Kv channel activity we can infer that we would expect an increase in vessel diameter. In fact, perfusion of lactate and $H_2O_2$ alone induced vasodilation, whereas the combined presence of lactate and $H_2O_2$ significantly enhanced both the Kv channel open probability and the vasodilatory response (**Fig. 2-4 and 2-6**). Additionally, it is crucial to understand the opposing functional responses of the Kvβ1 and Kvβ2 proteins in modifying Kv channel activity in response to altered metabolic conditions. Therefore, using our Kvβ1 overexpression model we found that priming of isolated arteries with lactate in the presence of $H_2O_2$ significantly impaired the observed vasodilatory response. Further supporting possible opposing roles for the Kvβ subunits to modify Kv channel activity and thus arterial diameter. Furthermore, these data demonstrate the ability to alter the composition of the Kvβ-subunit complex, or to modify the sensitivity of the catalytic component Kvβ-

subunits may provide a future pharmacological target. Finally, these findings further our understanding of the effects of altered local metabolism on Kv-mediated vasodilatory capacity and the role of the Kvβ-subunits as sensors of this change.

## Figures

**Figure 2-1.**

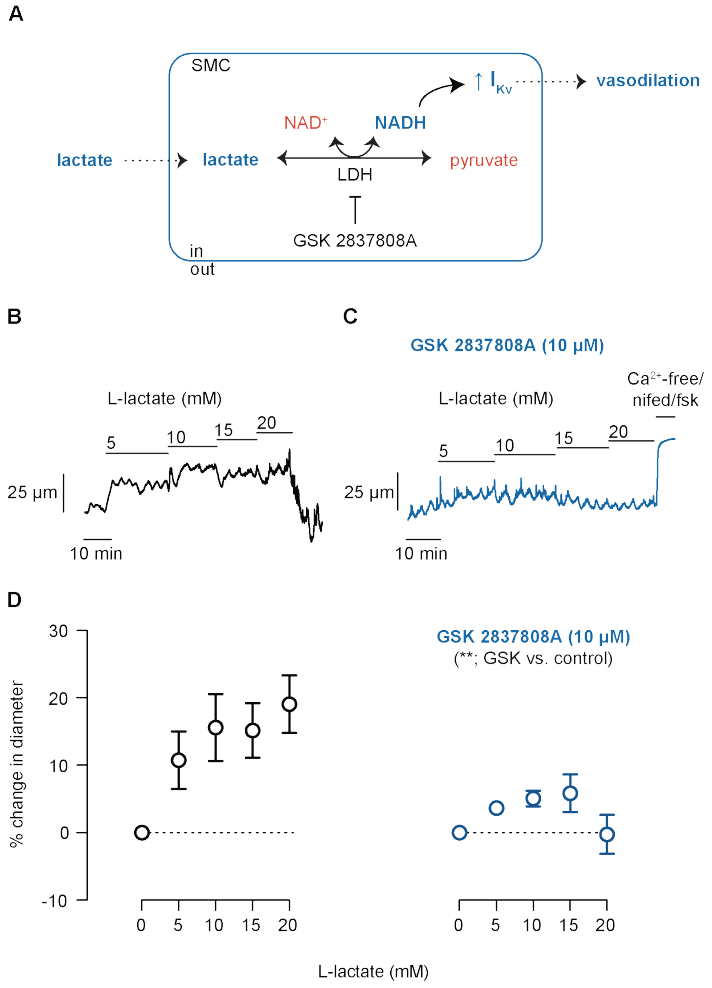


**Figure 2-1. Elevation of L-lactate promotes vasodilation via LDH activity.** (**A**) Scheme illustrating LDH-mediated interconversion of lactate to pyruvate, associated changes in NADH:NAD$^+$, and proposed impact on $I_{KV}$ underlying resistance artery dilation. (**B, C**) Representative arterial diameter recordings before and after application of L-lactate (5-20 mM) in abcence and presence of LDH inhibitor GSK 2837808A. (**D**) Summarized %-change in diameter from baseline in response to L-lactate ± GSK 2837808A. n = 3 arteries from 3 mice, P value, two-way ANOVA.

**Figure 2-2.**

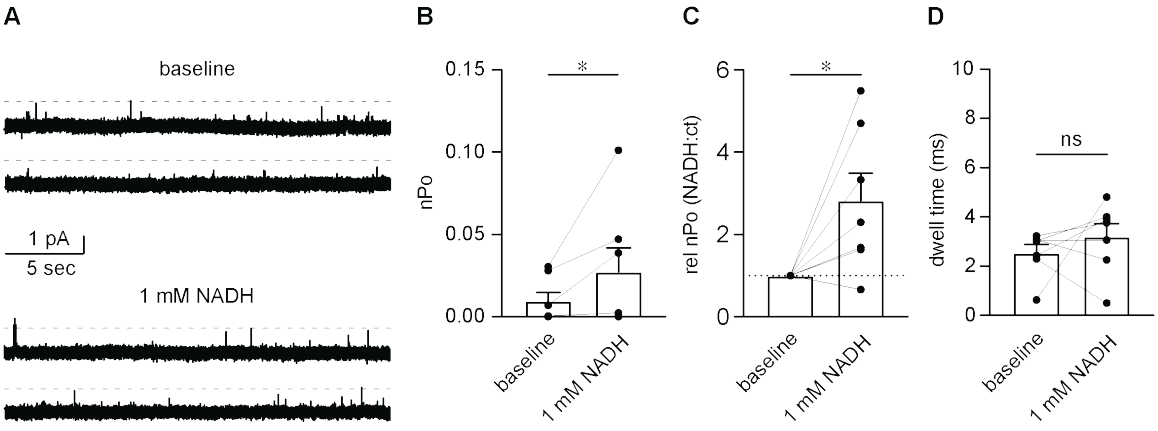


**Figure 2-2. NADH induces significant increase in nPo of isolated arterial myocytes.** (**A**) Representative recordings of single channel patch clamp under baseline conditions (top) and in the presence of 1 mM NADH (bottom). Administration of 1 mM NADH significantly increased Kv (**B**) nPo, and (**C**) relative nPo, but not dwell time (**D**). n = 7 cells from 6 mice each; Values on figure **B** produced a p-value of *p = 0.047 using the Wilcoxon matched-pairs signed rank test; values for figure **C** generated a p-value of *p = 0.031, utilizing the Wilcoxon Signed Rank Test; data for figure **D** ns: p = 0.399, Paired t-test.

**Figure 2-3**.

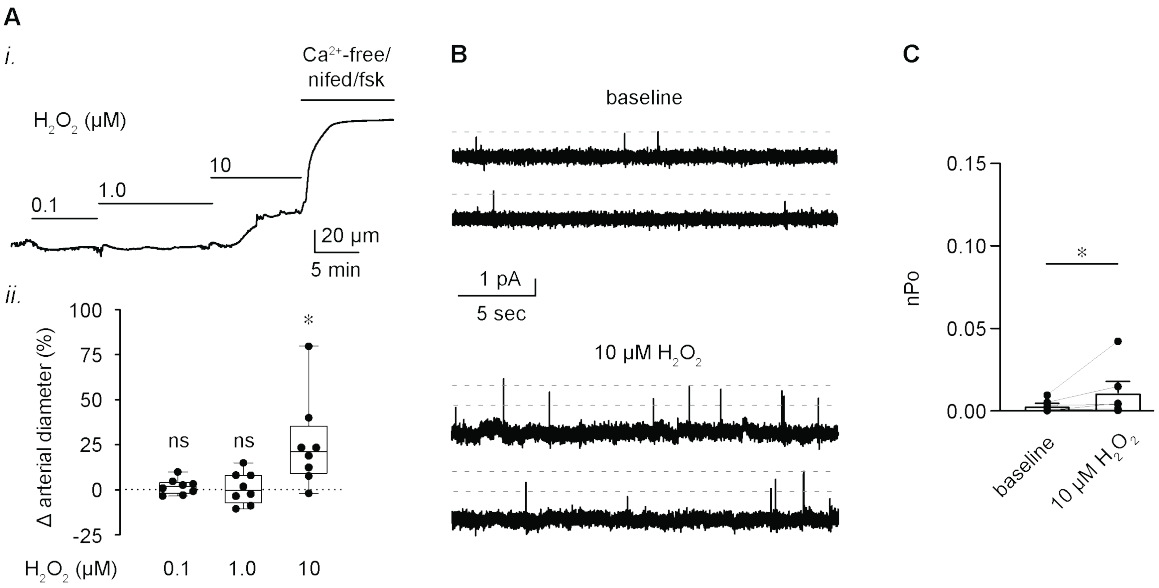


**Figure 2-3. 10 μM $H_2O_2$-induced increased vasodilation and Kv open channel probability.** (**A i.**) Example recording of arterial diameter in the absence and presence of bath $H_2O_2$ (0.1-10 μM). Maximum passive diameter was obtained at the end of the experiment in $Ca^{2+}$-free solution containing nifedipine (1μM) and forskoline (0.5 μM). (**A ii.**) Summary box and whisker plot of $H_2O_2$ (0.1-10 μM) induced vasodilation. n = 8 arteries from 5 mice; and Friedman test calculated *p = 0.011. (**B**) Representative single channel patch clamp traces of baseline (top) and 10 μM $H_2O_2$ (bottom). (**C**) Summary graph showing nPo of baseline and 10 μM $H_2O_2$. n = 6 cells from 5 mice; *$p < 0.05$; ns $p > 0.05$ vs. 0 μM (baseline control), repeated measures ANOVA.

**Figure 2-4.**

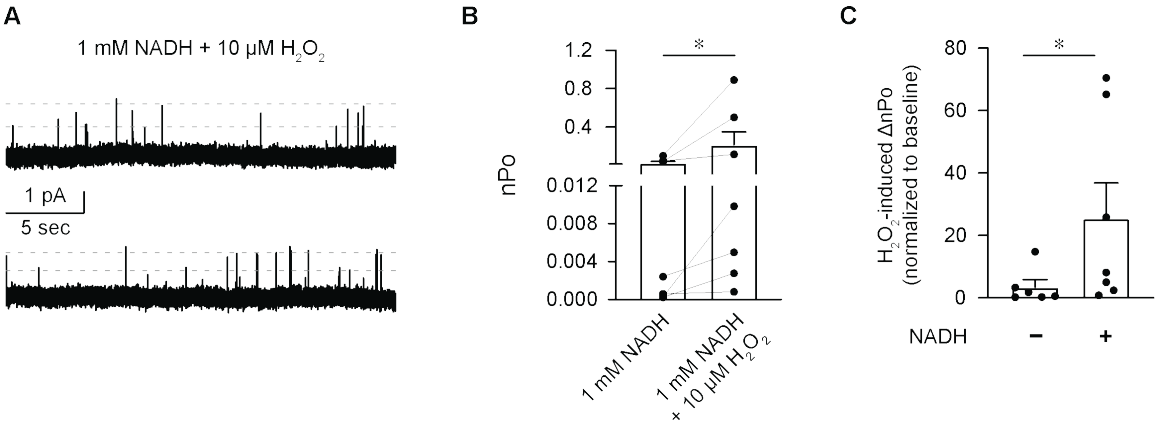


**Figure 2-4. Direct effects of $H_2O_2$ on native vascular Kv1 channels in the presence of NADH.** (**A**) (top) Representative single channel Kv1 recordings of 1 mM NADH and (bottom) subsequent perfusion of 10 μM $H_2O_2$ in the presence of 1 mM NADH. (B) Summarized mean ± SEM Kv1 open probabilities in the presence of 1 mM NADH and 1 mM NADH + 10 μM $H_2O_2$. n = 7 cells from 6 mice; *p = 0.016, Wilcoxon matched-pairs signed rank test. (**C**) Summary of $H_2O_2$-induced ΔnPo normalized to baseline. Data were quantified using Clampfit event search function to determine the time spent in the open state versus total recording time under each condition. Data are expressed for 1 mM NADH and 1 mM NADH + 10 μM $H_2O_2$ as relative to nPo under baseline conditions. n = 6-7 cells from 5-6 mice; *p = 0.042, unpaired t-test using Log-transformed data.

**Figure 2-5.**

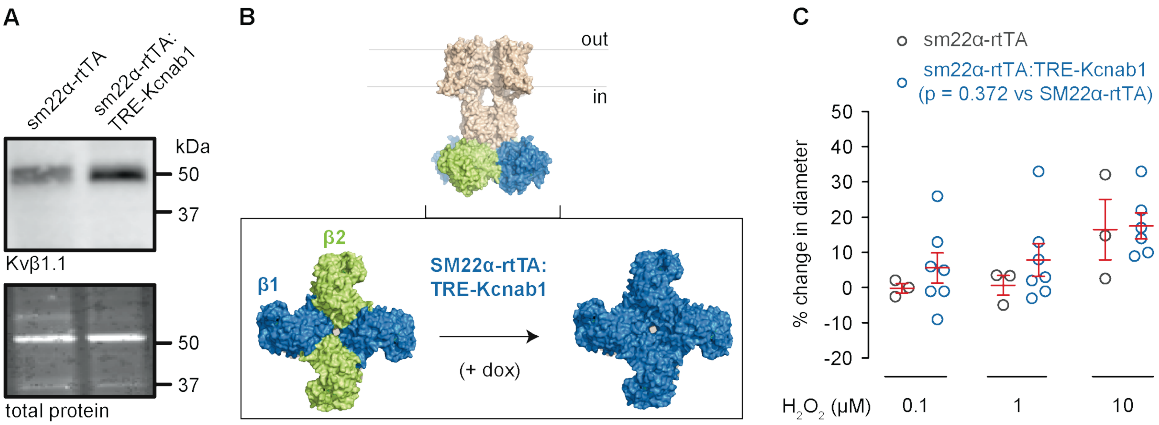


**Figure 2-5. $H_2O_2$-induced dilation is not affected by over-expression of Kvβ1 in smooth muscle.** (**A**) Representative image of Western Blot targeting Kvβ1 in samples of arterial resistance vasculature. (**B**) Representative figure of the proposed SM22α-rtTA:TRE-β1 Kv-complex model. (**C**) Summary of %-change in dilation in response to H2O2 at 0.1-10 uM in isolated mesenteric arteries from SM22α-rtTA (n = 7 arteries from 5 mice) and SM22α-rtTA:TRE-β1 mice (n = 7 arteries from 7 mice). $p > 0.05$, SM22α-rtTA vs. SM22α-rtTA:TRE-β1; two-way ANOVA.

**Figure 2-6.**

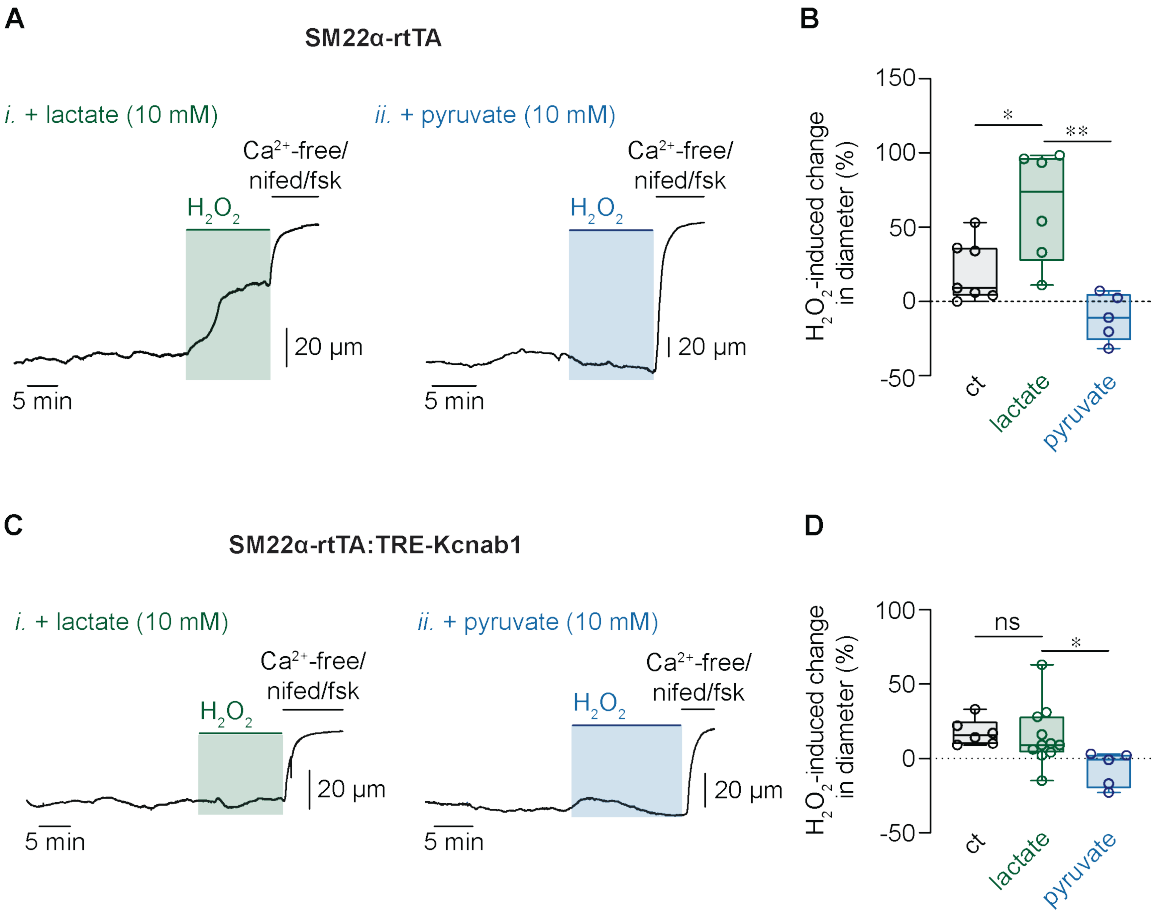


**Figure 2-6. Smooth muscle overexpression of Kvβ1 prevents redox modulation of $H_2O_2$-induced vasodilation.** (**A, C**) Representative arterial diameter traces obtained in the presence of either 10 mM lactate (**i.**) or 10 mM pyruvate (**ii.**) prior to application of 10 µM $H_2O_2$ in arteries from (**A**) SM22α-rtTA and (**C**) SM22α-rtTA:TRE-β1 mice. Maximum passive diameter was obtained at the end of the experiment as described above. Box-and-whiskers plot showing % change in diameter in response to $H_2O_2$ in the absence or in the presence of either 10 mM lactate or 10 mM pyruvate in arteries from (**B**) SM22α-rtTA mice (top; n =

5-7 arteries) or (**D**) SM22α-rtTA:TRE-β1 mice (bottom; n = 5-11 arteries). *p<0.05, **p<0.01; ns: p>0.05, one-way ANOVA with Sidaks multiple comparisons test.

# CHAPTER 5: EXERCISE-ENDHANCED CARDIAC FUNCTION AND MYOCARDIAL PERFUSION REQUIRE THE VOLTAGE-GATED POTASSIUM CHANNEL AUXILIARY SUBUNIT $K_V\beta2$.

## Introduction

Voltage-gated potassium (Kv) channels control membrane excitability in cells of the cardiovascular system. The coordinated activity of several types of Kv channels expressed in cardiac myocytes functions to return membrane voltage to resting potential after the upstroke of an action potential.[192] The importance of Kv channels to cardiac electrophysiology is underscored by the presence of arrhythmias under conditions in which Kv channel function is compromised.[193] Conversely, in vascular smooth muscle, the steady state activity of a subpopulation of sarcolemmal Kv channels maintains resting membrane potential and opposes depolarization-induced calcium influx via L-type voltage-gated $Ca^{2+}$ channels. Accordingly, several endogenous vasoactive substances evoke constriction or dilation via intracellular signaling cascades which culminate in the functional modulation of Kv channels. Thus, cardiovascular Kv channels mediate proper electrical signaling and by regulating myocyte contractility, play a profound role in maintaining cardiac pump function and vascular resistance to blood flow.

Native Kv channels reside in the sarcolemma of cardiac and vascular smooth muscle as macromolecular structures, consisting of four pore-forming α-

subunits that are variably associated with heteromeric assemblies of intracellular and transmembrane auxiliary β-subunits. Members of the Kv1 and Kv4 families associate with intracellular auxiliary Kvβ subunits, which confer A-type inactivation to otherwise non-inactivating outward $K^+$ currents. The Kvβ proteins are functional aldo-keto reductases and catalyze the reduction of aldehydes and ketones to alcohols using pyridine nucleotides (e.g., NADH) as cofactors for hydride transfer. The high affinity binding of both oxidized and reduced pyridine nucleotides has led to the proposal that the Kvβ proteins function as a link between intermediary metabolism and membrane excitability. Indeed, because the redox state of pyridine nucleotides bound to the Kvβ protein differentially regulates channel activation and inactivation properties, these proteins may be critical for Kv channel activation and modulation of cardiac action potential duration and blood flow during periods of increased oxygen consumption. Nonetheless, an in vivo role for Kvβ proteins has not been identified and their relevance to cardiovascular physiology remains poorly understood.

The principal physiological stimulus for increases in myocardial oxygen demand by cardiac muscle is an increase in physical activity such as aerobic exercise. During acute bouts of exercise, the heart increases oxidative energy production by ~6-fold to support higher cardiac output and systemic demand for blood flow. In response to intermittent hemodynamic stresses associated with recurrent exercise training, the heart remodels by increasing overall mass via increased cardiomyocyte size (i.e., hypertrophy). Extensive previous work has shown that physiologic cardiac growth in response to exercise involves enhanced

capacity for oxidative energy production. The importance of coronary vasodilation matching $O_2$ supply with cardiac demand is well understood. However, a gatekeeper of enhanced coronary blood flow in response to exercise has yet to be elucidated. Previous studies have shown that myocardial perfusion during increased cardiac work requires Kv1 channels and that exercise enhances Kv whole cell currents.[42,55,181] Additionally, little is currently known regarding the importance of proper electrical signaling in response to the physiologic adaptations to exercise.

In this study, we tested the in vivo importance of the Kvβ subunit complex in regulating exercise capacity as well as cardiac adaptations to exercise training. For this, we used a genetically engineered mouse in which the gene encoding the Kvβ2 subunit (*Kcnab2*) is ablated. We report that Kvβ2-null mice have impaired exercise capacity in an established protocol of forced treadmill exercise. Moreover, after four weeks of exercise training, enhancement of exercise capacity, physiologic cardiac growth, and myocardial perfusion was observed in wild type mice but was abolished in Kvβ2-null animals. Our data indicate that Kvβ proteins are important in vivo determinants of physiological cardiac adaptation to exercise and suggest a relationship between membrane excitability and exercise-induced remodeling of the cardiovascular system.

## Results

*Ablation of Kvβ2 impairs work done in naïve male mice.*

Naïve wild type (WT) and Kvβ2-null ($Kv\beta2^{-/-}$) male mice underwent an exercise capacity test after 2 days of familiarization with the forced treadmill apparatus (**Fig. 3-1 A, B**). Work is calculated as the distance run times sin(θ), where θ is the angle of treadmill, multiplied by the weight of the individual animals, calculated at each incline stage. Weight of animals was not significantly different between naive WT and $Kv\beta2^{-/-}$ animals (**Fig. 3-1 C**). However, run time, run distance and work were significantly lower in naïve $Kv\beta2^{-/-}$ male mice (**Fig. 3-1 D-F**). Blood lactate was measured from distal tail clips before and after initial ECT and mice were found to have significantly increased blood lactate concentrations at exhaustion (**Fig. 3-1 G**).

*Work done after 4-weeks forced treadmill running increases in WT but not $Kv\beta2^{-/-}$ male mice.*

After the initial ECT WT and $Kv\beta2^{-/-}$ male mice underwent 4-weeks FTR at 50% of maximum average capacity. Mice performed FTR for 40 minutes during week 1, 50 minutes week 2, and 60 minutes for weeks 3 and 4 (**Fig. 3-2 A**) followed by a second ECT. Ablation of $Kv\beta2^{-/-}$ did not significantly affect weight or run time (**Fig. 3-2 B, C**) compared with WT. However, run distance and work were significantly lower in $Kv\beta2^{-/-}$ male mice after 4-weeks FTR (**Fig. 3-2 D, E**).

*4-weeks exe enhanced cardiac function with dobutamine challenge.*

Cardiac diastolic function improved in WT male mice after 4-weeks exe. The percent change of end diastolic volume (EDV), the volume of the left ventricle (LV) when maximally dilated, was greater in WT exercised males than their sedentary controls that showed a significant decrease in EDV (**Fig. 3-3 A, C**). Additionally, end systolic volume (ESV), was significantly lower in WT sedentary animals suggesting greater maximal contraction with dobutamine challenge (**Fig. 3-3 B**). The percent change for both EDV and ESV from rest to stress was significantly depressed in sedentary WT mice compared to exercised mice (**Fig. 3-3 C**). Measures of cardiac function, ejection fraction (EF) and fractional shortening (FS) increased from rest with dobutamine challenge (a.k.a., stress) in all WT groups (**Fig. 3-3 D, E**). However, the percent change (a.k.a., difference of rest and stress) was significantly lower in exercised animals (**Fig. 3-3 F**). Global longitudinal strain (GLS), was not significantly enhanced after 4-weeks exercise training (**Fig. 3-3 G**). However, the percent change in GLS was significantly greater in WT exercised animals, compared with their sedentary controls (**Fig. 3-3 I**). Additionally, the global longitudinal strain rate, or the 'speed' at which the endocardial wall of the LV travels from diastole to systole was not significantly enhanced with 4-weeks forced treadmill exercise (**Fig. 3-3 H**).

*Exercise enhances Kvβ2 in coronary artery vascular smooth muscle cells.*

Exercise enhances Kv current density,[42] and the composition of the Kvβ-subunit complex determines the sensitivity of the channel to co-factors NADH and $NAD^+$ and modifies the vasodilatory response.[37,132,168] Therefore, we inferred that exercise enhances the presence of Kvβ2 over Kvβ1 in the Kv channel complex. Therefore, we utilized the proximity ligation assay which shows the associations of proteins within 40 nm. After 4-weeks of forced treadmill running that there was a significant increase in Kv1.5:Kvβ2 in coronary vascular smooth muscle cells from exercised WT male mice (**Fig. 3-4 B**). There was no significant increase in Kv1.5:Kvβ1 in exercised or sedentary controls.

*4-weeks of exercise enhanced cardiac function, and myocardial blood flow in WT male mice*.

Both sedentary and exercised male mice had significant increases in heart rate following dobutamine challenge (**Fig. 3-5 A**). However, cardiac output (CO; HRxSV) was significantly increased in only exercised animals (**Fig. 3-5 B**). The percent change in heart rate (HR) was significantly lower, and the percent change in (cardiac output) CO was significantly greater in exercised animals (**Fig. 3-5 C**). Relative myocardial blood flow (MBF) as a function of CO increased significantly in exercised WT mice (**Fig. 3-5 D**). The ΔMBF in respect to ΔCO also significantly increased after 4-weeks exercise training (**Fig. 3-5 E**).

*Ablation of Kvβ2 impairs the benefits of exercise to the heart.*

In Kvβ2$^{-/-}$ male mice, EDV was not significantly impacted by increased work, and exercise made no significant impact (**Fig. 3-6 A**). Both sedentary and exercised Kvβ2$^{-/-}$ mice had significant decreases in ESV with dobutamine challenge (**Fig. 3-6 B**). Additionally, EF and FS increased with dobutamine challenge but were not significantly different between sedentary and exercised groups (**Fig. 3-6 D, E**). However, the percent change in EF and FS were significantly lower in exercised Kvβ2$^{-/-}$ male mice compared with their sedentary controls (**Fig. 3-6 F**). Both GLS and GLSR were not significantly different between sedentary and exercised Kvβ2-/- male mice, however, the percent change in GLS was significantly greater after 4-weeks exe (**Fig. 3-6 G-I**).

*4-weeks of exercise did not enhance cardiac function, and myocardial blood flow in Kvβ2$^{-/-}$ male mice.*

In response to dobutamine challenge both sedentary and exercised Kvβ2-/- male mice had significant increases in HR and CO (**Fig. 3-7 A, B**). However, 4-weeks exe did not significantly change HR or CO as compared to sedentary controls. Additionally, percent change in both HR and CO significantly declined in exercised Kvβ2$^{-/-}$ male mice (**Fig. 3-7 C**). MBF as a function of CO significantly increased in sedentary Kvβ2$^{-/-}$ male mice with dobutamine challenge but did not exceed the declining MBFxCO of the exercised Kvβ2$^{-/-}$ male mice (**Fig. 3-7 D**). Additionally,

the ΔMBFxΔCO of exercised Kvβ2$^{-/-}$ male mice was lower than their sedentary controls (**Fig. 3-7 E**).

*Metabolic phenotyping in wild type and Kvβ2$^{-/-}$ animals.*

We assessed whether loss of Kvβ2 is associated with major alterations in metabolic phenotype or diurnal behavior patterns. For this, we performed indirect gas calorimetry ($VO_2$, $VCO_2$, RER, energy expenditure), measurements of activity (movement), and food and water consumption over a 24 hr period in Kvβ2$^{-/-}$ and age-matched wild (WT) type animals. Values of $VO_2$, $VCO_2$, RER, and energy expenditure were significantly higher at night (6 pm – 6 am) compared with day (6 am – 6 pm) for both WT and Kvβ2$^{-/-}$ mice (**Fig. 3-8 A-C**). While modest (<5%) increases in $VO_2$ and $VCO_2$ and decrease in RER were noted at night in Kvβ2$^{-/-}$ animals compared with wild type animals, day values were not different between groups. Both day and night values of energy expenditure were significantly increased (~5%) in Kvβ2$^{-/-}$ animals. However, no differences in day or night total activity levels, nor food and water consumption were found between Kvβ2$^{-/-}$ and wild type animals (**Fig. 3-8 D-F**).

*Exercise compliance is not impacted by ablation of Kvβ2.*

Following initial ECT, animals were subjected to an exercise training regimen consisting of a period of forced treadmill running 5 days per week for 4 weeks. At the end of the exercise training period, cardiac function was examined by

echocardiography. When animals were subjected to run for 40-60 minutes at 50% of their maximum exercise intensity determined during initial ECTs, there were no differences in protocol compliance between wild type and Kvβ2$^{-/-}$ for the duration of the exercise training procedure. As shown in Figure 3-9, the percent of completed exercise sessions and percent of total exercise time completed for the total four-week training period (>90% for each) was similar between experimental groups.

*Physiological hypertrophy following exercise training requires Kvβ2 subunits.*

Based on the afore-mentioned results, we further examined heart morphology in wild type versus Kvβ2$^{-/-}$ exercised and sedentary animals. Consistent with heart dimensions determined by echocardiography, at harvest (24 hours after final exercise session), we found a significant increase in heart weight, normalized to tibia length and body weight, in wild type animals undergoing exercise conditioning compared with age-matched wild type sedentary control animals (**Fig. 3-10 A-C**). Heart weight was not significantly different in sedentary WT or Kvβ2$^{-/-}$ animals. Additionally, we did not observe a significant increase in heart weight in Kvβ2$^{-/-}$ exercised animals compared with sedentary control animals.

*Kvβ2 subunits are required for exercise induced cardiomyocyte hypertrophy.*

We addressed whether changes in heart weight were associated with cardiac myocyte morphology. Figure 3-11 A shows transverse heart sections stained with

wheat germ agglutinin conjugated with Alexa Fluor 555 to identify sarcolemma of individual cardiac myocytes. Consistent with echocardiographic data and heart weight findings, we found that cardiac myocyte cross sectional area was significantly greater in hearts of wild type, but not Kvβ2, exercised animals compared with corresponding sedentary control hearts. Figure 3-11 C shows histograms of cardiac myocyte cross sectional area for wild type and Kvβ2 exercise and sedentary hearts.

Changes in biochemical markers of cardiac growth in exercise are abolished by deletion of Kvβ2. We examined whether changes in heart morphology in wild type exercised, but not $Kv\beta2^{-/-}$ exercised hearts, were associated with changes in biochemical markers of cardiac growth. Consistent with previous reports, we found that wild type animals undergoing exercise conditioning exhibited an increase in transcript expression of cited4, which has been shown to be an essential mediator of exercise-induced cardiac growth.[194,195] Moreover, a negative regulator of Cited4 expression, CEBPβ, was reduced in hearts from wild type exercise animals compared with sedentary control animals. A marker of pathological remodeling of the heart, NFATc2, was reduced in hearts of exercised animals compared with sedentary control animals. Remarkably, in contrast to hearts from wild type exercise animals, changes in the expression of Cited4, CEBPβ and NFATc2 were abolished in $Kv\beta2^{-/-}$ exercised animals. Together, our data suggest that Kvβ subunits, which are metabolic regulators or Kv1/4 channels, are critical mediators of the physiological hypertrophy response to exercise conditioning.

## Discussion

Regulation of membrane potential in cardiovascular smooth muscle cells is maintained predominantly via Kv channels. The activity of Kv channels greatly influences the vasodilatory state of the coronary artery. The Kv channel intracellular β-subunit is a catalytically active protein, capable of sensing changes in oxygen availability and nucleotide redox ratios. Greater $O_2$ consumption by the heart decreases available $O_2$ causing the Kvβ2 dependent hypoxia vasodilation response. We can infer that in vivo this hypoxia response would increase coronary artery diameter, coronary flow, and myocardial perfusion. Increased coronary diameter translates to greater myocardial perfusion to match the $O_2$ demands of the heart, this allows for sustained pump function, and prevents injury and death. Regular challenges of increased cardiac work (i.e., exercise) induce cardiac hypertrophy and an even greater need to meet myocardial blood flow demands. Therefore, I investigated the impact of exercise on Kv channel composition, exercise capacity, and myocardial perfusion, in naïve and 4-week trained WT, Kvβ2$^{-/-}$ male mice.

Increased cardiac work (i.e., demand) requires a matching of $O_2$ and nutrient supply (i.e., vasodilation). Briefly during the transitional state between rest and stress the needs demand of the heart exceeds the supply met by the coronary artery. Additionally, this uncoupling of $O_2$ supply and demand is paired with a shift in metabolism. The altered metabolism drives altered pyridine redox ratio (e.g., NADH). In chapter 3 of this manuscript, we uncovered a physiologically relevant

role of Kvβ2 as a sensor of altered $O_2$ and NADH (via LDH and L-lactate) to induce Kv-mediated vasodilation. From these findings we inferred that ablation of Kvβ2 would likely impair the coronary vasodilatory response to increased cardiac work. We tested our hypothesis that animals lacking Kvβ2 would experience an impaired exercise capacity, because of impaired coronary perfusion. Therefore we investigated whether in WT animals chronic bouts of increased work (e.g., exercise) would enhance myocardial perfusion, exercise capacity, and Kv1.5:Kvβ2 channel composition.

We found that exercise capacity was significantly impaired with the ablation of Kvβ2. We observed significantly greater exercise capacity in both naïve and 4-week trained WT mice, that was not observed in naïve or trained Kvβ2$^{-/-}$ male mice. Additionally, we found that in coronary aortic smooth muscle cells isolated from exercised WT male mice there was a significant increase in Kv1.5:Kvβ2 as compared with sedentary controls. Interestingly, Kv1.5:Kvβ1 did not significantly change with exercise. These support the hypothesis that exercise increases the presence of Kvβ2 over Kvβ1 in the Kv-complex. Further, this shift in the complex composition could enhance the vasodilatory capacity of the coronary artery to respond to increased cardiac work. Finally, using contrast echocardiography we were able to observe and quantify the myocardial perfusion in hearts from sedentary and exercised animals at rest and during pharmacological stress challenge. We found that after 4-weeks forced treadmill running WT male mice had significantly greater myocardial perfusion in response to the stress challenge. However, we did not observe this in exercised Kvβ2$^{-/-}$ mice, in-fact myocardial

perfusion was significantly impaired and declined in response to the stress challenge. From these data we can infer that loss of Kvβ2 in the coronary artery significantly impairs vasodilatory reserve and does not enhance vasodilation in response to increased cardiac work. Additionally, these data support our hypothesis, that the voltage-gated potassium channel intracellular β-subunit acting as a sensor of altered nucleotide redox ratios and oxygen availability is a necessary component in mediating the cardiovascular adaptive response to exercise. Insufficient myocardial perfusion during repeated bouts of increased work deprives the heart $O_2$ and nutrients. Potentially incurring a reliance on anaerobic, energy poor, no or low growth metabolic pathways. This work provides novel insight into the relationship and importance of exercise, cardiovascular adaptation, and regulation of membrane potential excitability.

## Figures

### Figure 3-1

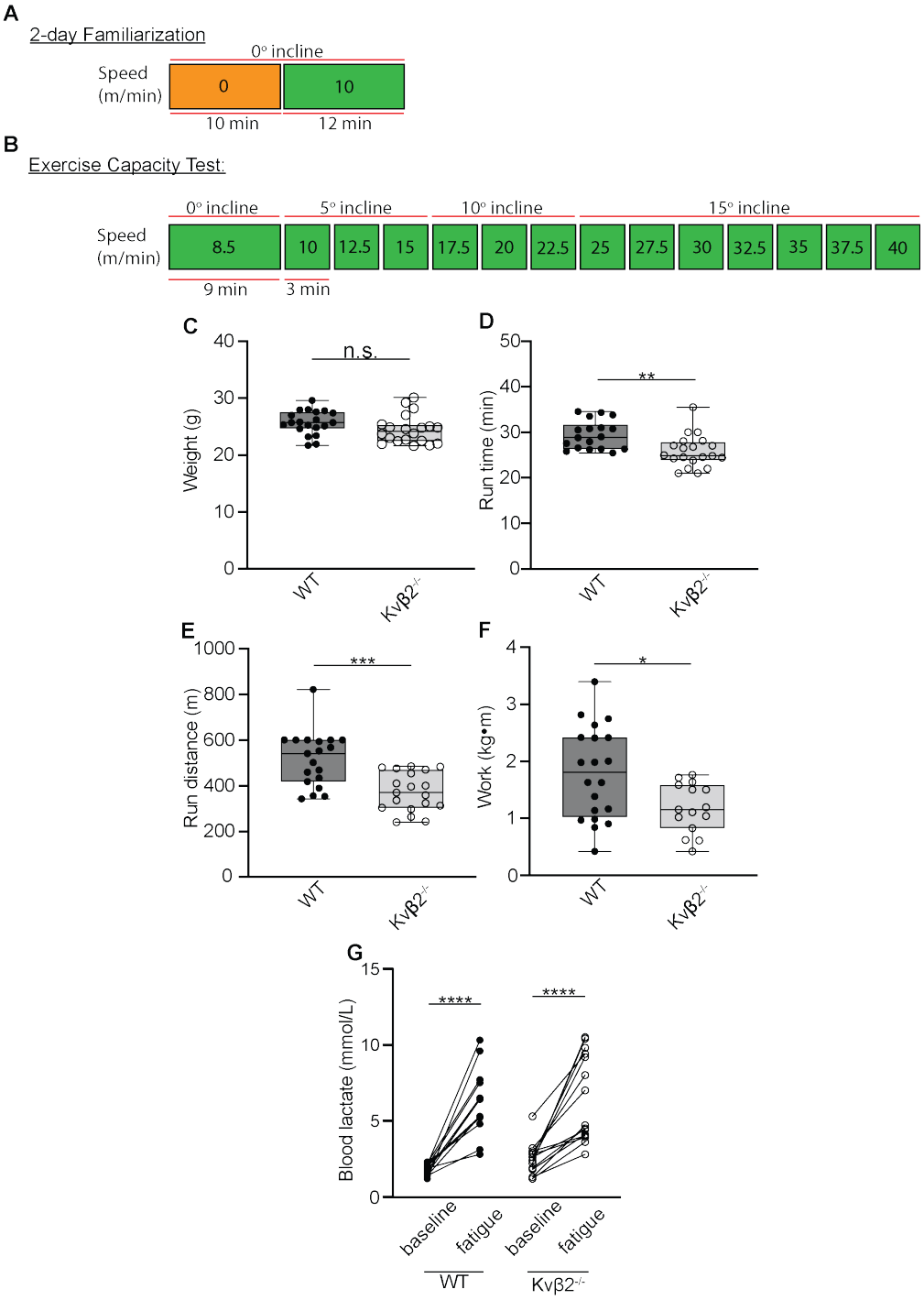


**Figure 3-1. Exercise capacity is impaired in naïve Kvβ2-knockout mice.** (a) Representative image showing the 2 days of familiarizing the animals to the treadmill and shock grid apparatus. (b) Exercise capacity protocol with incline,

speed and duration of each stage. (c) Weights of naive wildtype (WT) and Kvβ2-knockout ($Kv\beta2^{-/-}$) male mice. (d and e) Box and whiskey plots of run time and distance by WT and $Kv\beta2^{-/-}$ male mice. (f) Box and whisker plot of work done by WT and $Kv\beta2^{-/-}$ male mice. (g) Box and whisker plot of blood lactate measured at baseline and fatigue in WT and $Kv\beta2^{-/-}$ male mice.

**Figure 3-2**

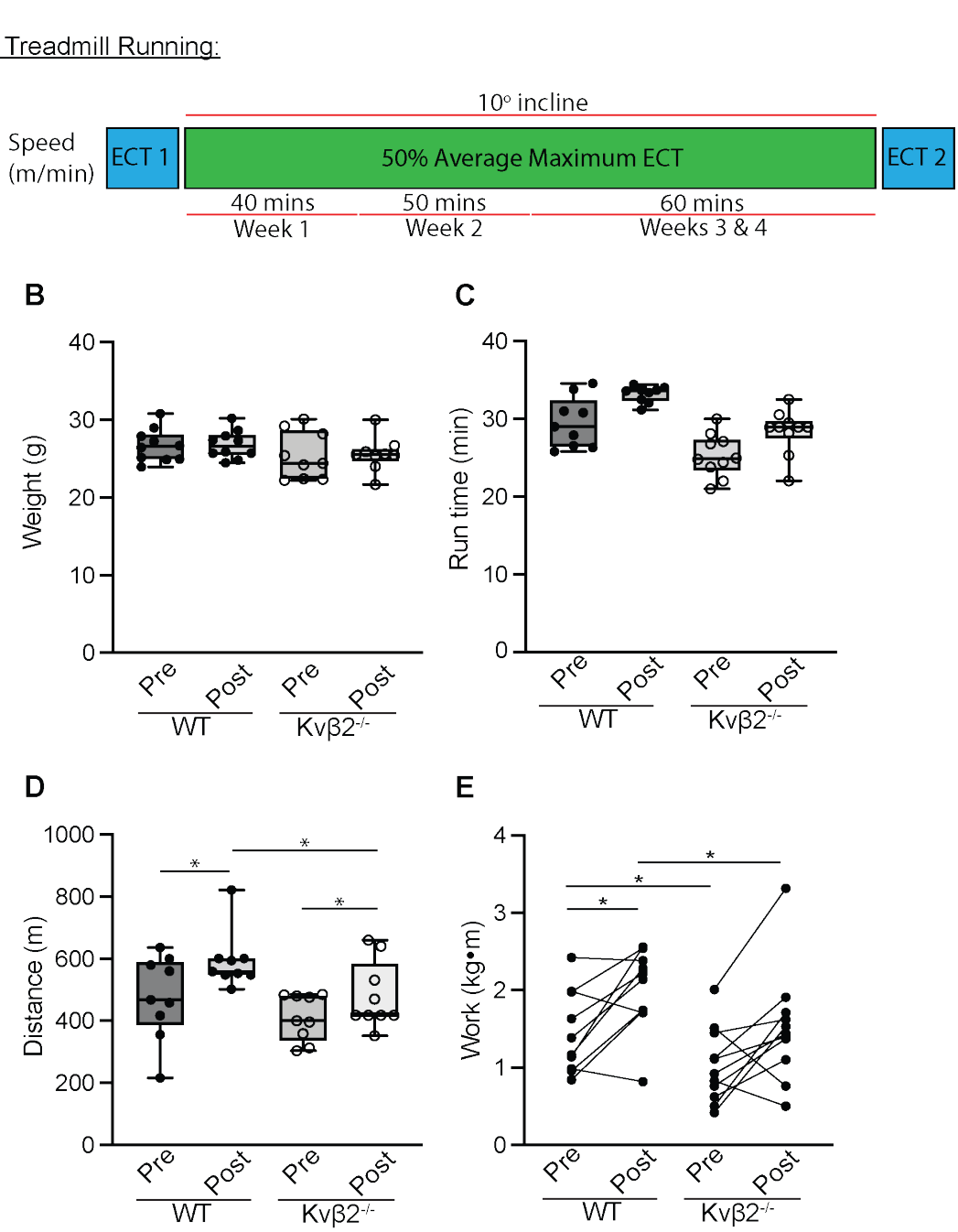


**Figure 3-2. Post 4-week forced treadmill running (FTR) exercise induced greater adaptation in WT male mice.** (A) Representative schematic of 4-week forced treadmill running (FTR) protocol. (B) Box and whisker plot of body weight of WT and Kvβ2$^{-/-}$ male mice pre- and post- 4-week exe. (C) Box and whisker plot

of run time and run distance in WT and Kvβ2$^{-/-}$ male mice after 4-week exe. (D) Paired dot and line plot of work conducted by WT and Kvβ2$^{-/-}$ male mice pre- and post- 4-week exe. P-value *<0.05.

**Figure 3-3**

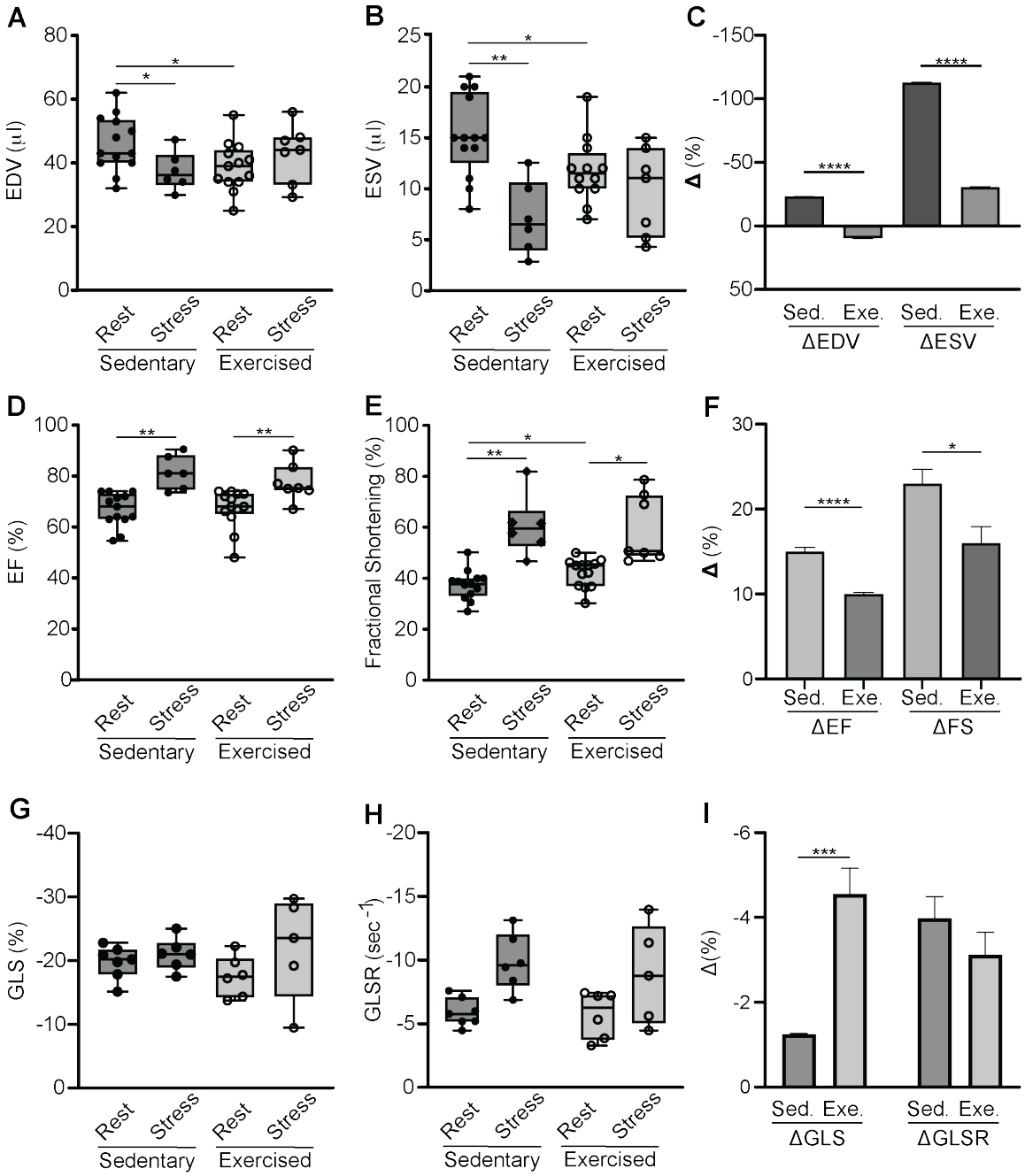


**Figure 3-3. 4-weeks exercise enhanced cardiac function in WT male mice.** (A, B, D, E, G, H) Box and whisker plots of end diastolic volume (EDV), end systolic volume (ESV), ejection fraction (EF), fractional shortening (FS), global longitudinal strain (GLS), and global longitudinal strain rate (GLSR). (C, F, I) Bar graphs

representing the percent change from rest to stress for EDV, ESV, EF, FS, GLS, and GLSR, respectively.

**Figure 3-4**

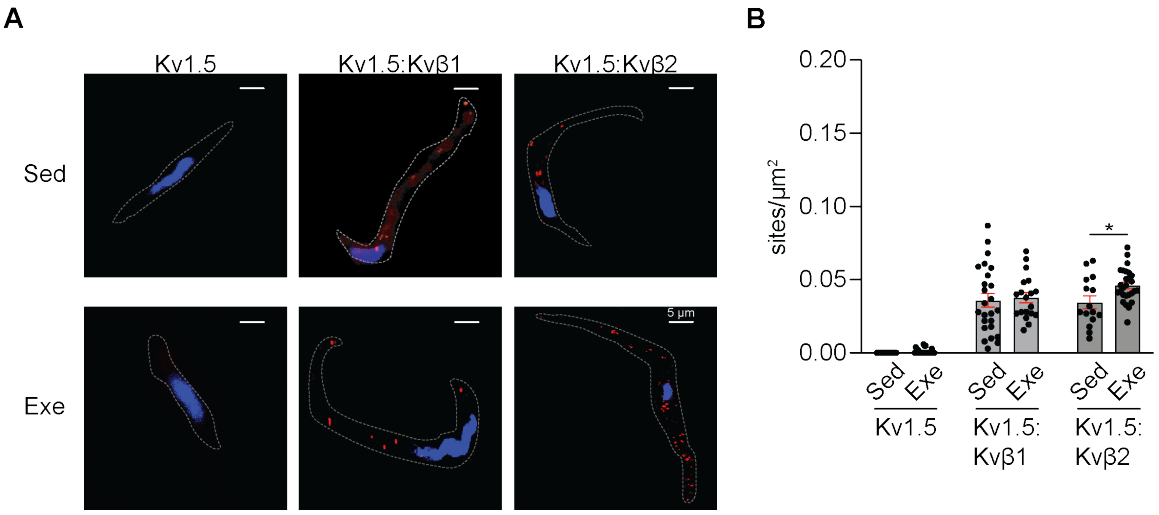


**Figure 3-4. 4-week exe increases Kv1.5:β2 proximity in isolated coronary vascular smooth muscle cells.** (A) Representative images of isolated coronary vascular smooth muscle cells from sedentary (top row) or exercised (bottom row) WT male mice (scale bars represent 5 μm). The nuclei are represented in blue (DAPI), and puncta in red (Cy3) represent either Kv1.5:Kvβ1 or Kv1.5:Kvβ2, as indicated by the column header. Scale bars = 5 μm. (B) Graphical representation of the quantified puncta from the respective conditions and targets. P-vale *<0.05.

**Figure 3-5**

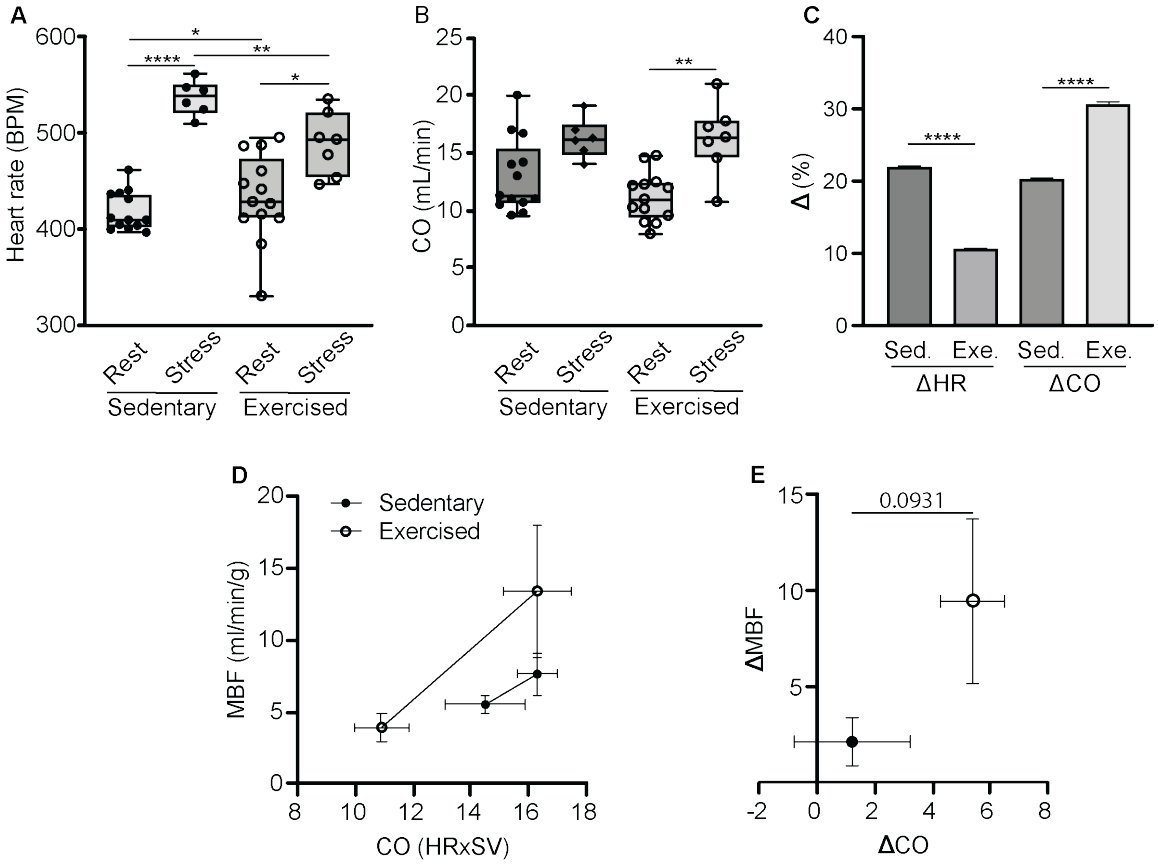


**Figure 3-5. 4-weeks of exercise enhanced cardiac function, and myocardial blood flow in WT male mice.** (A, B) box and whisker plot of heart rate (HR; bpm) and cardiac output (CO; HRxSV) from sedentary and exercised WT male mice. (C) Bar graph of the percent change (Δ%) from rest to stress of HR and CO in sedentary and exercised male mice. (D) Linear regression graph of myocardial blood flow (MBF) as a function of CO in sedentary (closed dot) and exercised (open dot) male mice. (E) XY graph of the ΔMBF as a function of ΔCO in sedentary (closed dot) and exercised (open dot) male mice.

**Figure 3-6**

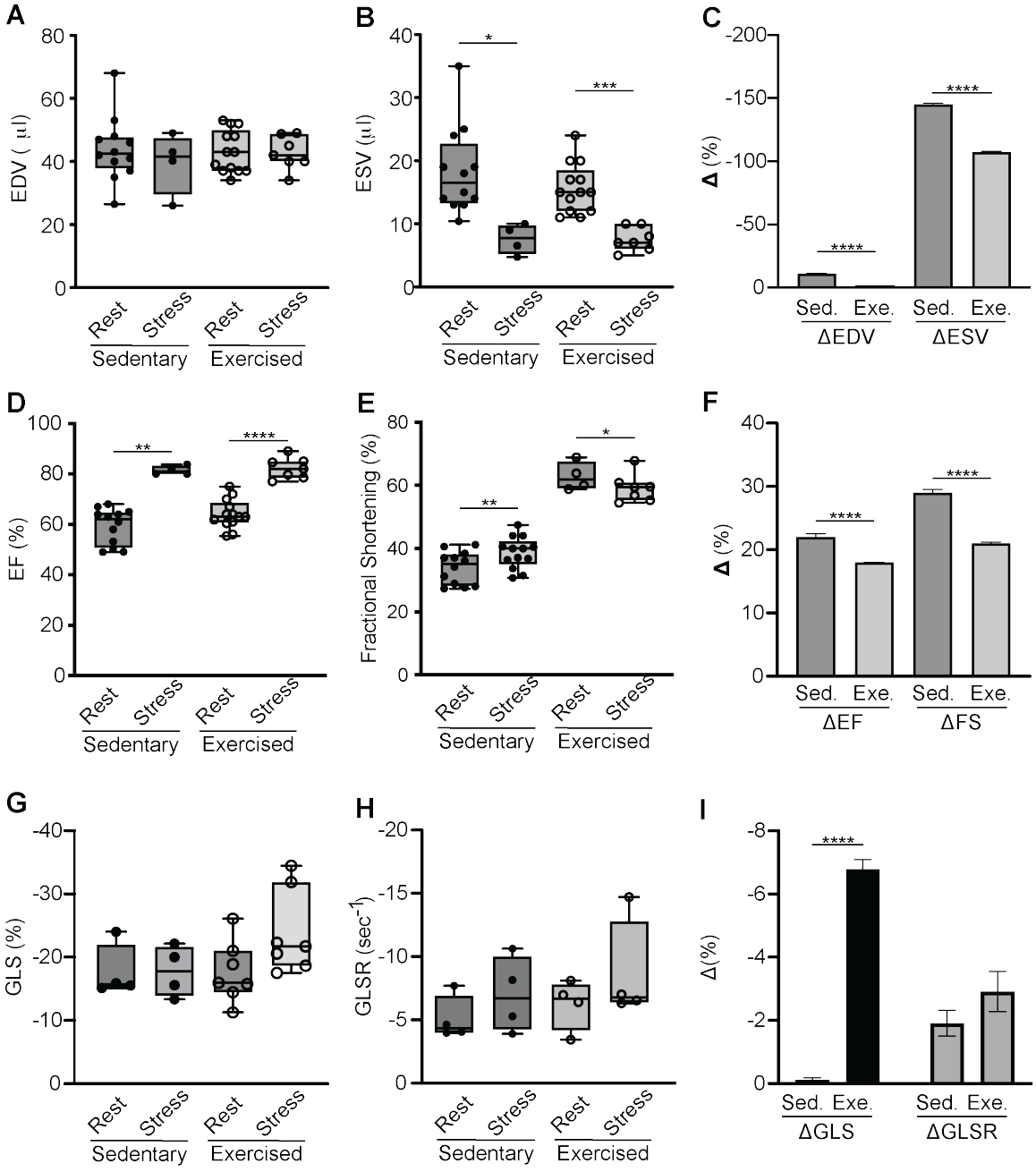


**Figure 3-6. 4-weeks exe had minimal impact on improving cardiac function in Kvβ2-/- male mice.** (A, B, D, E, G, H) Box and whisker plots of end diastolic volume (EDV), end systolic volume (ESV), ejection fraction (EF), fractional shortening (FS), global longitudinal strain (GLS), and global longitudinal strain rate

(GLSR). (C, F, I) Bar graphs representing the percent change from rest to stress for EDV, ESV, EF, FS, GLS, and GLSR, respectively.

**Figure 3-7**

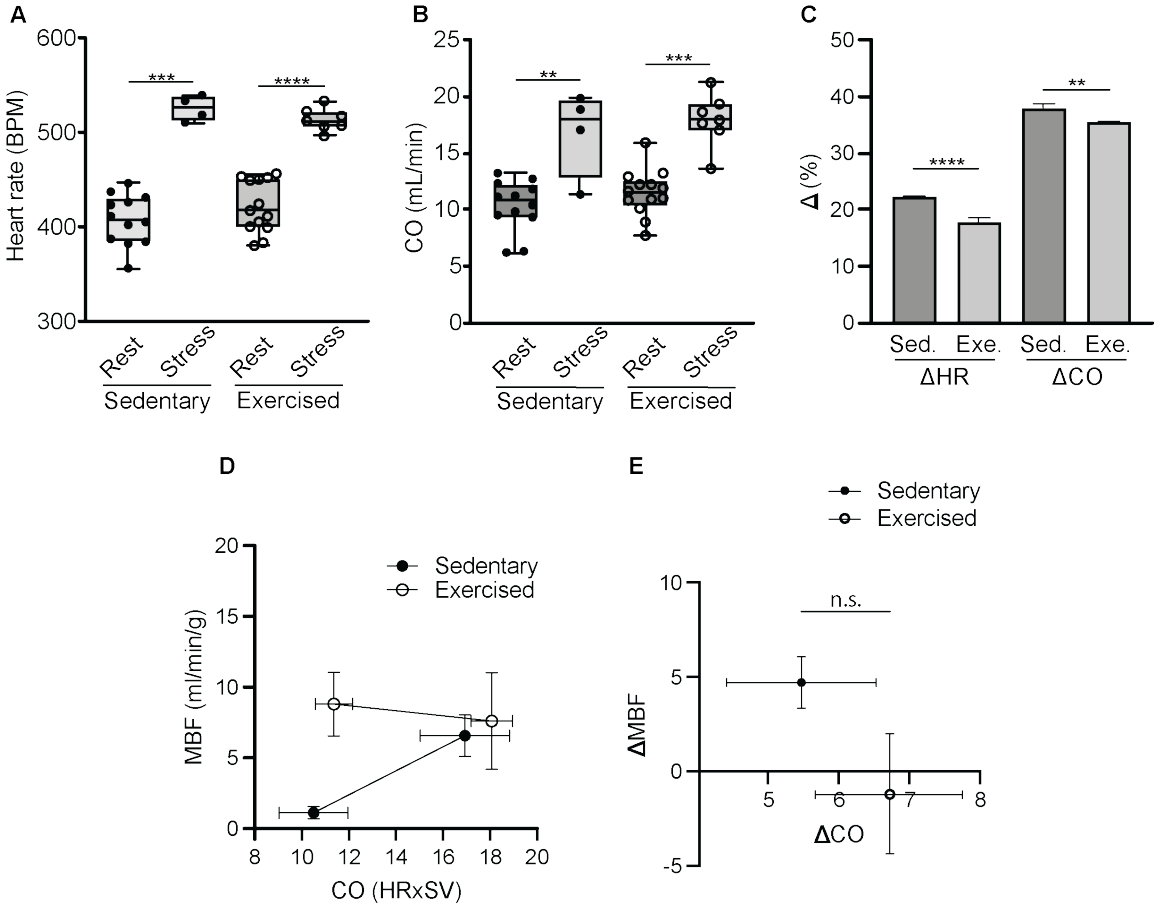


**Figure 3-7 4 weeks of exercise did not enhance myocardial blood flow in Kvβ2$^{-/-}$ male mice.** (A, B) box and whisker plot of heart rate (HR; bpm) and cardiac output (CO; HRxSV) from sedentary and exercised Kvβ2$^{-/-}$ male mice. (C) Bar graph of the percent change (Δ%) from rest to stress of HR and CO in sedentary and exercised male mice. (D) Linear regression graph of myocardial blood flow (MBF) as a function of CO in sedentary (closed dot) and exercised (open dot) male mice. (E) XY graph of the ΔMBF as a function of ΔCO in sedentary (closed dot) and exercised (open dot) male mice.

**Figure 3-8**

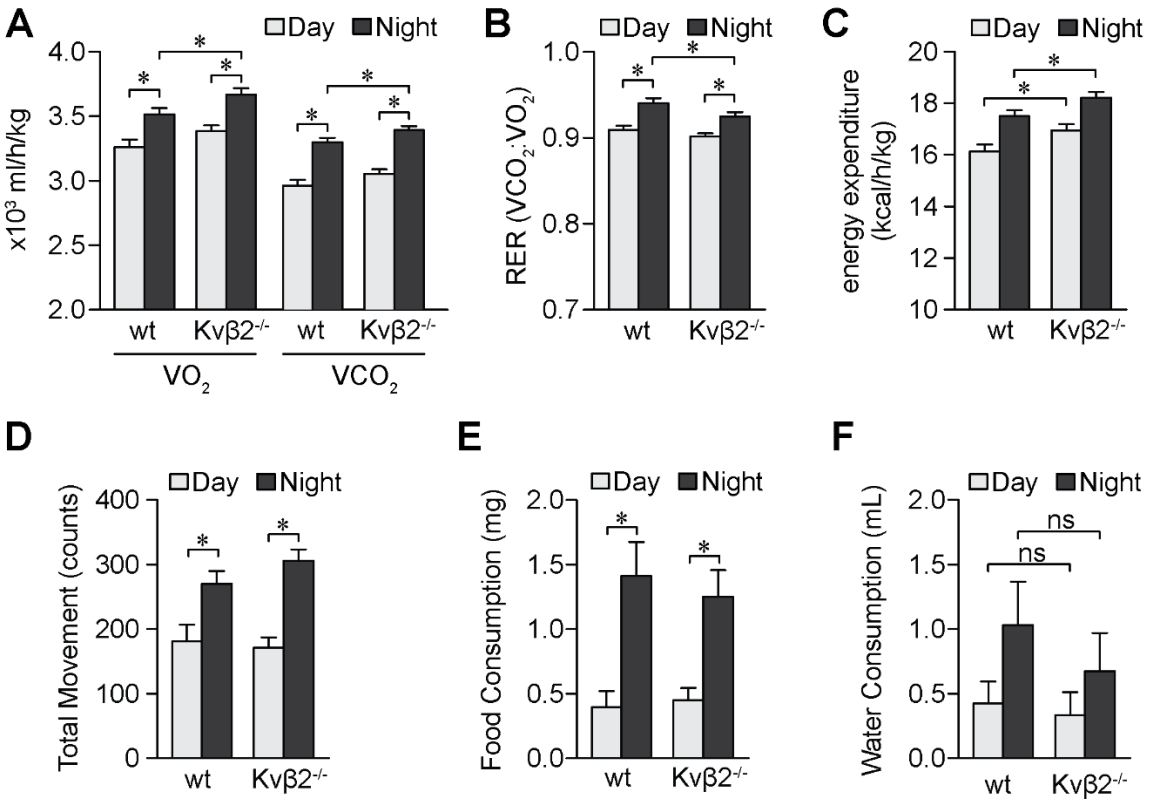


**Figure 3-8. Mice lacking Kvβ2 subunits same metabolic phenotype as WT male mice.** (**A-C**) Metabolic phenotyping of wild type and Kvβ2-null ($Kv\beta2^{-/-}$) animals (n = 8 animals each). Shown are day (6 am – 6 pm) and night (6 pm – 6 am) values of mean oxygen consumption ($VO_2$), carbon dioxide consumption ($VCO_2$) (**A**), respiratory exchange ratio (RER; $VCO_2$ : $VO_2$) (**B**), and energy expenditure (**C**). (**D-F**) Summaries of day and night total movement (sum of course and fine motion, **D**), food consumption (**E**), and water consumption (**F**). *P<0.05. ns: P>0.05.

**Figure 3-9**

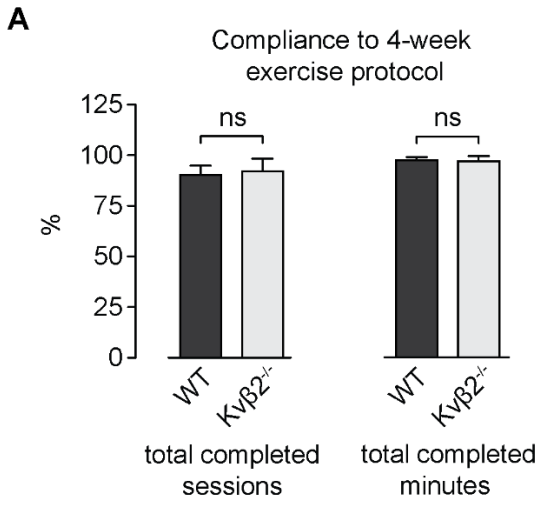


**Figure 3-9. Adaptations in exercise capacity following four weeks of treadmill running are attenuated in Kvβ2-null animals.** (**A**) Summary of exercise sessions and the total exercise time completed, expressed as a percent of the total exercise sessions time over a four week (5 days/week) treadmill exercise protocol, for wild type and Kvβ2$^{-/-}$ animals (n = 6 animals each). *P<0.05. ns: P>0.05.

**Figure 3-10**

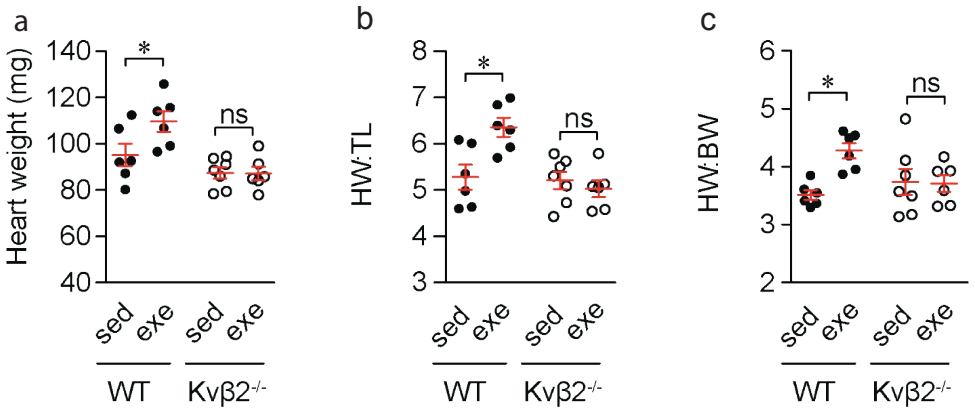


**Figure 3-10. Adaptive increases in heart size in wild type, but not Kvβ2-null animals following treadmill exercise conditioning.** (RWT = 2 x LVPWd / left ventricular internal diameter) (a-c) Summary of heart weight (HW) and heart weight normalized to tibia length (TL) and total body weight (BW) in sedentary and exercised wild type and Kvβ2$^{-/-}$ animals. *P<0.05, ns: P>0.05. n = 6 animals each group.

**Table 1: Body mass of sedentary and exercised wild type and Kvβ2-/- mice.**

| | **Body mass (g)** | **Lean mass (%)** | **Fat mass (%)** |
|---|---|---|---|
| Wild type | **Post-training** | | |
| *Sedentary* | 28 ± 1.2 | 72.3 ± 0.8 | 27.0 ± 0.8 |
| *Exercise* | 26 ± 1.1 | 80.2 ± 1.9* | 20.0 ± 1.8* |
| $Kv\beta2^{-/-}$ | | | |
| *Sedentary* | 25 ± 1.2 | 75.1 ± 1.8 | 24.9 ± 1.7 |
| *Exercise* | 25 ± 0.8 | 78.2 ± 0.5 | 21.8 ± 0.6 |

Values are mean ± SEM. *P<0.05 vs. sedentary. N = 6 animals per group.

**Table 2: Comparison of echocardiographic parameters in wild type and Kvβ2-/- exercised and sedentary mice and at baseline and during dobutamine challenge.**

| Baseline | | | | | | | | | | | | | |
|---|---|---|---|---|---|---|---|---|---|---|---|---|---|
| | Wildtype | | | | | | | Kvβ2-/- | | | | | |
| | Sedentary | | | Exercised | | | | Sedentary | | | Exercised | | |
| | Mean | | SEM | Mean | | SEM | | Mean | | SEM | Mean | | SEM |
| HR (bpm) | 419 | ± | 5.7 ♯♯♯ | 437 | ± | 14.3*, ♯♯ | | 409 | ± | 8 ♯♯♯♯ | 423 | ± | 8 ♯♯♯♯ |
| Endocardial Values | | | | | | | | | | | | | |
| EDV (µl) | 46 | ± | 2.42 ♯ | 39 | ± | 2.6* | | 44 | ± | 2.97 | 43 | ± | 1.88 |
| ESV (µl) | 15 | ± | 1.09 ♯♯♯ | 13 | ± | 1.85 ♯♯♯ | | 18 | ± | 1.97 ♯♯♯ | 16 | ± | 1.06 ♯♯♯ |
| SV (µl) | 32 | ± | 2.06 ♀ | 26 | ± | 1.4* | | 26 | ± | 1.42 | 28 | ± | 1.25 |
| EF (%) | 67 | ± | 1.84 ♀, ♯♯♯ | 68 | ± | 2.36 ♯♯ | | 59 | ± | 2.07 ♯♯♯ | 64 | ± | 1.59 ♯♯♯♯ |
| CO (ml/min) | 13 | ± | 0.91 ♀ | 11 | ± | 0.70 ♯♯ | | 11 | ± | 0.65 ♯♯ | 12 | ± | 0.56 ♯♯♯ |
| Chamber Diameter | | | | | | | | | | | | | |
| LVIDd (mm) | 3.64 | ± | 0.07 ♯♯♯ | 3.50 | ± | 0.09 ♯♯ | | 3.49 | ± | 0.08 ♯ | 3.56 | ± | 0.06 ♯ |
| LVIDs (mm) | 2.28 | ± | 0.08 ♯♯♯♯ | 1.99 | ± | 0.09 *, ♯♯♯ | | 2.31 | ± | 0.08 ♯♯♯♯ | 2.18 | ± | 0.05 ♯♯♯♯ |
| Wall Thickness | | | | | | | | | | | | | |
| LVPWd (mm) | 1.03 | ± | 0.06 | 1.14 | ± | 0.078 ♀ | | 0.94 | ± | 0.04 | 0.91 | ± | 0.06 |
| LVPWs (mm) | 1.47 | ± | 0.09 ♯ | 1.60 | ± | 0.069 ♀ | | 1.31 | ± | 0.04 | 1.32 | ± | 0.06 ♯ |
| LVAWd (mm) | 1.10 | ± | 0.07 | 1.19 | ± | 0.09 | | 1.04 | ± | 0.05 | 1.06 | ± | 0.04 |
| LVAWs (mm) | 1.54 | ± | 0.09 ♯♯♯ | 1.66 | ± | 0.09 | | 1.41 | ± | 0.05 ♯♯ | 1.57 | ± | 0.05 |
| RWT | 0.57 | ± | 0.03 ♯♯♯ | 0.65 | ± | 0.05 ♀ | | 0.54 | ± | 0.03 | 0.52 | ± | 0.04 |
| n | 13 | | | 13 | | | | 12 | | | 13 | | |

| Stress | | | | | | | | | | | | | |
|---|---|---|---|---|---|---|---|---|---|---|---|---|---|
| | Wildtype | | | | | | | Kvβ2-/- | | | | | |
| | Sedentary | | | Exercised | | | | Sedentary | | | Exercised | | |
| | Mean | | SEM | Mean | | SEM | | Mean | | SEM | Mean | | SEM |
| HR (bpm) | 537 | ± | 7.4 ** | 490 | ± | 12 | | 526 | ± | 7 | 514 | ± | 5 |
| Endocardial Values | | | | | | | | | | | | | |
| EDV (µl) | 37 | ± | 2 | 43 | ± | 3 | | 40 | ± | 5 | 43 | ± | 2 |
| ESV (µl) | 7 | ± | 1 | 10 | ± | 2 | | 7 | ± | 1 | 8 | ± | 1 |
| SV (µl) | 30 | ± | 1 | 33 | ± | 3 | | 32 | ± | 4 | 35 | ± | 2 |
| EF (%) | 81 | ± | 3 | 77 | ± | 3 | | 81 | ± | 1 | 82 | ± | 2 |
| CO (ml/min) | 16 | ± | 1 | 16 | ± | 1 | | 17 | ± | 2 | 18 | ± | 1 |
| Chamber Diameter | | | | | | | | | | | | | |
| LVIDd (mm) | 2.89 | ± | 0.18 | 3.02 | ± | 0.17 | | 3.20 | ± | 0.18 | 3.28 | ± | 0.09 |
| LVIDs (mm) | 1.18 | ± | 0.19 | 1.27 | ± | 0.21 | | 1.20 | ± | 0.13 | 1.34 | ± | 0.07 |
| Wall Thickness | | | | | | | | | | | | | |
| LVPWd (mm) | 1.39 | ± | 0.09 | 1.19 | ± | 0.09 | | 1.16 | ± | 0.09 | 1.13 | ± | 0.07 |
| LVPWs (mm) | 2.03 | ± | 0.14 | 1.79 | ± | 0.12 | | 1.77 | ± | 0.17 | 1.82 | ± | 0.05 |
| LVAWd (mm) | 1.41 | ± | 0.07 | 1.36 | ± | 0.09 | | 1.18 | ± | 0.08 | 1.10 | ± | 0.05 |
| LVAWs (mm) | 2.12 | ± | 0.08 | 1.89 | ± | 0.13 | | 1.94 | ± | 0.09 | 1.87 | ± | 0.04 |
| RWT | 1.00 | ± | 0.14 | 0.82 | ± | 0.10 | | 0.73 | ± | 0.08 | 0.69 | ± | 0.05 |
| n | 6 | | | 7 | | | | 4 | | | 7 | | |

Abbreviations: HR, heart rate; BPM, beats per minute; EDV, end diastolic volume; ESV, end systolic volume; SV, stroke volume; EF, ejection fraction; FS, fractional shortening; CO, cardiac output; LVIDd, left ventricular inner diameter at diastole; LVIDs, left ventricular inner diameter at systole; LVPWd, left ventricular posterior wall at diastole; LVPWs, left ventricular posterior wall at systole; LVAWd, left

ventricular anterior wall at diastole; LVAWs, left ventricular anterior wall at systole; RWT, relative wall thickness. P-value indicated as "*" is comparing sedentary to exercised within each group, "♀" compares sedentary to sedentary or exercised to exercised between each group, "♂" compares rest to stress within each group. Number of animals are listed at the bottom of the respective columns for each condition.

# CHAPTER 6: DISCUSSION, CONCLUSIONS AND FUTURE DIRECTIONS

## Discussion

A question that remains from the present study is whether the vasculature becomes sensitized as a response to cardiac hypertrophy or if the reverse is true. To better state this as multiple questions; 1) Does enhanced coronary vasodilation occur due to regular demands placed on the artery; or 2) is the heart able to undergo physiological hypertrophy because of the increased blood flow and sensitivity of the coronary artery? Both cardiac and arterial myocytes have similar Kv channel compositions including Kvβ1 and Kvβ2. However, due to the overwhelming influence of the Kv channel on membrane potential it is difficult to ascertain the individual tissues dependence on Kv channel composition. There exists a population of individuals with Brugada syndrome, where patients exhibit a point mutation in Kvβ2 expressed in the heart which during increased stress can cause them to experience dysrhythmias and sudden death.[193]. Furthermore, loss of Kvβ2 has been linked to epilepsy, poor prognosis of adenocarcinoma, issues with learning and memory retention, and Alzheimer's. [132,196-199] Understanding, the effect and prevalence of point mutations such as this in human populations may lead to addressing these questions.

The wide distribution of Kv channels and Kvβ-subunits throughout body make for greater complexity in using drugs to impair or enhance the channels activities. It is first important to understand which Kvα and Kvβ-subunits are highly expressed in which tissues. We have previously detailed what is known in the literature in Raph et al., 2018, "*Biochemical and physiological properties of K(+) channel-associated AKR6A (Kvβ) proteins*" and Dwenger, Raph et al., 2022, "*Diversification of potassium currents in excitable cells via Kvβ proteins.*" While there are several drugs and toxins such as, psora-4 (inhibits Kv1 channels) and Iberiotoxin (inhibits $BK_{Ca}$), little is known about drugs that target the Kvβ-subunits and enhance their enzymatic or Kv-modifying activities. There has been some research into inhibition of the Kvβ-subunits, Alka et al., 2014 found that DOPAC, cortisone, and valproate can all, directly or indirectly, impair Kvβ-subunit activity.[154] Additionally, Xu et al., 1997, showed that the Kvβ2-subunit can relieve or inhibit Kvβ1 inactivation of the Kv-channel.[157] However, there has been little if any works investigating whether enhancing the activity or sensitivity of the Kvβ-subunits is possible and in what contexts this may be beneficial. For instance, if as we have shown, enhanced Kvβ2 sensitivity, to signals of metabolic hyperemia, greatly increases vessel diameter and in turn myocardial perfusion. Then we can infer that a small molecular that similarly enhances Kvβ2 sensitivity might in-fact alleviate restricted myocardial perfusion in diabetic and obese individuals.

## Conclusions

The entirety of the work presented in this dissertation elucidates an important role of voltage-gated potassium channels and their intracellular β-

subunits as integral components of improved cardiovascular adaptation in response to exercise. The findings in these bodies of work demonstrate the following; 1) the composition of the Kvβ subunit complex significantly impacts vasodilation, $I_{KV}$, and myocardial blood flow; 2) the Kvβ2 subunit predominantly favors vasodilation in response to reduced nucleotide redox state; 3) vasodilation in response to $H_2O_2$ is modified by smooth muscle metabolic state via intracellular pyridine nucleotide redox state; 4) loss or displacement of the Kvβ2-subunit significantly impairs exercise capacity and cardiovascular adaptations to chronic exercise; 5) exercise drives an enhanced Kv:Kvβ2 relationship; 6) increased presence of Kvβ2 in the complex enhances myocardial perfusion. Collectively, I have shown that metabolic regulation of Kv1 activity, coronary vasoreactivity, and myocardial perfusion is modified by the composition of the Kvβ complex in arterial myocytes. Additionally, exercise-induced enhancement of MBF requires Kv channel remodeling to enhance Kvβ2 in the channel complex.

In the work contained in chapter 3, and further supported by appendix A, we demonstrated a physiologically relevant role for the Kvβ2-subunit as a sensor of altered $O_2$ availability and metabolic change. We demonstrated that in the absence of Kvβ2, during increased cardiac work, myocardial perfusion and sustained pump function are lost. From here, we further investigated the capacity of Kvβ2 to sense changes in $O_2$, and metabolism (i.e., L-lactate) at the isolated tissue level. We found that loss of Kvβ2 significantly impaired the vasodilatory capacity of isolated coronary and mesenteric small resistance arteries in response to hypoxia and L-lactate. Additionally, in whole cell and perforated patch clamp

experiments, we found that L-lactate significantly increased the Kv-mediated currents of coronary smooth muscle cells. In appendix A we utilized single channel patch clamp experiments to established that Kv:Kvβ2 single channel activity increases in response to NADH but not $NAD^+$. Further, in appendix A we established that there is a local increase in NADH:$NAD^+$ coronary tissues during increased cardiac work. From these findings we can summarize evidence that supports our hypothesis that: Kvβ2 is a sensor of shifts in $O_2$ and redox ratios during increased cardiac work. Further, that the loss of Kvβ2 diminishes Kv channel open probability and abolishes vasodilation in response to hypoxia and increased NADH. We can infer the loss of Kv-mediated vasodilation is due to impaired Kv facilitated membrane hyperpolarization. Interestingly we can use this to translates understand the phenomenon we observe with our *in vivo* contrast echocardiography experiments. In which we observed that loss of Kvβ2 significantly depresses myocardial perfusion in response to increased cardiac work.

In chapter 4 we address the complex question of how the Kv channel integrates multiple signals during altered metabolism. We further elucidated the role of the Kvβ subunits as sensors of altered metabolic conditions. First inhibiting the lactate dehydrogenase conversion of lactate and elevation of NADH, I found this significantly abolished lactate induced vasodilation. Further, using single channel patch clamp on isolated vascular smooth muscle cells I observed that addition of NADH significantly increased Kv channel activity. Additionally, I have shown that the endogenous vasodilator $H_2O_2$ induces vasodilation and increased

Kv channel activity. We furthered this investigation by inferring, based on the literature, that during increased cardiac work that local metabolites (NADH and $H_2O_2$) would also increase. As such, we concluded to investigate the effects of NADH and $H_2O_2$ at the level of the individual channel and isolated vessels. In the presence of both NADH and $H_2O_2$ I observed significant increases in $H_2O_2$-induced change in Kv channel open probability. Additionally, in isolated resistance arteries from WT animals I observed a significant increase in the vasodilatory response to $H_2O_2$ in the presence of NADH. Further, in arteries isolated from animals overexpressing Kvβ1 this phenomenon of an enhanced vasodilatory capacity in response to NADH and H2O2 was significantly abolished. These data demonstrate an enhanced vasodilatory capacity in response to metabolites that reflect conditions of increased cardiac work. Further, these data are evidence of a crucial role for the sensing capacity of Kvβ2 during altered metabolic conditions (i.e., increased cardiac work.

Regular exercise induces a chronic increase in cardiac work that demands greater $O_2$. The repeated responsiveness of coronary arteries to match blood flow needs drives an enhanced vasodilatory response met by the pairing of endogenous vasodilators (e.g., NADH and $H_2O_2$) and the increase in $O_2$ sensors (e.g., Kvβ2). The enhanced responsiveness and increased capacity of coronary blood flow creates a capacity for greater work and support for enhanced myocardial perfusion. I first tested whether the exercise capacity of naïve WT and Kvβ2-null animals differed, and we found that the Kvβ2-null animals did significantly less work than their WT counterparts. We then trained WT and Kvβ2-

null mice for 4 weeks using an established forced treadmill running protocol. Comparing WT exercised mice with their sedentary controls I observed a significant increase in exercise capacity. Additionally, utilizing the proximity ligation assay in coronary smooth muscle cells, I identified a significant increase in puncta associated with Kv1.5:Kvβ2 in WT exercised mice as compared with sedentary controls. Further, in Kvβ2-null exercised animals we saw a significantly depressed exercise capacity after 4-weeks of exercise training, as compared with the WT exercised group. Finally, we inferred from the work in chapter 3 that an impaired exercise capacity in the Kvβ2-null animals could result from impaired coronary vasodilatory capacity. Further, that this impaired coronary dilation would manifest as an impaired myocardial perfusion during increased cardiac stress. Therefore, we utilized the contrast echocardiography technique to visualize the rate of myocardial perfusion at rest and during pharmacologically induced increase in cardiac work. In WT exercised mice I observed a significant increase in the magnitude of myocardial perfusion as compared with sedentary controls. However, in the Kvβ2-null exercise animals had a significantly impaired myocardial perfusion as compared with their sedentary controls and WT exercised mice. Further reinforcing our hypothesis that Kvβ2 is a sensor of $O_2$ and altered local metabolic state as reflected by redox ratios. That the Kvβ2 sensor sensitizes or directly modifies Kv-mediated activity to favor a more hyperpolarized membrane potential, that translates to enhanced vasodilation. Loss of this enhanced vasodilatory capacity impairs myocardial perfusion and leads to impaired exercise capacity even after 4-weeks of exercise training.

## Future directions

Numerous cardiovascular diseases include some aspect of impaired resistance arterial function or reduced vasoactive responsiveness. There have been numerous reviews suggesting Kv and the Kvβ-subunits may be impaired in some disease states (i.e., diabetes). Interestingly, in diabetes there is often a nucleotide and ROS imbalance, as compared to observations in healthy individuals.[200] Certain stressors modify Kv1.5:Kvβ2, perhaps other stressors such as diabetes would favor enhanced Kv1.5:Kvβ1. We can infer, based on our studies and other publications, that enhanced Kvβ1 would favor a more vasoconstricted state. Any imbalance in both the signaling (i.e., decreased NADH) and positively responding sensor (Kvβ2) would suggest a detrimental outcome. There is also the potential that targeting the Kvβ subunits with small molecular to enhancer Kv channel activitiy may provide a novel means of enhancing vasodilation in diseases of non-obstructive vaso-dysfunction. Additionally, drugs that enhance the sensitivity of Kvβ2 in specific tissues with the intent of increasing tissue perfusion could reduce recovery time after injury, enhance myocardial perfusion in people with low exercise capacity. Conversely, targeting of Kvβ could be used to induce a vasoconstriction response to reduce blood loss, minimize internal bleeding, or reduce injury from myocardial reperfusion. Although we may speculate on the potential benefits of drugs targeting Kvβ any candidates would be decades away from clinical use.

## Study limitations

The present study presents novel insight into the physiological relevance of the Kvβ-subunits as regulators of vasodilation, myocardial perfusion, and in turn exercise capacity, however, there remain some limitations. The use of only male mice is disappointing, it is well established that in both exercise capacity, and cardiovascular adaptation that males and females differ.[201,202] As females make up approximately 49-51% of the human population, it is crucial to understand and establish relevant effects of disease and interventions (i.e., exercise) in both sexes. Additionally, the use of a global knockout animal model presents some difficulty in attributing outcomes to a single specific factor (i.e., Kvβ2). The present work would be greatly improved with the addition of either a tissue specific overexpression of Kvβ2 on the Kvβ2$^{-/-}$-background, or tissue specific overexpression of Kvβ1 to emulate the Kvβ2$^{-/-}$. The second condition is one we have previously shown works, associated interactions of Kv:Kvβ1 increase, while Kv:Kvβ2 decreases. This impaired both vasodilation in response to L-lactate and decreased myocardial blood flow in response to increased cardiac work similar to results observed in Kvβ2$^{-/-}$ animals.[37] Finally, the present study would have greatly benefited from the use of human subjects, and tissues. Researcher using animal models which may have evolved slight dissimilarities limit any direct comparison of results. Despite the existing moral and ethical questions around the use of both animal and human subjects in basic science research, it is important that we strive to further perfect our experimental models to better address the questions we are asking. Clinicians have shown that accurate echocardiographic measurements can reveal important

changes to cardiac function and myocardial perfusion.[203] Though despite the importance of the use of human subjects for the translational benefits we are limited by moral, ethical and financial bounds.

# REFERENCES


1. Mensah GA, Brown DW. An overview of cardiovascular disease burden in the United States. *Health Aff (Millwood)*. 2007;26:38-48. doi: 10.1377/hlthaff.26.1.38
2. Kendir C, van den Akker M, Vos R, Metsemakers J. Cardiovascular disease patients have increased risk for comorbidity: A cross-sectional study in the Netherlands. *Eur J Gen Pract*. 2018;24:45-50. doi: 10.1080/13814788.2017.1398318
3. Bassuk SS, Manson JE. Epidemiological evidence for the role of physical activity in reducing risk of type 2 diabetes and cardiovascular disease. *J Appl Physiol (1985)*. 2005;99:1193-1204. doi: 10.1152/japplphysiol.00160.2005
4. Pedersen BK, Saltin B. Exercise as medicine - evidence for prescribing exercise as therapy in 26 different chronic diseases. *Scand J Med Sci Sports*. 2015;25 Suppl 3:1-72. doi: 10.1111/sms.12581
5. Bramble DM, Lieberman DE. Endurance running and the evolution of Homo. *Nature*. 2004;432:345-352. doi: 10.1038/nature03052
6. Carrier DR. The advantage of standing up to fight and the evolution of habitual bipedalism in hominins. *PLoS One*. 2011;6:e19630. doi: 10.1371/journal.pone.0019630
7. Kinsey TE. Pheidippides and the Marathon run. *Br J Sports Med*. 1981;15:285-286. doi: 10.1136/bjsm.15.4.285
8. Grogan R. Run, Pheidippides, Run! The story of the Battle of Marathon. *Br J Sports Med*. 1981;15:186-189. doi: 10.1136/bjsm.15.3.186
9. Christensen DL, Nielsen TH, Schwartz A. Herodotos and Hemerodromoi: Pheidippides' Run from Athens to Sparta in 490 Bc from Historical and Physiological Perspectives. *Hermes-Z Klass Philo*. 2009;137:148-169.
10. Heiss HW, Barmeyer J, Wink K, Hell G, Cerny FJ, Keul J, Reindell H. Studies on the regulation of myocardial blood flow in man. I.: Training effects on blood flow and metabolism of the healthy heart at rest and during standardized heavy exercise. *Basic Res Cardiol*. 1976;71:658-675. doi: 10.1007/BF01906411
11. Heiss HW, Topfer M, Barmeyer J, Wink K, Huber G, Keul J. Studies on the regulation of myocardial blood flow in man. II. Effects of acute arterial hypoxia. *Clin Cardiol*. 1978;1:35-42. doi: 10.1002/clc.4960010106
12. Parodi O, De Maria R, Oltrona L, Testa R, Sambuceti G, Roghi A, Merli M, Belingheri L, Accinni R, Spinelli F, et al. Myocardial blood flow distribution in patients with ischemic heart disease or dilated cardiomyopathy undergoing heart transplantation. *Circulation*. 1993;88:509-522. doi: 10.1161/01.cir.88.2.509

13. Grynberg A, Demaison L. Fatty acid oxidation in the heart. *J Cardiovasc Pharmacol*. 1996;28 Suppl 1:S11-17. doi: 10.1097/00005344-199600003-00003
14. Erecinska M, Silver IA. ATP and brain function. *J Cereb Blood Flow Metab*. 1989;9:2-19. doi: 10.1038/jcbfm.1989.2
15. Fulghum K, Hill BG. Metabolic Mechanisms of Exercise-Induced Cardiac Remodeling. *Front Cardiovasc Med*. 2018;5:127. doi: 10.3389/fcvm.2018.00127
16. Kolwicz SC, Jr. An "Exercise" in Cardiac Metabolism. *Front Cardiovasc Med*. 2018;5:66. doi: 10.3389/fcvm.2018.00066
17. Kolwicz SC, Jr., Purohit S, Tian R. Cardiac metabolism and its interactions with contraction, growth, and survival of cardiomyocytes. *Circ Res*. 2013;113:603-616. doi: 10.1161/CIRCRESAHA.113.302095
18. Chandel NS. Glycolysis. *Cold Spring Harb Perspect Biol*. 2021;13. doi: 10.1101/cshperspect.a040535
19. Gertz EW, Wisneski JA, Stanley WC, Neese RA. Myocardial substrate utilization during exercise in humans. Dual carbon-labeled carbohydrate isotope experiments. *J Clin Invest*. 1988;82:2017-2025. doi: 10.1172/JCI113822
20. Juel C, Halestrap AP. Lactate transport in skeletal muscle - role and regulation of the monocarboxylate transporter. *J Physiol*. 1999;517 ( Pt 3):633-642. doi: 10.1111/j.1469-7793.1999.0633s.x
21. Pilegaard H, Domino K, Noland T, Juel C, Hellsten Y, Halestrap AP, Bangsbo J. Effect of high-intensity exercise training on lactate/H+ transport capacity in human skeletal muscle. *Am J Physiol*. 1999;276:E255-261. doi: 10.1152/ajpendo.1999.276.2.E255
22. Chinen I, Shimabukuro M, Yamakawa K, Higa N, Matsuzaki T, Noguchi K, Ueda S, Sakanashi M, Takasu N. Vascular lipotoxicity: endothelial dysfunction via fatty-acid-induced reactive oxygen species overproduction in obese Zucker diabetic fatty rats. *Endocrinology*. 2007;148:160-165. doi: 10.1210/en.2006-1132
23. Krylatov A, Maslov L, Tsibulnikov SY, Voronkov N, Boshchenko A, Downey J, Mentzer R. The Role of Reactive Oxygen Species, Kinases, Hydrogen Sulfide, and Nitric Oxide in the Regulation of Autophagy and Their Impact on Ischemia and Reperfusion Injury in the Heart. *Curr Cardiol Rev*. 2021;17:e230421186874. doi: 10.2174/1573403X16666201014142446
24. Krylatov AV, Maslov LN, Voronkov NS, Boshchenko AA, Popov SV, Gomez L, Wang H, Jaggi AS, Downey JM. Reactive Oxygen Species as Intracellular Signaling Molecules in the Cardiovascular System. *Curr Cardiol Rev*. 2018;14:290-300. doi: 10.2174/1573403X14666180702152436
25. Winter EM, Fowler N. Exercise defined and quantified according to the Systeme International d'Unites. *J Sports Sci*. 2009;27:447-460. doi: 10.1080/02640410802658461

26. Pinckard K, Baskin KK, Stanford KI. Effects of Exercise to Improve Cardiovascular Health. *Front Cardiovasc Med*. 2019;6:69. doi: 10.3389/fcvm.2019.00069
27. Liu Y, Lee DC, Li Y, Zhu W, Zhang R, Sui X, Lavie CJ, Blair SN. Associations of Resistance Exercise with Cardiovascular Disease Morbidity and Mortality. *Med Sci Sports Exerc*. 2019;51:499-508. doi: 10.1249/MSS.0000000000001822
28. Wilmot EG, Edwardson CL, Achana FA, Davies MJ, Gorely T, Gray LJ, Khunti K, Yates T, Biddle SJ. Sedentary time in adults and the association with diabetes, cardiovascular disease and death: systematic review and meta-analysis. *Diabetologia*. 2012;55:2895-2905. doi: 10.1007/s00125-012-2677-z
29. Metsios GS, Stavropoulos-Kalinoglou A, Veldhuijzen van Zanten JJ, Nightingale P, Sandoo A, Dimitroulas T, Kitas GD, Koutedakis Y. Individualised exercise improves endothelial function in patients with rheumatoid arthritis. *Ann Rheum Dis*. 2014;73:748-751. doi: 10.1136/annrheumdis-2013-203291
30. Stavropoulos-Kalinoglou A, Metsios GS, Veldhuijzen van Zanten JJ, Nightingale P, Kitas GD, Koutedakis Y. Individualised aerobic and resistance exercise training improves cardiorespiratory fitness and reduces cardiovascular risk in patients with rheumatoid arthritis. *Ann Rheum Dis*. 2013;72:1819-1825. doi: 10.1136/annrheumdis-2012-202075
31. Pedersen BK. Anti-inflammatory effects of exercise: role in diabetes and cardiovascular disease. *Eur J Clin Invest*. 2017;47:600-611. doi: 10.1111/eci.12781
32. Bruning RS, Sturek M. Benefits of exercise training on coronary blood flow in coronary artery disease patients. *Prog Cardiovasc Dis*. 2015;57:443-453. doi: 10.1016/j.pcad.2014.10.006
33. Bowles DK, Farrar RP, Starnes JW. Exercise training improves cardiac function after ischemia in the isolated, working rat heart. *Am J Physiol*. 1992;263:H804-809. doi: 10.1152/ajpheart.1992.263.3.H804
34. Chapman SB, Aslan S, Spence JS, Defina LF, Keebler MW, Didehbani N, Lu H. Shorter term aerobic exercise improves brain, cognition, and cardiovascular fitness in aging. *Front Aging Neurosci*. 2013;5:75. doi: 10.3389/fnagi.2013.00075
35. Gibb AA, McNally LA, Riggs DW, Conklin DJ, Bhatnagar A, Hill BG. Corrigendum: FVB/NJ Mice Are a Useful Model for Examining Cardiac Adaptations to Treadmill Exercise. *Front Physiol*. 2017;8:800. doi: 10.3389/fphys.2017.00800
36. Myers J, Prakash M, Froelicher V, Do D, Partington S, Atwood JE. Exercise capacity and mortality among men referred for exercise testing. *N Engl J Med*. 2002;346:793-801. doi: 10.1056/NEJMoa011858
37. Ohanyan V, Raph SM, Dwenger MM, Hu X, Pucci T, Mack G, Moore JBt, Chilian WM, Bhatnagar A, Nystoriak MA. Myocardial Blood Flow Control by Oxygen Sensing Vascular Kvbeta Proteins. *Circ Res*. 2021;128:738-751. doi: 10.1161/CIRCRESAHA.120.317715

38. Yoshinaga K, Beanlands RS, Dekemp RA, Lortie M, Morin J, Aung M, McKelvie R, Davies RF. Effect of exercise training on myocardial blood flow in patients with stable coronary artery disease. *Am Heart J*. 2006;151:1324 e1311-1328. doi: 10.1016/j.ahj.2006.03.008
39. Cole CR, Blackstone EH, Pashkow FJ, Snader CE, Lauer MS. Heart-rate recovery immediately after exercise as a predictor of mortality. *N Engl J Med*. 1999;341:1351-1357. doi: 10.1056/NEJM199910283411804
40. Cole CR, Foody JM, Blackstone EH, Lauer MS. Heart rate recovery after submaximal exercise testing as a predictor of mortality in a cardiovascularly healthy cohort. *Ann Intern Med*. 2000;132:552-555. doi: 10.7326/0003-4819-132-7-200004040-00007
41. Lombardo TA, Rose L, Taeschler M, Tuluy S, Bing RJ. The effect of exercise on coronary blood flow, myocardial oxygen consumption and cardiac efficiency in man. *Circulation*. 1953;7:71-78. doi: 10.1161/01.cir.7.1.71
42. Yang Y, Jones AW, Thomas TR, Rubin LJ. Influence of sex, high-fat diet, and exercise training on potassium currents of swine coronary smooth muscle. *Am J Physiol-Heart C*. 2007;293:H1553-H1563. doi: 10.1152/ajpheart.00151.2007
43. Nelson MT, Quayle JM. Physiological roles and properties of potassium channels in arterial smooth muscle. *Am J Physiol*. 1995;268:C799-822. doi: 10.1152/ajpcell.1995.268.4.C799
44. Duncker DJ, Bache RJ. Regulation of coronary blood flow during exercise. *Physiol Rev*. 2008;88:1009-1086. doi: 10.1152/physrev.00045.2006
45. Goodwill AG, Dick GM, Kiel AM, Tune JD. Regulation of Coronary Blood Flow. *Compr Physiol*. 2017;7:321-382. doi: 10.1002/cphy.c160016
46. Russell B, Motlagh D, Ashley WW. Form follows function: how muscle shape is regulated by work. *J Appl Physiol (1985)*. 2000;88:1127-1132. doi: 10.1152/jappl.2000.88.3.1127
47. Nakamura M, Sadoshima J. Mechanisms of physiological and pathological cardiac hypertrophy. *Nat Rev Cardiol*. 2018;15:387-407. doi: 10.1038/s41569-018-0007-y
48. Colan SD. Mechanics of left ventricular systolic and diastolic function in physiologic hypertrophy of the athlete heart. *Cardiol Clin*. 1992;10:227-240.
49. Colan SD, Sanders SP, MacPherson D, Borow KM. Left ventricular diastolic function in elite athletes with physiologic cardiac hypertrophy. *J Am Coll Cardiol*. 1985;6:545-549. doi: 10.1016/s0735-1097(85)80111-x
50. Tune JD, Richmond KN, Gorman MW, Feigl EO. Control of coronary blood flow during exercise. *Exp Biol Med (Maywood)*. 2002;227:238-250. doi: 10.1177/153537020222700404
51. Bazil JN, Beard DA, Vinnakota KC. Catalytic Coupling of Oxidative Phosphorylation, ATP Demand, and Reactive Oxygen Species Generation. *Biophys J*. 2016;110:962-971. doi: 10.1016/j.bpj.2015.09.036
52. Thengchaisri N, Kuo L. Hydrogen peroxide induces endothelium-dependent and -independent coronary arteriolar dilation: role of cyclooxygenase and

potassium channels. *Am J Physiol Heart Circ Physiol*. 2003;285:H2255-2263. doi: 10.1152/ajpheart.00487.2003
53. Spriet LL, Howlett RA, Heigenhauser GJ. An enzymatic approach to lactate production in human skeletal muscle during exercise. *Med Sci Sports Exerc*. 2000;32:756-763. doi: 10.1097/00005768-200004000-00007
54. Katz A, Sahlin K. Effect of decreased oxygen availability on NADH and lactate contents in human skeletal muscle during exercise. *Acta Physiol Scand*. 1987;131:119-127. doi: 10.1111/j.1748-1716.1987.tb08213.x
55. Ohanyan V, Yin L, Bardakjian R, Kolz C, Enrick M, Hakobyan T, Kmetz J, Bratz I, Luli J, Nagane M, et al. Requisite Role of Kv1.5 Channels in Coronary Metabolic Dilation. *Circ Res*. 2015;117:612-621. doi: 10.1161/CIRCRESAHA.115.306642
56. Gielen S, Hambrecht R. Effects of exercise training on vascular function and myocardial perfusion. *Cardiol Clin*. 2001;19:357-368. doi: 10.1016/s0733-8651(05)70222-8
57. Duncker DJ, Laxson DD, Lindstrom P, Bache RJ. Endogenous adenosine and coronary vasoconstriction in hypoperfused myocardium during exercise. *Cardiovasc Res*. 1993;27:1592-1597. doi: 10.1093/cvr/27.9.1592
58. Duncker DJ, van Zon NS, Pavek TJ, Herrlinger SK, Bache RJ. Endogenous adenosine mediates coronary vasodilation during exercise after K(ATP)+ channel blockade. *J Clin Invest*. 1995;95:285-295. doi: 10.1172/JCI117653
59. Borbouse L, Dick GM, Payne GA, Payne BD, Svendsen MC, Neeb ZP, Alloosh M, Bratz IN, Sturek M, Tune JD. Contribution of BK(Ca) channels to local metabolic coronary vasodilation: Effects of metabolic syndrome. *Am J Physiol Heart Circ Physiol*. 2010;298:H966-973. doi: 10.1152/ajpheart.00876.2009
60. Tune JD, Gorman MW, Feigl EO. Matching coronary blood flow to myocardial oxygen consumption. *J Appl Physiol (1985)*. 2004;97:404-415. doi: 10.1152/japplphysiol.01345.2003
61. Doerschug KC, Delsing AS, Schmidt GA, Haynes WG. Impairments in microvascular reactivity are related to organ failure in human sepsis. *Am J Physiol Heart Circ Physiol*. 2007;293:H1065-1071. doi: 10.1152/ajpheart.01237.2006
62. Aird WC. Discovery of the cardiovascular system: from Galen to William Harvey. *J Thromb Haemost*. 2011;9 Suppl 1:118-129. doi: 10.1111/j.1538-7836.2011.04312.x
63. Schneeweiss B. William Harvey's Anatomical study on the Motion of the Heart and Blood in Animals in the Discussion Field of contemporary Criticism. *Acta Conv Neo-Latini*. 2018;16:615-628. doi: 10.1163/9789004361553_053
64. Ramsingh B. On the Motion of the Heart and Blood in Animals: A New Edition of William Harvey's Exercitatio anatomica de motu cordis et sanguinis in animalibus. *Med Hist*. 2017;61:326-327. doi: 10.1017/mdh.2017.14

65. Giudicelli JF, Berdeaux A, Tato F, Garnier M. Left stellate stimulation: regional myocardial flows and ischemic injury in dogs. *Am J Physiol*. 1980;239:H359-364. doi: 10.1152/ajpheart.1980.239.3.H359
66. James TN. Anatomy of the coronary arteries in health and disease. *Circulation*. 1965;32:1020-1033. doi: 10.1161/01.cir.32.6.1020
67. Ogobuiro I, Wehrle CJ, Tuma F. Anatomy, Thorax, Heart Coronary Arteries. In: *StatPearls*. Treasure Island (FL); 2022.
68. Aalkjaer C, Boedtkjer D, Matchkov V. Vasomotion - what is currently thought? *Acta Physiol (Oxf)*. 2011;202:253-269. doi: 10.1111/j.1748-1716.2011.02320.x
69. Aalkjaer C, Nilsson H. Vasomotion: cellular background for the oscillator and for the synchronization of smooth muscle cells. *Br J Pharmacol*. 2005;144:605-616. doi: 10.1038/sj.bjp.0706084
70. Belz GG. Elastic properties and Windkessel function of the human aorta. *Cardiovasc Drugs Ther*. 1995;9:73-83. doi: 10.1007/BF00877747
71. Mulvany MJ, Aalkjaer C. Structure and function of small arteries. *Physiol Rev*. 1990;70:921-961. doi: 10.1152/physrev.1990.70.4.921
72. Simonsen U, Aalkjaer C. Small artery structure and function: a dual interaction with many players. *Basic Clin Pharmacol Toxicol*. 2012;110:2-4. doi: 10.1111/j.1742-7843.2011.00837.x
73. Kuo L, Davis MJ, Chilian WM. Myogenic activity in isolated subepicardial and subendocardial coronary arterioles. *Am J Physiol*. 1988;255:H1558-1562. doi: 10.1152/ajpheart.1988.255.6.H1558
74. Morales-Acuna F, Ochoa L, Valencia C, Gurovich AN. Characterization of blood flow patterns and endothelial shear stress during flow-mediated dilation. *Clin Physiol Funct Imaging*. 2019;39:240-245. doi: 10.1111/cpf.12564
75. Hill-Eubanks DC, Werner ME, Heppner TJ, Nelson MT. Calcium signaling in smooth muscle. *Cold Spring Harb Perspect Biol*. 2011;3:a004549. doi: 10.1101/cshperspect.a004549
76. Trexler AJ, Taraska JW. Regulation of insulin exocytosis by calcium-dependent protein kinase C in beta cells. *Cell Calcium*. 2017;67:1-10. doi: 10.1016/j.ceca.2017.07.008
77. Sudhof TC. Calcium control of neurotransmitter release. *Cold Spring Harb Perspect Biol*. 2012;4:a011353. doi: 10.1101/cshperspect.a011353
78. Bagur R, Hajnoczky G. Intracellular Ca(2+) Sensing: Its Role in Calcium Homeostasis and Signaling. *Mol Cell*. 2017;66:780-788. doi: 10.1016/j.molcel.2017.05.028
79. Dai L, Qian Y, Zhou J, Zhu C, Jin L, Li S. Hydrogen sulfide inhibited L-type calcium channels (CaV1.2) via up-regulation of the channel sulfhydration in vascular smooth muscle cells. *Eur J Pharmacol*. 2019;858:172455. doi: 10.1016/j.ejphar.2019.172455
80. Liu QH, Zheng YM, Korde AS, Yadav VR, Rathore R, Wess J, Wang YX. Membrane depolarization causes a direct activation of G protein-coupled receptors leading to local Ca2+ release in smooth muscle. *Proc Natl Acad Sci U S A*. 2009;106:11418-11423. doi: 10.1073/pnas.0813307106

81. Fill M, Copello JA. Ryanodine receptor calcium release channels. *Physiol Rev*. 2002;82:893-922. doi: 10.1152/physrev.00013.2002
82. Fill M, Ramos J. Calcium regulation of single cardiac ryanodine receptor channels. *J Muscle Res Cell Motil*. 2004;25:603-604.
83. Foskett JK, White C, Cheung KH, Mak DO. Inositol trisphosphate receptor Ca2+ release channels. *Physiol Rev*. 2007;87:593-658. doi: 10.1152/physrev.00035.2006
84. Jiang H, Stephens NL. Calcium and smooth muscle contraction. *Mol Cell Biochem*. 1994;135:1-9. doi: 10.1007/BF00925956
85. Geeves MA. The dynamics of actin and myosin association and the crossbridge model of muscle contraction. *Biochem J*. 1991;274 ( Pt 1):1-14. doi: 10.1042/bj2740001
86. Iring A, Jin YJ, Albarran-Juarez J, Siragusa M, Wang S, Dancs PT, Nakayama A, Tonack S, Chen M, Kunne C, et al. Shear stress-induced endothelial adrenomedullin signaling regulates vascular tone and blood pressure. *J Clin Invest*. 2019;129:2775-2791. doi: 10.1172/JCI123825
87. Olesen SP, Clapham DE, Davies PF. Haemodynamic shear stress activates a K+ current in vascular endothelial cells. *Nature*. 1988;331:168-170. doi: 10.1038/331168a0
88. Resnick N, Yahav H, Shay-Salit A, Shushy M, Schubert S, Zilberman LC, Wofovitz E. Fluid shear stress and the vascular endothelium: for better and for worse. *Prog Biophys Mol Biol*. 2003;81:177-199. doi: 10.1016/s0079-6107(02)00052-4
89. Paniagua OA, Bryant MB, Panza JA. Role of endothelial nitric oxide in shear stress-induced vasodilation of human microvasculature: diminished activity in hypertensive and hypercholesterolemic patients. *Circulation*. 2001;103:1752-1758. doi: 10.1161/01.cir.103.13.1752
90. Feletou M. Calcium-activated potassium channels and endothelial dysfunction: therapeutic options? *Br J Pharmacol*. 2009;156:545-562. doi: 10.1111/j.1476-5381.2009.00052.x
91. Leuranguer V, Gluais P, Vanhoutte PM, Verbeuren TJ, Feletou M. Openers of calcium-activated potassium channels and endothelium-dependent hyperpolarizations in the guinea pig carotid artery. *Naunyn Schmiedebergs Arch Pharmacol*. 2008;377:101-109. doi: 10.1007/s00210-008-0267-x
92. Dalsgaard T, Kroigaard C, Bek T, Simonsen U. Role of calcium-activated potassium channels with small conductance in bradykinin-induced vasodilation of porcine retinal arterioles. *Invest Ophthalmol Vis Sci*. 2009;50:3819-3825. doi: 10.1167/iovs.08-3168
93. Borysova L, Burdyga T. Evidence that NO/cGMP/PKG signalling cascade mediates endothelium dependent inhibition of IP(3)R mediated Ca(2)(+) oscillations in myocytes and pericytes of ureteric microvascular network in situ. *Cell Calcium*. 2015;58:535-540. doi: 10.1016/j.ceca.2015.08.006
94. Canty JM, Jr., Schwartz JS. Nitric oxide mediates flow-dependent epicardial coronary vasodilation to changes in pulse frequency but not mean flow in conscious dogs. *Circulation*. 1994;89:375-384. doi: 10.1161/01.cir.89.1.375

95. Liu Y, Gutterman DD. Vascular control in humans: focus on the coronary microcirculation. *Basic Res Cardiol*. 2009;104:211-227. doi: 10.1007/s00395-009-0775-y
96. Sandoo A, van Zanten JJ, Metsios GS, Carroll D, Kitas GD. The endothelium and its role in regulating vascular tone. *Open Cardiovasc Med J*. 2010;4:302-312. doi: 10.2174/1874192401004010302
97. Tang WH, Wang Z, Cho L, Brennan DM, Hazen SL. Diminished global arginine bioavailability and increased arginine catabolism as metabolic profile of increased cardiovascular risk. *J Am Coll Cardiol*. 2009;53:2061-2067. doi: 10.1016/j.jacc.2009.02.036
98. Knot HJ, Zimmermann PA, Nelson MT. Extracellular K(+)-induced hyperpolarizations and dilatations of rat coronary and cerebral arteries involve inward rectifier K(+) channels. *J Physiol*. 1996;492 ( Pt 2):419-430. doi: 10.1113/jphysiol.1996.sp021318
99. Park WS, Han J, Kim N, Ko JH, Kim SJ, Earm YE. Activation of inward rectifier K+ channels by hypoxia in rabbit coronary arterial smooth muscle cells. *Am J Physiol Heart Circ Physiol*. 2005;289:H2461-2467. doi: 10.1152/ajpheart.00331.2005
100. Ray CJ, Abbas MR, Coney AM, Marshall JM. Interactions of adenosine, prostaglandins and nitric oxide in hypoxia-induced vasodilatation: in vivo and in vitro studies. *J Physiol*. 2002;544:195-209. doi: 10.1113/jphysiol.2002.023440
101. Blitzer ML, Lee SD, Creager MA. Endothelium-derived nitric oxide mediates hypoxic vasodilation of resistance vessels in humans. *Am J Physiol*. 1996;271:H1182-1185. doi: 10.1152/ajpheart.1996.271.3.H1182
102. Blitzer ML, Loh E, Roddy MA, Stamler JS, Creager MA. Endothelium-derived nitric oxide regulates systemic and pulmonary vascular resistance during acute hypoxia in humans. *J Am Coll Cardiol*. 1996;28:591-596. doi: 10.1016/0735-1097(96)00218-5
103. Mott FW, Halliburton WD. On the Physiological Action of Choline and Neurine. *Br Med J*. 1899;1:1082-1083. doi: 10.1136/bmj.1.2001.1082
104. Furchgott RF, Zawadzki JV. The obligatory role of endothelial cells in the relaxation of arterial smooth muscle by acetylcholine. *Nature*. 1980;288:373-376. doi: 10.1038/288373a0
105. Kellogg DL, Jr., Zhao JL, Coey U, Green JV. Acetylcholine-induced vasodilation is mediated by nitric oxide and prostaglandins in human skin. *J Appl Physiol (1985)*. 2005;98:629-632. doi: 10.1152/japplphysiol.00728.2004
106. Ganz P, Vita JA. Testing endothelial vasomotor function: nitric oxide, a multipotent molecule. *Circulation*. 2003;108:2049-2053. doi: 10.1161/01.CIR.0000089507.19675.F9
107. Hodgkin AL, Huxley AF, Katz B. Measurement of current-voltage relations in the membrane of the giant axon of Loligo. *J Physiol*. 1952;116:424-448. doi: 10.1113/jphysiol.1952.sp004716
108. Nohl H, Gille L, Staniek K. The mystery of reactive oxygen species derived from cell respiration. *Acta Biochim Pol*. 2004;51:223-229. doi: 045101223

109. Lambert AJ, Brand MD. Reactive oxygen species production by mitochondria. *Methods Mol Biol*. 2009;554:165-181. doi: 10.1007/978-1-59745-521-3_11
110. Leto TL, Morand S, Hurt D, Ueyama T. Targeting and regulation of reactive oxygen species generation by Nox family NADPH oxidases. *Antioxid Redox Signal*. 2009;11:2607-2619. doi: 10.1089/ars.2009.2637
111. Hemnani T, Parihar MS. Reactive oxygen species and oxidative DNA damage. *Indian J Physiol Pharmacol*. 1998;42:440-452.
112. de Groot H. Reactive oxygen species in tissue injury. *Hepatogastroenterology*. 1994;41:328-332.
113. Sies H. Hydrogen peroxide as a central redox signaling molecule in physiological oxidative stress: Oxidative eustress. *Redox Biol*. 2017;11:613-619. doi: 10.1016/j.redox.2016.12.035
114. Liu Y, Gutterman DD. Oxidative stress and potassium channel function. *Clin Exp Pharmacol Physiol*. 2002;29:305-311. doi: 10.1046/j.1440-1681.2002.03649.x
115. Neo BH, Kandhi S, Wolin MS. Roles for soluble guanylate cyclase and a thiol oxidation-elicited subunit dimerization of protein kinase G in pulmonary artery relaxation to hydrogen peroxide. *Am J Physiol Heart Circ Physiol*. 2010;299:H1235-1241. doi: 10.1152/ajpheart.00513.2010
116. Saitoh S, Kiyooka T, Rocic P, Rogers PA, Zhang C, Swafford A, Dick GM, Viswanathan C, Park Y, Chilian WM. Redox-dependent coronary metabolic dilation. *Am J Physiol Heart Circ Physiol*. 2007;293:H3720-3725. doi: 10.1152/ajpheart.00436.2007
117. Huet O, Dupic L, Harrois A, Duranteau J. Oxidative stress and endothelial dysfunction during sepsis. *Front Biosci (Landmark Ed)*. 2011;16:1986-1995. doi: 10.2741/3835
118. Montezano AC, Touyz RM. Reactive oxygen species and endothelial function--role of nitric oxide synthase uncoupling and Nox family nicotinamide adenine dinucleotide phosphate oxidases. *Basic Clin Pharmacol Toxicol*. 2012;110:87-94. doi: 10.1111/j.1742-7843.2011.00785.x
119. Griffith TM, Edwards DH, Davies RL, Harrison TJ, Evans KT. Endothelium-derived relaxing factor (EDRF) and resistance vessels in an intact vascular bed: a microangiographic study of the rabbit isolated ear. *Br J Pharmacol*. 1988;93:654-662. doi: 10.1111/j.1476-5381.1988.tb10323.x
120. Griffith TM, Lewis MJ, Newby AC, Henderson AH. Endothelium-derived relaxing factor. *J Am Coll Cardiol*. 1988;12:797-806. doi: 10.1016/0735-1097(88)90324-5
121. Bauer V, Sotnikova R. Nitric oxide--the endothelium-derived relaxing factor and its role in endothelial functions. *Gen Physiol Biophys*. 2010;29:319-340.
122. Corbin JD, Cobb CE, Beebe SJ, Granner DK, Koch SR, Gettys TW, Blackmore PF, Francis SH, Wells JN. Mechanism and function of cAMP- and cGMP-dependent protein kinases. *Adv Second Messenger Phosphoprotein Res*. 1988;21:75-86.

123. Francis SH, Busch JL, Corbin JD, Sibley D. cGMP-dependent protein kinases and cGMP phosphodiesterases in nitric oxide and cGMP action. *Pharmacol Rev*. 2010;62:525-563. doi: 10.1124/pr.110.002907
124. Mustafa AK, Sikka G, Gazi SK, Steppan J, Jung SM, Bhunia AK, Barodka VM, Gazi FK, Barrow RK, Wang R, et al. Hydrogen sulfide as endothelium-derived hyperpolarizing factor sulfhydrates potassium channels. *Circ Res*. 2011;109:1259-1268. doi: 10.1161/CIRCRESAHA.111.240242
125. Hibino H, Inanobe A, Furutani K, Murakami S, Findlay I, Kurachi Y. Inwardly rectifying potassium channels: their structure, function, and physiological roles. *Physiol Rev*. 2010;90:291-366. doi: 10.1152/physrev.00021.2009
126. Isomoto S, Kondo C, Kurachi Y. Inwardly rectifying potassium channels: their molecular heterogeneity and function. *Jpn J Physiol*. 1997;47:11-39. doi: 10.2170/jjphysiol.47.11
127. Park WS, Son YK, Kim N, Ko JH, Kang SH, Warda M, Earm YE, Jung ID, Park YM, Han J. Acute hypoxia induces vasodilation and increases coronary blood flow by activating inward rectifier K(+) channels. *Pflugers Arch*. 2007;454:1023-1030. doi: 10.1007/s00424-007-0269-4
128. Ko EA, Han J, Jung ID, Park WS. Physiological roles of K+ channels in vascular smooth muscle cells. *J Smooth Muscle Res*. 2008;44:65-81. doi: 10.1540/jsmr.44.65
129. Park WS, Firth AL, Han J, Ko EA. Patho-, physiological roles of voltage-dependent K+ channels in pulmonary arterial smooth muscle cells. *J Smooth Muscle Res*. 2010;46:89-105. doi: 10.1540/jsmr.46.89
130. Jackson WF. Boosting the signal: Endothelial inward rectifier K(+) channels. *Microcirculation*. 2017;24. doi: 10.1111/micc.12319
131. Sancho M, Samson NC, Hald BO, Hashad AM, Marrelli SP, Brett SE, Welsh DG. K(IR) channels tune electrical communication in cerebral arteries. *J Cereb Blood Flow Metab*. 2017;37:2171-2184. doi: 10.1177/0271678X16662041
132. Dwenger MM, Raph SM, Baba SP, Moore JBt, Nystoriak MA. Diversification of Potassium Currents in Excitable Cells via Kvbeta Proteins. *Cells*. 2022;11. doi: 10.3390/cells11142230
133. Jiang Y, Lee A, Chen J, Cadene M, Chait BT, MacKinnon R. The open pore conformation of potassium channels. *Nature*. 2002;417:523-526. doi: 10.1038/417523a
134. MacKinnon R. Potassium channels. *FEBS Lett*. 2003;555:62-65. doi: 10.1016/s0014-5793(03)01104-9
135. MacKinnon R. Potassium channels and the atomic basis of selective ion conduction (Nobel Lecture). *Angew Chem Int Ed Engl*. 2004;43:4265-4277. doi: 10.1002/anie.200400662
136. Doyle DA, Morais Cabral J, Pfuetzner RA, Kuo A, Gulbis JM, Cohen SL, Chait BT, MacKinnon R. The structure of the potassium channel: molecular basis of K+ conduction and selectivity. *Science*. 1998;280:69-77. doi: 10.1126/science.280.5360.69

137. Mindnich RD, Penning TM. Aldo-keto reductase (AKR) superfamily: genomics and annotation. *Hum Genomics*. 2009;3:362-370. doi: 10.1186/1479-7364-3-4-362
138. Tipparaju SM, Barski OA, Srivastava S, Bhatnagar A. Catalytic mechanism and substrate specificity of the beta-subunit of the voltage-gated potassium channel. *Biochemistry*. 2008;47:8840-8854. doi: 10.1021/bi800301b
139. Tipparaju SM, Li XP, Kilfoil PJ, Xue B, Uversky VN, Bhatnagar A, Barski OA. Interactions between the C-terminus of Kv1.5 and Kvbeta regulate pyridine nucleotide-dependent changes in channel gating. *Pflugers Arch*. 2012;463:799-818. doi: 10.1007/s00424-012-1093-z
140. Tipparaju SM, Saxena N, Liu SQ, Kumar R, Bhatnagar A. Differential regulation of voltage-gated K+ channels by oxidized and reduced pyridine nucleotide coenzymes. *Am J Physiol Cell Physiol*. 2005;288:C366-376. doi: 10.1152/ajpcell.00354.2004
141. Mensah GA, Roth GA, Fuster V. The Global Burden of Cardiovascular Diseases and Risk Factors: 2020 and Beyond. *J Am Coll Cardiol*. 2019;74:2529-2532. doi: 10.1016/j.jacc.2019.10.009
142. Tsao CW, Aday AW, Almarzooq ZI, Alonso A, Beaton AZ, Bittencourt MS, Boehme AK, Buxton AE, Carson AP, Commodore-Mensah Y, et al. Heart Disease and Stroke Statistics-2022 Update: A Report From the American Heart Association. *Circulation*. 2022;145:e153-e639. doi: 10.1161/CIR.0000000000001052
143. Duncker DJ, Koller A, Merkus D, Canty JM, Jr. Regulation of coronary blood flow in health and ischemic heart disease. *Prog Cardiovasc Dis*. 2015;57:409-422. doi: 10.1016/j.pcad.2014.12.002
144. Khan MA, Hashim MJ, Mustafa H, Baniyas MY, Al Suwaidi S, AlKatheeri R, Alblooshi FMK, Almatrooshi M, Alzaabi MEH, Al Darmaki RS, et al. Global Epidemiology of Ischemic Heart Disease: Results from the Global Burden of Disease Study. *Cureus*. 2020;12:e9349. doi: 10.7759/cureus.9349
145. Nowbar AN, Gitto M, Howard JP, Francis DP, Al-Lamee R. Mortality From Ischemic Heart Disease. *Circ Cardiovasc Qual Outcomes*. 2019;12:e005375. doi: 10.1161/CIRCOUTCOMES.118.005375
146. Tibblin G, Wilhelmsen L, Werko L. Risk factors for myocardial infarction and death due to ischemic heart disease and other causes. *Am J Cardiol*. 1975;35:514-522. doi: 10.1016/0002-9149(75)90834-6
147. Salvo F, Bezin J, Bosco-Levy P, Letinier L, Blin P, Pariente A, Moore N. Pharmacological treatments of cardiovascular diseases: Evidence from real-life studies. *Pharmacol Res*. 2017;118:43-52. doi: 10.1016/j.phrs.2016.08.006
148. Kleschyov AL, Oelze M, Daiber A, Huang Y, Mollnau H, Schulz E, Sydow K, Fichtlscherer B, Mulsch A, Munzel T. Does nitric oxide mediate the vasodilator activity of nitroglycerin? *Circ Res*. 2003;93:e104-112. doi: 10.1161/01.RES.0000100067.62876.50
149. Ferrari R, Visioli O. Calcium channel blockers and ischaemic heart disease: theoretical expectations and clinical experience. *Eur Heart J*. 1991;12 Suppl F:18-24. doi: 10.1093/eurheartj/12.suppl_f.18

150. Mouhat S, Andreotti N, Jouirou B, Sabatier JM. Animal toxins acting on voltage-gated potassium channels. *Curr Pharm Des*. 2008;14:2503-2518. doi: 10.2174/138161208785777441
151. Wulff H, Castle NA, Pardo LA. Voltage-gated potassium channels as therapeutic targets. *Nat Rev Drug Discov*. 2009;8:982-1001. doi: 10.1038/nrd2983
152. Burg S, Attali B. Targeting of Potassium Channels in Cardiac Arrhythmias. *Trends Pharmacol Sci*. 2021;42:491-506. doi: 10.1016/j.tips.2021.03.005
153. Nerbonne JM, Guo W. Heterogeneous expression of voltage-gated potassium channels in the heart: roles in normal excitation and arrhythmias. *J Cardiovasc Electrophysiol*. 2002;13:406-409. doi: 10.1046/j.1540-8167.2002.00406.x
154. Alka K, Dolly JO, Ryan BJ, Henehan GT. New inhibitors of the Kvbeta2 subunit from mammalian Kv1 potassium channels. *Int J Biochem Cell Biol*. 2014;55:35-39. doi: 10.1016/j.biocel.2014.07.013
155. Park SW, Noh HJ, Sung DJ, Kim JG, Kim JM, Ryu SY, Kang K, Kim B, Bae YM, Cho H. Hydrogen peroxide induces vasorelaxation by enhancing 4-aminopyridine-sensitive Kv currents through S-glutathionylation. *Pflugers Arch*. 2015;467:285-297. doi: 10.1007/s00424-014-1513-3
156. Xie Z, Barski OA, Cai J, Bhatnagar A, Tipparaju SM. Catalytic reduction of carbonyl groups in oxidized PAPC by Kvbeta2 (AKR6). *Chem Biol Interact*. 2011;191:255-260. doi: 10.1016/j.cbi.2011.01.032
157. Xu J, Li M. Kvbeta2 inhibits the Kvbeta1-mediated inactivation of K+ channels in transfected mammalian cells. *J Biol Chem*. 1997;272:11728-11735. doi: 10.1074/jbc.272.18.11728
158. Hirst GD, Edwards FR. Sympathetic neuroeffector transmission in arteries and arterioles. *Physiol Rev*. 1989;69:546-604. doi: 10.1152/physrev.1989.69.2.546
159. Nelson MT, Patlak JB, Worley JF, Standen NB. Calcium channels, potassium channels, and voltage dependence of arterial smooth muscle tone. *Am J Physiol*. 1990;259:C3-18. doi: 10.1152/ajpcell.1990.259.1.C3
160. Hodgkin AL, Huxley AF. Currents carried by sodium and potassium ions through the membrane of the giant axon of Loligo. *J Physiol*. 1952;116:449-472. doi: 10.1113/jphysiol.1952.sp004717
161. Franco NH. Animal Experiments in Biomedical Research: A Historical Perspective. *Animals (Basel)*. 2013;3:238-273. doi: 10.3390/ani3010238
162. ElMaghawry M, Zanatta A, Zampieri F. The discovery of pulmonary circulation: From Imhotep to William Harvey. *Glob Cardiol Sci Pract*. 2014;2014:103-116. doi: 10.5339/gcsp.2014.31
163. Meijler FL, Meijler TD. Archetype, adaptation and the mammalian heart. *Neth Heart J*. 2011;19:142-148. doi: 10.1007/s12471-011-0086-4
164. Kass DA, Hare JM, Georgakopoulos D. Murine cardiac function: a cautionary tail. *Circ Res*. 1998;82:519-522. doi: 10.1161/01.res.82.4.519
165. Kaminskas LM, Boyd BJ, Porter CJ. Dendrimer pharmacokinetics: the effect of size, structure and surface characteristics on ADME properties. *Nanomedicine (Lond)*. 2011;6:1063-1084. doi: 10.2217/nnm.11.67

166. Reisner SA, Ong LS, Lichtenberg GS, Amico AF, Shapiro JR, Allen MN, Meltzer RS. Myocardial perfusion imaging by contrast echocardiography with use of intracoronary sonicated albumin in humans. *J Am Coll Cardiol*. 1989;14:660-665. doi: 10.1016/0735-1097(89)90107-1
167. Dwenger MM, Ohanyan V, Navedo MF, Nystoriak MA. Coronary microvascular Kv1 channels as regulatory sensors of intracellular pyridine nucleotide redox potential. *Microcirculation*. 2018;25. doi: 10.1111/micc.12426
168. Dwenger MM, Raph SM, Reyzer ML, Lisa Manier M, Riggs DW, Wohl ZB, Ohanyan V, Mack G, Pucci T, Moore JBt, et al. Pyridine nucleotide redox potential in coronary smooth muscle couples myocardial blood flow to cardiac metabolism. *Nat Commun*. 2022;13:2051. doi: 10.1038/s41467-022-29745-z
169. Feigl EO. Coronary physiology. *Physiol Rev*. 1983;63:1-205. doi: 10.1152/physrev.1983.63.1.1
170. Ralapanawa U, Sivakanesan R. Epidemiology and the Magnitude of Coronary Artery Disease and Acute Coronary Syndrome: A Narrative Review. *J Epidemiol Glob Health*. 2021;11:169-177. doi: 10.2991/jegh.k.201217.001
171. Nabel EG. Cardiovascular disease. *N Engl J Med*. 2003;349:60-72. doi: 10.1056/NEJMra035098
172. European Heart Network (2017) European Cardiovascular Disease Statistics 2017. https://ehnheart.org/cvd-statistics.html#:~:text=European%20Cardiovascular%20Disease%20Statistics%202017,all%20deaths%20in%20the%20EU. Accessed 18 March 2021.
173. Belcik JT, Mott BH, Xie A, Zhao Y, Kim S, Lindner NJ, Ammi A, Linden JM, Lindner JR. Augmentation of limb perfusion and reversal of tissue ischemia produced by ultrasound-mediated microbubble cavitation. *Circ Cardiovasc Imaging*. 2015;8. doi: 10.1161/CIRCIMAGING.114.002979
174. Eyre H, Kahn R, Robertson RM, Committee AAACW, Members AAACWC, Clark NG, Doyle C, Hong Y, Gansler T, Glynn T. Preventing cancer, cardiovascular disease, and diabetes: a common agenda for the American cancer society, the American diabetes association, and the American heart association. *Circulation*. 2004;109. doi: 10.1161/01.CIR.0000133321.00456.00
175. Timmis A, Townsend N, Gale CP, Torbica A, Lettino M, Petersen SE, Mossialos EA, Maggioni AP, Kazakiewicz D, May HT. European society of cardiology: cardiovascular disease statistics 2019. *Eur Heart J*. 2020;41. doi: 10.1093/eurheartj/ehz859
176. Nomura CH, Assuncao-Jr AN, Guimaraes PO, Liberato G, Morais TC, Fahel MG, Giorgi MCP, Meneghetti JC, Parga JR, Dantas-Jr RN, et al. Association between perivascular inflammation and downstream myocardial perfusion in patients with suspected coronary artery disease. *Eur Heart J Cardiovasc Imaging*. 2020;21:599-605. doi: 10.1093/ehjci/jeaa023

177. Goodwill AG, Noblet JN, Sassoon D, Fu L, Kassab GS, Schepers L, Herring BP, Rottgen TS, Tune JD, Dick GM. Critical contribution of KV1 channels to the regulation of coronary blood flow. *Basic Res Cardiol*. 2016;111:56. doi: 10.1007/s00395-016-0575-0
178. Ghosh S, Golbidi S, Werner I, Verchere BC, Laher I. Selecting exercise regimens and strains to modify obesity and diabetes in rodents: an overview. *Clin Sci (Lond)*. 2010;119:57-74. doi: 10.1042/CS20090389
179. Petrosino JM, Heiss VJ, Maurya SK, Kalyanasundaram A, Periasamy M, LaFountain RA, Wilson JM, Simonetti OP, Ziouzenkova O. Graded Maximal Exercise Testing to Assess Mouse Cardio-Metabolic Phenotypes. *PLoS One*. 2016;11:e0148010. doi: 10.1371/journal.pone.0148010
180. Brainard RE, Watson LJ, Demartino AM, Brittian KR, Readnower RD, Boakye AA, Zhang D, Hoetker JD, Bhatnagar A, Baba SP, et al. High fat feeding in mice is insufficient to induce cardiac dysfunction and does not exacerbate heart failure. *PLoS One*. 2013;8:e83174. doi: 10.1371/journal.pone.0083174
181. Ohanyan V, Yin L, Bardakjian R, Kolz C, Enrick M, Hakobyan T, Luli J, Graham K, Khayata M, Logan S, et al. Kv1.3 channels facilitate the connection between metabolism and blood flow in the heart. *Microcirculation*. 2017;24. doi: 10.1111/micc.12334
182. Kempf A, Song SM, Talbot CB, Miesenbock G. A potassium channel beta-subunit couples mitochondrial electron transport to sleep. *Nature*. 2019;568:230-234. doi: 10.1038/s41586-019-1034-5
183. Kilfoil PJ, Tipparaju SM, Barski OA, Bhatnagar A. Regulation of ion channels by pyridine nucleotides. *Circ Res*. 2013;112:721-741. doi: 10.1161/CIRCRESAHA.111.247940
184. Long SB, Campbell EB, Mackinnon R. Crystal structure of a mammalian voltage-dependent Shaker family K+ channel. *Science*. 2005;309:897-903. doi: 10.1126/science.1116269
185. Nishijima Y, Korishettar A, Chabowski DS, Cao S, Zheng X, Gutterman DD, Zhang DX. Shaker-related voltage-gated K(+) channel expression and vasomotor function in human coronary resistance arteries. *Microcirculation*. 2018;25. doi: 10.1111/micc.12431
186. Barron JT, Gu L, Parrillo JE. NADH/NAD redox state of cytoplasmic glycolytic compartments in vascular smooth muscle. *Am J Physiol Heart Circ Physiol*. 2000;279:H2872-2878. doi: 10.1152/ajpheart.2000.279.6.H2872
187. Rogers PA, Dick GM, Knudson JD, Focardi M, Bratz IN, Swafford AN, Jr., Saitoh S, Tune JD, Chilian WM. H2O2-induced redox-sensitive coronary vasodilation is mediated by 4-aminopyridine-sensitive K+ channels. *Am J Physiol Heart Circ Physiol*. 2006;291:H2473-2482. doi: 10.1152/ajpheart.00172.2006
188. Saitoh S, Zhang C, Tune JD, Potter B, Kiyooka T, Rogers PA, Knudson JD, Dick GM, Swafford A, Chilian WM. Hydrogen peroxide: a feed-forward dilator that couples myocardial metabolism to coronary blood flow.

*Arterioscler Thromb Vasc Biol*. 2006;26:2614-2621. doi: 10.1161/01.ATV.0000249408.55796.da
189. Xie W, Xu A, Yeung ES. Determination of NAD(+) and NADH in a single cell under hydrogen peroxide stress by capillary electrophoresis. *Anal Chem*. 2009;81:1280-1284. doi: 10.1021/ac802249m
190. Wong HS, Dighe PA, Mezera V, Monternier PA, Brand MD. Production of superoxide and hydrogen peroxide from specific mitochondrial sites under different bioenergetic conditions. *J Biol Chem*. 2017;292:16804-16809. doi: 10.1074/jbc.R117.789271
191. Farhana A, Lappin SL. Biochemistry, Lactate Dehydrogenase. In: *StatPearls*. Treasure Island (FL); 2022.
192. Nerbonne JM, Kass RS. Molecular physiology of cardiac repolarization. *Physiol Rev*. 2005;85:1205-1253. doi: 10.1152/physrev.00002.2005
193. Portero V, Le Scouarnec S, Es-Salah-Lamoureux Z, Burel S, Gourraud JB, Bonnaud S, Lindenbaum P, Simonet F, Violleau J, Baron E, et al. Dysfunction of the Voltage-Gated K+ Channel beta2 Subunit in a Familial Case of Brugada Syndrome. *J Am Heart Assoc*. 2016;5. doi: 10.1161/JAHA.115.003122
194. Eder RA, van den Boomen M, Yurista SR, Rodriguez-Aviles YG, Islam MR, Chen YI, Trager L, Coll-Font J, Cheng L, Li H, et al. Author Correction: Exercise-induced CITED4 expression is necessary for regional remodeling of cardiac microstructural tissue helicity. *Commun Biol*. 2022;5:696. doi: 10.1038/s42003-022-03671-8
195. Ding S, Gan T, Song M, Dai Q, Huang H, Xu Y, Zhong C. C/EBPB-CITED4 in Exercised Heart. *Adv Exp Med Biol*. 2017;1000:247-259. doi: 10.1007/978-981-10-4304-8_14
196. Heilstedt HA, Burgess DL, Anderson AE, Chedrawi A, Tharp B, Lee O, Kashork CD, Starkey DE, Wu YQ, Noebels JL, et al. Loss of the potassium channel beta-subunit gene, KCNAB2, is associated with epilepsy in patients with 1p36 deletion syndrome. *Epilepsia*. 2001;42:1103-1111. doi: 10.1046/j.1528-1157.2001.08801.x
197. Lyu Y, Wang Q, Liang J, Zhang L, Zhang H. The Ion Channel Gene KCNAB2 Is Associated with Poor Prognosis and Loss of Immune Infiltration in Lung Adenocarcinoma. *Cells*. 2022;11. doi: 10.3390/cells11213438
198. Perkowski JJ, Murphy GG. Deletion of the mouse homolog of KCNAB2, a gene linked to monosomy 1p36, results in associative memory impairments and amygdala hyperexcitability. *J Neurosci*. 2011;31:46-54. doi: 10.1523/JNEUROSCI.2634-10.2011
199. Raph SM, Bhatnagar A, Nystoriak MA. Biochemical and physiological properties of K(+) channel-associated AKR6A (Kvbeta) proteins. *Chem Biol Interact*. 2019;305:21-27. doi: 10.1016/j.cbi.2019.03.023
200. Wu J, Jin Z, Zheng H, Yan LJ. Sources and implications of NADH/NAD(+) redox imbalance in diabetes and its complications. *Diabetes Metab Syndr Obes*. 2016;9:145-153. doi: 10.2147/DMSO.S106087

201. Diaz-Canestro C, Montero D. Sex Dimorphism of VO(2max) Trainability: A Systematic Review and Meta-analysis. *Sports Med*. 2019;49:1949-1956. doi: 10.1007/s40279-019-01180-z
202. Konhilas JP, Maass AH, Luckey SW, Stauffer BL, Olson EN, Leinwand LA. Sex modifies exercise and cardiac adaptation in mice. *Am J Physiol Heart Circ Physiol*. 2004;287:H2768-2776. doi: 10.1152/ajpheart.00292.2004
203. Iliceto S, Marangelli V, Marchese A, Amico A, Galiuto L, Rizzon P. Myocardial contrast echocardiography in acute myocardial infarction. Pathophysiological background and clinical applications. *Eur Heart J*. 1996;17:344-353. doi: 10.1093/oxfordjournals.eurheartj.a014867
204. Messer JV, Wagman RJ, Levine HJ, Neill WA, Krasnow N, Gorlin R. Patterns of human myocardial oxygen extraction during rest and exercise. *J Clin Invest*. 1962;41:725-742. doi: 10.1172/JCI104531
205. Dick GM, Katz PS, Farias M, 3rd, Morris M, James J, Knudson JD, Tune JD. Resistin impairs endothelium-dependent dilation to bradykinin, but not acetylcholine, in the coronary circulation. *Am J Physiol Heart Circ Physiol*. 2006;291:H2997-3002. doi: 10.1152/ajpheart.01035.2005
206. Gulbis JM, Zhou M, Mann S, MacKinnon R. Structure of the cytoplasmic beta subunit-T1 assembly of voltage-dependent K+ channels. *Science*. 2000;289:123-127. doi: 10.1126/science.289.5476.123
207. Liu Y, Liu D, Heath L, Meyers DM, Krafte DS, Wagoner PK, Silvia CP, Yu W, Curran ME. Direct activation of an inwardly rectifying potassium channel by arachidonic acid. *Mol Pharmacol*. 2001;59:1061-1068. doi: 10.1124/mol.59.5.1061
208. Kilfoil PJ, Chapalamadugu KC, Hu X, Zhang D, Raucci FJ, Jr., Tur J, Brittian KR, Jones SP, Bhatnagar A, Tipparaju SM, et al. Metabolic regulation of Kv channels and cardiac repolarization by Kvbeta2 subunits. *J Mol Cell Cardiol*. 2019;137:93-106. doi: 10.1016/j.yjmcc.2019.09.013
209. Giese KP, Storm JF, Reuter D, Fedorov NB, Shao LR, Leicher T, Pongs O, Silva AJ. Reduced K+ channel inactivation, spike broadening, and after-hyperpolarization in Kvbeta1.1-deficient mice with impaired learning. *Learn Mem*. 1998;5:257-273.
210. McCormack K, Connor JX, Zhou L, Ho LL, Ganetzky B, Chiu SY, Messing A. Genetic analysis of the mammalian K+ channel beta subunit Kvbeta 2 (Kcnab2). *J Biol Chem*. 2002;277:13219-13228. doi: 10.1074/jbc.M111465200
211. Dick GM, Tune JD. Role of potassium channels in coronary vasodilation. *Exp Biol Med (Maywood)*. 2010;235:10-22. doi: 10.1258/ebm.2009.009201
212. El Gebeily G, El Khoury N, Mathieu S, Brouillette J, Fiset C. Estrogen regulation of the transient outward K(+) current involves estrogen receptor alpha in mouse heart. *J Mol Cell Cardiol*. 2015;86:85-94. doi: 10.1016/j.yjmcc.2015.07.013
213. Wellman GC, Quayle JM, Standen NB. Evidence against the association of the sulphonylurea receptor with endogenous Kir family members other than KATP in coronary vascular smooth muscle. *Pflugers Arch*. 1996;432:355-357. doi: 10.1007/s004240050144

214. Nystoriak MA, Zhang D, Jagatheesan G, Bhatnagar A. Heteromeric complexes of aldo-keto reductase auxiliary KVbeta subunits (AKR6A) regulate sarcolemmal localization of KV1.5 in coronary arterial myocytes. *Chem Biol Interact*. 2017;276:210-217. doi: 10.1016/j.cbi.2017.03.011
215. Syed AU, Reddy GR, Ghosh D, Prada MP, Nystoriak MA, Morotti S, Grandi E, Sirish P, Chiamvimonvat N, Hell JW, et al. Adenylyl cyclase 5-generated cAMP controls cerebral vascular reactivity during diabetic hyperglycemia. *J Clin Invest*. 2019;129:3140-3152. doi: 10.1172/JCI124705
216. Hung YP, Yellen G. Live-cell imaging of cytosolic NADH-NAD+ redox state using a genetically encoded fluorescent biosensor. *Methods Mol Biol*. 2014;1071:83-95. doi: 10.1007/978-1-62703-622-1_7
217. Wei K, Kaul S. Recent advances in myocardial contrast echocardiography. *Curr Opin Cardiol*. 1997;12:539-546. doi: 10.1097/00001573-199711000-00007
218. Nystoriak MA, O'Connor KP, Sonkusare SK, Brayden JE, Nelson MT, Wellman GC. Fundamental increase in pressure-dependent constriction of brain parenchymal arterioles from subarachnoid hemorrhage model rats due to membrane depolarization. *Am J Physiol Heart Circ Physiol*. 2011;300:H803-812. doi: 10.1152/ajpheart.00760.2010
219. Williamson JR. Glycolytic control mechanisms. 3. Effects of iodoacetamide and fluoroacetate on glucose metabolism in the perfused rat heart. *J Biol Chem*. 1967;242:4476-4485.
220. Sugiura Y, Katsumata Y, Sano M, Honda K, Kajimura M, Fukuda K, Suematsu M. Visualization of in vivo metabolic flows reveals accelerated utilization of glucose and lactate in penumbra of ischemic heart. *Sci Rep*. 2016;6:32361. doi: 10.1038/srep32361
221. Wilcox CS. Effects of tempol and redox-cycling nitroxides in models of oxidative stress. *Pharmacol Ther*. 2010;126:119-145. doi: 10.1016/j.pharmthera.2010.01.003
222. Quer G, Gouda P, Galarnyk M, Topol EJ, Steinhubl SR. Inter- and intraindividual variability in daily resting heart rate and its associations with age, sex, sleep, BMI, and time of year: Retrospective, longitudinal cohort study of 92,457 adults. *PLoS One*. 2020;15:e0227709. doi: 10.1371/journal.pone.0227709
223. Katritsis DG, Camm AJ. Atrioventricular nodal reentrant tachycardia. *Circulation*. 2010;122:831-840. doi: 10.1161/CIRCULATIONAHA.110.936591
224. Milani-Nejad N, Brunello L, Gyorke S, Janssen PM. Decrease in sarcoplasmic reticulum calcium content, not myofilament function, contributes to muscle twitch force decline in isolated cardiac trabeculae. *J Muscle Res Cell Motil*. 2014;35:225-234. doi: 10.1007/s10974-014-9386-9
225. Klocke FJ. Coronary blood flow in man. *Prog Cardiovasc Dis*. 1976;19:117-166. doi: 10.1016/0033-0620(76)90020-7
226. Weiss L, Lundgren Y. Chronic antihypertensive drug treatment in young spontaneously hypertensive rats: Effects on arterial blood pressure,

cardiovascular reactivity and vascular design. *Cardiovasc Res*. 1978;12:744-751. doi: 10.1093/cvr/12.12.744

227. Kuo L, Davis MJ, Chilian WM. Longitudinal gradients for endothelium-dependent and -independent vascular responses in the coronary microcirculation. *Circulation*. 1995;92:518-525. doi: 10.1161/01.cir.92.3.518
228. Kuo L, Chilian WM, Davis MJ. Coronary arteriolar myogenic response is independent of endothelium. *Circ Res*. 1990;66:860-866. doi: 10.1161/01.res.66.3.860
229. Kuo L, Davis MJ, Chilian WM. Endothelium-dependent, flow-induced dilation of isolated coronary arterioles. *Am J Physiol*. 1990;259:H1063-1070. doi: 10.1152/ajpheart.1990.259.4.H1063
230. Dick GM, Bratz IN, Borbouse L, Payne GA, Dincer UD, Knudson JD, Rogers PA, Tune JD. Voltage-dependent K+ channels regulate the duration of reactive hyperemia in the canine coronary circulation. *Am J Physiol Heart Circ Physiol*. 2008;294:H2371-2381. doi: 10.1152/ajpheart.01279.2007
231. Sun FH, Wong SH, Huang YJ, Chen YJ, Tsang KF. Substrate utilization during brisk walking is affected by glycemic index and fructose content of a pre-exercise meal. *Eur J Appl Physiol*. 2012;112:2565-2574. doi: 10.1007/s00421-011-2231-6
232. Sun SZ, Empie MW. Fructose metabolism in humans - what isotopic tracer studies tell us. *Nutr Metab (Lond)*. 2012;9:89. doi: 10.1186/1743-7075-9-89
233. Hwang K, Jeong DW, Lee JW, Kim IH, Chang HI, Kim HJ, Kim IY. Alteration of the NAD+/NADH ratio in CHO cells by stable transfection with human cytosolic glycerol-3-phosphate dehydrogenase: resistance to oxidative stress. *Mol Cells*. 1999;9:429-435.
234. Bhatnagar A, Das B, Gavva SR, Cook PF, Srivastava SK. The kinetic mechanism of human placental aldose reductase and aldehyde reductase II. *Arch Biochem Biophys*. 1988;261:264-274. doi: 10.1016/0003-9861(88)90341-4

# APPENDIX A

Pyridine nucleotide redox potential in coronary smooth muscle couples myocardial blood flow to cardiac metabolism.[6]

## Introduction

Blood flow to the heart is tightly coupled with cardiac workload and oxygen consumption.[45,169] Acute elevations of heart rate and myocardial contractile force, such as those that occur during a bout of strenuous physical activity, are associated with a higher rate of cardiomyocyte oxidative ATP production to support ion transport and sarcomeric function.[17] Although oxygen extraction from the arterial blood supply is near maximal at rest, sustained metabolic activity of the heart during stress requires an instantaneous reduction of coronary resistance and the consequent enhancement of myocardial perfusion.[204] Despite the importance of maintaining adequate myocardial oxygen delivery for the prevention of ischemic heart disease, molecular mechanisms that underlie the physiologic regulation of coronary blood flow remain poorly understood.

Local metabolic control of coronary arterial tone occurs in part via complex intercellular signaling between active cardiomyocytes and intramyocardial

[6] This is a final version of an article published as 168. Dwenger MM, Raph SM, Reyzer ML, Lisa Manier M, Riggs DW, Wohl ZB, Ohanyan V, Mack G, Pucci T, Moore JBt, et al. Pyridine nucleotide redox potential in coronary smooth muscle couples myocardial blood flow to cardiac metabolism. *Nat Commun*. 2022;13:2051. doi: 10.1038/s41467-022-29745-z

vasculature.[50] In this process, multiple factors likely coalesce to directly or indirectly modify the activity of ion channels in the sarcolemma of coronary smooth muscle cells (i.e., coronary arterial myocytes).[188] In particular, activation of redox-sensitive voltage-gated potassium channels (i.e., Kv1) in coronary arterial myocytes, upon increased myocardial oxygen demand, promotes rapid membrane hyperpolarization, reduced intracellular [$Ca^{2+}$], and vasodilation.[205] The native Kv1 holo-channel structure consists of four transmembrane pore-forming subunits that interface with four intracellular Kvβ subunits.[184,206] We previously observed that selective modifications to the Kvβ complex composition impact vasoreactivity and myocardial blood flow regulation; in particular, the loss of Kvβ2, or conversely the overabundance of Kvβ1.1 in vascular Kv1 channels results in suppression of metabolic vasodilatory function, and thereby disrupts the relationship between myocardial blood flow and cardiac workload.[37] Nonetheless, cellular responses to metabolic stress in the coronary circulation that ultimately promote Kvβ-dependent stimulation of Kv1 activity are unknown.

The Kvβ proteins are functionally active aldo-keto reductases (AKRs) that bind pyridine nucleotides (i.e., NAD(P)(H)) with high affinity. These proteins differentially regulate Kv1 function in heterologous systems and native excitable cells.[139,199,207,208] Accordingly, we tested the hypothesis that changes in myocardial oxygen consumption and demand modulate the redox ratio of pyridine nucleotides in arterial smooth muscle and thereby influence the regulatory mode of Kvβ proteins and Kv activity. Using a combination of *in vivo* and *ex vivo* approaches, we show that the intracellular NADH:$NAD^+$ ratio in arterial smooth muscle is

sensitive to changes in cardiac workload. Varying the intracellular NAD(P)H:NAD(P)$^+$ ratio to reflect enhanced myocardial metabolic demand potentiated Kv1 activity in a Kvβ2-dependent manner. Moreover, catalytic turnover of pyridine nucleotide cofactors by Kvβ2 was required for redox-sensitive modification of Kv1 function and vasoreactivity, and metabolic control of myocardial blood flow, underscoring the importance of Kvβ AKR enzymatic properties in cardiovascular physiology.

## Materials and Methods

*Animals and animal euthanasia:* All animal procedures were performed as approved by the Institutional Animal Care and Use Committees at the University of Louisville and Northeast Ohio Medical University. Genetically engineered mouse strains in which Kcnab1 or Kcnab2 genes were ablated (i.e., Kvβ1.1$^{-/-}$, Kvβ2$^{-/-}$, respectively)[209,210] or in which tyrosine 90 of Kvβ2 was mutated to phenylalanine (Kvβ2$^{Y90F}$)[210] were used for this study. Strain-matched wild type mice (WT; C57BL6N for Kvβ1.1$^{-/-}$, 129SvEv for Kvβ2$^{-/-}$) were used as controls (indicated in figure legends). Due to the potential for confounding effects of estrogen on the functional expression of vascular K$^+$ channels,[205,211-213] only male mice (aged-3-6 months) were used. All mice were bred in house and fed normal chow ad libitum. Mice were euthanized by sodium pentobarbital (150 mg/kg; i.p.) and thoracotomy, and tissues were excised immediately for *ex vivo* assessments as described below.

*Human tissue:* Deidentified human tissues, obtained through the Midwest Transplant Network, were kindly provided for this study by Dr. Tamer Mohamed (Division of Cardiovascular Medicine, University of Louisville). Branches of superficial and subepicardial left anterior descending coronary arteries were dissected from an excised heart (male, 52 yrs old; see **Table S1**) in ice-cold $Ca^{2+}$-free physiological saline solution consisting of (in mM): 140 NaCl, 5 KCl, 2 $MgCl_2$,10 HEPES, 10 glucose, pH 7.4. Arteries were enzymatically digested to isolate individual arterial myocytes as described below.

*Isolation of coronary arterial smooth muscle cells:* Hearts were excised and immediately transferred to ice-cold physiological saline solution containing (in mM): 134 NaCl, 6 KCl, 1 $MgCl_2$, 2 $CaCl_2$, 10 HEPES, and 7 glucose, pH 7.4. First and second-order branches of the left anterior descending coronary artery were manually dissected and smooth muscle cells were isolated as previously described.[214] Briefly, arterial segments were incubated at 37°C in $Ca^{2+}$-free physiological saline (composition described above), containing papain (1 mg/ml) and dithiothreitol (1 mg/ml) for 5 min with gentle agitation. Then, the solution was replaced with buffer containing trypsin inhibitor (1 mg/ml) and collagenase (type H, 1 mg/ml) and incubated at 37°C for an additional 5 min with gentle agitation. For human tissues, arterial myocytes were digested in collagenase (type H, 3 mg/mL; Sigma Aldrich), elastase (1 mg/mL; Sigma Aldrich), and bovine serum albumin (10 mg/mL; Sigma Aldrich) at 37°C for 30 min with gentle agitation. Digested tissues

were washed three times with ice-cold enzyme-free buffer. Cells were liberated by gentle trituration with a flame-polished glass pipette and kept on ice until use.

*Imaging Mass Spectrometry:* Hearts from anesthetized (sodium pentobarbital, 150 mg/kg, i.p.) mice that were acutely treated with dobutamine (10 mg/kg, i.p.) or vehicle (phosphate buffered saline; see **Figure 1**) were rapidly frozen with liquid $N_2$ and immediately excised and stored at -80°C. Thin sections (12 μm) of fresh frozen mouse hearts were obtained from a cryostat (Leica CM 1900) and thaw-mounted onto gold-coated stainless steel MALDI target plates. Serial sections were obtained for H&E staining on standard glass microscope slides. Four serial sections were obtained for each heart and used for imaging mass spectrometry (IMS). An automated sprayer (TM Sprayer, HTX Technologies) was used to apply the MALDI matrix to the tissues. 9-Aminoacridine (9AA, hydrochloride salt, Sigma-Aldrich A38401) was prepared at 5 mg/ml in 90% methanol and sprayed at 0.12 ml/min, 85°C, and 700 mm/min stage velocity. Eight passes were deposited at 3 mm track spacing, alternating horizontal and vertical positions between passes. Metabolite images were acquired on a 9.4T FT-ICR mass spectrometer (Bruker Solarix, Bruker Daltonics) in negative ionization mode at 20 μm spatial resolution. Data were acquired in CASI mode, with Q1 isolating m/z 86 with a 6 amu window with a detected mass range of 72-350 amu. Images were visualized with FlexImaging software (Bruker). Regions of interest were selected to encompass the coronary wall and the surrounding tissue. Spectra were averaged for each

region of interest, and the intensities for signals corresponding to lactate (m/z 89.0244) and pyruvate (m/z 87.0088) were exported.

*Smooth muscle and hiPSC-CM co-culture preparation and live-cell fluorescence imaging*: Vascular smooth muscle cells were isolated using previously described methods shown to yield highly pure CD31/CD45/lineage marker-negative and α-smooth muscle actin-positive cells.[215] Thoracic and abdominal aortae were excised and placed in ice-cold Dulbecco's Modified Eagle Media (DMEM) containing Fungizone™ (1:1000; Thermo Fisher Scientific). Vessels were cleaned of connective tissue, minced into 1 mm segments, and transferred to a sterile 15 ml tube and washed (3x) with cold Tyrode's solution containing (in mM): 126 NaCl, 44 KCl, 17 mM $NaHCO_3$, 1 $MgCl_2$, 10 Glucose, and 4 mM HEPES, pH 7.4. After washing, the solution was replaced with 1 ml of Tyrode's solution containing 1 mg/ml collagenase (Type 2, Worthington) and 20 μM $CaCl_2$. The tissue was incubated with intermittent agitation (4-5 hrs, 37ºC, 5% $CO_2$), centrifuged at 300 *x g*, and resuspended in DMEM containing 10% fetal bovine serum and 1% penicillin streptomycin. The cells were plated in 35 mM Primaria™ plates (Corning) for 5 days prior to use (P0-2) in imaging experiments.

Human induced pluripotent stem cells (iPSCs; line #SCVI15; Joseph Wu Laboratory, Stanford University) were reprised from cryogenic storage and plated on Matrigel (Corning)-coated tissue culture grade dishes. The iPSCs were subsequently propagated in a feeder-free environment using StemFlex Medium (Thermo Fisher Scientific), replaced every two days, and maintained under

standard incubation conditions (37 ºC with 5% atmospheric $CO_2$). When approaching 85% confluency, iPSCs underwent clump cell passaging using Versene dissociation agent (Thermo Fisher Scientific). Cells were then differentiated using the iPSC Cardiomyocyte Differentiation Kit (Thermo Fisher) following the manufacturer's instructions. Briefly, at ~75-80% confluency, cells were stimulated to differentiate by the addition of pre-warmed Cardiomyocyte Differentiation Medium A (day 1). On differentiation day 3, medium was replaced with pre-warmed Cardiomyocyte Differentiation Medium B. At differentiation day 5, medium was replaced with pre-warmed Cardiomyocyte Maintenance Medium and replenished every other day until differentiation day 10. At this time, differentiated cells were subjected to metabolic selection using cardiomyocyte enrichment medium (48.1 mL of glucose-free RPMI 1640 Medium, 1.7 mL of Bovine Albumin Fraction V 7.5% w/v, 0.4 mL of 1M sodium lactate, and 0.13 mL of 250x ascorbic acid solution). This solution was then replaced every other day for 5 days, after which, cultures were replenished with kit-supplied Cardiomyocyte Maintenance Medium with replacement every other day until use.

Plasmids for peredox-mCherry were obtained via Addgene (pcDNA3.1-Peredox-mCherry, #32383) and Ad-peredox-mCherry adenovirus was generated by insertion to an adenoviral backbone (Type 5, dE1/E3; Vector Biolabs). After reaching 50-80% confluency, arterial myocytes were treated with Ad-peredox-mCherry ($6.4x10^7$ PFUs, 50-100 MOI; 4 h at 37°C). During infection and thereafter, cells were maintained in antibiotic-free DMEM supplemented with 2% FBS. For arterial myocyte-iPSC-CM co-cultures, Ad-peredox-mCherry-treated (24 h) arterial

myocytes were seeded onto iPSC-CM monolayers, and the co-culture was maintained in DMEM supplemented with 5% FBS for 48 h prior to imaging.

Calibration of peredox-mCherry fluorescence for quantification of cytosolic NADH:$NAD^+$ was performed as previously described.[216] Briefly, cells were perfused with a baseline extracellular solution consisting of (in mM): 121.5 NaCl, 2 KCl, 25 $NaHCO_3$, 1.25 $NaH_2PO_2$, 1 $MgCl_2$, and 2 $CaCl_2$ (pH 7.4, maintained by aeration with 5% $CO_2$). Bath temperature was monitored throughout all experiments with a thermistor probe and maintained at 36.5-37.5°C. Green (ex 405, em 525) and red (ex 560, em 630) fluorescence was monitored during sequential application (10-15 min each) of lactate:pyruvate at ratios of 500, 160, 50, 20, and 6. At the end of each experiment, maximum and minimum green:red fluorescence was recorded in the presence of 10 mM lactate and 10 mM pyruvate, respectively. For experiments testing the effects of hypoxia and electrical stimulation of co-cultures, cells were bathed in DMEM/5% FBS in an enclosed stage-top incubation system (Warner Harvard Apparatus) to allow equilibration of the bath solution to controlled $O_2$ levels (1-5%). Co-cultures and arterial myocytes alone (i.e., in the absence of iPSC-CMs) were electrically paced from 1-3 Hz using platinum electrodes connected to a MyoPacer field stimulator (IonOptix). Fluorescence images were acquired using a Keyence BZ-X800 epifluorescence imaging system in time-lapse mode with a 4X objective lens. Images were captured every 20 seconds in brightfield, green (T-sapphire), and red (mCherry) channels. Image series were converted to .avi files and analyzed using FIJI software (NIH).

*Patch Clamp Electrophysiology:* Coronary arterial myocytes were isolated from mice as described above. Outward $K^+$ currents were recorded using the conventional whole-cell configuration of the patch clamp technique in voltage clamp mode of an Axopatch 200B amplifier (Axon Instruments). Borosilicate glass pipettes were pulled using a P-87 micropipette puller (Sutter Instruments) to a resistance of 5-7 MΩ and filled with a pipette solution containing (in mM): 87 $K^+$-aspartate, 20 KCl, 1 $MgCl_2$, 5 Mg-ATP, 10 EGTA, 10 HEPES, pH 7.2. In some experiments, pyridine nucleotides were added into the internal solution. Cells were allowed to adhere to a glass coverslip in a 0.25 ml recording chamber (Warner Instruments) and were bathed in a solution containing (in mM): 134 NaCl, 6 KCl, 1 $MgCl_2$, 0.1 $CaCl_2$, 10 Glucose, 10 HEPES. Series resistance was electronically compensated at ≥80%. Outward $K^+$ currents were recorded during a series of 500 msec step-wise depolarizations in 10 mV increments (-70 – +50 mV) from a holding potential of -70 mV. The voltage-dependence of activation was determined from tail currents elicited from repolarization to -40 mV. Voltage-dependence of inactivation was separately determined from a standard two-pulse voltage protocol in which cells were subjected to step-wise depolarizations (-100 – 50 mV) for 8 sec followed by 200 msec pulse to 50 mV.

Single Kv channel activity was recorded using the inside-out configuration of the patch clamp technique with symmetrical bath/pipette $K^+$ conditions. Glass pipettes (8-10 MΩ) were filled with a solution containing (in mM): 140 KCl, 1 HEDTA, 10 HEPES, and 0.0001 iberiotoxin (pH 7.3 with KOH). The bath solution consisted of (in mM): 140 KCl, 1 HEDTA, 10 HEPES, and 0.001 glibenclamide.

Excised membrane patches were held at a constant potential and stochastic channel activity was recorded in gap-free mode at a sampling frequency of 10 kHz. All electrophysiological data were analyzed using Clampfit 10 software (Axon Instruments). Whole cell current densities are expressed as the peak currents at each 500 msec depolarizing voltage step normalized to cell capacitance (pA/pF). $V_{0.5,act}$ and $V_{0.5,inact}$ are the voltages at half-maximum normalized current ($I/I_{max}$) determined from fitting data with a Boltzmann function. For single channel analysis, open probabilities (nPo) were determined from recordings that had stable channel activity for at least two minutes. Values of nPo and amplitude were determined using the single-channel search function in Clampfit 10 software.

*Echocardiography:* In vivo measurements of myocardial blood flow and cardiac function were performed as previously described.[37,55] Briefly, mice were anesthetized with isoflurane (3% induction, 1-2% maintenance; supplemental $O_2$ delivered at 1 L/min) and placed on a controlled heating platform in the supine position. A small incision was made on the right side of the neck for placement of a jugular venous catheter (sterile PE-50 tubing, prefilled with heparinized saline; 50 units/ml) to deliver contrast agent and drugs. For continuous monitoring of arterial blood pressure, a small incision was made on the hind limb and the femoral artery was isolated and cannulated with a 1.2 F pressure catheter (Transonic Systems), which was then advanced ~10 mm into the abdominal aorta. For myocardial contrast echocardiography (MCE), lipid-shelled microbubbles were prepared by sonication of decafluorobutane gas-saturated aqueous suspension of

distearoylphosphatidylcholine (2 mg/mL) and polyoxyethylene-40-stearate (1 mg/mL), and intravenously infused at ~5 x $10^5$ microbubbles/min. Imaging was performed using a Sequoia Acuson C512 imaging system (Siemens) with a high frequency linear array probe (15L8). A multi-pulse contrast specific pulse sequence was used to detect non-linear contrast signal at low mechanical index (MI = 0.18 – 0.25) and data were acquired during (i.e., destruction) and following (replenishment phase) a short 1.9 MI pulse sequence to destruct microbubbles within the acoustic field. Measurements were performed at baseline, after administration of the autonomic ganglionic blocker hexamethonium (5 mg/kg, i.v.), and subsequently after consecutive infusions of norepinephrine (0.5 – 5.0 μg/kg/min; 3 min each followed by 5 min washout). Mice that did not complete all norepinephrine infusions were excluded from the study. All data analyses and calculations of myocardial perfusion were conducted offline. Lab Chart 8 software (AD Instruments) was used for pressure and heart rate measurements.

For MCE, gain was adjusted to obtain images without myocardial signal in the absence of contrast agent infusion. Long axis images were acquired at a penetration depth of 2-2.5 cm. Images were analyzed to determine MBF by fitting intensity data from anterolateral regions of interest with an exponential function: $y = A(1 - e^{-\beta t})$ where $y$ is the signal intensity at time $t$, $A$ is the signal intensity at plateau during the replenishment phase (reflects microvascular cross sectional volume) and β is the initial slope corresponding to the volume exchange frequency.[173] Myocardial blood flow was estimated from 3-5 images per condition as the product of β x relative blood volume (RBV; myocardial to cavity signal

intensity).[173,217] MCE analyses were conducted in a genotype/treatment-blinded fashion.

*Ex vivo arterial diameter measurements:* Third and fourth order branches of the mesenteric arteries were dissected and kept in ice-cold isolation buffer consisting of (in mM): 134 NaCl, 6 KCl, 1 $MgCl_2$, 2 $CaCl_2$, 10 HEPES, 7 D-glucose, pH adjusted to 7.4 with NaOH. Arteries were cleaned of connective tissue and used for diameter measurements within 8 h of isolation. Vessels were cannulated in cold isolation buffer on flame polished glass micropipettes mounted in a linear alignment single vessel myograph chamber (Living Systems Instrumentation). After cannulation, the myography chamber was placed on an inverted microscope and arteries were equilibrated to temperature (37°C) and static intralumenal pressure (80 mmHg), maintained with a pressure servo control unit (Living Systems Instrumentation) under continuous superfusion (3-5 mL/min) of physiological saline solution (PSS) consisting of (in mM): 119 NaCl, 4.7 KCl, 1.2 $KH_2PO_4$, 1.2 $MgCl_2$, 7 D-glucose, 24 $NaHCO_3$, and 2 $CaCl_2$, maintained at pH 7.35-7.45 via aeration with 5% $CO_2$, 20% $O_2$ ($N_2$ balanced). Following equilibrium (45-60 min), intralumenal diameter was continuously monitored and recorded with a charge coupled device (CCD) camera and edge detection software (IonOptix). Experiments were performed to examine the effects of L-lactate (Sigma Aldrich) (5-20 mM) and $H_2O_2$ (0.1-10 μM) in arteries preconstricted with the synthetic thromboxane $A_2$ analogue U46619 (100 nM; Tocris Bioscience). At the end of each experiment, the maximum passive diameter was measured in the presence of $Ca^{2+}$-free PSS containing the

L-type $Ca^{2+}$ channel inhibitor nifedipine (1uM) and adenylyl cyclase activator forskolin (0.5 uM) as described previously.[214,218] Changes in diameter in response to L-lactate are expressed as the change from baseline (i.e., in the presence of 100 nM U46619) normalized to the difference between baseline and maximum passive diameters measured for each vessel.

*In situ proximity ligation:* Coronary arteries were enzymatically digested to isolate individual arterial myocytes, as described above, and allowed to adhere to glass microscope slides. After fixation with 4% paraformaldehyde (10 min, room temperature), cells were permeabilized with 0.1% triton-X100 and in situ proximity ligation was performed following manufacturer's instructions. Briefly, non-specific antibody binding sites were blocked with the supplied blocking reagent and cells were labelled with primary antibodies against Kv1.5 (Neuromab, 75-011, 1:50), Kvβ1 (Abcam, Ab174508, 1:100), and Kvβ2 (Aviva Systems Biology, ARP37678-t100, 1:100) overnight at 4°C. Cells were then treated with secondary oligonucleotide-conjugated probes, followed by ligation and rolling amplification by incubation with manufacturer-supplied ligase and polymerase, respectively. Sites of proximity were labelled with fluorophore (ex 554 nm, em 579 nm) and slides were mounted and sealed with coverslips. Brightfield and fluorescent images were captured using a 20x objective on a Keyence BZ-X800 All-in-One imaging system and fluorescent punctate sites and cell footprint area were quantified using FIJI software (NIH).

*Western blot:* Tissue lysates were obtained from mesenteric arteries (6-8 pooled segments of 3rd and 4th order branches) and homogenized in lysis buffer containing (in mM): 150 NaCl, 50 Tris-HCl, and 1 EDTA with 0.25% deoxycholic acid, 1% NP-40, and Complete Mini protease inhibitor cocktail (Roche; per manufacturer's instructions), pH 7.4. Tissue homogenates were sonicated on ice and centrifuged (10,000 xg, 10 min, 4°C). Supernatants were transferred to another tube and boiled with Laemmli sample buffer (10 min) and run on a Stain-free Mini-PROTEAN 4-20% polyacrylamide gel (Bio-Rad). Total protein was assessed prior to transfer using a myECL imager (Thermo Fisher Scientific). Following transfer of proteins to polyvinylidene fluoride (PVDF), membranes were blocked for non-specific binding with 5% milk (wt/vol) in tris-buffered saline (TBS) and incubated (overnight, 4°C) in primary antibodies against Kvβ2 (Neuromab, 75-021, 1:400) or α-tubulin (Sigma Aldrich, T5168, 1:4000) in TBS containing 0.1% Tween-20 (TBSt). After washing with TBSt (5x, room temperature), membranes were incubated with horseradish peroxidase (HRP)-conjugated secondary antibodies (anti-mouse IgG, Cell Signaling, 7076S, 1:3000). HRP was then detected with Pierce ECL Plus Western Blotting Substrate (Thermo Fisher Scientific) and a myECL imager (Thermo Fisher Scientific). Densitometry was performed for immunoreactive bands using FIJI software (NIH).

*Statistical Analysis:* Group data are presented as mean ± SEM, unless otherwise indicated. All data were analyzed with Prism 9 software (GraphPad Software) or SAS version 9.4 software (SAS Institute, Inc.). Normality was determined for

datasets by Shapiro-Wilk tests. Specific tests used to compare experimental groups are provided in figure legends. For normal data, unpaired or paired *t* tests were used to compare two groups and one-way ANOVA with post-hoc tests, as indicated, were used for multiple comparisons of three or more groups. Linear mixed models were used to test for interactions in time and genotype or treatment. For non-normal data, outcome variables were log-transformed for normality or nonparametric tests were used, as indicated. $P<0.05$ was considered statistically significant.

*Study approval:* All animal procedures were conducted as approved by Institutional Animal Care and Use Committees at the University of Louisville and Northeast Ohio Medical University, in accordance with guidelines set by the National Institutes of Health.

## RESULTS

**Cardiac workload-dependent changes in vascular pyridine nucleotide redox potential.** To test whether acute changes in cardiac workload and metabolic demand impact the redox state of the myocardium and coronary arterial wall *in vivo*, we used high spatial resolution imaging mass spectrometry (IMS) to visualize and compare relative levels of lactate and pyruvate in hearts of mice subjected to short-term (i.e., ~5 min) elevation of cardiac workload (high workload) with those from low workload control mice (see **Figure 1A**).[219] The intracellular lactate:pyruvate ratio is a sensitive surrogate indicator of redox state of the pyridine nucleotide pair - NADH:$NAD^+$ ; both ratios are highly sensitive to oxygen levels in tissues and rise dramatically during ischemia.[220] Hence, we tested whether transient changes of myocardial $O_2$ consumption caused by elevated workload modulate lactate:pyruvate in the heart and coronary vasculature. For this, we subjected mice to stress via administration of the β-adrenoceptor agonist dobutamine (10 mg/kg, i.p.) and hearts were frozen immediately (**Figure 1B**). Branches of the left anterior descending coronary arteries were identified in H&E-stained sections as regions of interest for IMS measurements. Exemplary IMS images for lactate (m/z 89.024), pyruvate (m/z 87.009), and merged lactate:pyruvate, in hearts from low and high workload mice are shown in **Figure 1C**. Comparison of signal intensities revealed significantly higher lactate:pyruvate in hearts from high workload mice relative to those in low workload mice both in the perivascular region and the coronary wall (**Figure 1C, D**). These data suggest that an acute increase in cardiac workload elevates the lactate:pyruvate ratio in the

intramyocardial vasculature, consistent with a rise in intracellular levels of NADH relative to $NAD^+$.

To determine directly whether the NADH:$NAD^+$ ratio in arterial smooth muscle cells is sensitive to local cardiomyocyte contractile function, we monitored cytosolic NADH:$NAD^+$ ratio using the genetically-encoded fluorescent biosensor peredox-mCherry (see **Figure S1A**).[216] Consistent with previous reports, we observed a reduction in peredox-mCherry green:red fluorescence in the presence of decreasing external lactate:pyruvate in arterial myocytes (**Figure S1**). At baseline, the cytosolic NADH:$NAD^+$ ratio estimated by this technique was 0.0027 ± 0.0001, which is consistent with previous estimates made in vascular smooth muscle of porcine carotid strips,[186] and indicated that most of the nucleotide is in its oxidized form ($NAD^+$). To examine whether the NADH:$NAD^+$ ratio in arterial myocytes is affected by the metabolic activity of cardiomyocytes, we seeded isolated arterial myocytes expressing peredox-mCherry on two-dimensional monolayers of induced pluripotent stem cell-derived cardiomyocytes (iPSC-CMs; **Figure 2A**). After incorporation of peredox-mCherry-positive arterial myocytes into iPSC-CM monolayers (**Figure 2B**), we monitored NADH:$NAD^+$ in arterial myocytes during step-wise increases in the frequency of electrical stimulation (1–3 Hz). Consistent with the redox modifications resulting from changes in cardiac workload seen *in vivo* (**Figure 1**), we observed a significant increase in arterial myocyte cytosolic NADH:$NAD^+$ as the pacing frequency was increased (**Figure 2C, D**). These frequency-dependent changes in NADH:$NAD^+$ were dependent on the presence of cardiomyocytes (frequency*group interaction, cardiac/arterial myocyte

vs. arterial myocytes alone, p = 0.0007, **Figure 2C, D**). Electrical pacing of co-cultures increased cytosolic NADH:$NAD^+$ in arterial myocytes to a similar degree as a reduction in chamber $O_2$ levels from 5 to 1% (**Figure S2**). Moreover, the significant elevation of arterial myocyte NADH:$NAD^+$ was prevented by the general redox cycling agent 4-hydroxy TEMPO (tempol; 1 mM; p = 0.1164, **Figure S3**), suggesting that this effect is at least partially dependent on cardiomyocyte-derived reactive oxygen species.[221] To test the possibility that the changes in pyridine nucleotide ratios seen *in vivo* after β-adrenergic stimulation (**Figure 1**) were due to direct agonist effects in arterial myocytes, we tested whether activation of β-adrenoceptors on arterial myocytes alters the cytosolic NADH:$NAD^+$ ratio. However, application of the synthetic catecholamine isoproterenol modestly reduced (e.g., 0.0018 ± 0.0010 in presence of 1 μM isoproterenol vs. 0.0022 ± 0.0001 at baseline), rather than enhanced, the NADH:$NAD^+$ ratio (**Figure S4**). Taken together, these data suggest that inotropic and chronotropic stimulation of cardiomyocytes elevates NADH:$NAD^+$ in adjacent arterial myocytes.

**Intracellular pyridine nucleotide redox states reflecting augmented $O_2$ demand increase coronary Kv1 activity.** Coronary arterial myocyte Kv1 channels are essential for proper metabolic hyperemia.[37,55,177,181,187] Under native conditions, these channels are associated with ancillary Kvβ proteins, which bind pyridine nucleotides with high affinity.[199,214] Based on results presented in Figures 1 and 2, we tested whether covaried pyridine nucleotide levels in smooth muscle that simulate altered myocardial $O_2$ demand could influence Kv1 activity. For this,

using the conventional whole-cell configuration of the patch clamp technique, we recorded voltage-dependent outward $K^+$ currents after internal dialysis of cells with altered NAD(P)H:NAD(P)$^+$ ratios, referred to hereafter as either "oxidized" or "reduced" nucleotide compositions (see **Table S2** for concentrations and ratios). Under the applied patch conditions and nucleotide-free internal solution, the Kv1-selective inhibitor psora-4 (500 nM) inhibited ~60% of the total outward $K^+$ current recorded from isolated coronary arterial myocytes (**Figure S5**). As shown in **Figure 3A**, the magnitude of $I_K$ recorded from coronary arterial myocytes perfused with reduced nucleotides was significantly higher than the current recorded from myocytes perfused with oxidized nucleotides (**Figure 3A,B – i.)**. No significant differences in $I_K$ density were observed between groups when the recordings were performed in the presence of 500 nM psora-4 (**Figure 3A,B – ii.**). Exemplary psora-4-sensitive $I_K$ and summarized current densities in the presence of either oxidized or reduced nucleotide ratios are shown in **Figure 3A,B – iii**. Reduced nucleotide conditions also promoted hyperpolarizing shifts in the voltage-sensitivity of activation and inactivation ($V_{0.5,act}$ and $V_{0.5,inact}$, respectively; **Figure 3C** and **Table S3**). These data support the notion that the intracellular redox ratio of pyridine nucleotides is a critical regulator of Kv1 activity, and that pyridine nucleotides at levels expected under conditions of high $O_2$ demand augment Kv1 current density.

In its native state, Kv1 associates with intracellular Kvβ, which is a key regulator of Kv1 gating. In the coronary vasculature, loss of the Kvβ2 subunit hampers coronary vasodilatory function and suppresses myocardial blood flow.[37]

In arterial myocytes, loss of Kvβ2 does not significantly impact basal $I_K$ density, but results in modest shifts in $V_{0.5,act}$ and $V_{0.5,inact}$ (**Figure S6**). However, deletion of Kvβ2 completely abolished the pyridine nucleotide sensitivity of Kv current. In contrast to effects observed in coronary arterial myocytes from wild type mice, no differences in $I_K$ density were observed between oxidized and reduced nucleotide conditions in cells from Kvβ2$^{-/-}$ mice **(Figure 3D)**. In addition, the loss of Kvβ2 proteins markedly altered the response in voltage-sensitivity to reduced nucleotides; whereas robust hyperpolarizing shifts in $V_{0.5,act}$ and $V_{0.5,inact}$ were observed in cells from wild type mice (**Figure 3C**), depolarizing shifts were observed in $V_{0.5,act}$ and $V_{0.5,inact}$ in arterial myocytes from Kvβ2$^{-/-}$ mice (**Figure 3E and Table S3**). Collectively, these data indicate that in coronary arterial myocytes, Kvβ2 imparts sensitivity of native Kv1 channels to pyridine nucleotide redox state.

**Direct potentiation of native coronary Kv1 channel activity by NADH.** We next tested whether an elevation of NADH in the cytosolic compartment would affect the activity of native coronary Kv1 channels. To test this, we measured the open probability of single Kv channels using the inside-out patch configuration. Unitary current amplitudes recorded over a range of voltage in the presence of $K_{ATP}$ and $BK_{Ca}$ channel inhibitors (i.e., glibenclamide and iberiotoxin, respectively) showed similar conductance values between patches from freshly isolated coronary arterial myocytes and Cos-7 cells expressing Kv1.5 (**Figure 4A, B**). Moreover, single channel events with amplitudes similar to that reported for Kv1 channels (+40 mV)[140] were abolished by application of 500 nM psora-4 in the bath solution

(**Figure 4C-D**), further supporting that channel activity observed under the specified conditions is mediated by Kv1 channels. At a holding potential of -40 mV, application of 1 mM NADH in the bath resulted in an immediate increase in Kv1 open probability ($nP_o$, **Figure 4E, F**). In contrast, no change in $nP_o$ was observed in the presence of $NAD^+$, suggesting that nucleotide-induced changes in Kv1 activity are dependent on redox state. Similar responses in channel activity in response to 1 mM NADH were observed in excised membrane patches from human coronary arterial myocytes (**Figure 4G**). Note that using in situ proximity ligation to assess Kv1 subunit interactions as previously described, we found that freshly isolated human coronary arterial myocytes, like murine cells, express Kv1 pore-forming subunits that interact with Kvβ1.1 and Kvβ2 proteins (**Figure S7**).[37,208,214] Whereas the NADH-induced increase in open probability was unaffected by ablation of Kvβ1.1, this effect was abolished in coronary arterial myocyte membrane patches from mice lacking Kvβ2 (**Figure 4H, I**). Together, these results indicate that NADH directly increases the activity of native coronary Kv1 channels and that the regulation of Kv1 by NADH is attributed to the Kvβ2 subunit.

**Redox control of Kv1 activity, vasodilation, and myocardial blood flow require intact enzymatic function of Kvβ2.** Considering that myocardial metabolism modifies coronary arterial myocyte pyridine nucleotide redox state and that this regulates Kv1 activity via the Kvβ2 subunit, we next tested whether this mode of regulation involves Kvβ2-mediated catalysis. Previous work has shown

that the Kvβ2 protein possesses weak aldehyde reductase activity that depends on a tyrosine residue at position 90 (Y90) for hydride transfer during the reductive catalytic cycle.[138,207] Therefore, to examine the role of Kvβ2-catalysis, we isolated arterial myocytes from mice in which the catalytic site tyrosine (Y90) of Kvβ2 is mutated to phenylalanine ($Kv\beta2^{Y90F}$). The abundance of Kvβ2 protein was not significantly different between arteries from $Kv\beta2^{Y90F}$ mice compared with those from wild type mice (**Figure S8**). In contrast to the NADH-induced increases in single Kv1 channel activity in coronary arterial myocytes from wild type mice (**Figure 4E, F**), no significant change in $nP_o$ was observed upon application of NADH in coronary arterial myocytes from $Kv\beta2^{Y90F}$ mice (**Figure 5A, B**). These observations suggest that catalytic turnover is essential for the redox regulation of Kv1 currents by Kvβ2. Next, we examined whether catalytic turnover is also required for redox-dependent vasoreactivity and regulation of myocardial blood flow in vivo. We previously reported that ablation of Kvβ2 suppresses redox-dependent vasodilation induced by elevated external L-lactate.[37] In agreement with these observations, we found that elevation of L-lactate caused vasodilation in arteries isolated from wild type mice; however, this effect was abolished in arteries from $Kv\beta2^{Y90F}$ mice (**Figure 5C**), indicating that Kv1-mediated vasodilation in response to changes in intracellular pyridine nucleotides depends entirely upon the catalytic activity of Kv□2. Moreover, vasodilation upon application of $H_2O_2$ (0.1 – 10 μM) was similarly abolished in arteries from $Kv\beta2^{Y90F}$ mice (**Figure 5D**), consistent with the role for Kvβ2 catalytic function in the physiologic vascular response to endogenous ROS production.

Next, to investigate whether Kv1-mediated regulation of myocardial blood flow depends similarly on catalytically active Kvβ2, we examined blood flow across a range of cardiac workloads, as described previously.[37,55] Intravenous infusion of norepinephrine led to similar increases in mean arterial pressure and heart rate in wild type and Kvβ2$^{Y90F}$ mice (**Figure 5E**). In wild type mice, increases in cardiac workload (double product of mean arterial pressure x heart rate) was accompanied by a proportional increase in myocardial blood flow (**Figure 5F**). Nonetheless, myocardial blood flow across the range of observed cardiac workloads was significantly suppressed in Kvβ2$^{Y90F}$ mice. The resultant suppression of blood flow upon loss of Kvβ2 catalytic function was comparable to that observed in mice lacking Kv1α subunits (i.e., Kv1.5 or Kv1.3) or Kvβ2. Collectively, these data indicate that pyridine nucleotide binding and catalytic cycling performed by Kvβ2 mediates the upregulated Kv1 activity underlying physiologic vasodilation and enhanced perfusion of the heart during acute metabolic stress.

## Discussion

The functional upregulation of voltage-gated $K^+$ channels in the coronary vasculature mediates metabolic hyperemia in the heart, yet the molecular events underlying how these channels sense changes in myocardial metabolism to dynamically regulate coronary arterial tone are unknown. In this study, we show that cardiac workload-dependent modifications to the pyridine nucleotide redox potential of coronary arterial myocytes promote enhanced Kv1 activity and vasodilation via the auxiliary Kvβ subunit complex (**Figure 6**). Catecholamine-

driven increases in cardiac work in vivo and high frequency stimulation of cardiomyocytes ex vivo increase the cytosolic NADH:$NAD^+$ ratio of proximal arterial myocytes, consistent with this redox couple serving as a modifiable vascular indicator of myocardial oxygen demand. Elevated levels of reduced pyridine nucleotides in coronary arterial myocytes promoted increases in Kv1 current density; and reduced (i.e., NADH), but not oxidized (i.e., $NAD^+$) nucleotides directly stimulated the activity of single native coronary Kv1 channels. Moreover, these effects were dependent on the presence of Kvβ2. Consistent with the concept that changes in pyridine nucleotide redox state and Kvβ2-mediated cofactor oxidation are required for nucleotide-sensitive upregulation of Kv1 activity, the ablation of Kvβ2 catalytic function abolished NADH-induced potentiation of Kv1 activity and vasodilation and suppressed myocardial blood flow.

The mechanical workload of the heart and rates of myocardial oxygen consumption are relatively stable at rest, yet can increase dramatically in response to environmental or physiologic cues. Resting heart rates in humans normally falls between 50-85 beats per minute,[222] although periods of extreme tachycardia can be sustained with rates up to 240 beats per min without lasting structural damage.[223] Likewise, conscious mice have heart rates of 500-700 beats per minute and can be increased to as high as 840 beats per minute.[224] Such large ranges of myocardial work among mammals are enabled by an intrinsic flexibility of myocardial metabolic activity. Under periods of stress, myocardial oxygen consumption can increase by as much as 10-fold relative to resting rates.[44] Nonetheless, sustaining a high metabolic rate during periods of stress requires

instantaneous and maintained increases in oxygen supply via arterial blood flow. Although extensive work has aimed to identify molecular processes regulating coronary perfusion as a function of cardiac metabolism, the underlying mechanism remains a fundamental enigma in cardiovascular physiology.[44,225]

Resistance sized arteries and arterioles of the coronary circulation maintain a partially constricted state from which they can readily dilate in response to local metabolic signals. In the absence of microcirculatory dysfunction, myocardial perfusion can increase 4-5-fold via reduced vascular resistance under conditions of high metabolic demand such as strenuous physical activity. For the heart to match oxygen supply to consumption, the coronary resistance arteries and arterioles modify their degree of tone in an orchestrated manner, by independently responding to metabolic, hemodynamic, and neurohumoral signals.[45] In particular, the sensing of changes in local tissue metabolism by arterioles directly controls the perfusion of the low-resistance coronary capillary bed.[226] Previous work has shown that small arterioles regulate their diameter in response to changes in local shear stress (flow-mediated dilation), which depends upon endothelium-derived nitric oxide, particularly in smaller arteries.[227-229] While there is currently no consensus, it is thought that coronary vascular resistance is dynamically regulated by the integration of local physical forces (pressure and flow), neurohumoral modulation, and exposure to vasodilator metabolites such as adenosine, $pO_2$, and pH. How these various factors influence the function of key effector pathways known to modulate coronary arterial myocyte function and vascular tone such as voltage-gated $K^+$ channels is unknown. The findings presented here provide evidence that

the capacity of vascular Kvβ proteins to sense pyridine nucleotide redox state and differentially control Kv1 activity is a missing link in the processes that couple myocardial metabolism with coronary arterial diameter and blood flow.

Several lines of evidence described above support a crucial role of the pyridine nucleotide sensing by Kvβ as a central event in the regulation of coronary blood flow. Previous work has shown that pharmacological inhibitors of Kv1 channels (4-aminopyridine, correolide) or genetic deletion of specific pore proteins that assemble as heteromeric Kv1 channels (Kv1.5, Kv1.3) dissociate changes in blood flow from metabolism, resulting in ischemia and cardiac pump dysfunction.[55,181,230] We have also reported that this behavior of Kv1 members depends upon their association with the intracellular auxiliary subunits – Kvβ, such that Kvβ2 promotes and Kvβ1 inhibits oxygen-dependent vasodilation.[37] Nevertheless, the mechanism by which Kvβ2 confers oxygen-sensitivity to vascular Kv1 channels has remained unclear. Although these channels consist of several auxiliary subunits,[214] the Kvβ subunits have a unique structure which allows high affinity binding to pyridine nucleotides[207] and low-rate catalysis of carbonyl substrates.[138] Because binding of Kvβ alters Kv gating,[140] changes in pyridine coenzymes in arterial myocytes in response to changes in $pO_2$ could in principle regulate Kv1 activity via interacting Kvβ proteins. Indeed, as reported in this study, we found that elevated tissue demand for oxygen increases the $NADH:NAD^+$ ratio in arterial myocytes and that the ratios of pyridine nucleotides achieved at low $pO_2$ augment Kv1 activity. Most cells maintain a low $NADH:NAD^+$ ratio under aerobic conditions. However, even marginal decreases in $O_2$ availability reduce the rate of

oxidative phosphorylation and can lead to the accumulation of NAD in its reduced form – i.e., NADH. This change in the redox state of the NADH/$NAD^+$ couple is closely reflected in the lactate:pyruvate ratio, which is determined in part by the activity of lactate dehydrogenase operating near equilibrium conditions.[219,231,232] Aside from changes in $O_2$ availability, altered NADH:$NAD^+$ induced by diffusible metabolites such as ROS or extracellular lactate results in vasodilation and this functional response is critically dependent on the expression and catalytic function of Kvβ2 (**Figure 5** and [37]). Loss of lactate-induced vasodilation in arteries from Kvβ-null animals indicates that the Kvβ complex itself, rather than the pore domain, impart pyridine nucleotide redox sensitivity to native vascular Kv1 channels. Moreover, our observation that the activity of Kv channels in coronary arteries is regulated directly by NADH:$NAD^+$ in proportion to ratios expected under low and high oxygen tensions, and that regulation is abolished by the loss of Kvβ2, provide compelling evidence of the unique redox sensitivity of the Kv1-Kvβ2 complex and its specific dependence on intracellular pyridine nucleotide redox state.

It is noteworthy that the effects of reduced pyridine nucleotides (i.e., NADH) on Kv1 activity extends to the coronary circulation of humans. Indeed, like in coronary arterial myocytes of mice, Kvβ proteins are abundant and associate with Kvα pore proteins in human coronary arteries (see Figure S7 and [185]). In large animals and small rodent models, voltage-gated $K^+$ channels have been identified as a key effector that establishes the relationship between myocardial oxygen consumption and perfusion; however, other redox sensitive cation channels (e.g., $K_{ATP}$, $BK_{Ca}$)[183] may be influenced by altered pyridine nucleotide levels to impact

either basal vascular tone, or vasoactive responses to metabolic stimuli. Moreover, it is also unclear whether the mechanism reported here extends to vascular beds outside of the heart. Our previous work indicates that Kvβ proteins are expressed and functional in small arteries and arterioles of peripheral tissues (e.g., mesenteric vessels).[37] Nonetheless, we speculate that organ-specific differences in tissue metabolism (e.g., basal and stress-related $O_2$ consumption) and associated metabolite generation may differentially impact smooth muscle pyridine nucleotide redox state, which our current study suggests is a key determinant of Kvβ function in the coronary vasculature. Additionally, the compositions of heteromeric Kvα:β complexes may be unique to a particular vascular bed to enable distinct functional responsiveness of Kv channels to changes in the local tissue environment.

Our observations are consistent with prior findings suggesting a role for reactive oxygen species signaling in regulating Kv activity in the coronary vasculature.[167,185,188] Specifically, elevated myocardial oxygen consumption is associated with increases in the levels of tissue hydrogen peroxide, a potent vasodilator that has effects on smooth muscle $K^+$ channels.[188] Our data showing that the antioxidant tempol prevents frequency-dependent elevation of NADH:$NAD^+$ in arterial myocytes is consistent with past reports suggesting that hydrogen peroxide and other forms of oxidative stress can acutely modify pyridine nucleotide redox ratios,[127,189,233] which we show directly influences Kv activity. It is likewise plausible that oxidant-induced effects on Kv function may result from increased NADPH-oxidase activity or direct channel modifications (e.g., cysteine oxidation). Nonetheless, our current data indicate that the binding of reduced

nucleotides to the Kv1 auxiliary subunit complex, presumably in the absence of these oxidative modifications, is sufficient to drive marked changes in Kv1 open probability. Furthermore, ablation of Kvβ2 catalytic function abolished NADH-evoked increases in channel activity and blunted vasodilation to both lactate and hydrogen peroxide, suggesting that Kvβ AKR function is central to the mechanism underlying the actions these physiological vasodilators. Based on these findings, we propose that changes in the levels of reduced nucleotides upon increased oxygen consumption enables direct stimulation of channel activity that is rapidly reversed upon catalytic cycling when nucleotide redox state returns to baseline. This mechanism is akin to that recently proposed in the excitability of Drosophila dorsal fan-shaped body neurons, in which ROS accumulation and the conversion of NADPH to $NADP^+$ by Hyperkinetic (orthologue of mammalian Kvβ), underlies slow A-type current inactivation, action potential frequency enhancement, and the induction of sleep.[182] That a similar mechanism may be operative with respect to blood flow regulation *in vivo* is supported by evidence showing that acute increases in cardiac workload promotes the accumulation of the lactate:pyruvate ratio in the intramyocardial vasculature. Although we could not directly measure NADH:$NAD^+$ ratio in vivo, the use of lactate:pyruvate ratio as a surrogate of pyridine nucleotide redox state is based on the tight coupled relationship between lactate:pyruvate and NADH:$NAD^+$ ratios amply demonstrated in previous studies.[219,231] Thus, it is plausible that under conditions of increased workload, increased oxygen consumption and demand alters coronary arterial myocyte redox state in favor of reduced NADH:$NAD^+$.

Despite strong evidence supporting this model, the specific processes underlying the workload-dependent effects on Kvβ function remain unclear. Perhaps the most intriguing finding of our study is the dependence of nucleotide sensing on the catalytic activity of Kvβ. In other aldo-keto reductases, the apo-protein can bind to pyridine nucleotides in the absence of substrate and the nucleotide is released only after its oxidation; the release of the nucleotide is usually the rate-limiting step in the catalytic cycle.[234] A similar kinetic mechanism may be operating in Kvβ,[138] which seems to be able to bind to nucleotides in the absence of any substrate.[207] However, for it to impact Kv gating, the cofactor must remain bound to the protein or undergo oxidation. Our observation that the regulation of Kv by Kvβ2 is abolished when the protein is catalytically incompetent favors the latter possibility – i.e., catalytic turnover of the protein is essential for the continued regulation of Kv gating under native conditions. Although this study did not aim to identify the in vivo substrates of Kvβ catalysis, our previous work suggests that lipid-derived aldehydes may be potential candidates for such regulation.[138,156] Further investigations are required to identify the substrate(s) that support Kvβ catalysis and thereby regulate Kv activity and vasodilation under conditions of varied myocardial oxygen demand. Nevertheless, our current observations offer the first example of a physiologic role for metabolic regulation of an ion channel by direct catalytic activity of its subsidiary subunit. Our findings therefore constitute a new paradigm for cellular oxygen sensing that may be an essential component of cardiovascular function in health and disease.

**Acknowledgements**

This work was supported by grants from the National Institutes of Health (HL142710, GM127607), American Heart Association (16SDG27260070), and the University of Louisville, School of Medicine.

## Figures with Legends

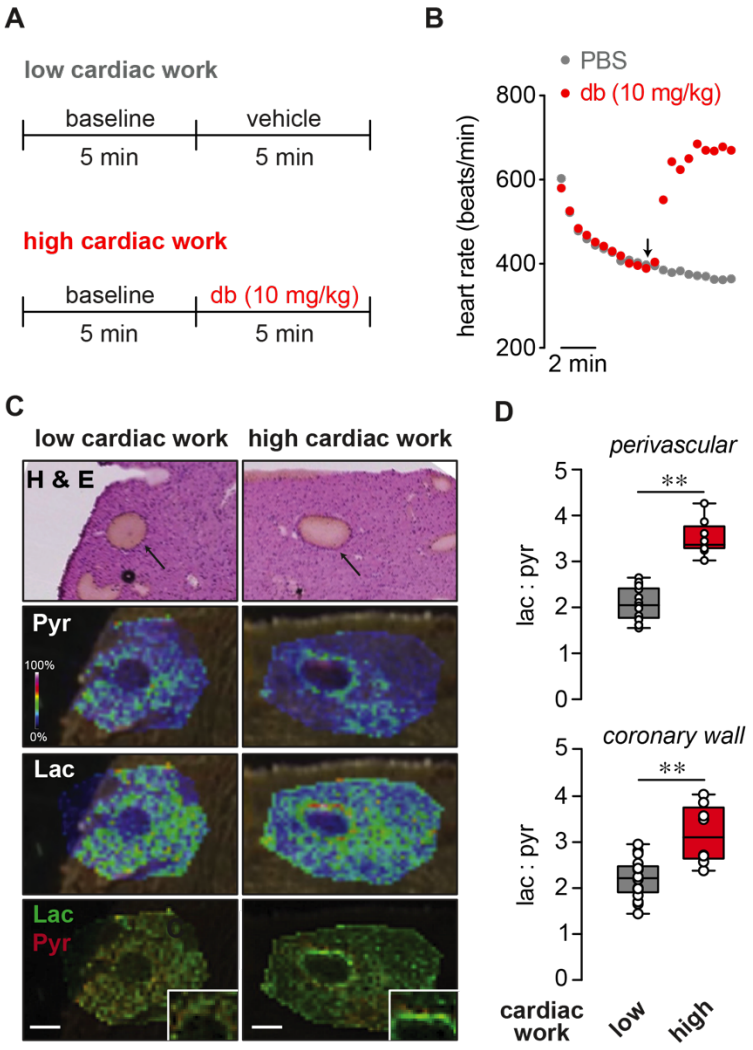


**Figure 1: Increased myocardial workload promotes local elevation of lactate:pyruvate ratio in the coronary arterial wall.** (**A**) Schematic showing protocol for induction of acute cardiac stress prior to collection of tissues for MALDI-MS imaging. To induce high cardiac work, anesthetized mice with stable heart rates of 400-450 bpm were treated with dobutamine (db; 10 mg/kg, i.p.). Heart rate was continuously monitored, and hearts were rapidly cryopreserved in the thoracic cavity and excised after 2-3 minutes of stabilized heart rate responses to either db or PBS

(vehicle). (**B**) Symbol plot showing exemplary heart rates recorded every 30 seconds before (i.e., during induction and stabilization of anesthesia) and after administration of either db (10 mg/kg; i.p.) or PBS. (**C**) Images of left ventricular intramyocardial coronary arteries in H & E-stained heart sections and corresponding intensity-coded MALDI-MS images showing lactate (Lac) and pyruvate (Pyr) relative to background signals in hearts from low and high cardiac work mice. x-y resolution: ~20 µm. Insets show magnified region of interest at coronary arterial wall. Scale bars represent 200 µm. (**D**) Box and whiskers plots showing lactate:pyruvate ratios in perivascular myocardium (region of interest within ~250 µm from coronary wall; *top*) and coronary wall (*bottom*) in hearts of low and high cardiac work mice. (low cardiac work: n = 16 technical replicates, 4 mice, high cardiac work group: n = 8 technical replicates, 2 mice), perivascular, $^{**}p < 0.0001$, coronary, $^{**}p = 0.0003$ (unpaired t test).

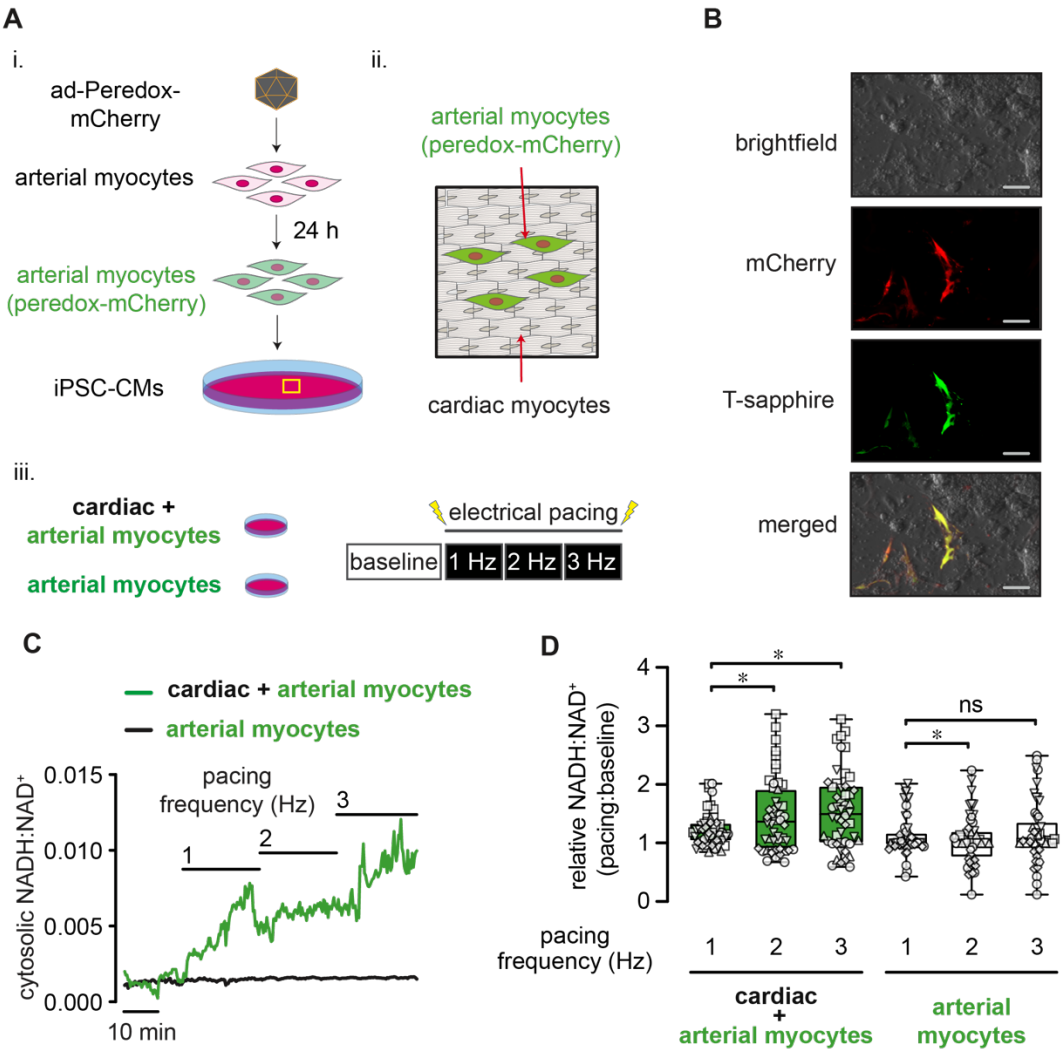


**Figure 2: Arterial myocyte NADH:NAD+ is sensitive to changes in proximal cardiomyocyte beating frequency.** (**A**) Schematic illustration depicting the preparation of arterial myocyte/induced pluripotent stem cell-derived cardiomyocyte (iPSC-CM) co-cultures. Primary aortic vascular smooth muscle cells (passage 0-2) were treated with adenovirus to express the NADH:NAD$^+$-sensitive fluorescent biosensor peredox-mCherry (*i.*). Arterial myocytes were then seeded and allowed to integrate (48 hr) onto a two-dimensional monolayer of iPSC-CMs (*ii.*). Imaging was performed on either arterial/cardiac co-cultured myocytes or arterial myocytes alone during electrical stimulation (1–3 Hz; *iii.*) while monitoring peredox-mCherry green:red fluorescence. (**B**) Exemplary brightfield and fluorescence images showing red (mCherry) and green (T-sapphire) fluorescence of peredox-mCherry expressing arterial myocytes in the presence of non-fluorescent cardiac myocytes in an arterial + cardiac myocyte co-culture. Scale bars represent 100 µm. (**C**) Exemplary time series of arterial myocyte NADH:NAD$^+$ in either an arterial/cardiac myocyte co-culture (green trace) or arterial myocytes alone ( – cardiac myocytes; black trace) at baseline (0 Hz) and during electrical stimulation (1–3 Hz). (**D**) Box and

whiskers plots summarizing fold-change in NADH:$NAD^+$ in arterial myocytes in arterial/cardiac myocyte co-cultures or arterial myocytes alone. Arterial/cardiac myocytes, n = 50 cells from 5 independent experiments, 2 vs. 1 Hz, *p = 0.0047; 3 vs. 1 Hz, *p = 0.0012; Arterial myocytes only, n = 52 cells from 6 independent experiments, 2 vs. 1 Hz, *p = 0.0029; 3 vs. 1 Hz, *p = 0.6574 (Linear mixed models, log-transformed NADH:$NAD^+$).

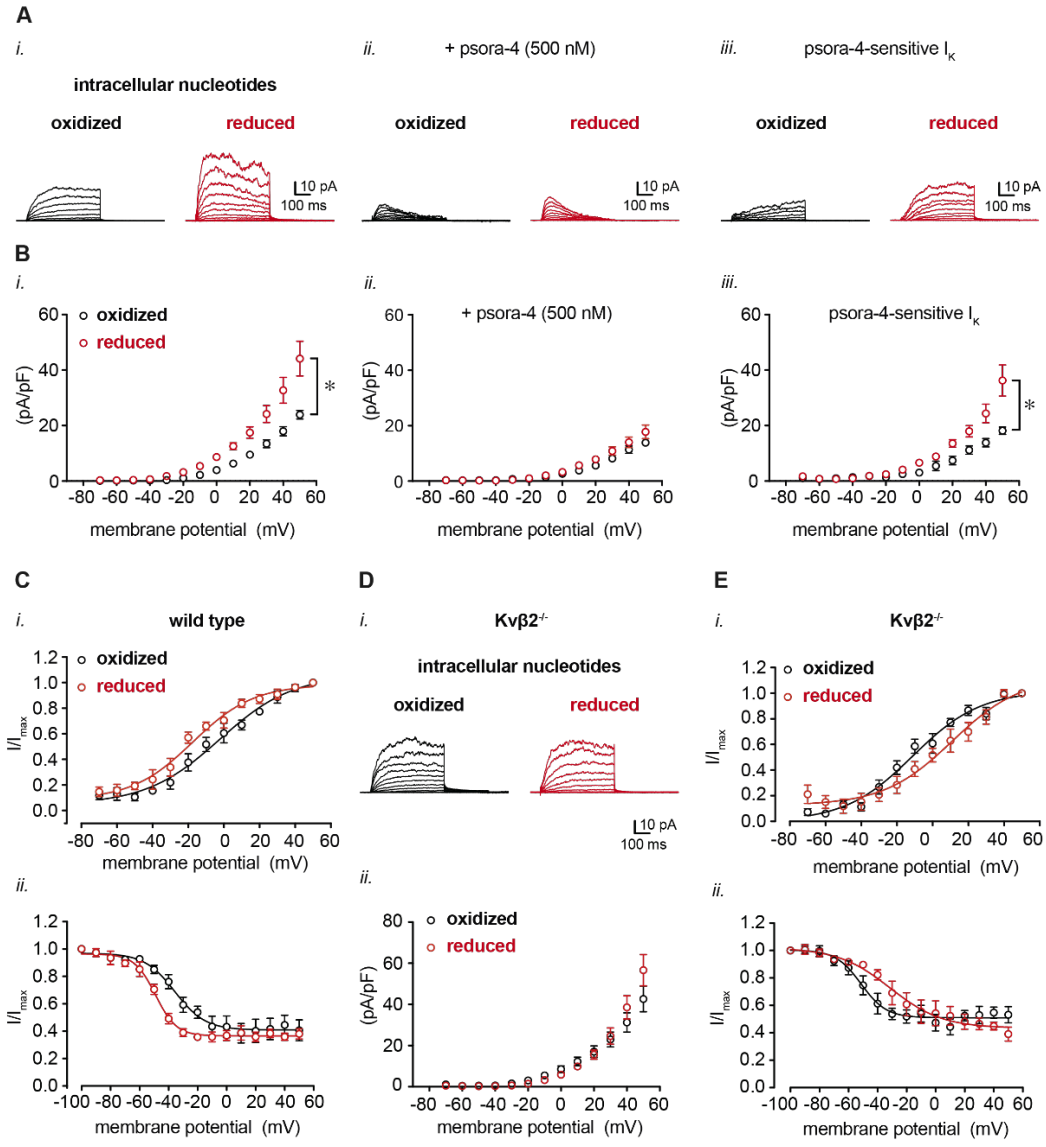

**Figure 3: Modulation of coronary arterial myocyte IKv upon changes in intracellular pyridine nucleotide redox potential.** Isolated coronary arterial myocytes were dialyzed with pyridine nucleotides at concentrations as indicated in **Table S2** for voltage-clamp recordings in the conventional whole cell configuration. (**A-B**) Representative outward $K^+$ currents (*A*) and $I_K$ densities (pA/pF; *B*) recorded in coronary arterial myocytes from wild type mice (129SvEv) in the presence of either oxidized or reduced pyridine nucleotide redox ratios. Recordings were performed in the absence (*i.*) and presence (*ii.*) of the Kv1 channel inhibitor psora-4 (500 nM). Representative psora-4-sensitive currents (i.e., total outward $I_K$ – psora-insensitive $I_K$) and summarized densities are shown in *iii.* panels. n = 5-6 cells, 4-5 mice for each. *P<0.001, oxidized vs. reduced (mixed effects analysis). (**C**) Summarized I/Imax from two-pulse activation voltage protocol (*i.*) and inactivation protocol (*ii.*) for coronary arterial myocytes from wild type mice in the presence of oxidized or reduced pyridine nucleotide ratios. Curves were fit with a Boltzmann function; $V_{0.5,act}$ and $V_{0.5,inact}$ are provided in **Table S3**. n = 5-6 cells, 4-5 mice for each. (**D**) Representative total outward $I_K$ and summarized $I_K$ density, as in A, recorded in coronary arterial myocytes from $Kv\beta2^{-/-}$ mice in the presence of either oxidized or reduced pyridine nucleotide ratios. n = 8-9 cells, 5 mice for each. (**E**) Plots showing summarized I/Imax with Boltzmann fittings, as in D, recorded from coronary arterial myocytes from $Kv\beta2^{-/-}$ mice. $V_{0.5,act}$ and $V_{0.5,inact}$ for each condition are provided in **Table S3.** n = 5-7 cells, 4-5 mice for each.

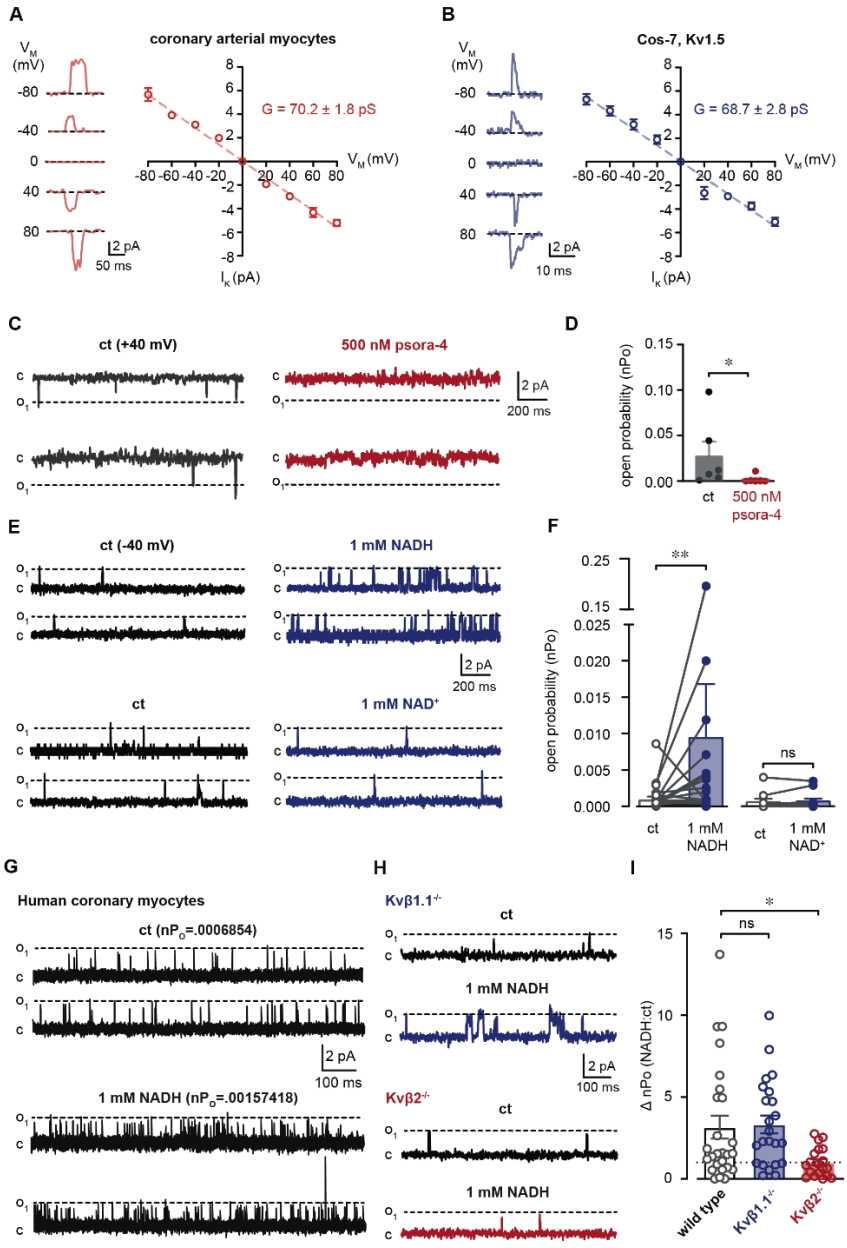


**Figure 4: Potentiation of native coronary Kv1 activity by NADH requires Kvβ2.** (**A-B**) Unitary $K^+$ channel currents (-80-80 mV as indicated, *left*) and summarized I-V relationships (*right*) from inside-out patch recordings from isolated coronary arterial myocytes (wild type 129SvEv, *A*) or Cos-7 cells transiently expressing Kv1.5 (*B*). *A*, n = 9 cells; *B*, n = 4 cells (**C**) Single $K^+$ channel activity in patches from coronary arterial myocytes at a holding potential of +40 mV in the absence and presence of

psora-4 (500 nM). (**D**) Summary of $K^+$ channel open probabilities (nPo) recorded in the absence and presence of 500 nM psora-4. n = 6 cells, *P<0.05 (paired t-test). (**E**) Representative single Kv current recordings (holding potential = -40 mV) in the absence (ct) and presence of 1 mM NADH (*top*) or 1 mM $NAD^+$ (*bottom*). (**F**) Summary of Kv channel nPo recorded before (ct) and after bath application of 1 mM NADH or $NAD^+$. **P<0.01 (paired t-test). (**G**) Single Kv channel currents recorded from freshly isolated human coronary arterial myocyte membrane patches before and after application of 1 mM NADH. nPo values for each condition are provided above each set of example traces. Data are representative of 4 independent experiments (one donor). (**H**) Inside-out patch recordings in coronary arterial myocyte membrane patches from Kvβ1.1$^{-/-}$ or Kvβ2$^{-/-}$ mice before and after application of 1 mM NADH. (**I**) Summary of fold-change in nPo (NADH:ct) in patches from wild type, Kvβ1.1$^{-/-}$, and Kvβ2$^{-/-}$ mice. *P<0.01 (Kruskal-Wallis test).

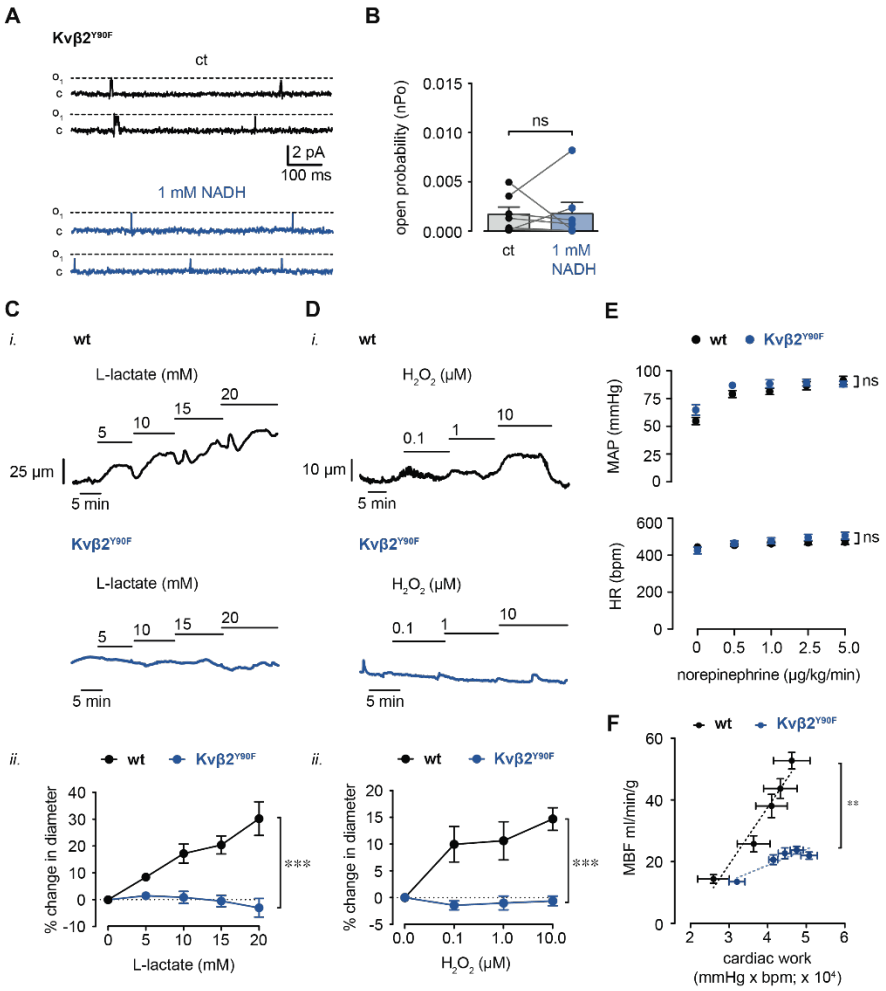


**Figure 5: Loss of Kvβ2 catalytic function prevents redox-mediated increases in Kv1 activity and vasodilation, and suppresses MBF.** (**A**) Inside-out recordings of Kv1 activity in membrane patches from Kvβ2$^{Y90F}$ mice before and after application of 1 mM NADH. (**B**) Summary of Kv1 open probabilities (nPo) in membrane patches form Kvβ2$^{Y90F}$ mice before and after application of 1 mM NADH. n = 6 cells from 3 mice; ns: P≥0.05 (Wilcoxon matched-pairs signed rank test). (**C**) Representative arterial diameter recordings in arteries from wild type (129SvEv) and Kvβ2$^{Y90F}$ mice in the absence and presence of L-lactate (5-20 mM) in the perfusate (*i.*); and, summary

of percent change in diameter in response to L-lactate (5-20 mM) relative to baseline (– L-lactate, *ii.*). ***P<0.001 (two-way repeated measures ANOVA). (**D**) Representative arterial diameter recordings in arteries from wild type (129SvEv) and Kvβ2$^{Y90F}$ mice in the absence and presence of $H_2O_2$ (0.1-10 μM) in the perfusate (*i.*); and, summary of percent change in diameter in response to $H_2O_2$ (0.1-10 μM) relative to baseline (– $H_2O_2$, *ii.*). ***P<0.001 (two-way repeated measures ANOVA). (**E**) Summary of mean arterial pressure (MAP) and heart rate (HR) in wild type and Kvβ2$^{Y90F}$ mice during intravenous norepinephrine infusion (0-5 μg/kg/min). n = 4 each, ns: P≥0.05 (two-way repeated measures ANOVA). (**F**) Summary of relationships between MBF (ml/min/g) cardiac work (pressure rate product; bpm x mmHg) in wild type (wt; 129SvEv) versus Kvβ2$^{Y90F}$mice. **P<0.01, slope wt vs. Kvβ2$^{Y90F}$, n = 4-6 mice, (linear regression).

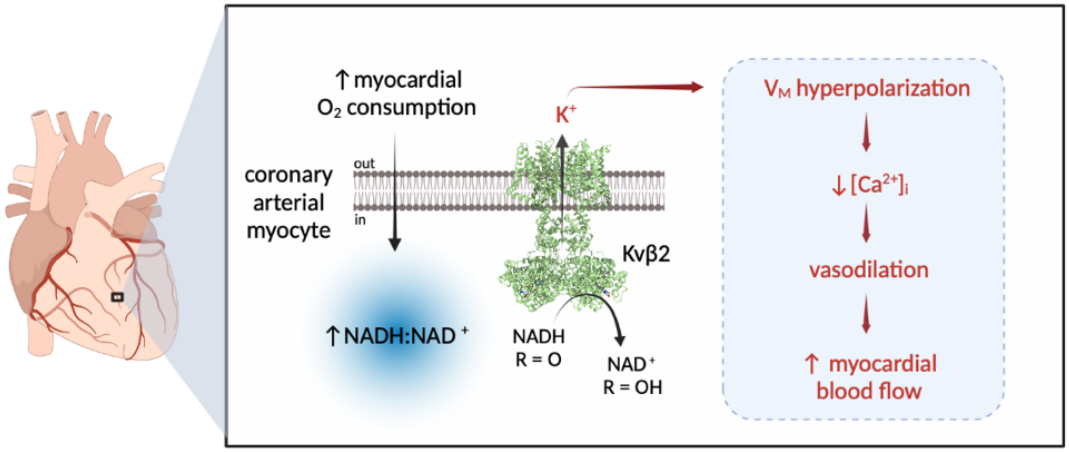


**Figure 6: Oxygen demand-sensitive coronary arterial myocyte NADH:NAD+ links blood flow to myocardial metabolism via Kvβ2 catalytic function.** Schematic representation showing proposed model of myocardial blood flow regulation via coronary pyridine nucleotide redox potential. Increases in myocardial oxygen consumption and cardiac workload promote the rapid elevation of intracellular NADH:$NAD^+$ in arterial myocytes in the wall of intramyocardial coronary arteries. This change in redox balance modulates the voltage-sensitivity of Kv1 gating via binding and enzymatic oxidation of NADH by Kv-associated Kvβ2 proteins. Resultant enhancement of steady-state $K^+$ efflux leads to membrane potential ($V_M$) hyperpolarization, reduction in intracellular $[Ca^{2+}]_I$, arterial myocyte relaxation, and vasodilation, thus increasing blood flow. Created with BioRender.com.

# APPENDIX B

Diversification of potassium currents in excitable cells via Kvβ proteins[7]

## 1. Introduction

Numerous physiological processes rely on coordinated cellular ionic currents me- diated by transmembrane ion channels. Tight regulation of K+ currents is critical for excitable cell functionality as the efflux of K+ along its electrochemical gradient is a primary means of cellular repolarization and maintenance of the resting membrane potential. Major classes of K+ channels that mediate this current include the two-transmembrane helix inwardly rectifying potassium channels (Kir), four-transmembrane tandem pore domain potassium channels (K2P), and six-transmembrane helix voltage-dependent potassium channels. These broader families are further divided into subfamilies; for example, Kir-related KATP potassium channels, voltage-gated (Kv) K+ channels, and voltage-sensitive $Ca^{2+}$-activated (KCa) potassium channels [1,2]. In complex organisms, the extensive diversity of potassium channel subtypes enables refinement of the K+ current morphology and membrane excitability in the context of cell-specific functionalities and persistently changing physiological conditions.

[7] This work was published as the following reference 132. Dwenger MM, Raph SM, Baba SP, Moore JBt, Nystoriak MA. Diversification of Potassium Currents in Excitable Cells via Kvbeta Proteins. *Cells*. 2022;11. doi: 10.3390/cells11142230

Voltage-gated K+ channels are widely expressed among excitable cells and participate in the control of membrane excitability in neurons, cardiomyocytes, and vascular smooth muscle, as well as other cell types. Unlike other voltage-gated ion channels (e.g., Nav, Cav), the Kv pore-forming complex is comprised of four distinct subunits (Kvα) that form the voltage-sensing, gating, and selectivity domains [3–5]. Kvα pore proteins are associated with several classes of cytoplasmic protein complexes that regulate subcellular localization and gating kinetics [4,6]. Kvβ proteins, which are predominantly associated with the Kv1 and Kv4 families, are functional aldo–keto reductases (AKRs) that catalyze the NAD(P)H-dependent reduction of carbonyl substrates to primary and secondary alco- hols [6]. Intriguingly, Kvβ AKR activity has been shown to regulate channel trafficking and gating [7,8]. Thus, the enzymatic properties of these associated proteins could conceivably couple membrane excitability to cell metabolism or vice versa. That is, Kvβ may regulate membrane potential according to the metabolic state of the cell or, alternatively, changes in membrane potential and channel gating may modify the local pyridine nucleotide redox potential and contribute to long-term remodeling processes [4].

Prior examination of cloned Kv subunits in heterologous systems has revealed important regulatory functions of Kvβ proteins. Building upon this foundation, more recent research has indicated key physiological roles for native Kvβ proteins in vivo [9–11]. Accordingly, in this review, we delineated the current knowledge of the roles for Kvβ proteins in regulating Kv currents and membrane excitability in the nervous and cardiovascular systems. Considering that Kvβ

proteins are associated with Kv1 and Kv4 channels, we focused our discussion on these channels. We also identified the knowledge gaps related to the complex physiological implications of cell-specific integration of distinct Kvα and β proteins and adaptive remodeling of heteromultimeric channel complexes.

## 2. Structural Determinants of the Kv Function

Intense investigation of Kv channels was inspired by early serendipitous observations of the shaking leg phenotype in mutant Drosophila melanogaster that were associated with aberrant K+ conductance and synaptic transmission [12–14]. The so-called Shaker locus was shown to underlie “A-type” outward K+ currents [15,16] mediated by a diverse array of N- and C-terminal channel splice variants [17–20]. The Shaker variants were identified as one of several channel subfamilies that also consists of the Shab, Shaw, and Shal proteins [21–23] corresponding to Kv1, Kv2, Kv3, and Kv4 vertebrate homologs, respectively [24–28]. Crude structural models of Kv multiprotein complexes were predicted via electrophysiological studies using various toxins; dendrotoxin was found to bind channels consisting of two discrete proteins with molecular masses of ~65 and 37 kDa [29,30]. Further sedimentation and electrophysiological analyses of toxin-bound proteins suggested an α4/β4 octameric assembly [31,32] which was later confirmed by X-ray crystallography [4] (Figure 1). Each Kvα protein within the pore tetramer consists of the voltage-sensing apparatus and the activation gate which transitions to the open state upon membrane depolarization to permit K+ conductance [4,33,34]. As channel activation proceeds, the selectivity filter slowly changes the conformation, returning the channel to an inactivated state (i.e., C-

type inactivation) [35,36]. Conversely, some Kv subtypes exhibit rapid channel inactivation via a “ball-and-chain” mechanism, in which an N-terminal peptide from either the α or β subunit occludes the channel pore [37,38].

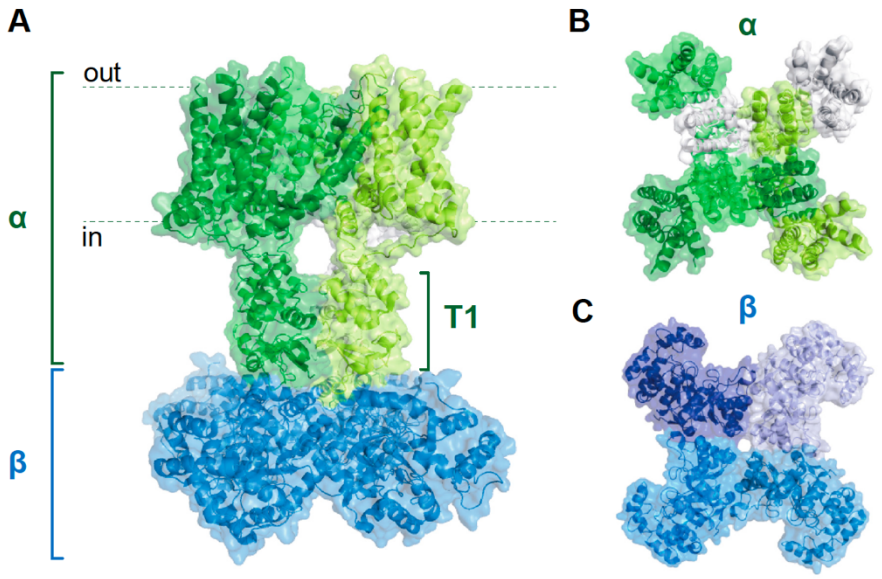


Figure 1. Kv1 α4β4 complex structure. (A) Sideview of the Kv1 holochannel structure showing interaction between the pore-forming α tetramer (green) and the intracellular Kvβ tetramer (blue). The intracellular T1 domain of the α subunits serves as a docking platform for the Kvβ subunits. (B,C) Top-down (B) and bottom-up (C) views of the structure shown in (A). Distinct peptides are shown with differential shading. Adapted with the Pymol software using protein database ID 7EJ1.

Whereas the Kvα N-terminus underlies rapid channel inactivation, this segment also forms an intracellular docking platform for physical interactions with Kvβ proteins. The N-terminal domains of each α subunit assemble to form the T1

structure, a hanging gondola-like feature that protrudes into the cytoplasm and interacts with the β complex (see Figure 1) [4,39–41]. Each of the four β subunits binds to N-terminal loops on the cytoplasmic face of the T1 tetramer [39]. These loops are unique to the Kv1 and Kv4 subfamilies and, accordingly, Kvβ subunits have only been shown to be associated with these channels [39]. Similar to the α complex, the tetrameric β assembly has fourfold symmetry, with each β subunit interacting with another in a side-to-end conformation [42]. This arrangement creates a β4 structure with a flat surface facing the membrane, promoting a stable interaction with the T1 domain [39,42]. Each β subunit consists of a triosephosphate isomerase (TIM) barrel composed of eight parallel β strands with intervening α helical sequences surrounding the perimeter [42]. Three mammalian genes encode Kvβ proteins (i.e., Kvβ1–3), each with conserved C-terminal regions and variable N-termini [38,43]. Generally, β1 and β3 proteins have longer N-terminal segments encoding inactivation peptides relative to β2 variants, which lack this structural motif [38,44]. Thus, the diversity of N-terminal peptide functionality among the Kvβ gene products may underlie their disparate regulatory roles, as discussed below [6].

Heterologous co-expression studies indicate that the Kvβ complex influences channel function. Generally, the assembly of Kv1 and Kv4 pore proteins with Kvβ increases whole- cell Kv current density and modifies voltage sensitivity. [6]. For example, co-expression of Kvβ proteins with Kv1.5 produced hyperpolarizing shifts in V0.5,act [45]. Likewise, heteromeric Kvβ complexes can accelerate N-type inactivation or impart rapid N-type inactivation to otherwise non-

inactivating pore complexes [6]. Depending on channel composition, these effects are mediated by N-terminal peptides within the Kvβ complex, the Kvα pore region, or both.

While co-expression studies have collectively indicated the potential for a vast array of mosaic Kvα/β assemblies, heteromerization is not entirely stochastic among all Kv subunits as only α and β splice variants of specific subfamilies can be associated with each other [23,46–49]. An exception to this subfamily specificity is the observation that “electrically silent” subfamilies (e.g., Kv9) require heteromerization with specific Kvα proteins for functional expression [50]. Structural determinants, such as the N-terminal docking site for the β subunit complex, restrict interactions between subunit subtypes [49,51–55]. Nonetheless, the molecular diversity garnered by heteromeric complex formation within subfamilies (see Figure 2) may be critical for precise control of membrane excitability in a manner that accommodates cell-specific processes. Moreover, the capability of Kv families to form heteromers with distinct functional profiles may enable adaptations in excitability in response to diverse environmental signals as discussed throughout the following sections.

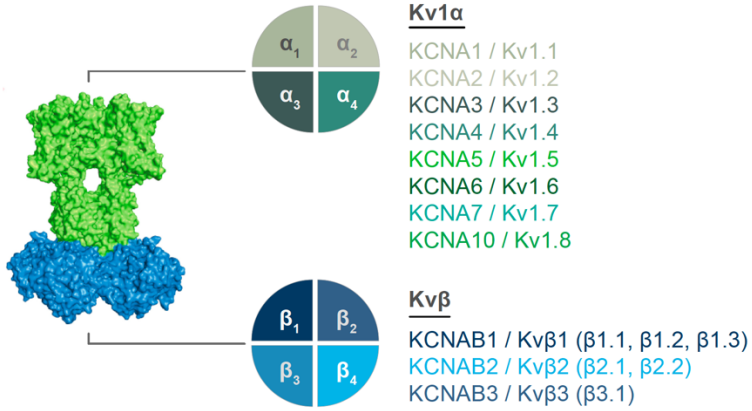

Figure 2. Molecular diversity of Kv1 complexes. Potential interacting subunits are show for Kv1α (top) and Kvβ (bottom) tetrameric structures. Gene names and corresponding proteins are listed. Known splice variants for Kvβ proteins are listed for each Kvβ in parentheses.

## 3. Enzymatic Properties and Regulatory Roles of Kvβ Proteins

Following their discovery, Kvβ proteins were found to have significant sequence homology with AKRs [56]. Indeed, it was later shown that Kvβ proteins catalyze the reduction of a range of carbonyl substrates via hydride transfer from NAD(P)H [57]. Thus, these findings led to the intriguing hypothesis that Kvβ proteins represent a molecular link between cellular redox state and membrane potential regulation. Similarly to other AKRs, Kvβ proteins are equipped with a C-terminal catalytic active site and a pyridine nucleotide cofactor-binding pocket [42]. Consistent with high-affinity cofactor binding, NADP+ remains bound via noncovalent interactions even after extensive washing of purified protein [42,58]. The active site conformation promotes ternary complex formation between the active site, the pyridine nucleotide cofactor, and the carbonyl substrate [59]. With this positioning, the catalytic tyrosine residue forms a hydrogen bond with the substrate and facilitates hydride transfer from the pyridine nucleotide cofactor to the carbonyl group [59]. Nonetheless, the catalytic rate for purified protein is slower than for other AKRs due to rate-limiting hydride transfer and cofactor release [7,59,60]. The active site binds pyridine nucleotides with and without a phosphate group [58], yet the predominant nucleotide used in vivo is unclear. Prior work has

suggested that Kvβ2 specifically uses NADPH, since substituting NADH for NADPH under otherwise identical conditions results in the loss of cofactor oxidation [7,59]. However, this discrepancy may be due to differences in binding affinities (Kd,NADPH < Kd,NADH) [58] and it is plausible that in a cellular setting, greater availability of cytosolic NAD(H) compared with NADP(H) may balance cofactor utility [58,61,62]. This remains unclear as experiments to test this hypothesis in native excitable cells have not been performed.

Perhaps more importantly, physiological carbonyl substrates for Kvβ and their impact on channel function have not been identified. Several in vitro studies show that purified Kvβ2 reduces a range of endogenous and exogenous carbonyls, yet seems more efficient in reducing aldehydes than ketones [59,63]. Along with C-nitro compounds, Kvβ2 readily reduces phenanthrenequinone, glycolytic byproduct methylglyoxal, and oxidized phospholipids (1-palmitoyl-2-oxovaleroyl phosphatidylcholine (POVPC) and 1-palmitoyl-2-arachidonoyl-sn-glycero-3-phosphocholine (PAPC)) [59,63]. The finding that Kvβ2 reduces the products of PAPC is consistent with the notion that Kvβ AKR activ- ity may be responsive to membrane oxidative stress under physiological or pathological conditions [63].

Although knowledge of physiological substrates and cofactors is lacking, several studies have shown that Kvβ-mediated AKR activity and pyridine nucleotide binding both contribute to dynamic regulation of the Kv function. Consistent with this, intracellular dialysis of Cos-7 cells expressing Kv1.5/Kvβ1.3 with NADPH or NADH reduces the steady-state current, enhances Kvβ-mediated

inactivation, and shifts V0.5,act to more hyperpolarized membrane potentials [64]. A similar regulatory role is also observed for the Kv1 channels associated with Kvβ2 and Kvβ3 proteins. Internal application of NADPH en- hances inactivation and reduces the steady-state current mediated by Kv1.5/Kvβ3 [45]. In contrast to Kvβ1 and Kvβ3, intracellular dialysis of NADPH shifts the voltage dependence of activation of Kv1.5/Kvβ2 complexes to hyperpolarized potentials with negligible effects on inactivation [45]. Moreover, C-terminal truncation of Kv1.5 (ΔC56 Kv1.5) eliminates the pyridine nucleotide sensitivity imparted by Kvβ2 [45]. These results suggest that inter- actions between Kvα C-termini and Kvβ pyridine nucleotide-binding pockets are critical for functional regulation of channel gating by changes in intracellular pyridine nucleotide redox state. It should be noted that whereas studies examining functional influences of Kvβ proteins on Kv currents have been performed in heterologous expression systems, further work is warranted to determine predominance of effects in the setting of heteromerization as is the case for native channels of excitable cells.

In addition to differential regulation of Kv activity via the pyridine nucleotide redox state, Kvβ catalytic activity itself may confer regulation of the channel function [65–67]. Moreover, mutations in both the cofactor-binding pocket and the AKR catalytic site of Kvβ1 and Kvβ2 have varied effects on Kv functional expression. Amino acid substitutions in the cofactor-binding pocket of Kvβ1 that lower the affinity for NADPH result in diffuse mem- brane and cytosolic localization, suggesting that cofactor binding may influence channel trafficking and membrane targeting [8,68]. However, subcellular localization was preserved for Kv1.2

channels expressed with catalytically inactive Kvβ2 mutants [8]. Yet, this result was not reproduced for all Kv1 complexes as mutations in both the binding pocket and the catalytic sites of Kvβ2 abolished Kvβ-mediated increases in Kv1.4 expression in Xenopus oocytes [69]. Thus, cofactor binding and catalysis may affect channel functional expression depending on the Kvα/β composition and cell type. The apparent contradictions in regulatory properties of Kvβ proteins, including effects on cellular trafficking and channel gating, suggest that their exact physiological contributions may be specific to the cell type and organ systems in which they are expressed. The following sections describe the recent works aiming to reveal more precise in vivo roles for specific Kv molecular assemblies found among different organ systems. Insights into the roles for Kvβ proteins and how adaptations in Kv composition may contribute to pathologic phenomena are discussed considering the aforementioned regulatory mechanisms.

## 4. Regulation of Neuronal Excitability

Kvβ proteins are heterogeneously distributed in the mammalian brain, with an over- lapping presence of Kvβ1 and β2 peptides across neuronal populations [70]. Expression studies have indicated that a significant population of heteromeric complexes consist of both Kvβ1 and Kvβ2 subunits [70,71]. Thus, neuronal homomers composed entirely of Kvβ1 are uncommon as this subunit is mostly found in complex with Kvβ2 [71]. Reciprocal coimmunoprecipitation experiments demonstrate that several Kv1α proteins form com- plexes with both Kvβ1 and Kvβ2 in the adult brain [72]. For instance, Kvβ2 is precipitated in complex with Kv1.1, Kv1.2, Kv1.4, and Kv1.6, whereas Kvβ1 is precipitated with Kv1.1 and Kv1.4, yet

in lower abundance than that observed for Kvβ2 [72]. These results support the notion that Kvβ2 is predominant in the mammalian brain and that a relatively lower abundance of Kvβ1 is found in the Kv1 and Kv4 channel complexes [72]. Comparable observations have been made in the human brain [71]. Considering that Kvβ3 is regionally isolated from other Kvβ subunits in the brain, it remains unclear whether β3 assembles in complexes with β1 or β2 [70,73].

Members of the Kv1 and Kv4 families control the neuronal action potential frequency via repolarization and by modulating the voltage threshold for action potential genera- tion [74]. Thus, the mosaic expression profile of Kvα and Kvβ subunits described above may contribute to varied action potential firing patterns among neuronal subpopulations. In particular, cell-specific expression patterns of Kvα/β combinations may balance the influence of transient A-type currents and delayed rectifier currents as required for spe- cific neuronal functions (Figure 3) [70–72]. For example, complexes consisting of Kv1.1 or Kv1.4 with Kvβ1 likely underlie the A-type current in neurons within cerebral gray matter, whereas complexes in which Kvβ2 predominates give rise to more slowly inactivating currents in neurons within cerebral white matter [70–72]. Thus, it is conceivable that co- ordinated expression patterns of Kvα and β proteins at the cellular and subcellular level mediate diverse excitability characteristics.

Modifications in the molecular identities of Kv assemblies and their subcellular lo- calization may also underlie key developmental changes in neuronal function. A fitting example of this is the observation that Kv1.1 channels are absent in axons of immature auditory nerve fibers but emerge in nodal structures

concurrent with the onset of hearing sensation [75]. Considering that Kv1.1 is associated with both Kvβ1 and Kvβ2 in the central nervous system [72], it is plausible that Kvβ-mediated modification of current density or voltage sensitivity contributes to spike generation and auditory fiber maturation. This is supported by a recently reported role in invertebrate neural development in which upregulated Kvβ2 was responsible for converting repetitive-firing zebrafish Mauthner cells into single spike-generating cells at four days post-fertilization [76].

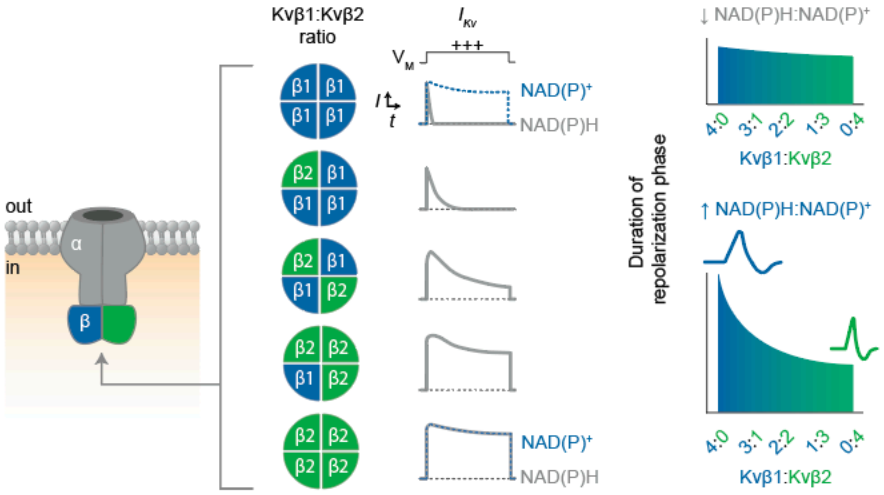


Figure 3. Proposed influence of the Kvβ1:Kvβ2 functional expression on IKv inactivation and repolarization. Schematic illustration depicting Kv α4β4 channel assembly (left) with possible combinations of Kvβ proteins present in native heteromultimeric structures. (Center) Expected impact of Kvβ stoichiometry on current inactivation rates is exemplified with theoretical trace recordings of de-polarization (+++) -evoked whole-cell IKv for cells expressing homogenous channel populations with the Kvβ ratios as indicated. Differential effects of the bound cofactor for β1(4) and β2(4) configurations are shown in dashed blue traces.

(Right) Predicted influence of differential Kvβ stochiometries on action potential duration in the presence of low and high cytosolic NAD(P)H:NADP+ ratios.

The wide range of the K+ current morphology imparted by the diversity of Kv com- plex compositions may be essential to the maturation of the central nervous system. Re- cent data demonstrate that hippocampal excitatory neural termini extensively express Kv1.1/1.2/Kvβ1 heteromers and that Kvβ1-mediated channel inactivation upon high- frequency stimulation elicits action potential broadening and, consequently, synaptic facilitation [77]. Along with direct effects on action potential morphology via modulating channel inactivation, Kvβ proteins may indirectly foster synaptic plasticity by way of cytoskeletal interactions that enable targeting and clustering of Kv channels at the neuronal membrane. For example, Kvβ2 anchors channels to the cytoskeleton in hippocampal neurons by interacting with the postsynaptic density protein ProSap2 [78]. Likewise, Kv channel clustering and targeting is regulated by Cdk-mediated phosphorylation of Kvβ2, which disrupts the interaction between the microtubule plus-end tracking protein EB-1, resulting in increased membrane localization [79]. In addition, Kv channel complexes inter- act with the post-synaptic density via associations between the C-terminal tail end of the transmembrane domain and PSD-95 proteins [80,81]. Interestingly, this interaction depends on C-terminal length; thus, alternative splicing can substantially influence interactions with PSD-95-anchoring proteins [80,81].

The chaperone functionality of Kvβ likely depends on cofactor binding and enzymatic turnover [8,68,69]. Moreover, interactions with PSD-95 and the C-

terminus of Kvα proteins may modulate the pyridine nucleotide sensitivity of neuronal Kv channels as this segment mediates sensitivity to changes in the intracellular NAD(P)+/NAD(P)H ratio [45]. Thus, axonal targeting of Kv channels could conceivably be sensitive to changes in the cellular redox status through this mechanism. Thus, future work to investigate the links between neuronal metabolism, redox state, and Kv subcellular localization and their impacts on excitability, development, and learning is warranted. Such functional relationships may be revealed by loss- or gain-of-function mutations to Kvβ AKR catalytic sites and cofactor- binding pockets, as well as phosphomimetics and cytoskeletal modifications [10,75,76].

Along with the potential effects of Kvβ-mediated regulation on Kv channel membrane targeting, AKR catalytic activity and cofactor binding could also influence the changes in action potential morphology that occur during the development of the central nervous system. For example, the formation of single-spiking patterns during auditory development, as described above, could also be regulated by Kvβ catalysis considering that the enzymatic functions of Kvβ1 and Kvβ2 enhance the Kv current density [7,65,75,76]. In contrast, synaptic facilitation related to learning processes appear to involve action potential broadening resulting from enhanced β1-mediated inactivation [77]. This effect may depend on cellular energetic and redox conditions during rapid action potential firing that ultimately serves to augment Kvβ1-mediated inactivation [77,82]. Consistent with this, repetitive neuronal firing elevates cytosolic NADH levels [82]. Since Kv inactivation is enhanced via Kvβ1 in the presence of reduced pyridine nucleotides

[64], elevated levels of NAD(P)H in neurons during rapid action potential firing may sustain or enhance Kv inactivation and thereby promote action potential prolongation (see Figure 3). Nonetheless, this hypothesis remains to be tested with electrophysiological experiments that examine whether native neuronal Kv1-mediated currents are sensitive to acute changes in pyridine nucleotide redox state.

While important questions surrounding the role of Kvβ AKR functionality persist, the recent works establish its role in connecting cellular metabolism and neuronal excitability as it relates to the initiation of arousal and sleep states. In this regard, the Drosophila ortholog of mammalian Kvβ, Hyperkinetic, has been isolated as a critical component for light-induced neuronal depolarization, enhanced action potential spiking, and behavioral arousal. Of particular importance, dynamic influences on K+ conductance may depend on the oxidation of Hyperkinetic-bound NADPH [83]. Another study has indicated that wakefulness in Drosophila causes the accumulation of reactive oxygen species derived from the electron transport chain, leading to the oxidation of Hyperkinetic-bound NADPH, reduced Shaker A-type current inactivation, and enhanced action potential firing rate, thus ultimately promoting sleep [84]. While the role of Kvβ AKR activity in mammalian sleep remains to be tested, these results warrant further research into the metabolic sensitivity of neuronal Kv1 channels as a potential target for treating a variety of sleep disorders.

### 5. Metabolic Regulation of Cardiac Repolarization

Precise control of the cardiac action potential relies on coordinated Kv channel activity in cardiomyocytes. Ventricular and atrial myocytes express several Kv pore proteins that interact with Kvβ, including Kv1.2, Kv1.4, Kv1.5, Kv4.2, and Kv4.3 [85–88]. Similar to expression patterns observed in the central nervous system, past studies have consistently shown the presence of Kvβ1 and Kvβ2 variants in association with Kvα subunits in the mammalian heart [86,89,90]. For instance, channel assemblies consisting of Kv4.2 and Kv4.3 with Kvβ1.1 [86,87], as well as Kv1.4, Kv1.5, Kv4.2, and Kv4.3 with Kvβ2 proteins [9] have been found in murine cardiomyocytes. Myocardial Kv1.5 proteins appear to be associated with both Kvβ1 and Kvβ2 subunits, whereas Kv1.4 subunits are associated with Kvβ1–3, and Kv4.3 channels mostly interact with KChIP proteins [88]. Nonetheless, subpopulations of individual α/β compositions are region-specific, which may give rise to distinct current profiles that underlie unique action potential morphologies in different regions of the heart [91]. Early phase 1 repolarization is largely mediated by the transient outward K+ current (Ito), which can be separated into two distinct components—i.e., fast (Ito,fast) and slow (Ito,slow) [92]. The differential manifestation of these components relies on expression patterns of Kv channels and their intracellular subunits; Ito,fast is mediated by Kv4.2 and Kv4.3 channels that assemble with KChIP2 and DPP6 [92], whereas Ito,slow is mediated by Kv1.4 coupled with Kvβ proteins [88,92]. On the other hand, atrial repo- larization features a unique component, IKur, mediated by Kv1.5–Kvβ channels [88,92]. Thus, regional heterogeneity in sarcolemmal abundance of Kvα and Kvβ proteins likely underlies differential regulatory

influences of K+ conductance on cardiac action potential waveforms, Ca2+ handling, and myocardial contractility.

Several studies have examined the impact of genetic ablation of Kvβ subunits on Kv currents and action potential waveforms in adult murine cardiomyocytes. Targeted disruption of Kcnab1 in mice has no overt effects on ECG morphologies or total peak IK density in isolated myocytes relative to wild-type mice [86]. Yet, kinetic analyses revealed a role of Kvβ1 in coordinating Ito; loss of Kvβ1 reduced Ito,fast and increased the Ito,slow density. The absence of Kvβ1 also shifted steady-state activation relative to wild-type myocytes by ~10 mV [86]. Conversely, mice lacking Kvβ2 exhibit reduced surface expression of all the reported binding partners [9]. This effect was associated with reduced Ito, IK,slow1, and IK,slow2 densities, action potential prolongation, and increased QT interval. Thus, expression of Kvβ proteins by cardiomyocytes appears to support the functional expression of K+ channels that orchestrate major repolarizing currents.

In addition to the purported roles in regulating Kv surface expression and basal Kv current densities, Kvβ proteins may also participate in the modulation of the Kv function and IKv upon fluctuations in myocardial metabolism such as those that may occur upon acute changes in cardiac workload and oxygen availability. In this regard, the results obtained thus far for native cardiac channels are consistent with past results indicating that the redox state of pyridine nucleotide cofactors bound to Kvβ differentially impact Kv gating in COS-7 cells. For instance, IKv recorded in myocytes isolated from wild-type mice, but not those from Kvβ2−/−

mice, showed accelerated inactivation when the cells were dialyzed with the pyridine nucleotide ratios that reflect hypoxic conditions [9]. Consistent with faster Kv inactivation under these conditions, parallel experiments showed increased monophasic action potential duration after the cells were treated with 20 mM external lactate to elevate intracellular [NADH]:[NAD+] [9]. Indeed, this delayed repolarization was readily reversed upon application of pyruvate (i.e., lowering [NADH]i:[NAD+]i) indicating the rapid reversibility of redox effects on the cardiac action potential. Beyond regulating cardiac electrophysiology upon acute changes in the cardiac workload, it is plausible that this mechanism to some extent underlies diurnal oscillations in heart rate and ventricular repolarization [93]. Surprisingly, redox modulation of repolarization requires the presence of both β subunits [9,87], indicating that Kvβ1 and Kvβ2 subunits may function together to confer metabolic sensitivity of current density and action potential duration. Although the dual requisite nature of Kvβ proteins in mediating pyridine nucleotide sensitivity of cardiac electrical properties is not clear, we speculate that this may arise from the net “priming” effect of each Kvβ protein on channel voltage sensitivities and inactivation rates that may enable further redox-dependent modulation.

Though current evidence supports the notion that Kvβ proteins have important roles in regulating cardiac electrophysiology, important questions remain to be addressed. In particular, these proteins appear to be linked with cardiac growth—sex-dependent hypertro- phy is associated with the loss of Kvβ1.1, whereas moderate cardiac atrophy is seen with the loss of Kvβ2 [9,11]. How these proteins may regulate cardiac myocyte size is unknown, but it may involve IKv-

dependent osmoregulation, altered activation of excitation–transcription processes, or voltage- or redox-dependent modulation of anabolic biosynthetic pathways. Disturbing the pyridine nucleotide sensing function of Kv channels and excitability may itself impact the metabolism of the heart. For instance, acute modifications in action po- tential duration in response to altered pyridine nucleotide redox state may represent a key feedback mechanism to regulate contractility and, thus, oxygen and energetic substrate demand. Along these lines, further work is warranted to address whether loss of either Kvβ1 or Kvβ2 may be protective or deleterious in the context of myocardial ischemia. Moreover, advancing knowledge of how these proteins regulate cardiac excitability could provide important insights into the development and progression of cardiac arrhythmias secondary to inherited or acquired metabolic disorders.

### 6. Control of Vascular Tone and Smooth Muscle Phenotype

Blood flow to tissues is largely determined by the contractility of vascular smooth muscle in small-diameter arteries and arterioles, which is in turn controlled by membrane potential and steady-state Ca2+ influx via voltage-dependent Ca2+ channels. Hence, sar- colemmal Kv channels are central feedback regulators of membrane depolarization in smooth muscle that counter depolarization-evoked Ca2+ influx [94]. Consistent with this, pharmacological inhibition of Kv1 channels causes marked vasoconstriction [95], indicating that tonic activity of these channels in smooth muscle cells of pressurized arteries and arterioles serves to oppose Ca2+ influx and vasoconstriction. Across species, multiple Kv proteins are abundant throughout the resistance vasculature and have been detected in

mesenteric, hepatic, retinal, placental, coronary, as well as pulmonary arteries [96–102]. Arterial smooth muscle cells express Kvα/β channel complexes to varying degrees de- pending on vessel location and size, including Kv1.2, Kv1.3, Kv1.4, Kv1.5, Kv1.6, Kv2.1, Kvβ1.1, Kvβ1.2, Kvβ2 [96–102]. Similar to other cell types discussed above, Kvβ1 and Kvβ2 variants co-assemble with native Kv1 channels in smooth muscle cells, yet their physiological roles related to the control of vascular Kv1 function, particularly with respect to oxygen sensing, have only recently been examined.

The diameter of small arteries and arterioles is sensitive to changes in tissue pO2 in a manner that serves to couple blood flow (i.e., oxygen delivery) with fluctuating metabolic demand. Redox-sensitive Kv1.5 channels expressed by smooth muscle cells have been recognized as an O2 sensor that contributes to pulmonary vasoconstriction in response to hypoxia [103,104]. Conversely, in coronary circulation, Kv1 channels represent end effectors that are activated to augment the arterial diameter and blood delivery upon changes in myocardial workload and oxygen consumption. The requirement of Kv1 channels in coronary metabolic vasodilation is supported by observations that mice lacking Kv1.5 or Kv1.1 proteins have severely blunted hyperemic responses to increased cardiac work [105,106]. These findings have been recapitulated in larger animals with the use of pharmacological Kv1 inhibitors [107,108]. Thus, available data collectively support a conserved oxygen-sensing role of Kv1 channels in the coronary vasculature. Nonetheless, the mechanisms contributing to redox control of these channels in the vasculature in the context of altered tissue metabolism are poorly

understood [109]. Our work recently found that Kvβ proteins that assemble with Kv1.x channels in smooth muscle are critical to the vasodilation secondary to metabolic stress. Whereas native channels in coronary smooth muscle cells assemble with Kvβ1 and Kvβ2 proteins in the same associated complex [100], these proteins have opposing roles in coordinating the oxygen sensitivity of coronary vascular tone and blood flow. Using a combination of murine models revealed that Kvβ2 is required for the physiological relationship between cardiac work and blood flow, whereas Kvβ1.1 has an inhibitory influence [110]. Moreover, using an inducible double transgenic model in which Kvβ1.1 is selectively overexpressed in smooth muscle, we found that modestly increasing the Kvβ1.1:Kvβ2 ratio in Kv1 channels recapitulates the effects of Kvβ2 deletion [110]. We propose that these opposing functional impacts on the Kv1 function likely reflect different functionalities of Kvβ N-termini and their response to redox shifts, although this remains to be tested directly. In support of this, we recently reported that the activity of native Kv1 channels in coronary smooth muscle is upregulated in the presence of NADH and that this response requires the presence of catalytically active Kvβ2 [111].

The findings described above are consistent with the concept that the heteromeric nature of Kvβ complexes may serve to finetune vasoregulation in an intrinsically flexible manner. Thus, we posit that smooth muscle cells may rely on oxygen-sensitive mechanisms that modulate Kvβ1:Kvβ2 functional expression in response to recurrent physiologic or pathologic stimuli to ultimately render the Kv1 function more or less responsive to metabolic cues [109,110]. For instance,

enhancement of the coronary Kv1 activity following chronic exercise conditioning likely contributes to the greater coronary flow reserve in exercise-adapted hearts [112]. Stimuli associated with physiological increases in myocardial oxygen consumption could conceivably evoke epigenomic or transcriptional regulatory processes influencing the abundance of Kv1-associated β proteins. Thus, altered molecular stoichiometry of the Kvβ complex may be a key driver of beneficial effects of exercise on coronary microvascular function.

In addition to their importance in regulating vascular tone, the recent works have shown that Kv1 channels participate in phenotypic modulation of vascular smooth muscle cells [113]. In particular, profiling ion channel expression in endoluminal lesions revealed that only two of the channel subunits measured, Kv1.3 and Kvβ2, were upregulated in proliferating smooth muscle [113]. Moreover, several studies have indicated that inhibition of Kv1.3 can prevent smooth muscle proliferation and migration in vitro as well as in the con- text of in vivo vascular injury models [114,115], thus prompting investigations into Kv1.3 inhibitors as therapeutics to prevent restenosis. While the precise mechanisms underlying this role of Kv1.3 in proliferation are still unclear, there is a clear role for voltage-dependent changes in the channel conformation that activate pro-proliferative pathways independent of the transmembrane ion flux [116]. This may involve depolarization-induced interactions with proliferation regulatory protein IQGAP3 and downstream Ras-dependent ERK activation [117]. Parallel to changes in ion channel expression, robust metabolic changes also occur during phenotypic modulation of vascular smooth muscle; transformation from contractile to synthetic

smooth muscle is associated with enhanced glycolysis, LDH activity, and glutamine utilization that facilitate proliferation and migration [118,119]. These metabolic shifts provide necessary substrates for these processes, but also modulate the cellular redox landscape related to the NAD(P)(H) levels and thus may influence the Kv1.3 conformation via Kvβ2 interactions. Thus, by integrating metabolic signals that occur as a result of exposure to growth stimuli, Kvβ may represent a key nodal target for novel therapeutics to prevent or reverse pathologic smooth muscle proliferation.

## 7. Summary and Remaining Questions to Be Addressed

The currently known physiological roles for Kvβ proteins discussed here are summarized in Figure 4. The wide-ranging physiological processes that require voltage-gated potassium channels are largely enabled by their extensive structural diversity. Indeed, the functional versatility of Kv channels is further extended by interactions with multiple types of associated proteins, the most abundant of which are Kvβs. Although substantial research effort over the past several decades has been devoted to an improved understanding of how these channels facilitate such diverse processes as learning and memory, sleep, muscle relaxation, and cell growth, new important questions should be addressed. Perhaps the most important question is related to the enzymatic functions of Kvβ proteins; while the catalytic mechanism has been resolved, the endogenous substrate(s) of Kvβ has not been unequivocally identified. Key gaps in knowledge remain as to how intracellular events, such as those involved in kinase/phosphatase signaling pathways, affect Kvβ catalysis. A number of phosphorylation target residues are

found with the N-terminus as well as the conserved C-terminal AKR domain of Kvβ proteins [79,120]. Whereas N-terminal serine phosphorylation appears to be critical for interactions with the cytoskeleton and cellular trafficking of channels, the role of target residues in the C-terminus is unknown. Whether phosphorylation of residues near the cofactor or substrate-binding pockets impacts catalytic function when Kvβ is assembled within α4β4 structures warrants investigation. Eluci- dating how phosphorylation impacts the enzymatic properties of Kvβ may advance the identification of which substrates are used by this protein in native cells under a variety of conditions.

As described above, there is now considerable evidence that catalytic cycling by Kvβ impacts Kv channel voltage sensitivity and gating. An additional question remains as to how Kvβ structural modification secondary to substrate/cofactor binding and release impacts the interacting Kvα pore proteins. Advanced computational modeling approaches may provide insight into the Kv structure–function relationships by examining Kvα/β as well as Kvβ/β interactions at each step in the Kvβ catalytic cycle to determine specific effects on the T1-interacting domain that influence positioning of the voltage sensor within the membrane. Furthermore, these efforts may reveal important information on whether the conformation of the Kvα voltage sensor and pores could influence substrate or cofactor binding and, thus, catalytic efficiency of Kvβ. Such evidence may reveal an important role in this channel–enzyme complex in processes of molecular memory via effects of membrane excitability on metabolism and redox-dependent transcriptional regulatory pathways. Future advances in these areas

could ultimately prove valuable for extending the capabilities of Kv modulators as research tools and therapeutics beyond pore blockers and openers to more specific agents that modify the strength of Kv metabolic sensing.

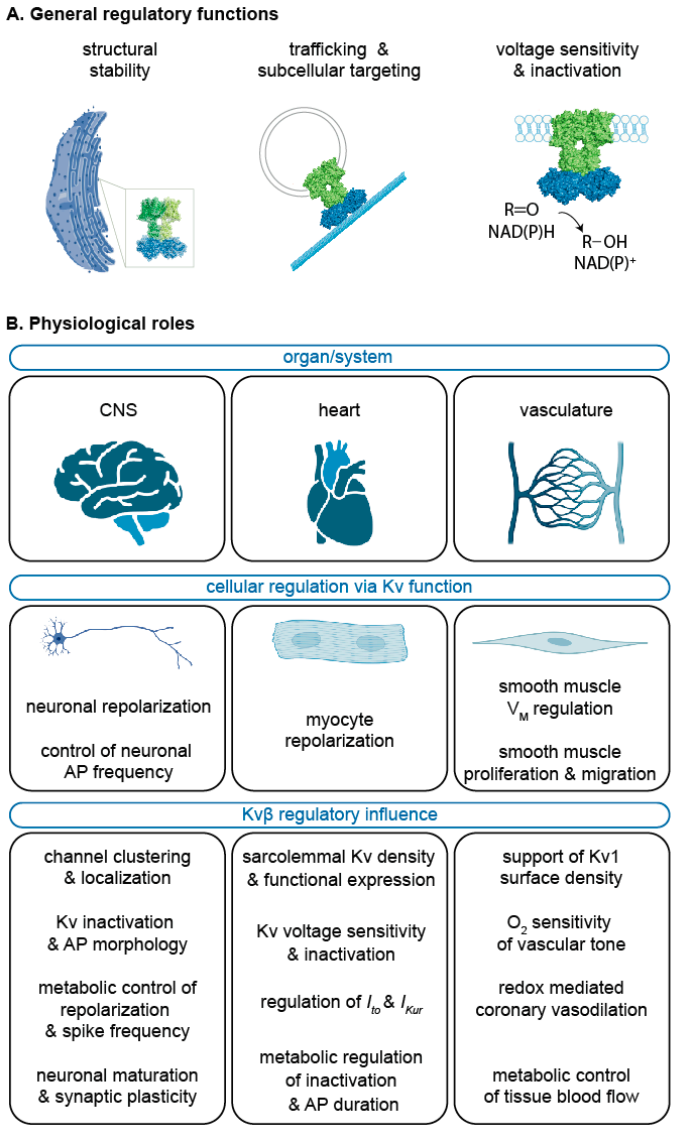


Figure 4. Summary of the Kvβ functional roles. General regulatory features or Kvβ (A) as discussed in Sections 2 and 3 and the key physiological roles for Kvβ proteins in the central nervous system (CNS), heart, and vasculature (B) as

discussed in Sections 4–6. Created with BioRender.com (accessed on 2 July 2022).

# APPENDIX C

## Biochemical and physiological properties of $K^+$ channel associated AKR6A (KVβ) proteins

Voltage-gated potassium (KV) channels play an essential role in the regulation of membrane excitability and thereby control physiological processes such as cardiac excitability, neural communication, muscle contraction, and hormone secretion. Members of the Kv1 and Kv4 families associate with auxiliary intracellular Kvβ subunits, which belong to the aldo-keto reductase superfamily. Electrophysiological studies have shown that these proteins regulate the gating properties of Kv channels. Although the three gene products encoding Kvβ proteins are functional enzymes in that they catalyze the nicotinamide adenine dinucleotide phosphate (NAD[P]H)-dependent reduction of a wide range of aldehyde and ketone substrates, the physiological role for these proteins and how each subtype may perform unique roles in coupling membrane excitability with cellular metabolic processes remains unclear. Here, we discuss current knowledge of the enzymatic properties of Kvβ proteins from biochemical studies with their described and purported physiological and pathophysiological influences.

The aldo-keto reductases (AKRs) comprise a group of oxidoreductase enzymes that catalyze the reduction of endogenous and xenobiotic carbonyl compounds. These enzymes are ubiquitous among eukaryotic and

prokaryotic organisms and share significant structural identity in that they all possess a C-terminal active site region within a triose-phosphate isomerase (TIM) barrel (α8/β8) motif with three loops at the base of the barrel that govern substrate binding.[94,95] The utility of this structural arrangement among the AKRs allows for flexibility in binding and metabolizing a wide range of chemical substrates that includes aliphatic and aromatic aldehydes and ketones, monosaccharides, steroids, and polycyclic aromatic hydrocarbons.[96-98] All AKRs require nicotinamide adenine dinucleotides (i.e., NAD(P)H) as a cofactor for hydride transfer [99] and their function can thus be modulated by the cellular redox state of electron carriers used in many intermediary metabolic reactions.

Most human AKRs are soluble monomeric proteins that are found in the cytosolic compartment. An exception to this are members of the AKR6 subfamily, which form tetrameric complexes that are associated with the pore-domains of voltage-gated potassium (Kv) channels (i.e., the Kvβ proteins).[100,101] The Kv channels are a large family of transmembrane $K^+$-permeable ion channels that, via regulation of membrane potential in excitable cell types, control numerous physiological processes, including neuronal excitability, hormonal secretion, and muscle contraction.[35,102,103] While this assembly between a catalytically active AKR and ion channel has stimulated several intriguing hypotheses regarding its evolutionary conservation and potential physiological role(s) [104], there is limited information about the potential *in vivo* role for the Kvβ proteins in the

cardiovascular, endocrine, and nervous systems, and it is unclear how these proteins may regulate diverse cellular physiological processes and pathophysiological development. While the enzymatic properties and cellular functions of the AKR family have been reviewed (readers are referred to [95,105]), we will discuss the enzymatic properties of the Kvβ proteins, including how these properties may relay metabolic information to the Kv channel gating apparatus. Additionally, these subunits may serve as molecular transducers that couple metabolism and membrane electrical signaling in excitable cell types. While underscoring key remaining questions that require further investigation, we discuss the potential efficacy of small molecules or peptides that selectively modulate Kvβ expression or functionality as a novel class of therapeutics that could prevent or reverse pathological changes, and therefore may be useful interventions for controlling excitability under a variety of different physiological and pathological conditions.

## Molecular and structural biology

In the human genome, there are ~35 genes encoding Kv channel pore proteins belonging to 12 subfamilies (i.e., Kv1.x – Kv12.x).[106] The basic Kv channel tertiary structure consists of a multi-subunit complex of pore-forming proteins with a diverse repertoire of associated auxiliary and regulatory proteins. The pore domain is formed by the tetrameric assembly of four distinct transmembrane subunits (α) that are arranged around a central axis to form a membrane-traversing ion conduction pore that is highly selective

(~10,000 fold more selective for $K^+$ than for $Na^+$) and efficient for $K^+$ transport (~$10^7$ $K^+$ ions $channel^{-1}$ $sec^{-1}$).[107-109] Kvα subunits are 70-100 kDa in mass and consist of six membrane-spanning α helices (S1-S6) with S1-S4 forming the voltage-sensor domain and the S5-S6 segments of each contributing to the pore lining with selectivity filter. A highly conserved series of positively charged arginine residues within the S4 region form the voltage sensor of the channel that responds to changes in membrane voltage to constrict or dilate the central pore.[110] In native channel complexes, members of a particular Kv family (e.g., Kv1) are known to interact with other functional members of the same family, giving rise to heteromeric alpha pore complexes with variable gating properties, which could ultimately increase diversity among functional channels.[111,112] This is thought to occur through highly conserved regions within the intracellular T1 domain, which also serves as a docking site for intracellular subunits. Association with conserved regions among accessory Kv proteins also allows for the formation of heterotetrameric auxiliary subunit complexes, which, as described below, may further add to the functional diversity of native channels.

Although the expression and assembly of four Kvα subunits is the minimum requirement to form a functional channel, association of the pore-domain with a diverse set of accessory subunits, such as Kvβ, KChAP, KChIP, and MinK, imparts multimodal regulatory features to Kv channels *in vivo.*[113] Members of the *Shaker* (Kv1) and *Shal* (Kv4) families are known to associate with Kvβ subunits.[114,115] The human genome contains three genes

that encode Kvβ proteins (KCNAB1, KCNAB2, KCNAB3) and their transcripts are alternatively spliced to generate additional variants. Early studies suggesting the functional importance of Kvβ proteins discovered that a leg shaking phenotype in *Drosophila melanogaster* (i.e., 'hyperkinetic') was the result of a mutation in a homologue of the mammalian Kvβ peptides. Subsequent sequence analyses led to the unexpected finding that the Kvβ subunits shared significant homology (15-30% amino acid identity) with members of the AKR superfamily.[104,116] Upon crystallization of Kv1.2-Kvβ2, it was found that Kvβ proteins possess a conserved C-terminal β-barrel structural fold with tightly bound nicotinamide cofactor and, consistent with findings from sequence alignments, the active site had all characteristic features of a catalytically active AKR, including a well- conserved cofactor binding site and a distinct substrate binding pocket.[100,117] Indeed, in these earlier reports on the X-ray crystal structure of a Kv channel complex, and more recently in a study demonstrating the single-particle cryo-electron microscopic structure of Kv1.2-Kvβ2 expressed in lipid nanodiscs [118], electron density could be resolved from $NADP^+$ that was bound to the β subunits.

The active site structure of the AKR6 family is unique in that the α8/β8 motif has an additional helix attached to a long loop between β9 and α7 near the cofactor binding pocket.[95] The functional significance of this modification that is shared among AKR6 members is not presently clear. At the quaternary level, the β1 and β2, which are perpendicular to the central axis of the barrel, along with the α2-β5-α3 region, form the intersubunit interface region that

participates in β tetramerization, while the α5-α6 region interacts with the T1 docking domains of the Kvα proteins.[100,101] Thus, via the T1 domain, the active site of Kvβ can influence the conformation of the voltage sensing apparatus and thereby impact gating properties because of catalytic activity and/or pyridine nucleotide cofactor binding.

## Enzymology and channel biophysics

A prerequisite for investigating and understanding the potential physiological or pathological roles of the Kvβ proteins is a thorough understanding of their catalytic properties and the identification of potentially relevant endogenous or xenobiotic carbonyl substrates. The Kvβ proteins bind pyridine nucleotides, with binding affinities in the low micromolar range (i.e., 0.1-4 μM). The proteins display a ~10-fold greater affinity for NADP(H) compared to NAD(H) cofactors.[119] Considering that in most metabolically active cells, the NADPH:$NADP^+$ ratio is substantially higher than that of NADH:$NAD^+$, while the absolute concentration of NADP(H) is much lower than that of NAD(H) [120,121], the cofactor predominantly used by Kvβ proteins *in vivo* is not clear and likely varies with respect to cell type. Kvβ2 catalyzes the reduction of a wide range of aldehydes and ketones, although preferential binding and reduction of aldehydes versus ketones, and higher catalytic efficiency for aromatic aldehydes was reported for this subunit.[122] For example, Kvβ2 shows higher catalytic activity with aromatic carbonyls such as

phenanthrenequinone than with straight chain aldehydes such as acrolein or 4-oxo-nonenal.[122] Little or no activity was observed with steroids such as cortisone. Significantly, the protein was also found to be active with products of lipid peroxidation, such as 1-palmitoyl, 2-oxovaleroyl, phosphatidyl choline (POVPC). Given that POVPC and related aldehydes are generated during the oxidation of unsaturated fatty acids in the plasma membrane and that Kvβ is tethered within close proximity to the membrane, it appears plausible that the catalytic function of Kvβ may be to detoxify lipid peroxidation products and thereby protect Kv channels from oxidative damage. Alternatively, binding to lipid peroxidation products could be a potential regulatory mechanism that could alter Kv kinetics under conditions of oxidative stress (e.g., to trigger apoptosis). Although future studies are required to distinguish between these possibilities and to identify other endogenous substrates, the catalytic reactivity of the protein with aldehydes could represent an important link that would regulate Kv channel activity as a function of Kvβ catalysis (regulation of electrical activity by metabolism) or Kvβ catalysis by Kv activity (regulation of metabolism by electrical activity). In either scenario, the link between metabolism and excitability could represent a regulatory mode with profound implications for neural, cardiac, and muscle excitability.

The catalytic activity of Kvβ2 has been found to be sensitive to both pH and ionic strength. Measurements of the enzyme activity at various pH and ionic concentrations found that enzyme activity is maximal between pH 7.2-7.4 and relatively insensitive to varied phosphate concentrations between

100 mM and 250 mM. Yet, at low phosphate concentrations (≤ 50 mM), enzymatic activity is significantly decreased [122-124] and is not impacted by the addition of NADH and or $NAD^+$, suggesting that the enzyme functions most effectively at a specific ionic strength. As with other AKRs such as aldose reductase and aldehyde reductase, the mechanism of Kvβ catalysis is consistent with an ordered bi- bi rapid equilibrium reaction in which the nucleotide cofactor is the first to bind and the last to dissociate. Consistent with this, the binding affinities for NADPH and $NADP^+$ by Kvβ2 are significantly different, as NAD(P)H binds with 4-times greater affinity than $NADP^+$. The sequence of cofactor and substrate binding was confirmed using variable concentrations of 4-NB and NADPH to establish the initial velocity, the starting rate of enzymatic activity. When plotting initial velocity against the different NADPH concentrations, a rapid equilibrium mechanism was predominant, indicative of NADPH binding prior to substrate.[122]

The cofactor binding kinetics for Kvβ2, determined by monitoring the reduction in fluorescence of the Kvβ2 reporter fluorescence by addition of each respective cofactor, provided insight into the phasic behavior and rate limitation of catalysis.[123] By measuring the dependence of observed $k_{fast}$ and $k_{slow}$ of kinetic traces on NADP(H) concentration, it was suggested that the binding of NAD(P)H to Kvβ could be described as a three-step process consisting of rapid formation of a loose enzyme-cofactor association, a slow conformational change that securely seats the cofactor in the active site of the enzyme, and further stabilization of the NADPH cofactor to its binding

site.[122,123] The binding of $NADP^+$, however, follows the two step model of binding affinity, suggesting that the second conformational change observed with NADPH binding that prevents nucleotide exchange is absent in the binding of oxidized nucleotide.[123] Moreover, studies performed using mutant Kvβ2 in which the catalytic site tyrosine (Y90) is replaced with phenylalanine ($Kvβ2^{Y90F}$) suggest that high affinity nucleotide binding is not significantly impacted by loss of catalytic function.[122]

By binding of cofactors to the Kvβ subunits, Kv channel activation and inactivation are sensitive to changes in intracellular pyridine nucleotide redox state, which is reflected in the ratio of intracellular $NAD(P)H/NAD(P)^+$.[124] Modulation of Kv activity by oxidized and reduced pyridine nucleotides is determined by the identity of Kvβ subunits present.[125,126]Unlike Kvβ1 and Kvβ3, the Kvβ2 subunit lacks an inactivating N-terminus tail-like structure.[127,128] Despite this structural difference, Kvβ2 has a common binding affinity to the α subunit T1 domain.[100] Consistent with this, the C-terminal domain of the Kvα subunits is critical for proper association between the Kvα and β subunits.[126,129] The underlying region of importance in the Kv1α C-terminal domain lies between Arg-543 and Val-583 of Kv1.5, a region with differential affinities for NAD(P)H-bound versus NAD(P)+-bound Kvβ. Thus, nucleotide-dependent modification in subunit binding affinity and associated conformational changes within the Kvα transmembrane region may represent a potential mechanism whereby Kvβ redox sensing could alter channel biophysical properties.

The mechanism and biochemical role of cofactor binding in Kvβ-mediated catalysis are like that observed with other AKRs, such as aldose reductase. As with other AKRs, NAD(P)H binding promotes a change in protein conformation that stabilizes the cofactor within the catalytic pocket.[123] The affinity of this interaction produces a large change in free energy that drives catalysis. As little energy is derived from substrate binding to achieve the transition state, the protein can bind a range of carbonyl substrates. This mode of high affinity binding to pyridine coenzyme seems well-suited for ion channel regulatory functions of Kvβ, as it reduces the constraints of aldehyde binding and renders the cofactor binding pocket an effective sensor of intracellular pyridine nucleotides. Thus, physiological changes in intracellular NAD(P)H:NAD(P)$^+$ could readily impact Kv gating and membrane potential regulation. Under conditions of high intracellular NAD(P)H:NAD(P)$^+$ ratio, binding of reduced cofactor generally enhances the degree and rate of channel inactivation.[124,126] However, this effect can be effectively 'turned off' upon completion of a catalytic cycle resulting in substrate reduction and cofactor oxidation. Accordingly, the net effect of AKR enzymatic function on Kv channel activity likely reflects dynamic homeostatic balance between pyridine nucleotide redox potential as well as the concentrations and molecular identities of local aldehyde and ketone substrates, which collectively reflect cellular and subcellular metabolic activity.

## Physiological roles

*Regulation of membrane excitability by cellular metabolism*: Considering that Kv channel gating is modulated by intracellular pyridine nucleotides via the Kvβ complex as stated above, these proteins have been proposed as a link between cellular function and metabolic activity. However, a clear view of how the Kvβ proteins operate and modify channel gating behavior in their native cellular and tissue environments has not yet emerged. Complicating this issue native Kv channels likely consist of heteromeric assemblies of multiple gene products and splice variants, which have not yet been functionally characterized. Moreover, the expression levels of Kvα and β proteins and how their stoichiometry within a given population of functional channels is determined may be cell specific. It is also conceivable that the molecular identity of predominant subunits utilized by a cell may be modified because of changing metabolic cues. Considering the functional diversity imparted by variable N-termini of the Kvβ subtypes, the ratio of Kvβ2:Kvβ1/3 present in the Kv auxiliary complex could have a significant impact on inactivation (**Schematic 1**).

**Schematic 1**

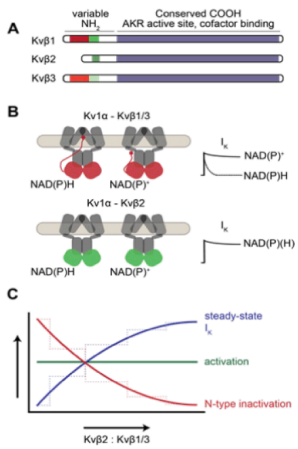


**Schematic 1: Balanced redox regulation of whole cell $I_{Kv}$ by differential incorporation of Kvβ proteins in heteromultimeric channels.** (**A**) Schematic of Kvβ1, Kvβ2, and Kvβ3 amino acids showing conserved COOH terminal region (blue) and variable N-termini (green/red). Several splice variants which differ in the N-terminal domain have been found for Kvβ1 (1.1-1.3 and Kvβ2 (2.1, 2.2). Ball-and-chain inactivation domain is shown in red. *Adapted from* [68]. (**B**) Differential regulation of Kv channel inactivation by Kvβ1/3 (red) and Kvβ2 (green) in the presence of oxidized and reduced pyridine nucleotides. *Adapted from* [101]. Kv channels expressed in membranes of excitable cells represent heterogeneous populations of structures with varying β subunit compositions. Channels that assemble with Kvβ1/Kvβ3 proteins demonstrate enhanced inactivation upon binding to reduced pyridine nucleotides. Conversely, sensitivity of channel inactivation to pyridine nucleotide redox is absent in channels that associate with Kvβ2, which does not contain the ball-and-chain. (**C**) Graph showing proposed regulation of Kv channel activation, inactivation, and single channel and whole-cell $I_{Kv}$ as the ratio of expressed Kvβ2:Kvβ1 or Kvβ3 is increased. A reduction in channel inactivation with increased Kvβ2:Kvβ1/3 in native Kv channels could produce an increase in single channel Kv activity and elevation in steady-state $I_K$, which may lead to significant alteration in membrane excitability and responsiveness to changes in cellular metabolism. Solid lines represent predicted observed effects on whole cell Kv activation, inactivation, and $I_K$. Dashed lines show plausible graded effects of Kvβ2:Kvβ1/3 ratio on inactivation and $I_K$.

For example, in channels with non- inactivating Kvα pore subunits (e.g., Kv1.5) and predominantly Kvβ2 subunits, channel inactivation may be slower, as C-type inactivation would be the primary mode of inactivation.[127] Conversely, in channels consisting of variants of Kvβ1 or 3, channel inactivation likely occurs within a faster time frame, as these subunits would contribute to rapid N-type inactivation. In addition to interaction and regulation of Kvα function by the Kvβ proteins, interaction between multiple types of Kvβ can influence the net function of the Kvβ complex on channel gating. For example, incorporation of Kvβ2 can lead to significant inhibition of N-type inactivation imposed by Kvβ1 subunits within the same channel complex.[130] Nonetheless, the extent to which these subunits impact channel activation and inactivation would also be dependent upon pyridine nucleotide redox

ratios in the submembrane compartment, as discussed above. Thus, it is plausible that the cell could dynamically fine-tune the regulatory properties of membrane potential to changing metabolic conditions by altering the ratio of Kvβ subunits within the population of functional membrane-inserted channels. In the remainder of this section, I will provide a brief overview of the importance of Kv channels to the cardiovascular, nervous, endocrine, and immune systems, and how the functional expression of Kvβ may influence physiological processes of excitable cells types within each.

*Cardiovascular system*: In the mammalian heart, multiple types of Kv channels mediate outward $K^+$ currents with variable activation and inactivation properties that collectively shape the cardiac action potential.[131,132] Attesting to the importance of Kv channel function to cardiac physiology is the robust association between cardiac arrhythmias with mutations in Kv channel subunit genes [133,134], as well as defective ventricular action potential repolarization in mice lacking Kv proteins.[135-137] The murine heart is known to express Kvβ1.1, Kvβ1.2, and Kvβ2 proteins.[138] Kvβ1 associates primarily with proteins of the Kv4 family and loss of Kvβ1 reduces the abundance of Kv4.3 in the sarcolemma, blunts transient outward $K^+$ current, and prevents modulation of action potential duration by changes in pyridine nucleotide redox state.[138,139] The physiological role of Kvβ2 remains unclear. Considering that the heart expresses multiple Kvβ subtypes, it is plausible that the promiscuous association between both Kvβ1 and Kvβ2

proteins with Kv1 and Kv4 channels contributes to priming cardiac Kv channels for modulation of channel inactivation. Under conditions of altered nucleotide redox (e.g., altered cardiac workload stress, ischemia), this influences the duration of the early and intermediate phases of repolarization of the action potential.

The Kv channels expressed by vascular smooth muscle are a predominant regulator of vascular tone, and therefore control blood flow and organ perfusion.[140] Kv1 expression and function has been reported in a number of vascular beds, including coronary, pulmonary, mesenteric, and cerebral arteries, among others.[141] Inhibition of Kv1 channels induces vasoconstriction, suggesting that Kv1 channels are tonically active in vascular smooth muscle to oppose vascular tone development.[142] However, little is known regarding the expression and function of Kvβ subunits in the vasculature. Our laboratory recently reported that murine coronary arterial myocytes express heteromeric assemblies of Kvβ complexes in association with Kv1.5 alpha subunits, and that genetic deletion of Kvβ2 reduces the membrane expression of Kv1.5 [143], similar to that reported in neurons and heterologous expression systems.[144,145] Although we and others have speculated that these subunits may play an important regulatory role in coupling tissue oxygen demand with vasodilatory function in various vascular beds [12,146,147], further research is needed to increase our understanding of how the Kvβ proteins operate in the vasculature and how these may participate in functional or metabolic hyperemic responses.

Unlike most peripheral arteries and arterioles, hypoxia causes rapid and profound vasoconstriction of pulmonary arteries.[148] This phenomenon, referred to as “hypoxic pulmonary vasoconstriction” (HPV), is thought to be an important physiological response of the pulmonary circulation that shunts blood away from under-ventilated lung tissue.[149] However, excessive HPV can lead to pulmonary hypertension, right ventricular hypertrophy, and heart failure.[150] Kv1 channels regulate pulmonary vascular smooth muscle membrane potential and mediate the HPV response.[151,152] HPV is significantly impaired after genetic deletion of redox sensitive Kv1.5 channels, and *in vivo* gene transfer of Kv1.5 normalizes HPV in a model of chronic pulmonary hypertension.[153,154] The association of the Kv1 channels of the pulmonary vasculature with Kvβ proteins may be integral to the HPV response. In support of this, bovine pulmonary arteries exhibit a significant increase in Kvβ1.1 expression with further progression towards higher order pulmonary arteries and arterioles.[155] Higher expression of Kvβ1.1 may impart enhanced inactivation to Kv channels in small vessels in which HPV is apparent by allowing sensing of increases in NADH:NAD ratio upon a decrease in mitochondrial oxidative metabolism during periods of hypoxia.[156] Nonetheless, the precise role of the Kvβ1 subunits in the HPV response has not been directly tested.

*Nervous system*: Multiple types of Kv channels expressed in the central nervous system control membrane potential and excitability of neurons, and

coordinate diverse processes such as action potential propagation and back propagation, neurotransmitter release, and apoptosis.[157] The altered activity or expression of Kv channel proteins in the nervous system has been associated with human pathological conditions such as epilepsy, multiple sclerosis, and Alzheimer's disease.[158-161] Neurons express multiple Kv alpha subunits that form functional channels, confer A-type $K^+$ currents, and likely associate with Kvβ proteins, including dendritic Kv4.1, Kv4.2 and Kv4.3 subunits [162-164] and presynaptic Kv1.4 subunits.[162] Variants of all three Kvβ gene products have been found in the brain, with Kvβ2 being the predominant form [165-171], suggesting that Kv1 and Kv4 channels may assemble into heteromers with considerable functional diversity that may participate in the determination of neuronal phenotype. In addition to modulation of channel activation and inactivation characteristics, Kvβ proteins may play a chaperone role and regulate the subcellular targeting of specific populations of Kv channels to distinct neuronal regions (i.e., axonal versus dendritic targeting).[144,145] Genetic deletion of Kvβ2 in mice increases mortality, reduces body weight and results in defects in thermoregulatory processes [172], whereas mice lacking Kvβ1.1 have reduced Kv current inactivation, frequency-dependent spike broadening, and slower afterhyperpolarization compared with wild type mice. These changes in neuronal electrical signaling are associated with impaired learning and memory in water maze and social transmission tasks.[173] Although definitive evidence is lacking, it is possible that changes in brain electrical activity could be strongly modulated by Kvβ-

dependent regulation of Kv1 and Kv4 activity during periods of altered neuronal cytosolic redox potential, for example, changes in glucose metabolism.

*Endocrine and immune systems*: Multiple Kv channel subtypes also participate in the physiological regulation of membrane potential in several cell types outside of the cardiovascular and nervous systems. Studies have suggested that these channels, via regulation of $Ca^{2+}$ influx, also control hormonal secretion in cells of the endocrine system. For example, in pancreatic beta cells, an increase in $Ca^{2+}$ influx following increased cellular ATP:ADP ratio and inhibition of ATP-sensitive $K^+$ channels ($K_{ATP}$) stimulates the release of insulin.[161,174] Repolarization of the cell back to resting potential and cessation of the secretory process, is mediated, in part, by Kv-mediated outward $K^+$ currents, which are likely mediated by a variety of Kv channel subtypes, including Kv1, Kv2, Kv4.[175] Although the expression profile of associated Kvβ proteins in pancreatic islets is not known, modulation of Kv activity by these subunits may be essential to proper electrical signaling following a glucose-induced rise in $NADPH:NADP^+$ ratio in beta cells.[176] In addition, Kv1 channels have also been shown to be expressed by cells of the immune system.[57] Kv1.5 and Kv1.3 are the predominant Kvα proteins in macrophages and inhibition of Kv1 channels can prevent macrophage activation and proliferation.[177-179] Bone marrow-derived macrophages express all known variants of Kvβ1, and Kvβ2.1 proteins [180]; LPS- and TNF-

α induced activation differentially impact the abundance of these proteins and modify channel inactivation. This suggests that modification of Kv1 channel pore and auxiliary subunit composition may reflect an adaptive mechanism that could alter the functional properties of cells in the immune system.

## Therapeutic implications

Based on current knowledge of the physiological roles of Kvβ proteins, it is plausible that these proteins and their functional properties may represent an advantageous therapeutic target over conventional pharmacological ion channel blockers for several conditions. Classical inhibitors of AKRs show little inhibition of Kvβ-mediated catalysis, and currently, only a few pharmacological agents are known to impact Kvβ function; these act primarily as inhibitors of catalytic activity or by disrupting the association between the Kvβ and Kvα T1 docking domain. A recent study identified the acidic dopamine metabolite 3,4-dihydroxphenylacetic acid (DOPAC) as an effective inhibitor of Kvβ2-mediated reduction of 4-nitrobenzaldehyde, inhibiting the production of 4-nitrobenzyl alcohol by ~40% [181], albeit at supraphysiological concentrations. Additional nonendogenous inhibitors such as the cardioprotective drug resveratrol and plant derived flavonoid rutin, only slightly inhibit Kvβ2 catalytic activity by ~38% each. Alternatively, corticosteroids, such as cortisone, directly interact with Kvβ to increase Kv1 channel activity through binding near the cofactor binding pocket and the inter-subunit interface, resulting in dissociation of the Kvβ from the

channel.[182] There are currently no known pharmacological agonists that can selectively enhance Kvβ catalytic function. Further elucidation of compounds that can selectively modulate the function of the proteins may be valuable as novel therapeutics for the treatment of multiple disorders. Although the possibility for using compounds identified by these initial studies as Kvβ modulators as therapeutics is unlikely, they provide a useful foundation for further research into more beneficial chemical analogues that may possess more specific biological actions resulting from altering Kvβ function while avoiding off target effects.

# CURRICULUM VITAE

Sean M. Raph, BA, MS, MS
Center for Cardiometabolic Science
University of Louisville
580 South Preston Street, Room 219
Louisville, Kentucky, 40202
(207) 877-5858
Sean.Raph@Louisville.edu

## Education

05/2012 B.A. in Biology
University of Maine at Farmington
Farmington, ME

05/2015 M.S. in Biological Sciences
University of Southern Maine
Portland, ME

12/2020 M.S. in Pharmacology and Toxicology
University of Louisville
Louisville KY

12/2022 Ph.D. in Pharmacology and Toxicology
University of Louisville
Louisville KY

## Academic Appointments

2012–2015 *Graduate Research Assistant, Masters Candidate*
Department of Biology
University of Southern Maine

2018–2021 *Graduate Research Assistant, Masters Candidate*
Department of Pharmacology and Toxicology
University of Louisville

2021–pres. *Graduate Research Assistant, Doctoral Candidate*
Department of Pharmacology and Toxicology
University of Louisville

**Professional memberships and activities**

Society of Toxicology, 2017–2018
American Heart Association 2019–2021
American Society for Pharmacology and Experimental Therapeutics 2020–2021

**Honors and awards**

2019 Research!Louisville Research Symposium: 2nd place Masters candidate poster
2019 Southeast Regional IDeA Research Conference: Best Poster Award in Environmental Research and Cardiovascular Disease, Graduate Student Division

**Abstracts**

1. **Raph, SM**, Dwenger, MM, Nystoriak, MA. Integrated redox sensitivity of vascular Kv1 channels. Experimental Biology, April 2–5, 2022, Philadelphia, Pennsylvania.
2. Dwenger, MM, **Raph, SM**, Ohanyan, V, Chilian, WM, Bhatnagar, A, Nystoriak, MA. Mechanisms underlying physiologic coupling of myocardial metabolism and blood flow. Society for Heart and Vascular Metabolism, September 23–24, 2021, Jena, Germany (virtual).
3. **Raph, SM**, Nystoriak, MA. Oxidoreductase activity of voltage-gated potassium channel-associated auxiliary subunit mediates vasodilation to altered intracellular redox state. University of Louisville Cardiovascular Research Symposium, April 16, 2019, University of Louisville, Cardiovascular Institute, Health Sciences Campus, Louisville, Kentucky.
4. **Raph, SM**, Nystoriak, MA. $K_V\beta2$ Mediates Vasodilation in Response to Redox Changes of the NADH:$NAD^+$ Ratio. Research!Louisville, September 10–12, 2019, Center for Translational Research Building, University of Louisville, Health Sciences Campus, Louisville, Kentucky.
5. **Raph, SM**, Nystoriak, MA. Redox changes in the NADH:$NAD^+$ ratio induces vasodilation via the $K_V1$ redox sensing subunit $K_V\beta2$. Southeast regional IDeA Conference, November 6–8, 2019, The Galt House, Louisville, Kentucky.
6. **Raph, SM**, Bhatnagar, A, Nystoriak, MA. The enzymatic function of Kvβ2 contributes to resistance artery vasodilation. The FASEB Journal *34 (S1)*, 1-1.

**Publications**

1. Dwenger MM, **Raph SM**, Baba SP, Moore JBIV, Nystoriak MA. Diversification of potassium currents in excitable cells via Kvβ proteins. 2022. *Cells*. 11: 2230. PMC9317154. Review.
2. Dwenger MM, **Raph SM**, Reyzer ML, Lisa Manier M, Riggs DW, Wohl ZB, Ohanyan V, Mack G, Pucci T, Moore JB 4th, Hill BG, Chilian WM, Caprioli RM, Bhatnagar A, Nystoriak MA. Pyridine nucleotide redox potential in

coronary smooth muscle couples myocardial blood flow to cardiac metabolism. 2022. *Nature Communications*. 13: 2051. PMC9018695.
3. Ohanyan V*, **Raph SM***, Dwenger MM, Hu X, Pucci T, Mack GD, Moore JB, Chilian WM, Bhatnagar A, Nystoriak MA. Myocardial blood flow control by oxygen sensing vascular Kvβ proteins. 2021. *Circulation Research*. 128: 738. PMC8486354. (*Co-first authors).
4. **Raph SM**, Bhatnagar A, Nystoriak MA. Biochemical and physiological properties of K+ channel associated AKR6A (Kvβ) proteins. 2019. *Chemico-Biological Interactions*. 305: 21. PMC6584034. Review.